

広島大学学位請求論文

The Chemistry of Unstable Molecules
with Unusual Electronic Structures:
Anti-aromatic 16π Porphyrins and
Cyclic Aromatic Remote Carbenes

(特異な電子構造を有する不安定分子の化学：
反芳香族性 16π ポルフィリン及び
環状芳香族リモートカルベン)

2015 年

広島大学大学院理学研究科

化学専攻

菅原 峻

The Chemistry of Unstable Molecules with
Unusual Electronic Structures: Anti-aromatic
16 π Porphyrins and Cyclic Aromatic Remote
Carbenes

(特異な電子構造を有する不安定分子の化学：
反芳香族性 16 π ポルフィリン及び環状芳香族リ
モートカルベン)

広島大学大学院理学研究科
化学専攻

菅原 峻

目次

1. 主論文

The Chemistry of Unstable Molecules with Unusual Electronic Structures: Anti-aromatic 16π Porphyrins and Cyclic Aromatic Remote Carbenes

(特異な電子構造を有する不安定分子の化学：反芳香族性 16π ポルフィリン及び環状芳香族リモートカルベン)

菅原 峻

2. 公表論文

3. 参考論文

主論文

The Chemistry of Unstable Molecules with
Unusual Electronic Structures: Anti-aromatic
 16π Porphyrins and Cyclic Aromatic Remote
Carbenes

Department of Chemistry,
Graduate School of Science
Hiroshima University

Shun, SUGAWARA

Contents

Chapter 1. General Introduction

1-1. Unstable Molecules with Unusual Electronic Structures	2
1-2. Porphyrins	3
1-3. Aromaticity and Antiaromaticity	4
1-4. Previously Isolated 16 π Porphyrins	6
1-5. Purpose of This Work 1	8
1-6. Carbenes	9
1-7. Spin Multiplicity and Electronic Effects of Adjacent Substituents	10
1-8. Stable Singlet Carbenes	12
1-9. Cyclic Aromatic Carbenes	14
1-10. Purpose of This Work 2	15
References	16

Chapter 2. Synthesis and Characterization of the Most Distorted 16 π Porphyrin: 16 π Octaisopropyltetraphenylporphyrin (OiPTPP)

2-1. Introduction	22
2-2. Synthesis and Characteriation	23
2-3. Comparison of Distortion with OiBTPP analogs	27
2-4. Conclusions and Outlook	29
Experimental Section	32
References	37

Chapter 3. Synthesis, Characterization, and Spectroscopic Analysis of Anti-aromatic Benzofused Metalloporphyrins

3-1. Introduction	40
3-2. Synthesis and Characterization	42
3-3. Crystal Structures	46
3-4. Evaluation of Antiaromaticity by ^1H NMR Spectroscopy and NICS Calculations	52
3-5. Magnetic Circular Dichroism (MCD) spectra and MO analysis	54
3-6. Excited-state Relaxation Dynamics	64
3-7. Electrochemistry and Electrosynthesis	67
3-8. Conclusions and Outlook	72
Experimental Section	73
References	79

Chapter 4. Anti-aromatic 16π Porphyrin Metal Complexes with meso-Alkyl Substituents

4-1. Introduction	84
4-2. Synthesis and Characterization	84
4-3. Evaluation of Antiaromaticity	89
4-4. Conclusions and Outlook	91
Experimental Section	92
References	97

Chapter 5. Synthesis of the Most Anti-aromatic 16π Porphyrin: An Octaethylporphyrin Zinc(II) Complex with No meso-Substituents

5-1. Introduction	100
5-2. Results and Discussion	101
5-3. Conclusions and Outlook	105
Experimental Section	106
References	107

Chapter 6. Synthesis of New Cyclic Aromatic Carbene Ligands Bearing Remote Amino Groups and Their Palladium(II) Complexes

6-1. Introduction	110
6-2. Theoretical Calculation	111
6-3. Synthesis and Characterization	112
6-4. Catalytic Activity	115
6-5. Conclusions and Outlook	115
Experimental Section	116
References	125

Chapter 7. 1,8-Disubstituted Xanthyldene-based Remote Carbenes: Photolytic Generation and Isolation of Low-coordinate Palladium(II) Complex

7-1. Introduction	128
7-2. Synthesis	129
7-3. Photolysis of Tosylhydrazones	134
7-4. Metal Complexes	139
7-5. Conclusions and Outlook	143
Experimental Section	144
References	158

Chapter 8. Synthesis of C4 Cumulene featuring Xanthyldene Derivative Units

8-1. Introduction	162
8-2. Synthesis and Characterization	163
8-3. Electronic Properties	166
8-4. Conclusions and Outlook	168
Experimental Section	169
References	171

Chapter 9. Attempted Synthesis of Tridentate Pincer-type Cyclic Aromatic Remote Carbene Ligands

9-1. Introduction	174
9-2. Results and Discussion	175
9-3. Conclusions and Outlook	176
Experimental Section	177
References	179

Chapter 10. Conclusions and Outlook

10-1. Summary of Anti-aromatic 16 π Porphyrins	182
10-2. Summary of Cyclic Aromatic Remote Carbenes	186

List of Publication

Acknowledgement

Chapter 1

General Introduction

1-1. Unstable Molecules with Unusual Electronic Structures

A number of molecules composing biological systems, chemical materials, and other organic substances in our world possess enough stability for their existence and frequent usage. In order to serve their functions appropriately, it is essential that they should be durable for a long period as well as resistant to external stimuli (*i.e.* air, moisture, and light). In contrast, unstable molecules, which are not able to exist under normal environmental conditions, exhibit peculiar structures, properties, and reactivity derived from their unusual electronic structures, which have intrigued a lot of chemists for decades. For example, reactive intermediates have played a pivotal role to elucidate reaction mechanisms although most of them can be only detected in terms of spectroscopic methods due to their short lifetimes.^[1] However, owing to scientist's persistent endeavor and recent progress of measuring instruments and computations, explorations of the fascinating structures and properties have become available in recent years. In addition to the fundamental elucidation, there are unlimited potentialities for their applications including organic electronic materials, activation of small molecules, and development of functional catalysts.

In the field of main group and organometallic chemistry, molecular architecture including ligand design is a key to stabilize unstable species as isolable forms since several strategies for stabilizing such unstable species with suitable ligand systems have enabled us to isolate them.^[2] Despite the thermodynamic and kinetic stabilities derived from electronic and steric perturbations of ancillary functional groups, their reactivity and electronic structure still remain unchanged in several cases (Figure 1). Thus, investigations of unstable molecules stabilized by suitable ligand systems highly worth challenging. Among them, we have focused on developing reasonable ligands for “isolable” anti-aromatic 16π porphyrins and cyclic aromatic carbenes.

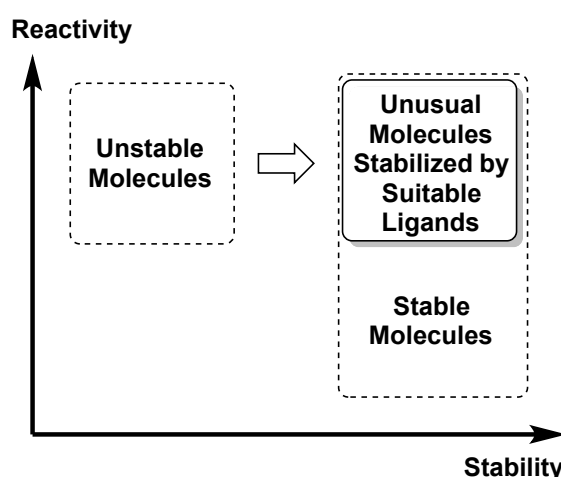


Figure 1. General idea about the correlation between stability and reactivity.

1-2. Porphyrins

Porphyrins are well known as biologically important components in our life. Indeed, biological systems contain a number of porphyrin-based molecules, which are crucial for bioorganic reactions found inside creatures and plants of the Earth. For instance, heme-containing proteins are based on porphyrin iron complexes bearing functions to transport gaseous oxygen to bodies in respiration, and photosynthesis of chlorophylls are taken place because of light harvesting ability of the porphyrin segments. Therefore, porphyrins have been widely investigated by chemists in both fundamental and applied research fields.^[3]

The basic framework for porphyrins consists of four pyrrole subunits connected with four methine carbons and countless numbers of the derivatives with substituents at the β or/and meso positions have been developed due to their photochemical properties, electrochemical characters, and catalytic functions. Besides, expanded and contracted derivatives, which are known as expanded porphyrins for the former and subporphyrins for the latter, have been intensively explored by Osuka and coworkers for recent years, revealing their intriguing structures and peculiar properties.^[2d, 2e] Porphyrins and all of the derivatives possess several features, that is, metal binding ability with central amine and imine moieties, structural deformation caused by the steric hindrance between peripheral substituents, and accessible redox transformation. In particular, the redox behaviors of basic porphyrins have played a crucial role to clarify mechanisms to transfer the electrons in biological reactions such as photosynthesis and oxygen carrier. While conventional porphyrins have 18π electrons in their conjugated system and extra stability derived from Hückel aromaticity (*vide infra*), their redox states can change from neutral (18π) to doubly oxidized species (16π), cation radical (17π), anion radical (19π), and, doubly reduced species (20π) (Figure 2). The cation radical complexes have been well investigated in the isolated forms because one-electron oxidation is likely to be easily occurred.^[4] However, isolated examples with other electronic structures are still rare due to their unstable nature caused by dearomatization, especially characterization and isolation of “anti-aromatic” 16 and 20 π -electron states were one of the biggest challenges in this research field.

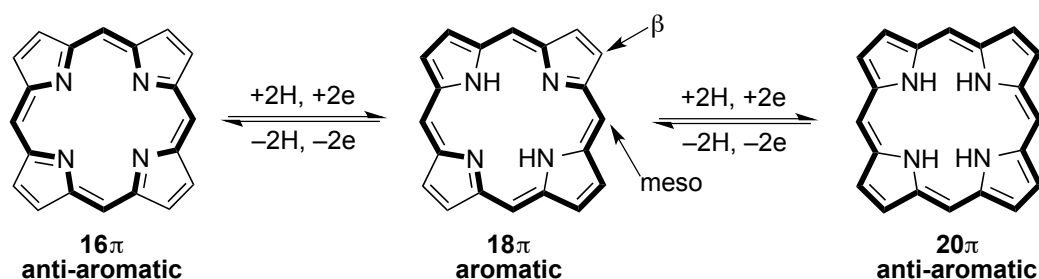


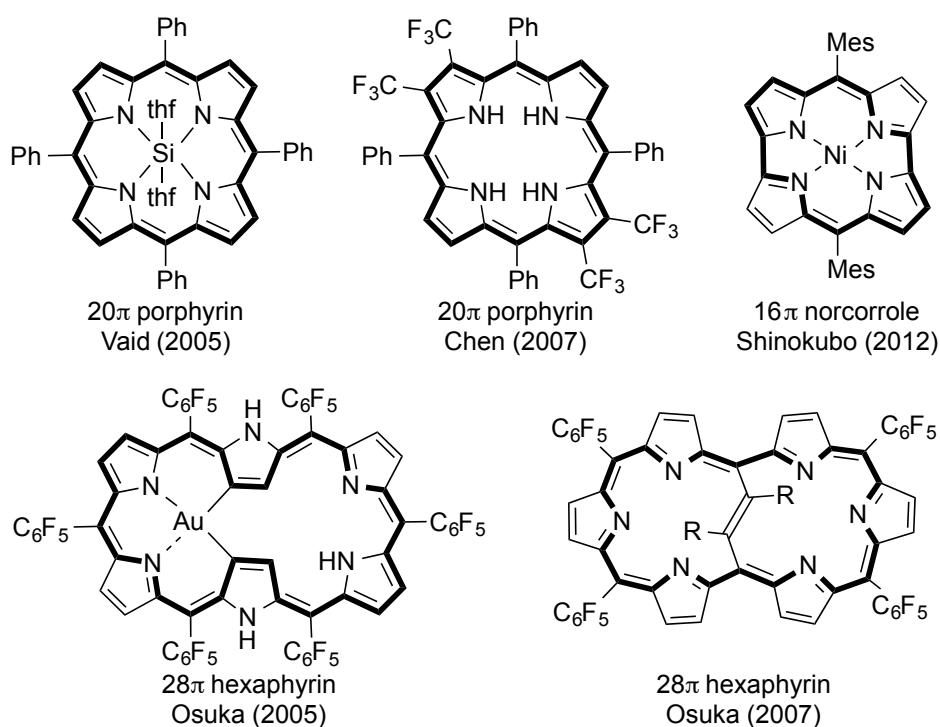
Figure 2. Redox transformation among 16, 18, and 20 π -electron porphyrin cores.

1-3. Aromaticity and Antiaromaticity

Aromaticity is one of common basic notions in organic chemistry. In general, planar and cyclic unsaturated molecules, which have the number of π -electrons equaled to $4n+2$ ($n = 0, 1, 2, \dots$) in their successive conjugated circuit, can exhibit aromatic nature with extra stability caused by electron delocalization. In contrast, π systems, which have the number of π -electrons equaled to $4n$, are classified as anti-aromatic molecules. The index of aromaticity and antiaromaticity is widely known as Hückel's rule proposed by Erich Hückel in 1931. However, there is no precise quantitative definition for aromaticity and the concept is not directly measurable experimentally. Thus, we should consider whether or not the molecule has aromaticity with several criteria: (i) structure, (ii) energy, and (iii) magnetic properties.^[5] (i) Most of the aromatic molecules possess equalized bond lengths on their conjugated bonds due to π -electron delocalization. However, note that some of the non-aromatic molecules such as polybenzenoid hydrocarbons and highly conjugated acyclic compounds also show small difference of their bond lengths as if they have aromatic nature. (ii) Aromatic molecules possess enhanced resonance energies (REs) and the aromatic stabilization energies (ASEs) in principle, but the criterion is difficult to evaluate even in simple molecular systems since the values were dependent on the equations and reference molecules. Instead, the better evaluated value than ASE was obtained by the isomerization stabilization energy (ISE) proposed by Schleyer *et al.* in 2002.^[6] (iii) ^1H NMR chemical shifts are the most reliable experimental tools to evaluate aromaticity and antiaromaticity. In the ^1H NMR spectra of aromatic molecules, the signals of the outer protons of the porphyrin ring exhibit low-field shifts due to the diatropic ring current, whereas those of anti-aromatic molecules are shifted to high field due to the paratropic ring current.^[7] In addition to the experimental criteria, nucleus-independent chemical shifts (NICS) developed in 1996 have become the most popular magnetic criterion to define aromaticity and antiaromaticity of π systems by computational method, in which a dummy atom is placed at the center of a ring.^[8] Negative values are expected for aromatic molecules, whereas positive values are found in anti-aromatic molecules. With these criteria, aromaticity of porphyrin derivatives has been scrutinized for long period of time.

As yet, antiaromaticity has not been fully established since a limited number of anti-aromatic molecules have been known thus far due to their unstable nature. With respect to anti-aromatic porphyrins and their derivatives, the species with longer π -electron conjugated chains than 20π electrons have emerged in recent years. For example, some of anti-aromatic 20π porphyrins and their derivatives mostly generated by chemical reduction were fully characterized by X-ray structural analysis, photophysical measurements, and NMR spectroscopy.^[9] In addition, metal complexes of expanded porphyrins showed distinct anti-aromatic properties and some of them were found to be stable even when exposed to air and moisture.^[10] Furthermore, topological changes of expanded porphyrins induced Möbius aromaticity and antiaromaticity in which the definition of the number of π electrons was opposite to that of Hückel's rule.^[11] The molecules with Möbius topology and the number of π electrons equaled to $4n$ indicate Möbius aromaticity, whereas those with $4n+2$ π electrons possess Möbius antiaromaticity.

Compared to the above-mentioned porphyrin derivatives with more than 20π electrons, anti-aromatic species with 16π electrons have been scarcely known as the isolated forms. In fact, isolation of the 16π porphyrins have been accomplished only by us and Vaid's group.^[12, 13] In 2005, we have firstly found that highly distorted porphyrins (e.g. octaethyltetraphenylporphyrin and octaisobutyltetraphenylporphyrin) were effective to isolate the corresponding 16π porphyrins by oxidative reaction. Then, our successive discoveries with other porphyrin ligands were intensively achieved in recent years, whereas Vaid et al. only reported that the doubly oxidized tetraphenylporphyrin lithium(I) complex showed antiaromaticity derived from 16π electron conjugated circuit in 2006 (see more details in the next section). As for the porphyrin derivatives, gram-scale synthesis of norcorrole nickel(II) complex with strong anti-aromatic nature was reported by Shinokubo *et al.* in 2012 and the peculiar reactivity and application to an electrode-active material were also investigated.^[14] Thus, anti-aromatic porphyrins and their derivatives have been paid much attention due to their fundamental properties and potential applications.



Topology	Number of π electrons	
	$4n+2$	$4n$
Hückel	Aromatic	Anti-aromatic
Möbius	Anti-aromatic	Aromatic

Figure 3. Examples of Hückel anti-aromatic molecules and basic rule to define aromatic or anti-aromatic nature by the number of π electrons and topology.

1-4. Previously Isolated 16 π Porphyrins

While exploring highly distorted porphyrin – main group element complexes,^[15] we fortunately found that the dilithiated salt of octaethyltetraphenylporphyrin (OETPPH₂) or octaisobutyltetraphenylporphyrin (OiBTTPH₂) could be reacted with SOCl₂ to afford doubly oxidized octaalkyltetraphenylporphyrins (OETPP or OiBTTP) with a 16 π -electron core (Figure 4).^[12a] From the results of this study, we disclosed three features for 16 π porphyrins: (i) structural deformation, (ii) bond alternation, and (iii) clear difference in the UV-vis absorptions. As for (i), X-ray structural analysis revealed that our isolated metal-free 16 π porphyrins were more distorted than the corresponding 18 π analogs, although the 18 π porphyrins were also distorted by the steric repulsions between peripheral substituents compared to less substituted porphyrins such as tetraphenylporphyrins (TPP) or octaethylporphyrins (OEP). While OETPP was gradually decomposed in the CH₂Cl₂ solution, the stability of OiBTTP was largely enhanced due to the more distorted structure. Thus, these results suggested that stability of 16 π porphyrins was correlated closely with the degree of distortion of the porphyrin core. With respect to (ii), X-ray structures of the 16 π porphyrins showed distinct bond alternation in the porphyrin core, suggesting that the molecules were non-aromatic or anti-aromatic. Finally, as for (iii), the UV-vis absorption of 16 π porphyrins showed highly blue-shifted Soret-like bands observed at 280-330 nm and no peak in the Q-band region, while the absorption of the corresponding 18 π porphyrins appeared at 440-450 nm as Soret-bands and at 550-590 nm as Q-bands. These experimental features were revealed for full characterization of the first isolated 16 π porphyrins.

Contemporaneously, Vaid *et al.* also found that the oxidation of dilithiated tetraphenylporphyrin ((TPP)Li₂) with thianthrenium tetrafluoroborate (Thn⁺BF₄[−]) enabled them to isolate 16 π [(TPP)Li^I]⁺[BF₄][−] (Figure 4) and they reported the results during a year after our initial report.^[13] This complex was the first example of the 16 π porphyrin metal complex at that time. Since all of their efforts to remove the central lithium(I) cation were to no avail, the highly planar 16 π TPP would be too unstable to exist as a metal-free state, suggesting that coordination to the central metal provided the further stabilization as well as structural deformation upon oxidation.

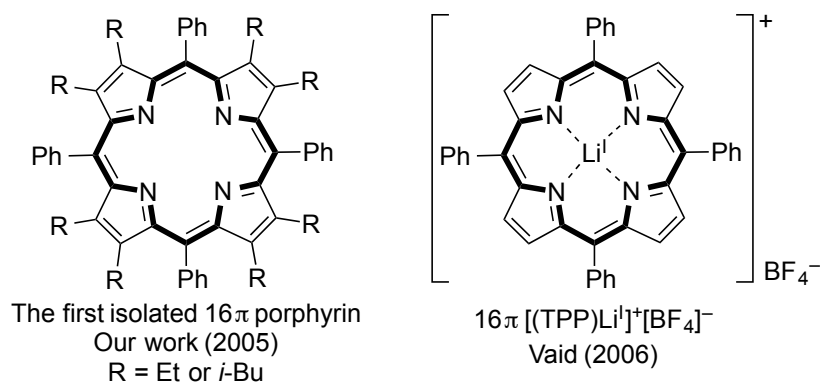
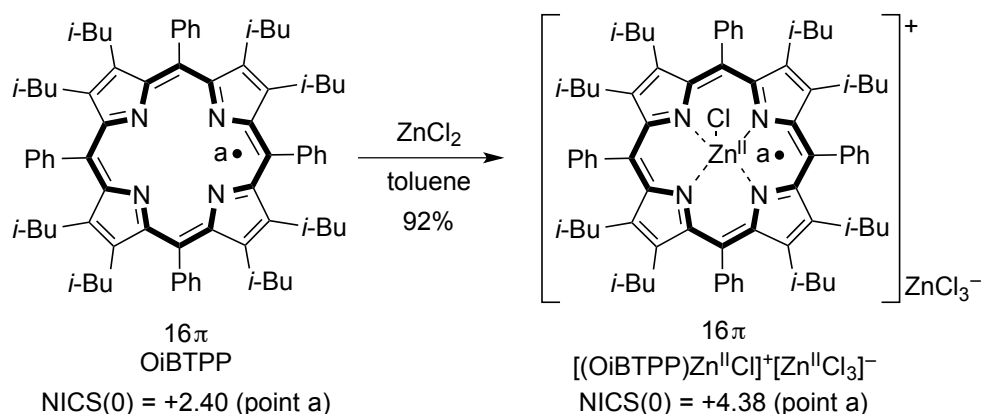


Figure 4. The previously isolated 16 π porphyrins investigated by us and Vaid's group.

In order to achieve comprehensive understandings for reactivity of our 16 π porphyrins, we examined reactions of the metal-free 16 π porphyrin (OiBTTP) with various metal reagents after elucidating that SbCl₅ is a reliable strong oxidant to generate the metal-free 16 π porphyrins.^[12b] Although the reaction of the metal-free OiBTTP with SnCl₂ followed by ethanolysis gave the OiBTTP tin(IV) complex with 18 π electrons in a redox manner and other low-valent metals such as Zn⁰, Cu⁰, and Pd⁰ were not incorporated to the center, the reaction with divalent ZnCl₂ cleanly produced the 16 π -electron porphyrin zinc(II) complex, [(OiBTTP)Zn^{II}Cl]⁺[Zn^{II}Cl₃]⁻, in 92% yield and the crystal structure was unambiguously determined by single crystal X-ray analysis (Scheme 1). The structure of the 16 π -electron zinc(II) complex was also largely distorted than the corresponding 18 π analog in accordance with the structural change of the metal-free porphyrins. To gain further insights into the electronic structures of 16 π porphyrins, magnetic circular dichroism (MCD) studies in conjunction with ZINDO/S calculations supported to identify the electronic transitions of the UV-vis spectra of the isolated 16 π porphyrins. In addition, electrochemical and thin-layer UV-vis spectroelectrochemical measurements revealed that the redox behavior of the 16/18 π metal complexes were to be reversible, whereas the metal-free 16 π porphyrin can be reduced electrochemically to afford an unidentified 18 π decomposed products. It's noteworthy that nucleus-independent chemical shift (NICS) calculations of our highly distorted 16 π porphyrins showed the positive but small value at the inner point of the macrocycles, indicating that the ring current was weakly paratropic and the species essentially possessed non-aromatic nature, with only weak antiaromaticity. Therefore, our previous study clarified that the isolated 16 π porphyrins with 12 peripheral substituents were stabilized by highly structural deformation caused by steric hindrance between the substituents at the expense of their anti-aromatic properties.



Scheme 1. Reaction of metal-free 16 π OiBTTP with ZnCl₂ to give a 16 π porphyrin zinc(II) complex and NICS(0) values of the 16 π porphyrins at the inner point of the porphyrin core.

1-5. Purpose of This Work 1

As described above, our findings and Vaid's discovery about the isolable 16π porphyrins opened the further investigations to elucidate intriguing structures and electronic properties of the species. In our previous work, antiaromaticity of our 16π porphyrins was significantly decreased by highly deformed structures and the assessment could be carried out only with NICS calculations because there is no measurable proton directly connected to the porphyrin macrocycles of octaalkyltetraphenylporphyrins. In contrast, Vaid's 16π porphyrin possessed the measurable protons at the β positions and high-field shifts of the β -protons in the ^1H NMR spectrum were observed, which the peak was found at 5.94 ppm and corresponded to a chemical shift typical of alkene protons rather than that of aromatic 18π porphyrins. However, it would be more effective to evaluate the antiaromaticity in terms of the ^1H NMR shifts of meso protons since the meso protons were directly bonded to the porphyrin core and subjected to the influence of paratropic ring current derived from anti-aromatic nature of 16π porphyrins. In addition, the relationship between planarity and antiaromaticity is still elusive due to a few isolable examples of the 16π porphyrins. Thus, further investigations of 16π porphyrins are crucially important and worth challenging.

In this thesis, comprehensive studies of a series of isolable 16π porphyrins are discussed. In order to disclose the correlation between the planarity and the antiaromaticity of 16π porphyrins, various porphyrin skeletons were developed to accomplish the goal of this study (Figure 5). In chapter 2, we discuss the most distorted 16π porphyrin, octaisopropyltetraphenylporphyrin, which was newly synthesized from a hitherto unknown diisopropylpyrrole.^[12d] The structures and electronic states of the benzo-fused 16π porphyrin metal complexes investigated by X-ray analysis, MCD spectroscopy as well as transient absorption spectroscopy are described in Chapter 3.^[12e] In Chapter 4, the most planar 16π porphyrin zinc(II) complex bearing a meso-alkyl substituent is explained.^[12c] Finally, although the structural study could not be accomplished due to the rapid decomposition, the most anti-aromatic 16π porphyrin measured by ^1H NMR spectroscopy is reviewed in Chapter 5.^[12f]

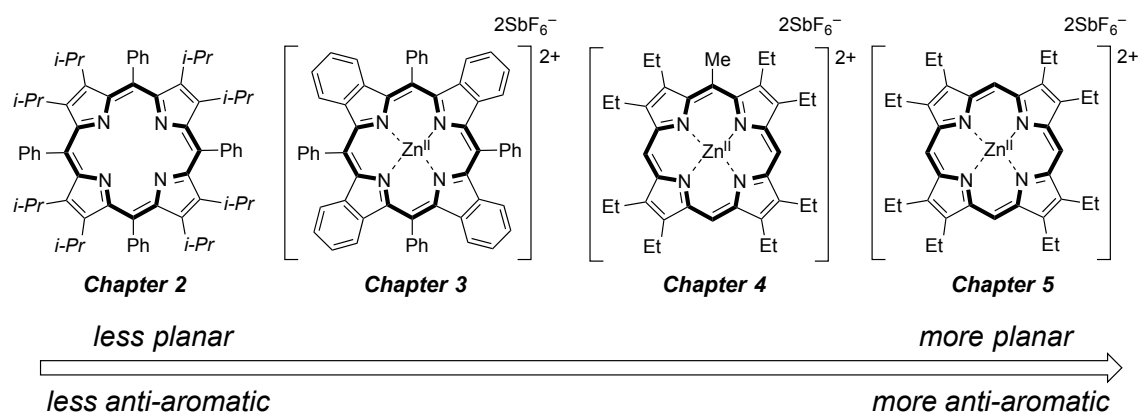


Figure 5. A series of 16π porphyrins prepared in this thesis and the correlation between planarity and antiaromaticity.

1-6. Carbenes

Carbenes $R_2C:$ are well known as neutral divalent carbon compounds with only six valence electrons. Thus, carbenes have two nonbonding orbitals and two unoccupied electrons. Since the electrons can occupy the vacant orbital and the spins are arranged parallel or anti-parallel, carbenes have two ground state multiplicity, *i.e.* singlet and triplet. Historically, the species have been considered as reactive intermediates for a long period, but they have played a crucial role in the field of both organic and organometallic chemistry (Figure 6). Although carbenes had been recognized as type of radicals prior to 1950, pioneering works reported by Hine^[16a] and Doering^[16b] in 1950's ignited much interest in carbene research as organic chemistry. Concurrently, Fischer *et al.* accomplished integration of these potential ligands into organometallic chemistry in 1964 because of the discovery of the first carbene tungsten complex.^[17] After a few years of the landmark findings, Öfele^[18] and Wanzlick^[19a] firstly reported preparation of the metal complexes with *N*-heterocyclic carbenes as ligands, respectively. These complexes were synthesized via deprotonating reaction of the imidazolium salt with metal-containing reagents, which had sufficient basicity. Meanwhile, Wanzlick *et al.* attempted isolation of the free carbene generated by deprotonation of the imidazolium salt with *t*-BuOK, but their work was to no avail.^[19b] Finally, in another two decades, Bertrand *et al.* accomplished the first isolation of persistent carbenes, (phosphino)(silyl)carbenes, in the liquid form in 1988, and moreover, Arduengo *et al.* achieved the first single crystal X-ray structural analysis of *N*-heterocyclic carbenes (NHCs) in 1991 (Figure 7).^[20] Triggered by these epoch-making discoveries, carbene chemistry has rapidly expanded from fundamental study of the reactivity and structure to application to functional organic and organometallic catalysts and stabilization of unusual molecules.^[21] Therefore, development of newly designed carbenes should be highly worthwhile for inflating the scope of carbene chemistry.

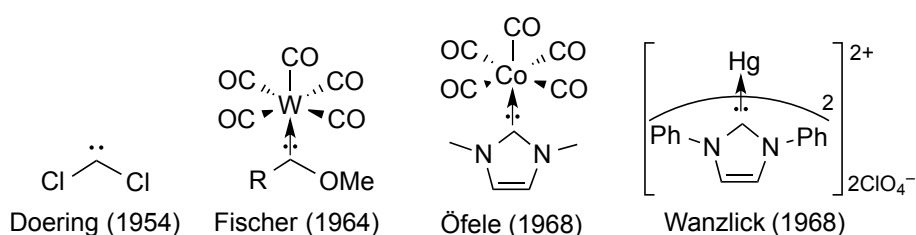


Figure 6. Early discoveries of carbene chemistry including the metal complexes.

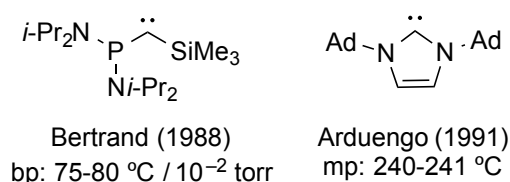


Figure 7. The first isolation of persistent carbenes by Bertrand and Arduengo.

1-7. Spin Multiplicity and Electronic Effects of Adjacent Substituents

As described in the above section, carbenes have two multiplicity of the ground state (*i.e.* singlet and triplet) derived from electron configuration of two non-bonding electrons.^[21b, c] In order to determine the multiplicity, the geometry at the carbene carbon atom as well as electronic effects of adjacent substituents is highly important. As for the former, either linear or bent structures can be possible for the geometry at the carbene carbon atom. An sp -hybridized carbene carbon atom provides the linear structure, which has two energetically degenerated p orbitals. While the triplet state can be largely stabilized in this geometry, most carbenes indeed show bent structures composed of sp^2 -hybridized carbon atom. A σ orbital of the carbene is stabilized by s character in comparison with the original p orbital. The occupation of the two empty orbitals with a parallel spin orientation leads to a triplet ground state ($\sigma^1 p^1$, Figure 8). On the other hand, two electrons occupy the σ orbital with an antiparallel spin orientation to be the singlet ground state ($\sigma^2 p^0$). Although the electronic states are energetically unfavorable, a less stable singlet state ($\sigma^0 p^2$) and an excited singlet state with a parallel spin orientation ($\sigma^1 p^1$) are possible but negligible to discuss in this thesis. The spin multiplicity of carbenes plays a crucial role to decide their reactivity. In fact, the singlet carbenes have a filled σ orbital and a vacant p orbital resulting that the singlet carbenes possess an ambiphilic character. In contrast, the triplet carbenes have two unpaired electrons and are generally behaved as diradicals.

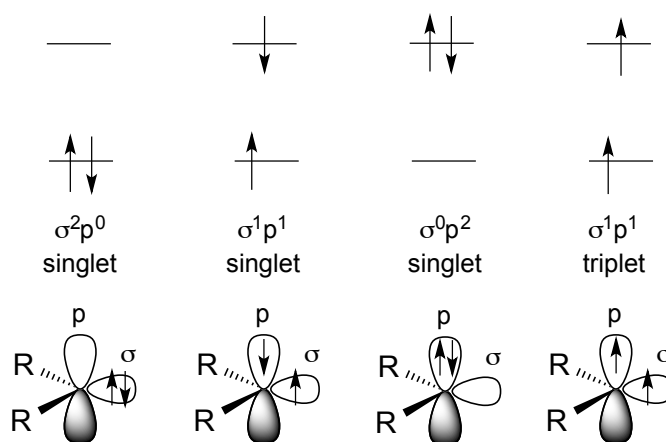


Figure 8. Electronic states of carbenes.

It is critical to understand the energy difference between the singlet and triplet states (ΔE_{ST}) since ΔE_{ST} is strongly related to electronic structure and reactivity of carbenes. In particular, the adjacent substituents at the carbene carbon atom have a significant influence on the spin multiplicity of the ground state. The electronic perturbation of the substituents can be considered as inductive and mesomeric effects. It is well known that σ -electron withdrawing group can stabilize the singlet state since the negative inductive effect lowers the relative energy of non-bonding σ orbital whereas the energy level of p orbital are unaffected.^[22] On the other hand, the triplet ground state can be stabilized by substituents with σ -electron donating properties due to the decrease of the energy gap between the σ and p orbital.

Although inductive effects partially dictate the multiplicity, mesomeric effects of the adjacent substituents should be more crucial factor to determine the ground state.^[23] The substituents can be categorized into two types depending on their electronic properties: π -donor substituents (X) which provide π electrons to the vacant p orbital of carbenes (e.g. $-\text{NR}_2$, $-\text{F}$, $-\text{OR}$, ...), and π -acceptor substituents (Z) which withdraw π electrons from the carbene center (e.g. $-\text{CF}_3$, $-\text{BR}_2$, $-\text{SiR}_3$, ...).^[24] Thus, the singlet carbenes can be classified according to the combination of these substituents: the highly bent carbenes X_2C : (push-push type), quasi-linear carbenes XZC : (push-pull type), or quasi-linear carbenes Z_2C : (pull-pull type) (Figure 9). While pull-pull type carbenes have still not been found as the isolable form, most of the isolable carbenes are regarded as push-push or push-pull types. For example, lone pair electrons of two adjacent nitrogen atoms are given to the vacant p orbital in stable N,N' -diaminocarbenes, which can be considered as push-push type carbenes. Also, Bertrand's (phosphino)(silyl)carbenes can be regarded as push-pull type carbenes since there are a π -electron donation from the phosphino group and a π -electron withdrawing effect of the silyl group. Thus, fine-tuning of the adjacent substituents is a key for designing stable carbenes.

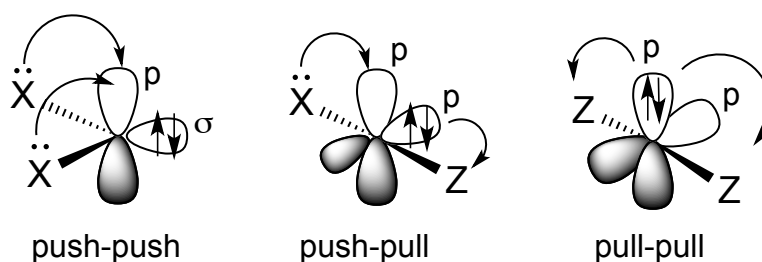


Figure 9. Mesomeric effects of the adjacent substituents.

Steric effects of the substituents are not so important but cannot be negligible. Bulky substituents can kinetically stabilize carbenes inhibiting the dimerization of carbenes. However, electronic effects dominate the stability of carbenes in some cases more than the kinetic stabilization. For example, N,N' -diaminocarbene with N -methyl groups could be isolated as the free form although the species was not kinetically stabilized by the small N -methyl groups, indicating the steric effects are not critical for their stability.^[25] Nonetheless, steric effects have also played an important role for increasing the stability of carbenes, and additionally, increasing catalytic activity in their metal complexes. Indeed, the carbene-palladium complexes bearing bulky substituents at the nitrogen atoms exhibit higher catalytic activity than when the complex has less sterically hindered ligands.^[26]

1-8. Stable Singlet Carbenes

After the first isolation of stable singlet carbenes accomplished by Bertrand and Arduengo,^[20] the number of fundamental and applied researches in carbene chemistry has been exponentially increasing. Above all, *N*-heterocyclic carbenes (NHCs) have been widely utilized in the research fields from organometallic chemistry to main-group chemistry. In organometallic chemistry related to NHCs, development of Grubbs' catalysts coordinated with NHCs, which possessed outstanding catalytic activity in olefin metathesis reactions, was generally recognized as the most famous and successful example.^[27] In the meantime, unusual main-group molecules have been successively isolated in terms of base-stabilized methods which firstly proposed by Robinson *et al.* as shown in his work on the first isolated base-stabilized diborene.^[28] All of these findings were achieved due to strong σ -donating ability of NHCs as well as their easier preparation. Thus, there are lots of possibilities to extend the chemistry by means of development of new singlet carbene ligands with different electronic structures.

Taking advantage of strong π -electron donating ability of nitrogen or phosphorus atoms, stable carbenes with only one adjacent heteroatom have been intensively developed by Bertrand's group (Figure 10). In their earlier works, two examples of acyclic stable carbenes with only one heteroatom were isolated with the full characterizations including X-ray structural analysis,^[29] but these acyclic carbenes could not form the stable metal complexes because of energetically unfavorable complexation derived from the wide carbene bond angle, which was in marked contrast to NHCs. Thus, their mind turned into designing cyclic stable carbenes with consideration for the future application to organometallic catalysts. Among the large number of their discoveries, cyclic (alkyl)(amino)carbenes (CAACs) have been predominantly utilized as ligands for highly active catalysts and base-stabilized unusual main-group species.^[21f] CAACs were firstly isolated in 2005 and their improved synthesis was also reported two years later.^[30] In comparison to NHCs, it is remarkable for CAACs to exert stronger σ -donating and π -accepting properties due to the replacement of one σ -withdrawing and π -donating adjacent nitrogen atom by one σ -donating but not π -donating adjacent carbon atom. In other words, the highest occupied molecular orbital (HOMO) is higher and lowest unoccupied molecular orbital (LUMO) is lower than those of NHCs. In addition, the steric demand of CAACs is different from that of NHCs owing to the presence of a quaternary carbon atom next to the carbene center.

Since stronger π -accepting property of CAACs was found to be prominent for stabilization of electron-rich species and activation of inert small molecules, fine-tunings of *N,N'*-diaminocarbenes have also been investigated in recent years (Figure 10). For example, Bertrand *et al.* developed a cyclic diamino carbene with a pyramidalized nitrogen atom, which exhibited the enhanced electrophilicity without diminishing its nucleophilicity equaled to that of conventional NHCs.^[31] Furthermore, Bielawski *et al.* recently succeeded in isolating *N,N'*-diamidocarbenes (DACs) with 6-membered ring and their study revealed that DACs have the lowest energy level of LUMO among all of the *N*-heterocyclic carbenes.^[32] Thus, DACs showed the peculiar reactivity with various organic substrates such as olefins,

alkynes, nitriles, amines, and small molecules. It should be noted that these carbenes could be isolated and used as reactants although the species possess high reactivity.

Furthermore, a new generation of stable carbene species beyond above-mentioned classical carbenes has steadily appeared in their free forms (Figure 10). Thus far, these compounds have been also recognized as “abnormal” or “remote” carbenes (aNHCs or rNHCs) due to the presence of nitrogen atoms at the different positions from those of “conventional” NHCs. However, note that Bertrand proposed that these new species should be named as mesoionic carbenes (MICs) since no reasonable canonical resonance forms could be drawn for them. Although there are only a few isolated examples for aNHCs and rNHCs presented by Bertrand’s group, experimental and theoretical studies demonstrated that these newer carbenes have stronger electron-donating properties than NHCs.^[33] Owing to this feature, catalytic activity of NHC/MIC mixed complexes used in ring closure metathesis reactions was superior to that of the ordinary catalysts.^[34] Thereby, much attention has been paid towards exploring newly designed aNHCs and rNHCs because of their high potentialities as ligands for activating transition-metal catalysts and stabilizing unusual reactive molecules.^[35]

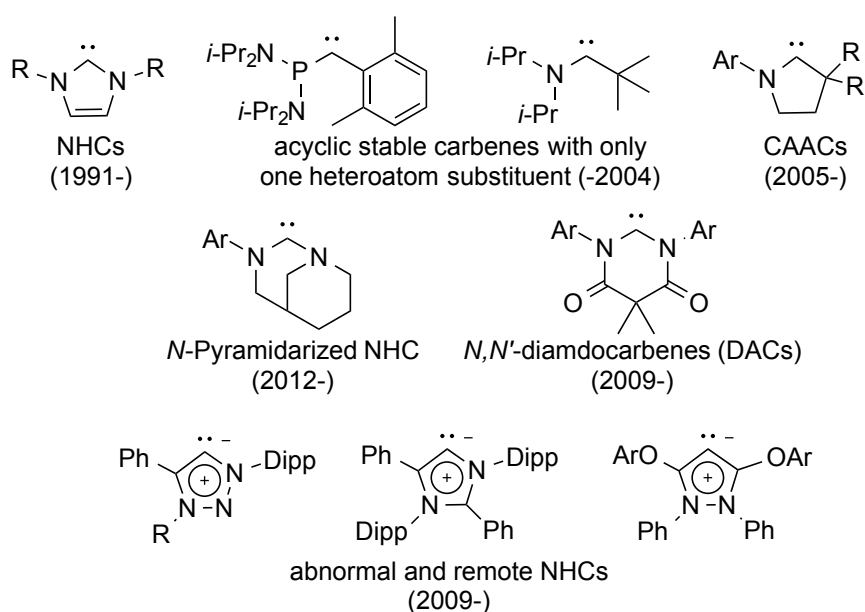


Figure 10. Isolated singlet carbenes with different electronic states compared to conventional NHCs.

1-9. Cyclic Aromatic Carbenes

Cyclic aromatic carbenes are derivatives of diphenylcarbenes bearing the bridged atom placed at the *para*-position of the carbene carbon atom (Figure 11). Previous work on cyclic aromatic carbenes, investigated as transient species by Schuster *et al.*, revealed that the ground state multiplicity was dependent on the identity of the bridged heteroatom.^[36] As for xanthylidene which is the oxygen-bridged cyclic aromatic carbene, the ground state was determined to be singlet. It was rationalized that the aromatic HOMO enhanced by the electron-donating oxygen substituent interacted with p orbital of the carbene moiety to provide a lower occupied orbital and a higher unoccupied orbital, resulting in increasing the energy gap between HOMO and LUMO (Figure 11). In contrast, boraanthrylidene that is the boron-bridged cyclic aromatic carbene was found to have the triplet ground state. In this case, the electron-deficient orbital of the boron atom decreases the energy of aromatic LUMO, so this lower LUMO has an interaction with p orbital of the carbene moiety to generate a lower singly occupied orbital and an unoccupied orbital (Figure 11). Since the resulting energy gap between σ orbital originated from the carbene moiety and the lower semi-occupied orbital should be narrow, the triplet ground state is more favorable than the singlet ground state. As described above, cyclic aromatic carbenes are intriguing motifs for designing newly carbenes because of these unusual electronic states depending on the bridged atom. In addition, there are a few papers on preparation of the carbene metal complexes, but little is known about their structures and catalytic properties other than the catalytic ability of a sole acridinylidene palladium(II) complex.^[37] Thus, we decided to explore the cyclic aromatic carbene derivative bearing a remote amino groups (see the following section).^[38] After publishing our first report on the carbene, theoretical calculations based on our structural motif were performed by Schaefer III *et al.* and their study revealed that the bridged atom on the central ring played an important role for the tuning effect on the carbene singlet-triplet energy gap.^[39] Therefore, synthesis and characterization of isolable cyclic aromatic carbene derivatives have been paid much attention and are highly worth challenging.

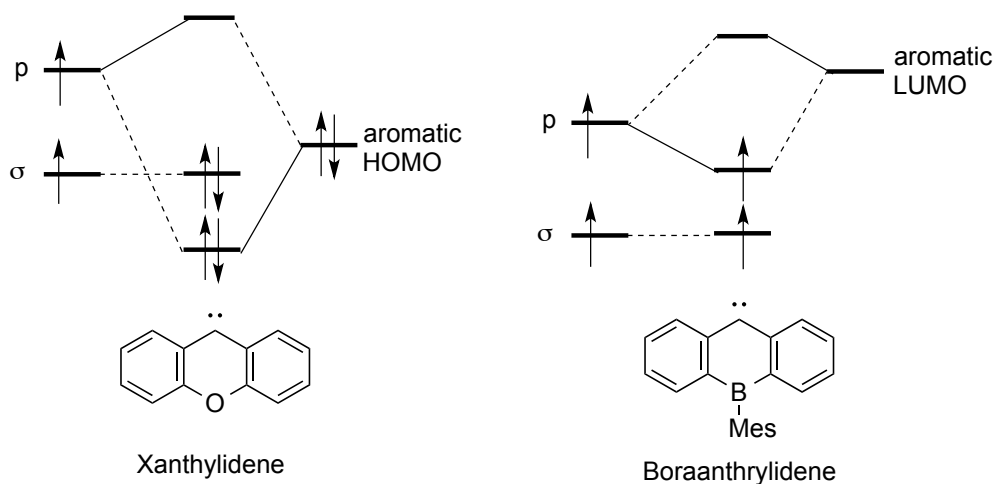


Figure 11. Orbital interactions for xanthylidene and boraanthrylidene.

1-10. Purpose of This Work 2

As described in the above chapters, cyclic aromatic carbenes have been less investigated so far and there was only a report on application of the carbene metal complexes to catalysts.^[37c] Thus, we envisioned that isolation of cyclic aromatic carbenes would be a milestone to make the ligand more versatile. In order to achieve this goal, we envisaged that introduction of electron-donating amino groups at the conjugated position of the carbene carbon atom could thermodynamically stabilize the free carbenes. In addition, further substitution of the aromatic rings would make them to be more fascinating ligands since the bulky substituents for kinetic stabilization or further donating groups as the bidentate or tridentate ligands would be introduced by means of coupling reactions. Provided that the carbenes would possess even higher HOMO and lower LUMO than CAACs, the electronic state of the carbene should be completely different from that of the conventional stable carbenes. Therefore, we decided to focus on preparing the newly designed cyclic aromatic carbene derivatives and proposing their application to the metal complexes and other unusual molecules as the ligands.

In this thesis, synthesis, characterization, and application of newly designed cyclic aromatic carbenes bearing remote amino groups are discussed. At first, our calculations to seek the reasonable ligands and synthesis of the xanthyldene derivative bearing remote amino groups at the 3,6-positions are described in Chapter 6.^[38a] As shown in Chapter 7, the further substitution of the xanthyldene derivatives at the 1,8-positions by two phenyl groups were achieved and the sterically bulky phenyl groups provided isolation of the low-coordinated palladium(II) complex as well as photophysical studies of the xanthyldene derivatives via laser flash photolysis.^[38b] In Chapter 8, we discuss synthesis of the carbene-stabilized C4 cumulenes with the xanthyldene ligand. Finally, attempted synthesis of pincer-type ligands based on the xanthyldene derivatives is stated in Chapter 9.

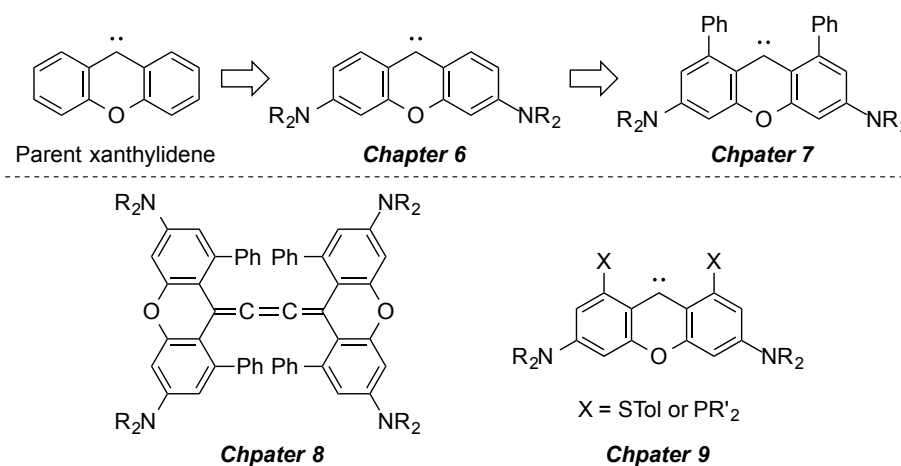


Figure 12. Our designed cyclic aromatic carbene bearing remote amino groups and potential applications of the ligands.

References

- [1]. M. S. Singh, *Reactive Intermediates in Organic Chemistry: Structure, Mechanism, and Reactions*, Wiley-VCH, Weinheim, **2014**, p1-273.
- [2]. Reviews: a) W. A. Herrmann, C. Köcher, *Angew. Chem. Int. Ed. Engl.* **1997**, *36*, 2162-2187; b) M. Melaimi, M. Soleilhavoup, G. Bertrand, *Angew. Chem. Int. Ed.* **2010**, *49*, 8810-8849; c) R. C. Fischer, P. P. Power, *Chem. Rev.* **2010**, *110*, 3877-3923; d) A. Osuka, E. Tsurumaki, T. Tanaka, *Bull. Chem. Soc. Jpn.* **2011**, *84*, 679-697; e) S. Saito, A. Osuka, *Angew. Chem. Int. Ed.* **2011**, *50*, 4342-4373; f) M. Asay, A. Sekiguchi, *Bull. Chem. Soc. Jpn.* **2012**, *85*, 1245-1261; g) H. Braunschweig, R. D. Dewhurst, *Angew. Chem. Int. Ed.* **2013**, *52*, 3547-3583; h) M. Abe, *Chem. Rev.* **2013**, *113*, 7011-7088; i) Y. Wang, G. H. Robinson, *Inorg. Chem.* **2014**, *53*, 11815-11832.
- [3]. a) *The Porphyrin Handbook* (Eds.: K. M. Kadish, K. M. Smith, R. Guilard), Academic Press, San Diego, 2000; b) *Handbook of Porphyrin Science* (Eds.: K. M. Kadish, K. M. Smith, R. Guilard), World Scientific Publishing, Singapore, **2010**.
- [4]. a) S. Konishi, M. Hoshino, M. Imamura, *J. Am. Chem. Soc.* **1982**, *104*, 2057-2059; b) H. Song, R. D. Orosz, C. A. Reed, W. R. Scheidt, *Inorg. Chem.* **1990**, *29*, 4274-4282; c) G. S. Nahor, P. Neta, P. Hambright, L. R. Robinson, *J. Phys. Chem.* **1991**, *95*, 4415-4418; d) T. R. Holman, M. P. Hendrich, L. Que, Jr., *Inorg. Chem.* **1992**, *31*, 939-941; e) Y. Tokita, K. Yamaguchi, Y. Watanabe, I. Morishima, *Inorg. Chem.* **1993**, *32*, 329-333; f) W. R. Scheidt, *J. Bio. Inorg. Chem.* **2001**, *6*, 727-732; g) K. M. Kadish, M. Lin, E. V. Caemelbecke, G. D. Stefano, C. J. Medforth, D. J. Nurco, N. Y. Nelson, B. Krattinger, C. M. Muzzi, L. Jaquinod, Y. Xu, D. C. Shyr, K. M. Smith, J. A. Shelnutt, *Inorg. Chem.* **2002**, *41*, 6673-6687.
- [5]. Z. Chen, C. S. Wannere, C. Corminboeuf, R. Puchta, P. v. R. Schleyer, *Chem. Rev.* **2005**, *105*, 3842-3888.
- [6]. P. v. R. Schleyer, F. Puhlhofer, *Org. Lett.* **2002**, *4*, 2873.
- [7]. M. Stępień, B. Szyszko, L. Latos-Grażyński, *J. Am. Chem. Soc.* **2010**, *132*, 3140-3152.
- [8]. P. v. R. Schleyer, C. Maerker, A. Dransfeld, H. Jiao, N. J. R. v. E. Hommes, *J. Am. Chem. Soc.* **1996**, *118*, 6317-6318.
- [9]. a) E. Vogel, I. Grigat, M. Köcher, J. Lex, *Angew. Chem.* **1989**, *101*, 1687-1689; *Angew. Chem. Int. Ed. Engl.* **1989**, *28*, 1655-1657; b) J. Setsune, K. Kashiwara, K. Wada, H. Shiozaki, *Chem. Lett.* **1999**, 847-848; c) J. A. Cissell, T. P. Vaid, A. L. Rheingold, *J. Am. Chem. Soc.* **2005**, *127*, 12212-12213; d) A. Weiss, M. C. Hodgson, P. D. W. Boyd, W. Siebert, P. J. Brothers, *Chem. Eur. J.* **2007**, *13*, 5982-5993; e) H.-e. Song, J. A. Cissell, T. P. Vaid, D. J. Holten, *J. Phys. Chem. B* **2007**, *111*, 2138-2142; f) C. Liu, D.-M. Shen, Q.-Y. Chen, *J. Am. Chem. Soc.* **2007**, *129*, 5814-5815; g) X.-G. Chen, C. Liu, D.-M. Shen, Q.-Y. Chen, *Synthesis* **2009**, 3860-3868; h) T. P. Vaid, *J. Am. Chem. Soc.* **2011**, *133*, 15838-15841.
- [10]. a) S. Mori, A. Osuka, *J. Am. Chem. Soc.* **2005**, *127*, 8030-8031; b) M. Suzuki, A. Osuka, *J. Am.*

- Chem. Soc.* **2007**, *129*, 464-465; c) S. Mori, K. S. Kim, Z. S. Yoon, S. B. Noh, D. Kim, A. Osuka, *J. Am. Chem. Soc.* **2007**, *129*, 11344-11345; d) A. Muranaka, O. Matsushita, K. Yoshida, S. Mori, M. Suzuki, T. Furuyama, M. Uchiyama, A. Osuka, N. Kobayashi, *Chem. Eur. J.* **2009**, *15*, 3744-3751; e) M. -C. Yoon, S. Cho, M. Suzuki, A. Osuka, D. Kim, *J. Am. Chem. Soc.* **2009**, *131*, 7360-7367; f) H. Mori, Y. M. Sung, B. S. Lee, D. Kim, A. Osuka, *Angew. Chem. Int. Ed.* **2012**, *51*, 12459-12463; g) K. Naoda, H. Mori, A. Osuka, *Chem. Asian. J.* **2013**, *8*, 1395-1398; h) T. Yoneda, Y. M. Sung, J. M. Lim, D. Kim, A. Osuka, *Angew. Chem. Int. Ed.* **2014**, *126*, 13385-13389.
- [11]. Z. S. Yoon, A. Osuka, D. Kim, *Nat. Chem.* **2009**, *1*, 113-122.
- [12]. a) Y. - Yamamoto, A. - Yamamoto, S. Furuta, M. Horie, M. Kodama, W. Sato, K.-y. Akiba, S. Tsuzuki, T. Uchimar, D. Hashizume, F. Iwasaki, *J. Am. Chem. Soc.* **2005**, *127*, 14540-14541; b) Y. Yamamoto, Y. Hirata, M. Kodama, T. Yamaguchi, S. Matsukawa, K.-y. Akiba, D. Hashizume, F. Iwasaki, A. Muranaka, M. Uchiyama, P. Chen, K. M. Kadish, N. Kobayashi, *J. Am. Chem. Soc.* **2010**, *132*, 12627-12638; c) T. Kakui, S. Sugawara, Y. Hirata, S. Kojima, Y. Yamamoto, *Chem. Eur. J.* **2011**, *17*(29), 8005-8008; d) S. Sugawara, M. Kodama, Y. Hirata, S. Kojima, Y. Yamamoto, *J. Porphyrins. Phthalocyanines.* **2011**, *15*, 1326-1334; e) S. Sugawara, Y. Hirata, S. Kojima, Y. Yamamoto, E. Miyazaki, K. Takimiya, S. Matsukawa, D. Hashizume, J. Mack, N. Kobayashi, Z. Fu, K. M. Kadish, Y. M. Sung, K. S. Kim, D. Kim, *Chem. Eur. J.* **2012**, *18*(12), 3565-3581; f) S. Hiramatsu, S. Sugawara, S. Kojima, Y. Yamamoto, *J. Porphyrins. Phthalocyanines.* **2013**, *17*(12), 1183-1187.
- [13]. J. A. Cissell, T. P. Vaid, G. P. A. Yap, *Org. Lett.* **2006**, *8*, 2401-2404.
- [14]. Norcorrole is a porphyrin derivative which lacks two meso carbon atoms from a regular porphyrin: a) T. Ito, Y. Hayashi, S. Shimizu, J. -Y. Shin, N. Kobayashi, H. Shinokubo, *Angew. Chem. Int. Ed.* **2012**, *51*, 8542-8545; b) T. Fukuoka, K. Uchida, Y. M. Song, J. -Y. Shin, S. Ishida, J. M. Lim, S. Hiroto, K. Furukawa, D. Kim, T. Iwamoto, H. Shinokubo, *Angew. Chem. Int. Ed.* **2014**, *53*, 1506-1509; c) J. -Y. Shin, T. Yamada, H. Yoshikawa, K. Awaga, H. Shinokubo, *Angew. Chem. Int. Ed.* **2014**, *53*, 3096-3101; d) T. Yoneda, Y. M. Sung, J. M. Lim, D. Kim, A. Osuka, *Angew. Chem. Int. Ed.* **2014**, *126*, 13385-13389.
- [15]. a) Y. Yamamoto, R. Nadano, M. Itagaki, K.-y. Akiba, *J. Am. Chem. Soc.* **1995**, *117*, 8287-8288; b) A. Yamamoto, W. Satoh, Y. Yamamoto, K.-y. Akiba, *Chem. Commun.* **1999**, 147-148; c) Y. Yamamoto, K.-y. Akiba, *J. Organomet. Chem.* **2000**, *611*, 200-209; d) K.-y. Akiba, R. Nadano, W. Satoh, Y. Yamamoto, S. Nagase, Z. Ou, X. Tan, K. M. Kadish, *Inorg. Chem.* **2001**, *40*, 5553-5567.
- [16]. a) J. Hine, *J. Am. Chem. Soc.* **1950**, *72*, 2438-2445; b) W. v. E. Doering, A. K. Hoffmann, *J. Am. Chem. Soc.* **1954**, *76*, 6162-6165.
- [17]. E. O. Fischer, A. Maasböl, *Angew. Chem. Int. Ed. Engl.* **1964**, *3*, 580-581.
- [18]. K. Öfele, *J. Organometat. Chem.* **1968**, *12*, P42-P43.
- [19]. a) H. -W. Wanzlick, H. -J. Schönherr, *Angew. Chem. Int. Ed. Engl.* **1968**, *7*, 141-142; b) H.-J.

- Schönherr, H.-W. Wanzlick, *Justus Liebigs Ann. Chem.* **1970**, 731, 176-179.
- [20]. a) A. Igau, H. Grutzmacher, A. Baceiredo, G. Bertrand, *J. Am. Chem. Soc.* **1988**, 110, 6463-6466; b) A. J. Arduengo, III, R. L. Harlow, M. Kline, *J. Am. Chem. Soc.* **1991**, 113, 361-363.
- [21]. Reviews: a) W. A. Herrmann, C. Köcher, *Angew. Chem. Int. Ed. Engl.* **1997**, 36, 2162-2187; b) D. Bourissou, O. Guerret, F. P. Gabbaï, G. Bertrand, *Chem. Rev.* **2000**, 100, 39-91; c) F. E. Hahn, M. C. Jahnke, *Angew. Chem. Int. Ed.* **2008**, 47, 3122-3172; d) T. Dröge, F. Glorius, *Angew. Chem. Int. Ed.* **2010**, 49, 6940-6952; e) M. Melaimi, M. Soleilhavoup, G. Bertrand, *Angew. Chem. Int. Ed.* **2010**, 49, 8810-8849; f) D. Martin, M. Melaimi, M. Soleilhavop, G. Bertrand, *Organometallics* **2011**, 30, 5304-5313; g) H. Braunschweig, R. D. Dewhurst, *Organometallics* **2014**, 33, 6271-6277.
- [22]. a) J. F. Harrison, *J. Am. Chem. Soc.* **1971**, 93, 4112-4119; b) C. W. Bauschlicher, Jr., H. F. Schaefer III, P. S. Bagus, *J. Am. Chem. Soc.* **1977**, 99, 7106-7110; c) J. F. Harrison, R. C. Liedtke, J. F. Liebman, *J. Am. Chem. Soc.* **1979**, 101, 7162-7168; d) D. Feller, W. T. Borden, E. R. Davidson, *Chem. Phys. Lett.* **1980**, 71, 22-26.
- [23]. a) R. Hoffmann, G. D. Zeiss, G. W. Van Dine, *J. Am. Chem. Soc.* **1968**, 90, 1485-1499; b) N. C. Baird, K. F. Taylor, *J. Am. Chem. Soc.* **1978**, 100, 1333-1338.
- [24]. I. Fleming, *Frontier Orbitals and Organic Chemical Reactions*, Wiley, New York, **1976**.
- [25]. A. J. Arduengo, III, H. V. R. Dias, R. L. Harlow, M. Kline, *J. Am. Chem. Soc.* **1992**, 114, 5530-5534.
- [26]. C. Valente, S. Çalimsiz, K. H. Hoi, D. Mallik, M. Sayah, M. G. Organ, *Angew. Chem. Int. Ed.* **2012**, 51, 3314-3332.
- [27]. M. Scholl, S. Ding, C. W. Lee, R. H. Grubbs, *Org. Lett.* **1999**, 1, 953-956.
- [28]. Y. Wang, B. Quillian, P. Wei, C. S. Wanne, Y. Xie, R. B. King, H. F. Schaefer III, P. v. R. Schleyer, G. H. Robinson, *J. Am. Chem. Soc.* **2007**, 129, 12412-12413.
- [29]. a) C. Buron, H. Gornitzka, V. Romanenko, G. Bertrand, *Science* **2000**, 288, 834-836; b) S. Sole, H. Gornitzka, W. W. Schoeller, D. Bourissou, G. Bertrand, *Science* **2001**, 292, 1901-1903; c) E. Despagne, H. Gornitzka, A. B. Rozhenko, W. W. Schoeller, D. Bourissou, G. Bertrand, *Angew. Chem. Int. Ed.* **2002**, 41, 2835-2837; d) E. Despagne-Ayoub, S. Sole, H. Gornitzka, A. B. Rozhenko, W. W. Schoeller, D. Bourissou, G. Bertrand, *J. Am. Chem. Soc.* **2003**, 125, 124-130; e) V. Lavallo, J. Mafhouz, Y. Canac, B. Donnadieu, W. W. Schoeller, G. Bertrand, *J. Am. Chem. Soc.* **2004**, 126, 8670-8671.
- [30]. a) V. Lavallo, Y. Canac, C. Präsang, B. Donnadieu, G. Bertrand, *Angew. Chem. Int. Ed.* **2005**, 44, 5705-5709; b) R. Jazzar, R. D. Dewhurst, J.-B. Bourg, B. Donnadieu, Y. Canac, G. Bertrand, *Angew. Chem. Int. Ed.* **2007**, 46, 2899-2902.
- [31]. a) D. Martin, N. Lassauque, B. Donnadieu, G. Bertrand, *Angew. Chem. Int. Ed.* **2012**, 51, 6172-6175; b) D. Martin, C. E. Moore, A. L. Rheingold, G. Bertrand, *Angew. Chem. Int. Ed.* **2013**, 52, 7104-7017; c) D. Martin, N. Lassauque, F. Steinmann, G. Mannuel, G. Bertrand, *Chem, Eur. J.*

- 2013**, *19*, 14895-14901.
- [32]. Selected papers for *N,N'*-diamidocarbenes: a) T. W. Hudnall, C. W. Bielawski, *J. Am. Chem. Soc.* **2009**, *131*, 16039-16041; b) T. W. Hudnall, J. P. Moerdyk, C. W. Bielawski, *Chem. Commun.* **2010**, *46*, 4288-4290; c) J. P. Moerdyk, C. W. Bielawski, *Nat. Chem.* **2012**, *4*, 275-280; d) J. P. Moerdyk, C. W. Bielawski, *J. Am. Chem. Soc.* **2012**, *134*, 6116-6119; e) J. P. Moerdyk, G. A. Blake, D. T. Chase, C. W. Bielawski, *J. Am. Chem. Soc.* **2013**, *135*, 18798-18801; f) J. P. Moerdyk, C. W. Bielawski, *Chem. Eur. J.* **2013**, *19*, 14773-14776.
- [33]. a) V. Lavallo, C. A. Dyker, B. Donnadiou, G. Bertrand, *Angew. Chem. Int. Ed.* **2008**, *47*, 5411-5414; b) I. Fernández, C. A. Dyker, A. DeHope, B. Donnadiou, G. Frenking, G. Bertrand, *J. Am. Chem. Soc.* **2009**, *131*, 11875-11811; c) E. Aldeco-Perez, A. J. Rosenthal, B. Donnadiou, P. Parameswaran, G. Frenking, G. Bertrand, *Science* **2009**, *326*, 556-559; d) D. Mendoza-Espinosa, B. Donnadiou, G. Bertrand, *J. Am. Chem. Soc.* **2010**, *132*, 7264-7265; e) G. Guisado-Barrios, J. Bouffard, B. Donnadiou, G. Bertrand, *Angew. Chem. Int. Ed.* **2010**, *49*, 4759-4762; f) G. Ung, G. Bertrand, *Chem. Eur. J.* **2011**, *17*, 8269-8272.
- [34]. B. K. Keitz, J. Bouffard, G. Bertrand, R. H. Grubbs, *J. Am. Chem. Soc.* **2011**, *133*, 8498-8501.
- [35]. a) Y. Han, V. Huynh, G. K. Tan, *Organometallics* **2007**, *26*, 6581-6585; b) H. G. Raubenheimer, S. Cronje, *Dalton Trans.* **2008**, 1265-1272; c) A. A. Turov, A. T. Normand, M. S. Nechaev, *Dalton Trans.* **2009**, 7015-7028; d) O. Schuster, L. Yang, H. G. Raubenheimer, M. Albrecht, *Chem. Rev.* **2009**, *109*, 3455-3478; e) M. Iglesias, M. Albrecht, *Dalton Trans.* **2010**, *39*, 5213-5215; f) G. Ung, J. Rittle, M. Soleilhavoup, G. Bertrand, J. C. Peters, *Angew. Chem. Int. Ed.* **2014**, *53*, 8427-8431.
- [36]. a) S. C. Lapin, B. E. Brauer, G. B. Schuster, *J. Am. Chem. Soc.* **1984**, *106*, 2092-2100; b) S. C. Lapin, G. B. Schuster, *J. Am. Chem. Soc.* **1985**, *107*, 4243-4248.
- [37]. a) K. H. Dötz, J. Pfeiffer, *Chem. Commun.* **1996**, 895; b) J. Pfeiffer, K. H. Dötz, *Organometallics* **1998**, *17*, 4353-4361; c) S. K. Schneider, P. Roembke, G. R. Julius, H. G. Raubenheimer, W. A. Herrmann, *Adv. Synth. Catal.* **2006**, *348*, 1862-1873.
- [38]. a) S. Sugawara, S. Kojima, Y. Yamamoto, *Chem. Commun.* **2012**, *48*, 9735-9737; b) S. Sugawara, M. Abe, Y. Fujiwara, M. Wakioka, F. Ozawa, Y. Yamamoto, *Eur. J. Inorg. Chem.* **2015**, 534-541.
- [39]. Y. Zeng, J. Feng, Y. Xie, H. F. Schaefer III, *J. Org. Chem.* **2014**, *79*, 2926-2933.

Chapter 2

Synthesis and Characterization of the Most Distorted 16π Porphyrin: Octaisopropyltetraphenylporphyrin (OiPTPP)

2-1. Introduction

According to the previous work on 16π porphyrins by us and Vaid *et al.*, two methods for stabilizing 16π porphyrins have been established: (i) deformation of the conjugated core^[1a] and (ii) metallation^[2]. Specifically, as for (i), the isolation of metal-free 16π octaalkyltetraphenylporphyrins were made possible by stabilization brought about by deformation of the conjugated core induced by steric hindrance between the peripheral substituents.^[1a] In addition, it was found that the more hindered octaisobutyltetraphenylporphyrin (OiBTTP), having iso-butyl groups at the β position of the porphyrin core, is more stable than octaethyltetraphenylporphyrin (OETTP) having ethyl groups instead, according to evaluations by the time course of decomposition monitored by UV-vis spectroscopy. As for (ii), Vaid's group revealed that the introduction of a central metal is also effective for stabilizing 16π porphyrin metal complexes during their study of tetraphenylporphyrin lithium(I) complex $[(\text{TPP})\text{Li}^+][\text{BF}_4]^-$.^[2] Concerning the first stabilizing effect among the three, we envisioned that a 16π porphyrin more sterically hindered than OiBTTP should be more stable. Therefore, we designed novel octaisopropyltetraphenylporphyrin (OiPTTP), having isopropyl substituents at the β -positions in the place of the isobutyl groups in OiBTTP, since the isopropyl substituents were expected to induce more steric hindrance between the β -substituents and the meso-phenyl groups (Figure 1). Highly distorted 16π porphyrins would also be interesting in light of the fact that core distortions in 18π porphyrins are known to be strongly related with reactivity in biological systems.^[3] In this chapter, we report on the synthesis and structural characterization of novel metal-free 16π OiPTTP and related 18π metal complexes.

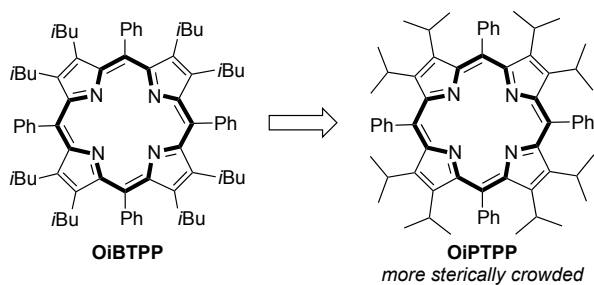
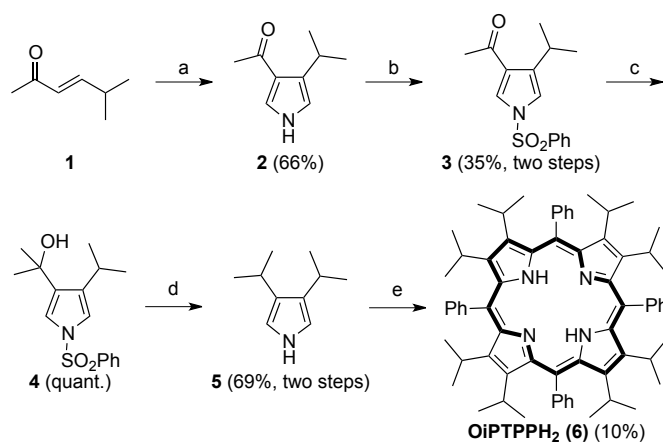


Figure 1. Working hypothesis for stabilizing the 16π porphyrin by increasing steric repulsion between the substituents.

2-2. Synthesis and Characterization

While octaisopropylporphyrin (OEPH₂) which has no substituents at the meso-positions was synthesized by Gross et al. about three decades ago,^[4] there have been no reports on the synthesis of octaisopropyltetraphenylporphyrin (OiPTPPH₂, **6**), which in principle could be prepared in a similar manner. However, since the reported method contained a process requiring special instrumentation, we sought a different synthetic route toward **6** starting from commercially available 5-methyl-3-hexen-2-one (**1**) as described in Scheme 1. In the proposed route, we chose the widely recognized Lindsey method^[5] to obtain **6** from 3,4-diisopropylpyrrole (**5**), which has not been isolated before. This is probably due to its supposed unstable nature that could make it difficult to purify.

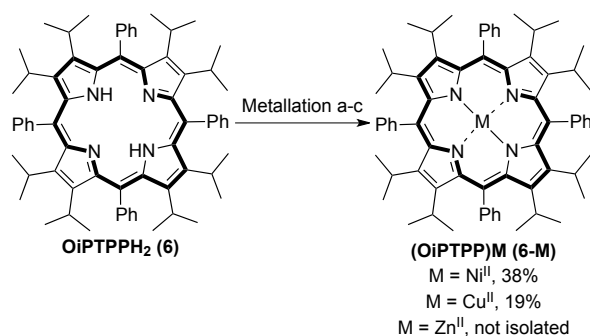


Scheme 1. The synthetic route for 18 π octaisopropyltetraphenylporphyrin (OiPTPPH₂, **6**). (a) TosCH₂NC, NaH, ether/DMSO; (b) (i) KOH, EtOH, (ii) ClSO₂Ph, acetone; (c) CH₃MgBr, ether; (d) (i) NaOH, MeOH, (ii) LiAlH₄, THF; (e) (i) PhC(O)H, BF₃•Et₂O, CH₂Cl₂, (ii) DDQ, toluene.

Treatment of **1** with *p*-tolylsulfonylmethyl isocyanide and sodium hydride gave 3-acetyl-4-isopropylpyrrole (**2**) in 66% yield. In order to introduce a methyl group into the acetyl moiety of **2** without side reactions, it was anticipated that the nitrogen atom of pyrrole should be protected. Thus, the hydrogen atom on the nitrogen atom was substituted with a benzenesulfonyl group by the reaction of **2** with base followed by benzenesulfonyl chloride to give **3** in 35% yield from **2**. After protection, the methylated species **4** was formed, quantitatively, by the reaction of **3** with 3.0 eq. of MeMgBr in dry ether. The product **4** gradually underwent dehydration even in the presence of trace amounts of acid (even in CDCl₃) to give a byproduct with a 2-propenyl substituent. Reduction of **4** using LiAlH₄ after removal of the protecting group by treatment with sodium hydroxide gave the desired 3,4-diisopropylpyrrole (**5**) in ca. 69% yield over two steps.^[6] It was essential to carry out deprotection prior to reduction, since reduction of **4** was sluggish. Product **5** contained a small amount of impurities that could not be removed even after vacuum-distillation and recrystallization. Thus, the successive condensation reaction under Lindsey

conditions was carried out with crude **5**, to afford 18π OiTPPPH₂ (**6**) in ca. 10% yield as a product that could not be fully purified.

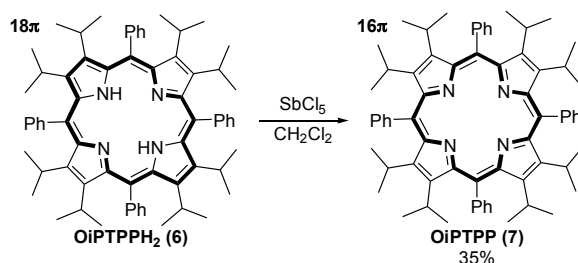
In order to assess the features of our new sterically hindered porphyrin, we turned our attention to metal-complexes. We also envisaged that purification of the free-base 18π porphyrin might be possible via a metallation-chromatographic separation-demetallation process. Since purification of metal-free 16π porphyrin **7** was expected to be difficult due to its anticipated unstable nature, purification of the precursor free-base 18π species seemed to be crucial. Thus, crude free-base **6** was treated with nickel(II) acetate, copper(II) acetate and zinc(II) acetate to give their respective metal complexes (**6-M**; M = Ni^{II}, Cu^{II}, Zn^{II}) as chromatographically purifiable species, as shown in Scheme 2. Complex **6-Ni** had enough stability to enable us to carry out manipulations in the open air. However, complexes **6-Zn** and **6-Cu** underwent gradual demetallation in the open air to give the corresponding free-base **6**. Particularly, **6-Zn** had a greater tendency to undergo demetallation than **6-Cu**. Furthermore, free-base **6** resulting from **6-Zn** was highly pure as evaluated by ¹H NMR spectroscopy. Therefore, **6-Zn** was purposely treated with acid to furnish pure **6**, and this was used for the subsequent oxidation reaction (vide infra). The UV-vis spectrum of pure **6** showed absorptions at 483 and 707 nm as Soret and Q bands, respectively. In comparison with the Soret bands of OETPPH₂ and OiBTTPPH₂ (446 and 462 nm, respectively), that of **6** is highly red-shifted, indicating that OiTPPPH₂ is more distorted out of conjugation than OETPPH₂ and OiBTTPPH₂. All attempts to crystallize **6** for X-ray diffraction analysis were to no avail and thus a direct structural comparison could not be conducted.



Scheme 2. Metallation of 18π OiTPPPH₂ (**6**). (a) M = Ni^{II}, Ni^{II}(OAc)₂ • 4H₂O, DMF, (b) M = Cu^{II}, Cu^{II}(OAc)₂ • H₂O, THF, (c) M = Zn^{II}, Zn^{II}(OAc)₂, THF.

In our previous study of OiBTTPPH₂, it was found that the reaction using SbCl₅ as the oxidizing agent proceeded cleanly to give the corresponding 16π porphyrin with high reproducibility.^[1b] In accordance, 18π OiTPPPH₂ (**6**) was treated with SbCl₅ and the corresponding 16π OiTPPP (**7**) was obtained as a brown solid in moderate yield (Scheme 3). Single crystals of **7** could be obtained by recrystallization using off-the-shelf hexane/CH₂Cl₂ and the structure was unambiguously confirmed by the X-ray analysis as shown in Figure 2. The crystal lattice of **7** was found to contain two molecules of H₂O per porphyrin molecule. The metal-free 16π porphyrin **7** is stable in the solid state and in CH₂Cl₂ in the

absence of water, but the species rapidly degraded to an unidentified 18π species in protic solvents such as methanol. To compare the stability between 16π OiTPP and OiBTPP, the time courses of decomposition were monitored by UV-vis spectroscopy using highly pure CH_2Cl_2 with 1 drop of methanol. Although this evaluation is qualitative, it was found that the decomposition of **7** was undoubtedly slower than that of 16π OiBTPP, in accordance with our expectations. The UV-vis spectrum of **7** showed Soret-like bands at 280 and 330 nm, which are highly blue-shifted relative to corresponding absorptions of free-base 18π porphyrin **6** (Figure 3). Interestingly, the maximum absorbances of the Soret-like band are slightly blue-shifted in comparison with those of 16π OETPP (339 nm) and OiBTPP (331 nm).



Scheme 3. Oxidation reaction of 18π OiTPPPH₂ (**6**) with SbCl_5 .

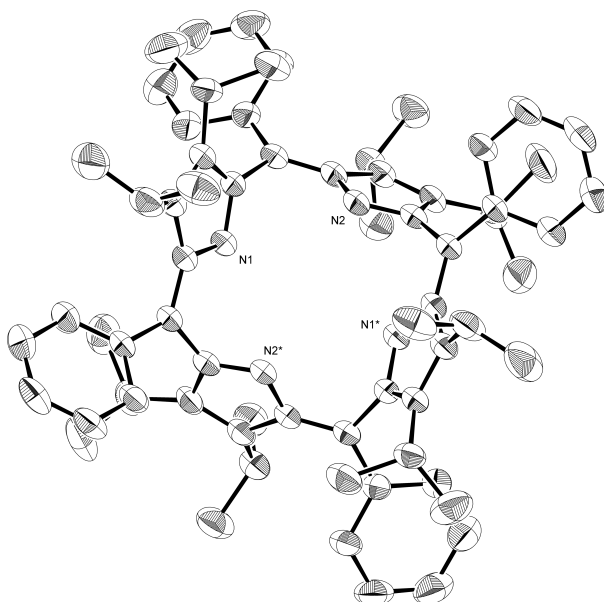


Figure 2. The ORTEP drawing of 16π OiTPPP (**7**) with the thermal ellipsoids shown at the 50% probability level. Two molecules of water are included per complex in the crystals. All hydrogen atoms and the water molecules are omitted for clarity.

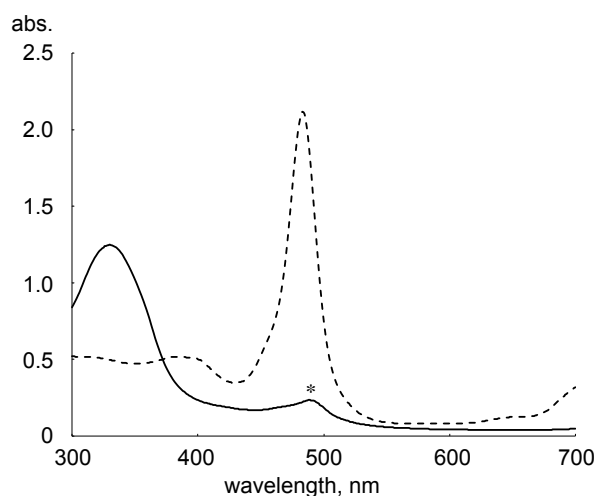
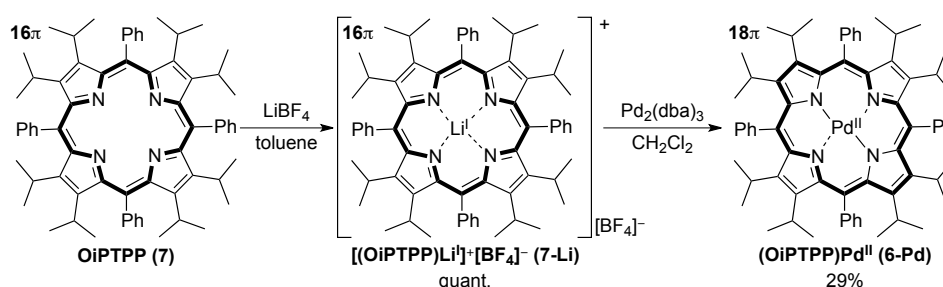


Figure 3. The UV-vis spectra of 18 π OiTPPPH₂ (**6**; broken line) and 16 π OiTPPP (**7**; solid line) in CH₂Cl₂. The asterisk * corresponds to the absorbance of a decomposition product.

Next, in order to investigate the reactivity of **7**, reaction with a zero-valent metal reagent was examined. As in the study of 16 π OiBTTP, ^[1b] the reaction of **7** with LiBF₄ afforded the 16 π OiTPPP lithium(I) complex (**7-Li**) as an intermediate which could not be isolated and then treatment of **7-Li** with Pd₂(dba)₃ (dba = dibenzylideneacetone) gave the 18 π OiTPPP palladium(II) complex (**6-Pd**) in 29% yield (Scheme 4). It was necessary to convert metal-free **7** to its lithium complex for this reaction to proceed. Therefore, it can be assumed that **7-Li** was first reduced by zero-valent Pd to furnish 18 π **6-Li** as an intermediate which subsequently underwent metal exchange, as in the case of the 16 π OiBTTP lithium(I) complex. ^[1b] The structure of **6-Pd** was determined by the X-ray structural analysis (Figure 4). The crystal lattice of **6-Pd** was found to contain a molecule of H₂O per complex.



Scheme 4. Reaction of 16 π OiTPPP with LiBF₄ followed by Pd₂(dba)₃.

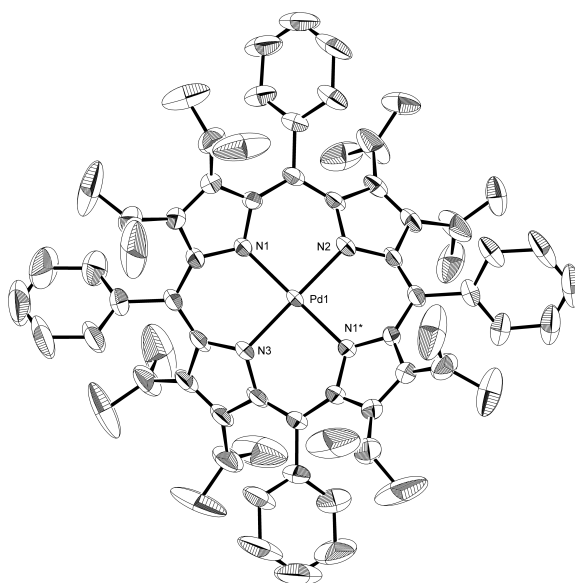


Figure 4. The ORTEP drawing of 18π (OiPTPP) Pd^{II} (**6-Pd**) with the thermal ellipsoids shown at the 50% probability level. Two molecules of water are included per complex in the crystals. All hydrogen atoms and the water molecules are omitted for clarity.

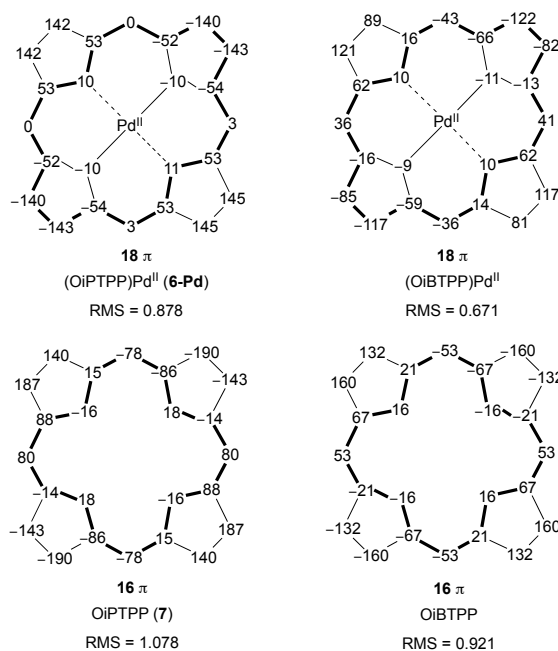
2-3. Comparison of Distortion with OiBTPP analogs

As Table 1 shows, although structural comparison with free-base 18π OiTPPH₂ cannot be made, it is unambiguous that there are bond alternations in the porphyrin core of metal-free 16π OiPTPP (**7**), as previously reported for 16π OETPP and OiBTPP. This character is unique to nonaromatic and anti-aromatic porphyrins. The deviation of each atom from the mean plane defined by the 24 core atoms for **6-Pd** and **7** is shown as numerals (in units of picometers) in Figure 5 and the root-mean-square values of these deviations (RMS value), which are indicators of the degree of overall distortion of the porphyrin core, are given in Table 1. As the data show, the RMS value of **6-Pd** is 0.878. Since the corresponding Pd complex has been structurally identified in the previously most sterically hindered OiBTPP series, a comparison was carried out between **6-Pd** and the OiBTPP palladium(II) complex. The RMS value of **6-Pd** is larger by +0.207, suggesting that overall, the OiPTPP skeleton is more distorted than the OiBTPP framework. As for shape, while the OiBTPP palladium(II) complex is twisted in pseudo- C_2 style away from pseudo- C_{2v} symmetry, **6-Pd** has nearly perfect C_{2v} symmetry, with large deviations in the β -positions of the pyrrole rings. This can be considered to be a consequence of the increased steric hindrance between neighboring peripheral substituents. The RMS value of metal-free 16π porphyrin **7** is 1.078 which is larger than those of metal-free 16π OETPP and OiBTPP (0.836 and 0.921, respectively), indicating that **7** is the most distorted 16π porphyrin to date. The values of distortion compared between OiPTPP (**7**) and OiBTPP show that the shapes are practically the same with pseudo- C_2 symmetry but with larger deviations for the former.

Table 1. Structural parameters of the porphyrin cores.

compound	no. of π electrons	difference of average bond distances (Å)		RMS ^[c]	
		$\Delta(\text{N}-\text{C}_\alpha)^{[a]}$	$\Delta(\text{C}_m-\text{C}_\alpha)^{[b]}$		
(OiPTPP)Pd ^{II} ^[d]	18	0.000(5)	0.000(7)	0.878	
OiPTPP ^[d]	16	0.109(4)	0.125(4)	1.078	
(OiBTPP)Pd ^{II} ^[e]	18	0.003(5)	0.001(5)	0.671	
[(TPP)Li ^I] ⁺ [BF ₄] ⁻ ^[f]	16	0.092(3)	0.105(3)	0.381	
OETPP ^[e]	16	0.114(3)	0.118(4)	0.836	
OiBTPP ^[e]	16	0.114(3)	0.122(4)	0.921	

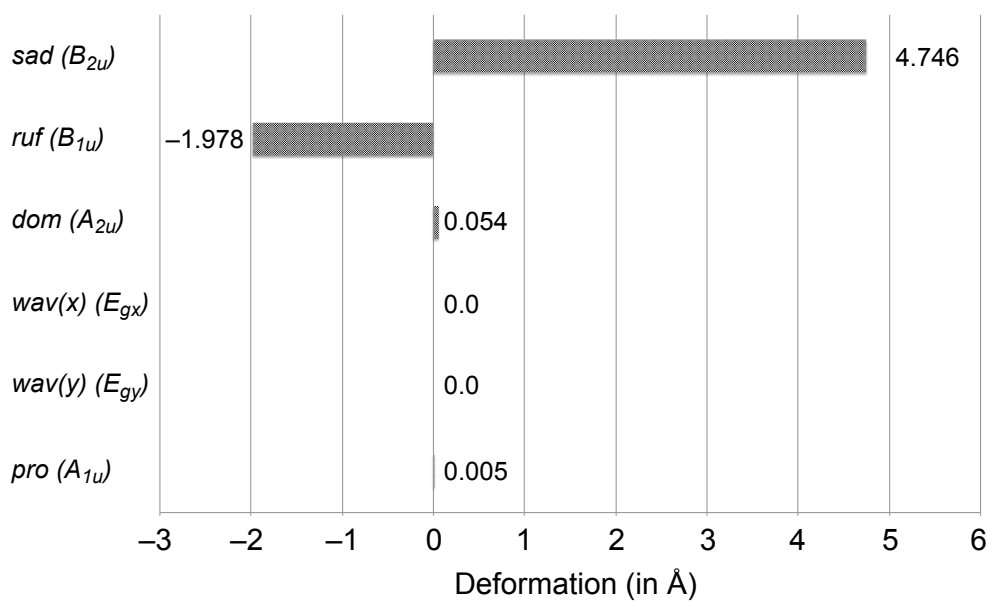
[a] Difference in the average bond distance between $\text{N}-\text{C}_{\alpha 1}$ and $\text{N}-\text{C}_{\alpha 2}$. [b] Difference in the average bond distance between $\text{C}_m-\text{C}_{\alpha 1}$ and $\text{C}_m-\text{C}_{\alpha 2}$. [c] The root-mean-square of the distance of each atom from the mean plane defined by the 24 core atoms. [d] This work. [e] Ref [1b]. [f] Ref [2].

**Figure 5.** The deviation of each atom from the mean plane defined by the 24 core atoms in units of picometers.

To evaluate the modes of distortion in more detail, the normal-coordinate structural decomposition (NSD) technique was applied on **6-Pd** and **7** using their X-ray crystal structures.^[7] This is a method that decomposes the total out-of-plane distortion into saddling (*sad*, B_{2u}), ruffling (*ruf*, B_{1u}), doming (*dom*, A_{2u}), waving [*wav*(x), *wav*(y); E_g], and propelling (*pro*, A_{1u}) based upon molecular vibrations. The calculated results are shown in Figure 6 and 7. As for 16π OiPTPP (**7**), the saddle (B_{2u}) and ruffle (B_{1u}) deformations were prominent compared with other modes (Figure 6). In contrast, the 18π (OiPTPP)Pd^{II} (**6-Pd**) shows saddle deformation with no contribution of the ruffle deformation (Figure 7). Although this is not a direct comparison between complexes with the same atom composition, these results indicate that the new 16π species has an additional mode of deformation in accordance with the previously examined OiBTTP system.

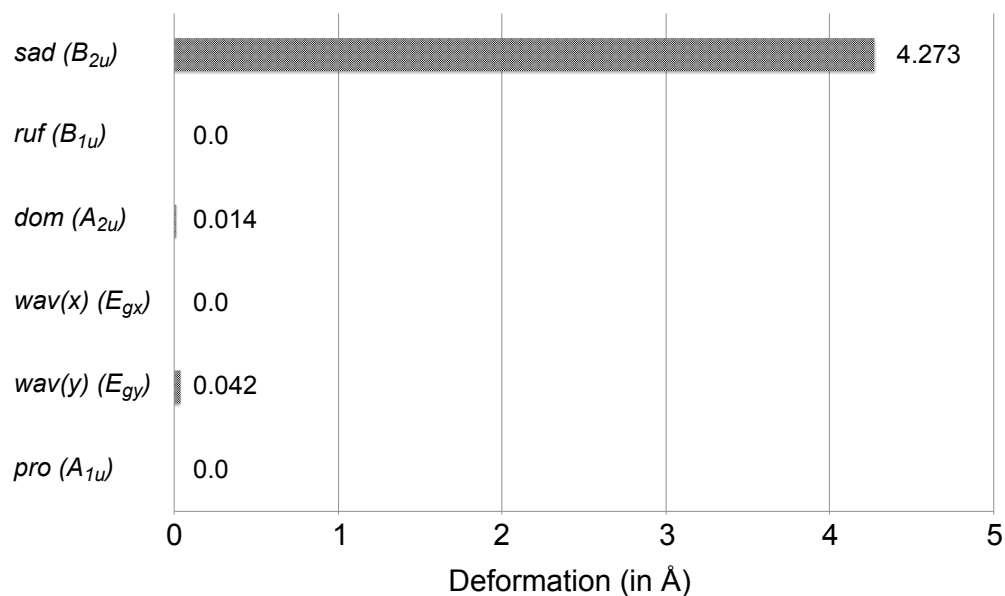
2-4. Conclusions and Outlook

On the basis of previous studies, we assumed that increasing the distortion of the porphyrin core would raise the stability of 16π porphyrins. In turn, we anticipated that this could be realized by increasing steric hindrance between peripheral substituents, namely, changing the isobutyl groups in 16π OiBTTP to isopropyl groups. Therefore, we decided to prepare it from its 18π precursor. Previously unreported 18π octaisopropyltetraphenylporphyrin (OiTPPH₂) was prepared from previously uncharacterized 3,4-diisopropylpyrrole. Metallation of OiTPPH₂ afforded new 18π OiPTTP metal complexes. Oxidation of the 18π porphyrin with SbCl₅ furnished the corresponding metal-free 16π octaisopropyltetraphenylporphyrin (OiPTPP). X-ray structural analysis revealed that this novel species is the most distorted known 16π porphyrin, in agreement with our working hypothesis. The reaction of 16π OiPTPP with LiBF₄ followed by Pd₂(dba)₃ afforded the corresponding 18π OiPTTP palladium(II) complex. X-ray analysis revealed that this complex was highly distorted compared with its 18π OiBTTP palladium(II) complex counterpart. Based upon the fact that the introduction of metals to the porphyrin core is more difficult compared with other well-known ordinary porphyrins, it seems that our highly hindered porphyrins lose flexibility, thus allowing the incorporation of only certain metals and in turn favoring the free-base form. Thus, it can be rationalized that the distortion effect coupled with the electron donating effect of the peripheral alkyl groups has made the formation of the metal-free 16π porphyrin highly favorable for the OiPTTP system.



basis	Dip	dip	B2g	B1g	Eu(x)	Eu(y)	A1g	A2g
min.	2.1124	0.3370	-0.0083	0.1702	-0.0007	-0.0001	-2.0386	-0.5264
ext.	2.3402	0.2844	-0.0084	0.1705	-0.0007	-0.0001	-2.0400	-0.5349
			-0.0268	0.0178	0.0002	0.0006	-0.4310	-0.9096
comp.	2.8104	0.0003	0.0327	0.1856	0.0011	0.0011	2.5959	1.060
basis	Doop	doop	B2u	B1u	A2u	Eg(x)	Eg(y)	A1u
min.	5.1417	0.1967	4.7456	-1.9782	0.0543	0.0000	-0.0000	0.0049
ext.	5.2771	0.0377	4.7231	-1.9782	0.0532	0.0000	-0.0000	0.0049
			-1.1674	-0.2202	-0.0264	0.0000	-0.0000	0.0041
comp.	5.2821	0.0000	4.8905	1.9949	0.0606	0.0000	0.0000	0.0064

Figure 6. Out-of-plane displacements (minimal basis) and full normal-coordinate structural decomposition (NSD) values for OiPTPP (7) calculated using the X-ray crystal structure.



basis	Dip	dip	B2g	B1g	Eu(x)	Eu(y)	A1g	A2g
min.	1.0767	0.1564	0.0002	0.0454	0.0002	0.0248	-1.0754	0.0001
ext.	1.1665	0.1259	0.0002	0.0455	0.0002	0.0247	-1.0768	0.0001
			-0.0004	0.0080	0.0004	-0.0101	-0.4487	-0.0003
comp.	1.3461	0.0000	0.0006	0.0506	0.0008	0.0470	1.3444	0.0005
basis	Doop	doop	B2u	B1u	A2u	Eg(x)	Eg(y)	A1u
min.	4.2734	0.0787	4.2732	-0.0000	0.0140	0.0000	0.0415	0.0000
ext.	4.3012	0.0121	4.2638	-0.0000	0.0125	0.0000	0.0404	0.0000
			-0.4864	-0.0000	-0.0350	-0.0000	-0.0307	-0.0000
comp.	4.3018	0.0000	4.3013	0.0000	0.0380	0.0000	0.0526	0.0000

Figure 7. Out-of-plane displacements (minimal basis) and full normal-coordinate structural decomposition (NSD) values for (O_iPTPP)Pd^{II} (**6-Pd**) calculated using the X-ray crystal structure.

Experimental Section

General. Melting points were measured with a Yanagimoto micro melting point apparatus and are uncorrected. Column chromatography was carried out using Merck neutral alumina 1077. ^1H NMR (400 MHz) spectra were recorded using a JEOL EX-400 or AL-400 spectrometer. The chemical shifts are reported (σ scale) from internal tetramethylsilane. UV-visible spectra were recorded using a Shimadzu UV-2200 spectrophotometer using Nacalai Tesque spectroscopic grade dichloromethane as the solvent for spectroscopic measurements. The elemental analyses were performed using a Perkin-Elmer 2400 CHN elemental analyzer. Mass spectra were measured with SX102A (JEOL) by using the ESI-TOF method in the positive ion mode with acetonitrile solution samples. Crystals suitable for the X-ray structural determination were mounted on a Rigaku SCXmini CCD diffractometer and irradiated with graphite monochromated Mo-K α radiation ($\lambda = 0.71073 \text{ \AA}$) for data collection. The data were processed using the SCXmini program package (Rigaku). The structures were solved by a direct method using the SIR-2004 program.^[8] Refinement on F^2 was carried out by full-matrix least-squares using the SHELXL-97 program.^[9] All non-hydrogen atoms were refined using anisotropic thermal parameters except for disordered atoms. The hydrogen atoms and disordered atoms were included in the refinement with isotropic thermal parameters. The crystallographic data are summarized in Table 2. NSD analyses of the X-ray structures were carried out with the web-based NSD computational engine program available for general use at <http://jasheln.unm.edu>.

Synthesis of 3-Acetyl-4-isopropylpyrrole (2).

A solution of 5-methyl-3-hexen-2-one (**1**) (5-methyl-3-hexen-2-one : 5-methyl-4-hexen-2-one = 75 : 25, 25.0 mL, 142 mmol) and *p*-tolylsulfonylmethyl isocyanide (27.4 g, 140 mmol) in dry ether/DMSO (2:1) (270 mL) was added dropwise into a suspension of sodium hydride (20.6 g, 429 mmol) in a way that the ether gently refluxed under cooling with ice. After stirring at rt for 40 min, the mixture was carefully hydrolyzed by addition of water (250 mL) under cooling with ice. Then the organic layer was separated and the aqueous phase was extracted with ether (50 mL \times 3), and the collected organic layer was dried over K_2CO_3 . After the organic layer was evaporated, the residue was recrystallized from $\text{CH}_2\text{Cl}_2/n$ -hexane to give 3-acetyl-4-isopropylpyrrole **2** (14.1 g, 93.2 mmol, 66%) as a white solid. M.p. 115-116 $^\circ\text{C}$ (lit. 99-102 $^\circ\text{C}$)^[10]; ^1H NMR (CDCl_3 , 400 MHz): δ = 1.21 (6H, d, J = 6.8 Hz), 2.42 (3H, s), 3.48 (1H, sept., J = 6.8 Hz), 6.61 (1H, s), 7.38 (1H, s), 8.61 ppm (1H, s); ^{13}C NMR (CDCl_3 , 100 MHz): δ = 23.5 (CH_3), 25.5 (CH), 28.1 (CH_3), 115.4 (CH), 122.8 (C), 125.6 (CH), 133.3 (C), 193.8 ppm (C); elemental analysis calcd (%) for $\text{C}_9\text{H}_{13}\text{NO}$: C 71.49, H 8.67, N 9.26; found: C 71.50, H 8.96, N 9.18.

Synthesis of N-Phenylsulfonyl-3-acetyl-4-isopropylpyrrole (3).

KOH pellets (6.70 g, 119 mmol) were added to a solution of 3-acetyl-4-isopropylpyrrole **2** (14.4 g, 95.2 mmol) in EtOH (900 mL) at rt, and the mixture was stirred for 5 min. After the solvent was evaporated,

the residue was redissolved in acetone (900 mL). Benzenesulfonyl chloride (13.0 mL, 102 mmol) was added to the solution and a precipitate was formed instantly. After stirring at rt for 30 min, the solvent was evaporated, and the product mixture was extracted with CH_2Cl_2 (30 mL \times 3), and the collected organic layer was washed with water (50 mL \times 3), then dried over K_2CO_3 . After the organic layer was evaporated, the residue was subjected to neutral alumina column chromatography (Brockman grade I, *n*-hexane : CH_2Cl_2 = 1 : 2). The first fraction was evaporated, and the product was recrystallized from CH_2Cl_2 /*n*-hexane to give *N*-phenylsulfonyl-3-acetyl-4-isopropylpyrrole **3** (9.65 g, 33.1 mmol, 35%) as a white solid. M.p. 77-78 °C (decomp.); ^1H NMR (CDCl_3 , 400 MHz): δ = 1.13 (6H, d, J = 6.8 Hz), 2.40 (3H, s), 3.35 (1H, sept., J = 6.8 Hz), 6.91 (1H, s), ca. 7.7 (1H, s), 7.54-7.91 ppm (5H, m); elemental analysis calcd (%) for $\text{C}_{15}\text{H}_{17}\text{NO}_3\text{S}$: C 61.83, H 5.88, N 4.86; found: C 62.14, H 6.02, N 4.86.

Synthesis of 3-(1-Hydroxy-1-methylethyl)-4-isopropyl-*N*-phenylsulfonylpyrrole (**4**).

A solution of methylmagnesium bromide (0.96 M solution in THF, 66.5 mL, 61.8 mmol) was added dropwise to a solution of *N*-phenylsulfonyl-3-acetyl-4-isopropylpyrrole **3** (6.00 g, 20.6 mmol) in dry ether (150 mL) at 0 °C. After stirring at rt for 5 h, sat. NH_4Cl aq. (10 mL) was carefully added dropwise to the mixture. The product was extracted with ether (30 mL \times 3), and the collected organic layer was washed with water (30 mL \times 3), then dried over K_2CO_3 . After the organic layer was evaporated, the residue was recrystallized from CH_2Cl_2 /*n*-hexane to give 3-(1-hydroxy-1-methylethyl)-4-isopropyl-*N*-phenylsulfonylpyrrole **4** (quant.) as a white solid. M.p. 95-97 °C (decomp.); ^1H NMR (CDCl_3 , 400 MHz): δ = 1.15 (6H, d, J = 6.8 Hz), 1.48 (6H, s), 3.13 (1H, sept., J = 6.8 Hz), 6.90 (1H, d, J = 2.4 Hz), 6.95 (1H, d, J = 2.4 Hz), 7.47-7.82 (5H, m); elemental analysis calcd (%) for $\text{C}_{16}\text{H}_{21}\text{NO}_3\text{S}$: C 62.51, H 6.89, N 4.56; found: C 60.19, H 6.64, N 4.31.

Synthesis of 3,4-Diisopropylpyrrole (**5**).

A solution of NaOH (1.12 g, 28.0 mmol) in water (15 mL) was added to a solution of 3-(1-hydroxy-1-methylethyl)-4-isopropyl-*N*-phenylsulfonylpyrrole **4** (6.24 g, 20.2 mmol) in MeOH (20 mL) under the open air. After the solution was refluxed for 15 h, the solvent was evaporated. The product was extracted with ether (20 mL \times 2), washed with water (30 mL \times 2), and the collected organic layer was dried over K_2CO_3 . After the organic layer was evaporated, a suspension of LiAlH_4 (2.32 g, 61.1 mmol) in dry THF (60 mL) was carefully added dropwise to the residue in dry THF (60 mL), and the resulting mixture was refluxed for 5 h. Then the mixture was cooled to rt and ether (150 mL) was added, followed by ca. 2 N NaOH aq. (15 mL) to hydrolyze the excess LiAlH_4 . After the addition of additional water (30 mL) under cooling with ice, the ether layer was separated and the aqueous suspension was extracted with ether (100 mL). The collected organic layer was washed with water (100 mL), dried over K_2CO_3 , and the solvent was evaporated to give 3,4-diisopropylpyrrole **5** (2.10 g, 13.9 mmol, 69%) as an unstable yellow solid. M.p. 47-48 °C; ^1H NMR (CDCl_3 , 400 MHz): δ = 1.21 (12H, d, J = 7.2 Hz), 2.88

(2H, sept, $J = 7.2$ Hz), 6.50 (2H, d, $J = 2.4$ Hz), 7.88 ppm (1H, br s); ^{13}C NMR (CDCl_3 , 100 MHz): $\delta = 24.1$ (CH_3), 24.5 (CH), 112.2 (CH), 128.8 ppm (C).

Synthesis of Octaisopropyltetraphenylporphyrin (OiTPPH₂) (6).

Benzaldehyde (1.61 mL, 15.8 mmol) was added to a solution of 3,4-diisopropylpyrrole **5** (2.10 g, 13.9 mmol) in CH_2Cl_2 (2.1 L). The solution was stirred for 15 min at rt. After the reaction vessel was shielded from ambient light, the solution was stirred for 7 h in the presence of a catalytic amount of boron trifluoride diethyl etherate (0.18 mL, 1.4 mmol) and the then solvent was evaporated. 2,3-dichloro-5,6-dicyano-1,4-benzoquinone (DDQ) (3.21 g, 14.1 mmol) was added to a solution of the residue in toluene (1.0 L). After the solution was refluxed for 1 h and DDQ derivative was filtered, and the solution was diluted with toluene. Then the solvent was evaporated, the product mixture was extracted with CH_2Cl_2 (100 mL), and the combined organic layer was washed with NaHCO_3 aq. (100 mL \times 3), then dried over K_2CO_3 . The solvent was evaporated and the residue was subjected to neutral alumina column chromatography (Brockman grade III) using CH_2Cl_2 and then 2% MeOH in CH_2Cl_2 as eluents. The solution was evaporated in vacuo. The residue was redissolved in CH_2Cl_2 and was filtered to remove eluted alumina particles. The solvent was evaporated to give OiTPPH₂ **6** (327 mg, 0.343 mmol, 10%) as a green solid.

Synthesis of (OiTPP)Ni^{II} (6-Ni).

Under Ar, a suspension of (OiTPP)H₂ **6** (173 mg, 0.183 mmol) and excess $\text{Ni}^{\text{II}}(\text{OAc})_2 \cdot 4\text{H}_2\text{O}$ (413 mg, 1.66 mmol) in DMF (5 mL) was heated at reflux for 3 h. The reaction mixture was filtered and the filtrate was evaporated. The mixture was extracted with CH_2Cl_2 (20 mL \times 2), and the collected organic layer was washed with water (20 mL \times 2), brine (20 mL) and dried over Na_2SO_4 . After the solvent was evaporated, the residue was subjected to neutral alumina column chromatography (Brockman grade I, CH_2Cl_2). The first purple fraction was evaporated to give (OiTPP)Ni^{II} (**6-Ni**) (71 mg, 0.070 mmol, 38%) as a purple solid. An analytic sample was obtained by recrystallization from EtOH/ CH_2Cl_2 . M.p. >300 °C; ^1H NMR (CDCl_3 , 400 MHz, CDCl_3): $\delta = 0.49$ (24H, br s), 1.00 (24H, br s), 2.48 (8H, br s) 7.52-7.71 (12H, m) 7.99-8.08 ppm (8H, m); UV/vis (CH_2Cl_2): λ_{max} (log ϵ) = 341 (4.36), 451 (5.26), 572 (4.17), 609 nm (407); elemental analysis calcd (%) for $\text{C}_{68}\text{H}_{76}\text{N}_4\text{Ni} + 0.5\text{EtOH}$: C 80.38, H 7.72, N 5.43; found: C 80.34, H 7.84, N 5.66.

Synthesis of (OiTPP)Cu^{II} (6-Cu).

Under Ar, a suspension of (OiTPP)H₂ **6** (191 mg, 0.201 mmol) and excess $\text{Cu}^{\text{II}}(\text{OAc})_2 \cdot \text{H}_2\text{O}$ (403 mg, 2.02 mmol) in dry THF (40 mL) was heated to reflux for 3 h. The reaction mixture was filtered through neutral alumina column chromatography (Brockman grade I, CH_2Cl_2) and the filtrate was evaporated to give (OiTPP)Cu^{II} (**6-Cu**) (38 mg, 0.038 mmol, 19%) as a green solid. An analytic sample was obtained

by recrystallization from EtOH/CH₂Cl₂. M.p. >300 °C; elemental analysis calcd (%) for C₆₈H₇₆N₄Cu+EtOH: C 79.39, H 7.80, N 5.29; found: C 79.24, H 7.59, N 5.48.

Synthesis of (OiPTPP)Zn^{II} (**6-Zn**) and pure free-base 18 π OiPTPPH₂ (**6**).

Under Ar, a suspension of (OiPTPP)H₂ **6** (218 mg, 0.229 mmol) and excess Zn^{II}(OAc)₂·H₂O (219 mg, 1.19 mmol) in dry THF (20 mL) was heated to reflux for 2 h. After the excess salt was removed by filtration, the solvent was evaporated. The residue was subjected to neutral alumina column chromatography (Brockman grade I, CH₂Cl₂), and the first fraction was collected and evaporated to give (OiPTPP)Zn^{II} (**6-Zn**) as a green solid. Yield: 76 mg (33%). However, the product underwent gradual demetallation and thus the spectra of pure **6-Zn** could not be obtained. However, this species was found to be a good precursor for free-base **6**. Thus, the complex was dissolved in CH₂Cl₂ and treated with 1M HCl. After separation of the layers, the aqueous layer was extracted with CH₂Cl₂, and the combined organic layer was washed with brine and then dried over Na₂SO₄ to give free-base **6** (39 mg, 0.035 mmol, 55%). ¹H NMR (CDCl₃, 400 MHz): δ = 0.90 (24H, m), 1.27 (24H, m), 2.67 (8H, br s), 7.82 (12H, m), 8.48 ppm (8H, m); UV-vis (CH₂Cl₂): λ_{max} = 483, 707 nm.; MS (EI): m/z : calcd. for [M]⁺ 952; found 952.

Synthesis of 16 π OiPTPP·2H₂O (**7**).

A solution of antimony pentachloride (1.0 M solution in CH₂Cl₂, 3.0 mL, 3.0 mmol) was added to a solution of OiBTPPH₂ **6** (728 mg, 0.662 mmol) in dry CH₂Cl₂ (100 mL) at -78 °C. After stirring at -78 °C for 3 h, sat. NaHCO₃ aq. (ca. 10 mL) was carefully added dropwise to the mixture. The mixture was washed with sat. NaHCO₃ aq. (20 mL \times 2). After the solvent was evaporated, the residue was subjected to neutral alumina column chromatography (Brockman grade III, CH₂Cl₂). The first brown fraction was evaporated to give OiPTPP·2H₂O **7** (248 mg, 0.261 mmol, 35%) as a brown solid. M.p. 235-236 °C (decomp.); ¹H NMR (CDCl₃, 400 MHz): δ = 0.27 (12H, d, J = 7.0 Hz), 1.01 (12H, d, J = 7.0 Hz), 1.12 (12H, d, J = 7.0 Hz), 1.20 (12H, d, J = 7.0 Hz), 2.69 (4H, sept., J = 7.0 Hz), 3.19 (4H, sept., J = 7.0 Hz), 7.40 ppm (20H, br s); UV-vis (CH₂Cl₂): λ_{max} (log ϵ) = 280 (4.52), 330 nm (4.76); elemental analysis calcd (%) for C₆₈H₇₆N₄+3H₂O: C 81.40, H 8.24, N 5.58; found: C 81.52, H 8.24, N 5.39.

Synthesis of (OiPTPP)Pd^{II} (**6-Pd**).

Under Ar, excess LiBF₄ (90 mg, 0.096 mmol) was added to a solution of OiPTPP·2H₂O **7** (82 mg, 0.086 mmol) in dry toluene (5 mL). The reaction mixture was stirred for 1 h at rt. After the excess LiBF₄ was removed by filtration, the filtrate was evaporated to give OiPTPP·LiBF₄ (**7-Li**) in quantitative yield. Pd₂(dba)₃·CHCl₃ (93 mg, 0.090 mmol) was added to a solution of the generated OiPTPP·LiBF₄ complex in dry THF (10 mL) and the reaction mixture was stirred for 34 h at rt. After the excess Pd₂(dba)₃·CHCl₃ was removed by filtration, and the filtrate was evaporated. The residue was subjected to neutral alumina column chromatography (Brockman grade I, CH₂Cl₂). The first red fraction was evaporated to give

(OiPTPP)Pd^{II} **6-Pd** (26 mg, 0.025 mmol, 29%) as a red solid. M.p. > 300 °C; UV/vis (CH₂Cl₂): λ_{max} (log ϵ) = 332 (4.39), 455 (5.18), 567 (4.29), 608 nm (4.12); ¹H NMR (CDCl₃, 400 MHz): δ = 0.45 (24H, d, J = 7.0 Hz), 0.99 (24H, d, J = 7.0 Hz), 2.80 (8H, br s), 7.57-7.77 (12H, m), 8.21 ppm (8H, br s); elemental analysis calcd (%) for C₆₈H₇₆N₄Pd+CH₂Cl₂+H₂O: C 71.52, H 6.96, N 4.84; found: C 71.82, H 7.03, N 4.77.

Table 2. Crystallographic data for **6-Pd** and **7**.

	6-Pd	7
Formula	C ₆₈ H ₇₆ N ₄ OPd	C ₆₈ H ₈₀ N ₄ O ₂
Mol wt	1071.73	985.36
Crystal system	monoclinic	monoclinic
Space group	<i>P</i> 2 ₁ /m	<i>C</i> 2/c
Color	red	brown
Habit	plate	plate
Cryst dims, mm	0.50x0.25x0.10	0.35x0.27x0.25
<i>a</i> , Å	11.0257(4)	32.102(2)
<i>b</i> , Å	21.8893(8)	8.8603(6)
<i>c</i> , Å	15.3442(5)	25.4264(16)
α , deg	90	90
β , deg	11.4770(10)	128.4692(14)
γ , deg	90	90
<i>V</i> , Å ³	3445.7(2)	5662.3(6)
<i>Z</i>	2	4
<i>D</i> _{calc} , g cm ⁻³	1.033	1.156
Abs coeff, mm ⁻¹	0.308	0.069
<i>F</i> (000)	1132	2128
Temp, K	173	173
Reflections	36339	28498
Independent	8099	6493
<i>R</i> _{int}	0.0658	0.0987
Parameters	348	335
<i>R</i> ₁ [<i>I</i> > 2 σ (<i>I</i>)]	0.0763	0.0840
<i>wR</i> ₂ (all data)	0.2508	0.2570
Goodness of fit	1.114	1.052
solv for crystallization	ethanol/CH ₂ Cl ₂	hexane/CH ₂ Cl ₂

References

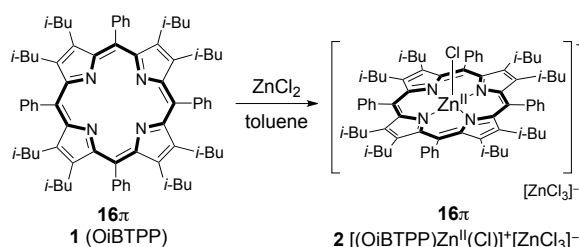
- [1] a) Y. Yamamoto, A. Yamamoto, S.-y. Furuta, M. Horie, M. Kodama, W. Sato, K.-y. Akiba, S. Tsuzuki, T. Uchimar, D. Hashizume, F. Iwasaki, *J. Am. Chem. Soc.* **2005**, *127*, 14540-14541; b) Y. Yamamoto, Y. Hirata, M. Kodama, T. Yamaguchi, S. Matsukawa, K.-y. Akiba, D. Hashizume, F. Iwasaki, A. Muranaka, M. Uchiyama, P. Chen, K. M. Kadish, N. Kobayashi, *J. Am. Chem. Soc.* **2010**, *132*, 12627-12638.
- [2] J. A. Cissell, T. P. Vaid, G. P. A. Yap, *Org. Lett.* **2006**, *8*, 2401-2404.
- [3] J. A. Shelnutt, X. Z. Song, J. G. Ma, S. L. Jia, W. Jentzen, C. J. Medforth, *Chem. Soc. Rev.* **1998**, *27*, 31-41. and references herein.
- [4] a) H. J. Callot, A. Louati, M. Gross, *Angew. Chem. Int. Ed.* **1982**, *21*, 285; b) H. J. Callot, A. Louati, M. Gross, *Bull. Soc. Chim. Fr.* **1983**, *2*, 317-320.
- [5] J. S. Lindsey, I. C. Schreiman, H. C. Hsu, P. C. Kearney, A. M. Marguerettaz, *J. Org. Chem.* **1987**, *52*, 827-836.
- [6] R. Greenhouse, C. Ramirez, J. M. Muchowski, *J. Org. Chem.* **1985**, *50*, 2961.
- [7] a) W. Jentzen, X. Z. Song, J. A. Shelnutt, *J. Phys. Chem. B* **1997**, *101*, 1684-1699.; b) R. E. Haddad, S. Gazeau, J. Pécaut, J. C. Marchon, C. J. Medforth, J. A. Shelnutt, *J. Am. Chem. Soc.* **2003**, *125*, 1253-1268.
- [8] M. C. Burla, M. Caliendo, B. Carrozzini, G. L. Cascarano, L. De Caro, C. Giacovazzo, G. Polidori, R. Spagna, *J. Appl. Cryst.* **2005**, *38*, 381-388.
- [9] G. M. Sheldrick, *Acta Crystallogr. Sect. A* **2008**, *64*, 112-122.
- [10] A. Lavecchia, R. Costi, M. Artico, G. Miele, E. Novellino, A. Bergamini, E. Crespan, G. Maga, R. D. Santo, *Chem. Med. Chem.* **2006**, *1*, 1379-1390.

Chapter 3

Synthesis, Characterization, and Spectroscopic Analysis of Anti-aromatic Benzofused Metalloporphyrins

3-1. Introduction

In one of our previous studies, a variety of metal reagents were reacted with metal-free octaisobutyltetraphenylporphyrin (OiBTPP, **1**), which has a 16π -electron system, in an attempt to synthesize a series of 16π OiBTPP-metal complexes.^[1] The ultimate goal was to carry out a comprehensive investigation of the electronic properties of 16π -electron porphyrin metal complexes. Unfortunately, only the 16π $[(\text{OiBTPP})\text{Zn}^{\text{II}}(\text{Cl})]^+[\text{Zn}^{\text{II}}\text{Cl}_3]^-$ complex (**2**) was found to have a 16π -electron system. The nucleus-independent chemical shifts (NICS) of **1** and **2** are essentially non-aromatic with only weak anti-aromatic character. The chemical oxidation reactions of 18π -electron OiBTPP-metal complexes were also attempted to no avail, and the singly oxidized 17π porphyrin cation radical was obtained instead in the case of copper(II) (*i.e.* $[(\text{OiBTPP})\text{Cu}^{\text{II}}]^+[\text{SbF}_6]^-$).^[1b]



Scheme 1. Reaction of **1** with ZnCl_2 to give 16π -electron $[(\text{OiBTPP})\text{Zn}^{\text{II}}(\text{Cl})]^+[\text{Zn}^{\text{II}}\text{Cl}_3]^-$ (**2**).

A potential alternative strategy for forming stable 16π porphyrinoids is to use tetraphenyl-tetrabenzoporphyrin (TPTBP) as the ligand, since the ligand is expected to be more rigid and hence more planar than porphyrin ligands. The 16π -electron systems of TPTBPs are expected to be stabilized by the presence of four benzo-rings with 6π -electrons. These moieties arguably possess partial *o*-quinodimethane character in the context of 18π porphyrins (Figure 1). Based upon this reasoning, we examined the oxidation of $(\text{TPTBP})\text{Cu}^{\text{II}}$ (**3**) and $(\text{TPTBP})\text{Zn}^{\text{II}}$ (**6**) and have successfully isolated and fully characterized novel 16π -electron $[(\text{TPTBP})\text{Cu}^{\text{II}}(\text{H}_2\text{O})]^{2+} \cdot 2[\text{SbF}_6]^-$ (**4**) and $[(\text{TPTBP})\text{Zn}^{\text{II}}(\text{H}_2\text{O})_2]^{2+} \cdot 2[\text{SbF}_6]^-$ (**7**) complexes, which turned out to be much more stable than previously isolated 16π porphyrin complexes, and a novel 17π -electron cation radical complex $[(\text{TPTBP})\text{Cu}^{\text{II}}]^+[\text{SbF}_6]^-$ (**5**). The three copper(II) species represent the first example of a series of identical metalloporphyrin structures with 16 , 17 , and 18π -electrons to be isolated and fully characterized. In this chapter, we report a systematic assessment of the optical spectroscopy of these species. The main spectral bands are assigned based on a combined study of magnetic circular dichroism (MCD) spectra and TD-DFT calculations, and the excited state relaxation dynamics are elucidated by femtosecond transient absorption studies. It is the first time this latter approach has been applied to 16π metal porphyrinoid complexes. Half-wave potentials for the stepwise electrochemical conversions between 16π Cu^{II} **4** or 16π Zn^{II} **7**, and their 18π forms, Cu^{II} **3** or Zn^{II} **6**, were measured in dichloromethane and benzonitrile utilizing

cyclic voltammetry at a glassy carbon electrode. The reversibility and progress of the reactions upon reducing the 16π M^{II} derivatives to their 18π forms or upon oxidizing the 18π M^{II} species to their 16π forms was monitored by UV-visible spectroscopy in a thin-layer cell and resulting spectra for the electrogenerated 16, 17 and 18π compounds are compared to UV-vis spectra for the same species obtained by chemical methods.

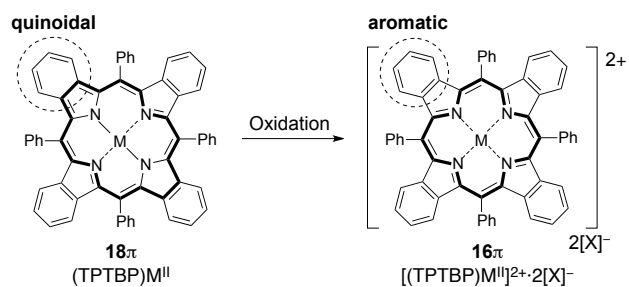


Figure 1. Working hypothesis for the stabilizing effect of the peripheral benzo-rings in the benzofused 16π porphyrin.

3-2. Synthesis and Characterization

The (TPTBP)Cu^{II} complex was selected to explore the feasibility of using chemical oxidation to form 16 π TPTBPs due to the anticipated lowering of the oxidation potential relative to (OiBTTP)Cu^{II}, since we had previously obtained only the singly oxidized porphyrin radical cation in that context. The parent 18 π -electron (TPTBP)Cu^{II} (**3**) complex was prepared using a literature method.^[2] The cyclic voltammogram of **3** in CH₂Cl₂ contains reversible oxidation steps at +0.56 V and +0.86 V vs SCE (SCE vs Fc = 0.46 V, Figure 2). As anticipated, the second oxidation potential is somewhat lower than that of the OiBTTP copper(II) complex (+1.10 V vs SCE, Figure 3). This implies that the introduction of the peripheral benzo-rings is an effective strategy for lowering the oxidation potential. The relatively high value for the second oxidation indicates that the oxidation of **3** to the doubly oxidized state requires a strong oxidizing reagent with an oxidation potential of more than +0.40 V vs ferrocenium.

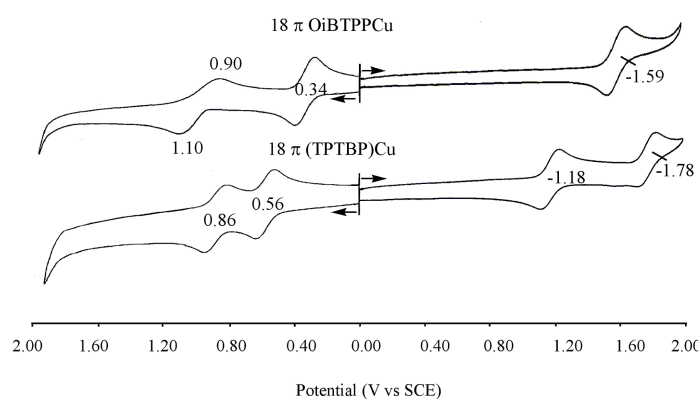
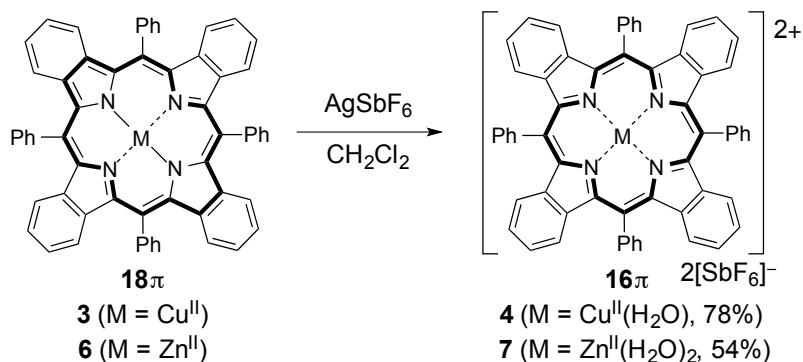


Figure 2. Cyclic voltammograms of (OiBTTP)Cu^{II} and (TPTBP)Cu^{II} (**3**) in CH₂Cl₂, 0.1 M TBAP.

The oxidation of **3** was, therefore, attempted with silver(I) hexafluoroantimonate (AgSbF₆).^[3] The use of 3.3 eq. of AgSbF₆ yielded the desired 16 π copper(II) complex. After many attempts crystals were eventually obtained once the use of “off the shelf” rather than pure solvents was identified as the key to successfully carrying out the crystallization. The complex was isolated in 78% yield as a brown crystalline solid in the form of [(TPTBP)Cu^{II}(H₂O)]²⁺·2[SbF₆]⁻ (**4**), bearing one equivalent of water molecules due to traces present in the organic solvent (Scheme 2). The intentional addition of water led to decomposition, however. This implies that the stability of the 16 π complex is comparable to that of 16 π OiBTTP zinc(II) complex (**2**) as would be anticipated, based on the stabilization of the 16 π porphyrinoid π -system due to the four peripheral 6 π benzo-rings. The electronic absorption spectrum of **4** in CH₂Cl₂ contains bands at 328, 410 and 540 nm (Figure 3a), which are shifted to the blue relative to the corresponding bands in the spectrum of **3**, which lie at 447, 457 and 646 nm. Similar absorption bands are



Scheme 2. Oxidation of 18 π (TPTBP)M (**3**: M = Cu^{II}, **4**: M = Zn^{II}) with AgSbF₆ to give 16 π metal complexes.

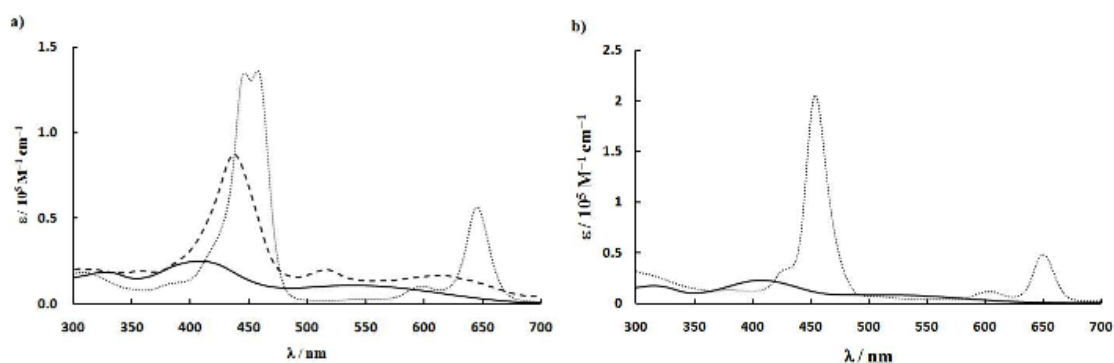
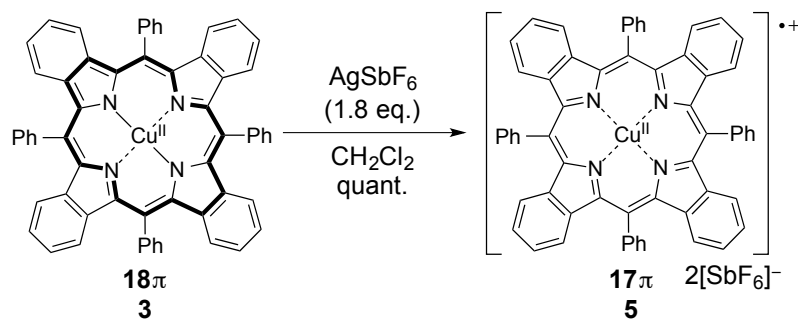


Figure 3. The UV-vis spectra of TPTBP copper(II) and zinc(II) complexes: a) copper(II) complexes **3** ($c = 11.0$ mM; dotted line), **4** ($c = 16.7$ mM; solid line), and **5** ($c = 82.8$ mM; broken line) in CH₂Cl₂. b) zinc(II) complexes **6** ($c = 8.40$ mM; dotted line) and **7** ($c = 43.3$ mM; solid line) in CH₂Cl₂.

obtained in CH₂Cl₂ containing 0.1 M TBAP as the supporting electrolyte (see below). The peak in the Q band region at 540 nm is characteristic of the 16 π [(TPTBP)Cu^{II}(H₂O)]²⁺·2[SbF₆][−] complex. Complex **4** slowly decomposes in solution to another species in a nearly quantitative manner, with the 17 π species being the obvious candidate, despite the relatively high stability of this product in the solid state. A single oxidation of **3** was, therefore, attempted with 1.8 eq. of AgSbF₆, and the reaction resulted in the formation of 17 π -electron cation radical complex, [(TPTBP)Cu^{II}]^{•+}[SbF₆][−] (**5**), quantitatively, as an air-stable species (Scheme 3). The electronic absorption spectrum of **5** contains bands slightly blue-shifted to 437 and 517 nm relative to those of **3** (Figure 3a), which correspond closely with those of the decomposition product of the 16 π porphyrin copper(II) complex (The electrogenerated 17 π species has bands at 438 and 517 nm, see later discussion). Unlike in the case of [(OETPP)Cu^{II}]^{•+}X[−] (X = ClO₄, I),^[4] the signals are broadened in the ¹H NMR spectrum of **5** in CDCl₃ at ambient temperatures as is also the case in the spectrum of 18 π complex **3** (Figure 4). No sharpening of the signals is observed in CD₂Cl₂ when the measurement temperature is lowered to −60 °C (Figure 5) and only minor differences are observed in the



Scheme 3. Oxidation of 18π (TPTBP)Cu^{II} (**3**) with AgSbF₆ to give 17π copper(II) complex (**5**).

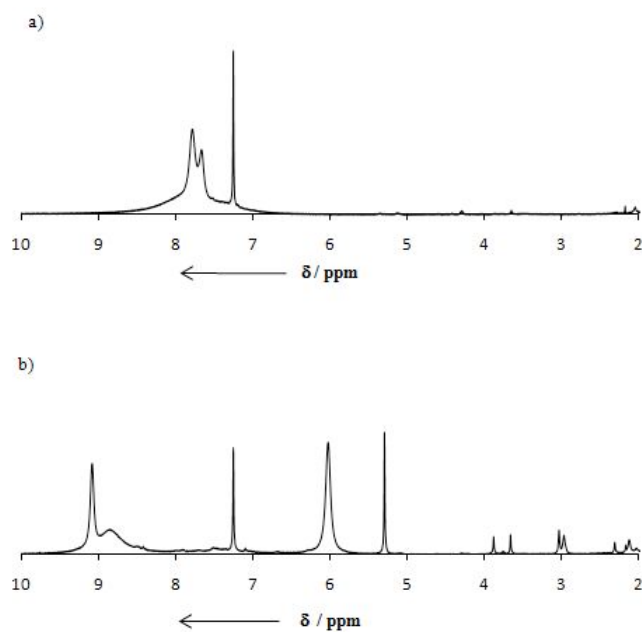


Figure 4. ¹H NMR spectra of a) **3** in CDCl₃ and b) **5** in CDCl₃.

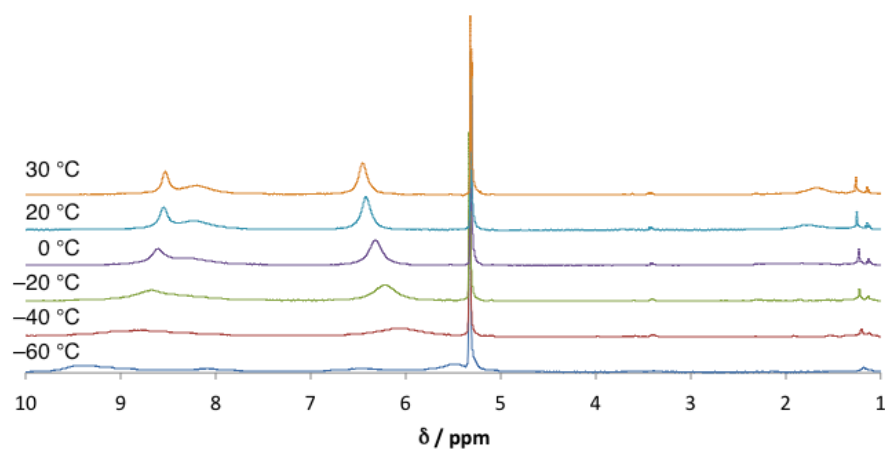


Figure 5. ¹H NMR spectra of **5** at various temperatures in CD₂Cl₂.

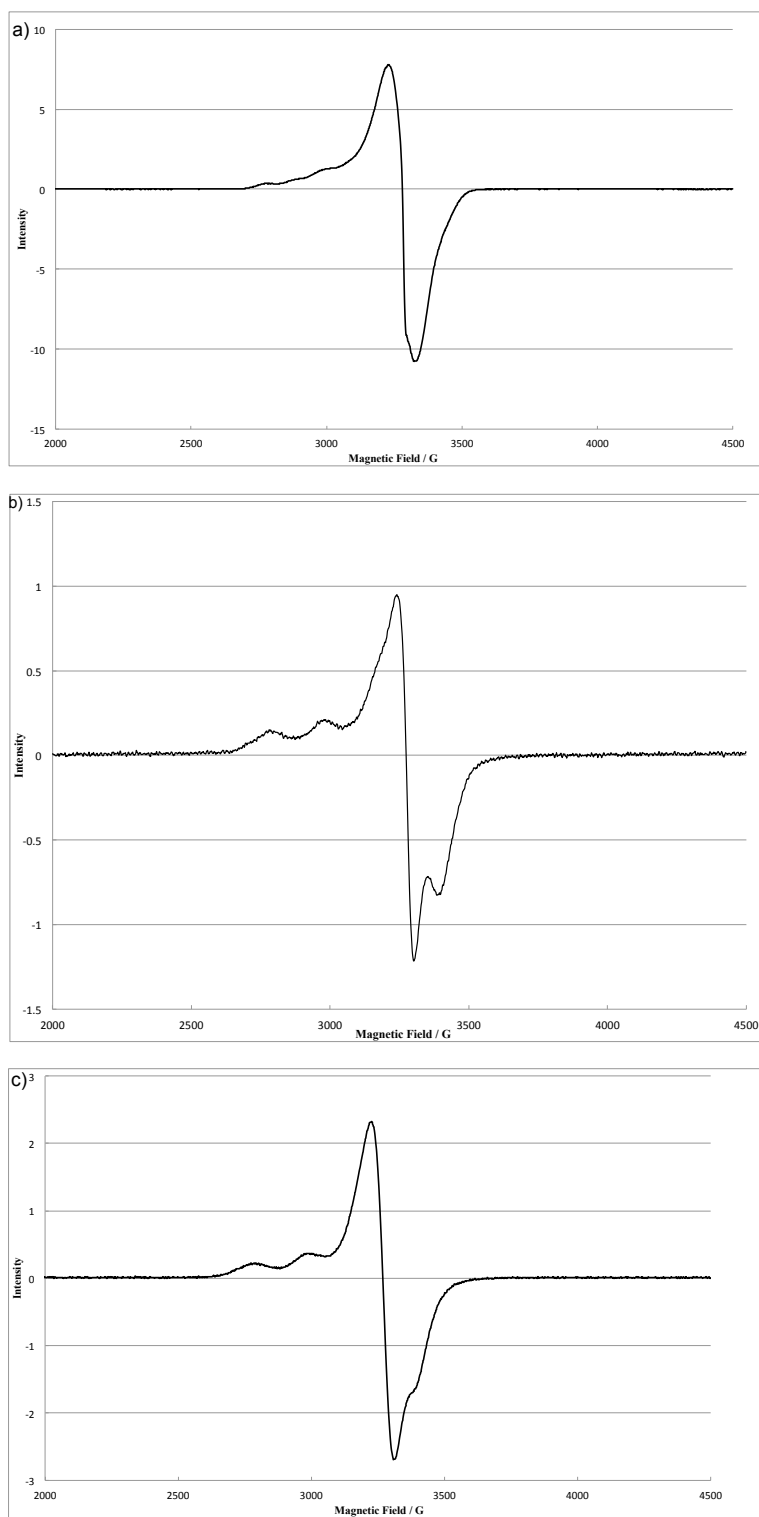


Figure 6. ESR spectra of a) $18\pi(\text{TPTBP})\text{Cu}^{\text{II}}$ (**3**), b) $17\pi [(\text{TPTBP})\text{Cu}^{\text{II}}] \cdot [\text{SbF}_6]^-$ (**5**) and c) $16\pi [(\text{TPTBP})\text{Cu}^{\text{II}}]^2 \cdot 2[\text{SbF}_6]^-$ (**4**) at 85 K. The g values are 2.050 for a), 2.052 for b) and 2.056 for c), respectively.

ESR spectra of **3** - **5** (Figure 6), which is consistent with an absence of antiferromagnetic coupling between the unpaired electrons of the copper(II) center and the porphyrin ring. The observed oxidation potentials and theoretical calculations (*vide infra*) provide further evidence that the +2 oxidation state of the copper center is retained during the oxidation processes.

The successful preparation of a 16 π copper(II) complex demonstrates that the TPTBP ligand facilitates the 2-electron chemical oxidation of the porphyrinoid ligand in metal complexes. The oxidation of the zinc(II) complex was subsequently attempted so that the antiaromaticity of the 16 π species can be evaluated by ^1H NMR spectroscopy due to the diamagnetic character of the central metal (*vide infra*). The 18 π -electron (TPTBP) Zn^{II} (**6**) complex was prepared using a literature method.^[5] The introduction of the fused benzo-rings results in a greater decrease in the oxidation potentials than previously reported octaalkyltetraphenylporphyrins. The 18 π TPTBP complex was, therefore, treated with 5.7 eq. of AgSbF_6 and the 16 π zinc(II) complex was successfully isolated in 54% yield as a brown crystalline solid in the form of $[(\text{TPTBP})\text{Zn}^{\text{II}}(\text{H}_2\text{O})_2]^{2+} \cdot 2[\text{SbF}_6]^-$ (**7**) (Scheme 2). The electronic absorption spectrum of **7** contains bands at 316, 407 and 510 nm (Figure 3b), which are blue-shifted relative those observed in the spectrum of the parent 18 π complex at 454, 604 and 650 nm (Figure 3b). The stability of the 16 π porphyrin zinc(II) complex in the solid state is comparable to that of the 16 π $[(\text{O}i\text{BTPP})\text{Zn}^{\text{II}}(\text{Cl})]^+[\text{Zn}^{\text{II}}\text{Cl}_3]^-$ and $[(\text{TPTBP})\text{Cu}^{\text{II}}(\text{H}_2\text{O})]^{2+} \cdot 2[\text{SbF}_6]^-$ species (**2** and **4**). In solution, although the 16 π zinc(II) complex gradually decomposes in a manner similar to the 16 π copper(II) complex, different products are obtained. While the copper(II) species decomposes to form a 17 π radical cation (*vide supra*), the decomposition product of the zinc(II) species has a characteristic absorption band at 493 nm, which is not observed in the spectrum of the 17 π $[(\text{TPTBP})\text{Zn}^{\text{II}}]^{+\cdot}$ radical species generated by electrochemical oxidation.^[6] When the single chemical oxidation of **12** was carried out with AgSbF_6 , a species was obtained with a spectrum identical to that reported previously for the 17 π species. Attempts to identify the decomposition product in the case of the zinc(II) complex have met with failure. Despite many attempts, crystals suitable for X-ray analysis could not be obtained, for the either the decomposition product or the 17 π zinc(II) radical species that was prepared by chemical oxidation.

3-3. Crystal Structures

The crystal structures of **3-7** were unambiguously determined by single crystal X-ray diffraction analysis. The ORTEP drawings of **3** (two independent molecules) and **4** - **7** are shown in Figures 7^[7] and 8-11, respectively, with selected structural parameters summarized in Table 1. As shown in Figure 8 and 11, there are two counter anions (SbF_6^-) for each porphyrin molecule in the crystal structures of the 16 π species **4** and **7**, which confirms the presence of metal porphyrin dications. The counter anions are well separated from the metal ions with the closest $\text{M} \cdots \text{F}$ distances being 4.004 Å for **4** ($\text{M} = \text{Cu}^{\text{II}}$) and 3.909 Å for **7** ($\text{M} = \text{Zn}^{\text{II}}$), so it is safe to conclude that there is no interaction. Solvated

water molecules lie in the axial positions relative to the metal ions ($M\cdots O$ distances are 2.225 Å for **4** and 2.216 Å, 2.232 Å for **7**). As shown in Table 1, the distance between the Cu^{II} ion and the mean plane consisting of the four nitrogen atoms ($M\cdots \Delta 4N$) is slightly longer in the structure of **4** (0.142 Å) than in that of **3** (0.010, 0.003 Å). The $M\cdots \Delta 4N$ distances of the TPTBP copper(II) complex tends to increase as the number of the π electrons decreases. In the structure of the 17π complex, the closest $Cu^{II}\cdots F$ and the $Cu^{II}\cdots \Delta 4N$ distances are 5.256 Å and 0.040 Å, respectively. In contrast, the $M\cdots \Delta 4N$ distance of the 16π zinc(II) complex **7** (0.001 Å) is significantly shorter than that of the parent 18π complex (0.293 Å). This can be attributed to the difference in the coordination numbers: the former is a 6-coordinate zinc(II) complex whereas the latter is a 5-coordinate. Table 1 also contains the average bond distances of the C_m-C_α and $N-C_\alpha$ bonds. In contrast to the heteroaromatic **3** and **6** complexes, alternating bond lengths are clearly observed on the inner perimeter of the ligand π -system of both of the doubly oxidized metal complexes **4** and **7**, where both the $N-C_{\alpha 1}$ and $N-C_{\alpha 2}$ and the $C_m-C_{\alpha 1}$ and $C_m-C_{\alpha 2}$ distances are markedly different with the average differences being 0.095 Å ($\Delta(N-C_\alpha)$) and 0.111 Å ($\Delta(C_m-C_\alpha)$) in the copper(II) complex, and 0.098 Å ($\Delta(N-C_\alpha)$) and 0.102 Å ($\Delta(C_m-C_\alpha)$) in the zinc(II) complex, respectively. This is consistent with what was observed in the structure of the 16π $[(O_iBTTP)Zn^{II}(Cl)]^+[Zn^{II}Cl_3]^-$ complex.

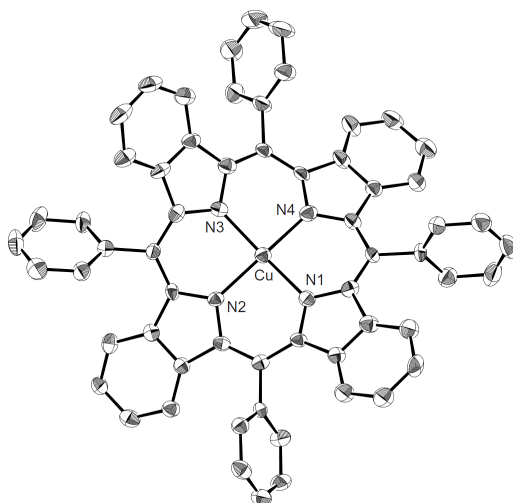


Figure 7. The ORTEP drawing of $(TPTBP)Cu^{II}$ (**3**, two independent molecules) with the thermal ellipsoids shown at the 50% probability level. All hydrogen atoms and the solvated molecules (CH_2Cl_2 and CH_3OH) are omitted for clarity. Selected bond lengths (Å) and angles ($^\circ$) for molecule 1: Cu1-N1, 1.977(5); Cu1-N2, 1.980(6); Cu1-N3, 1.969(5); Cu1-N4, 2.002(5); N1-Cu1-N2, 91.2(2); N1-Cu1-N3, 169.8(2); N1-Cu1-N4, 90.9(2); N2-Cu1-N3, 89.8(2); N2-Cu1-N4, 171.0(2); N3-Cu1-N4, 89.7(2). Selected bond lengths (Å) and angles ($^\circ$) for molecule 2: Cu2-N5, 1.979(5); Cu2-N6, 1.976(5); Cu2-N7, 1.977(5); Cu2-N8, 1.971(5); N5-Cu2-N6, 90.1(2); N5-Cu2-N7, 169.8(2); N5-Cu2-N8, 90.5(2); N6-Cu2-N7, 90.8(2); N6-Cu2-N8, 170.2(2); N7-Cu2-N8, 90.4(2).

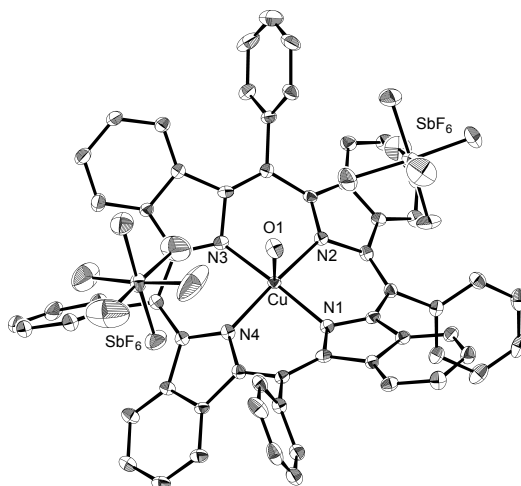


Figure 8. ORTEP diagrams of the 16π $[(\text{TPTBP})\text{Cu}^{\text{II}}(\text{H}_2\text{O})]^{2+} \cdot 2[\text{SbF}_6]^-$ and complexes (**4**). The thermal ellipsoids are scaled to the 50% probability level. All hydrogen atoms and the molecules are omitted for clarity. Selected lengths (Å) and angles (°): Cu1–N1, 1.987(4); Cu1–N2, 1.999(4); Cu1–N3, 1.996(4); Cu1–N4, 1.989(4); Cu1–O1, 2.225(4); N1–Cu1–N2, 89.89(16); N1–Cu1–N3, 173.51(17); N1–Cu1–N4, 89.32(17); N1–Cu1–O1, 92.63(16); N2–Cu1–N3, 89.93(17); N2–Cu1–N4, 170.11(16); N2–Cu1–O1, 96.90(16); N3–Cu1–N4, 89.74(17); N3–Cu1–O1, 93.83(17); N4–Cu1–O1, 92.99(16).

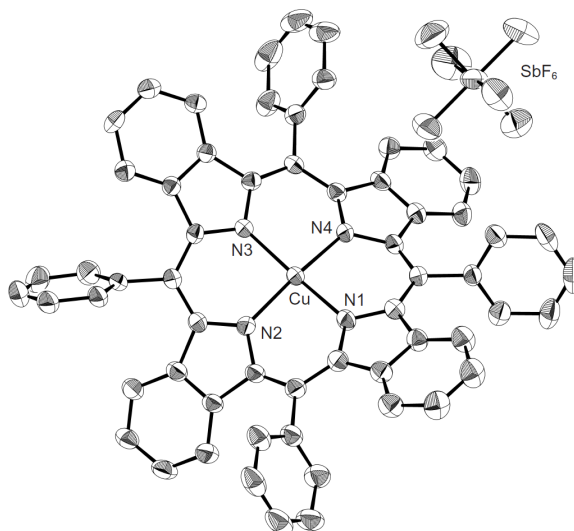


Figure 9. The ORTEP drawing of $[(\text{TPTBP})\text{Cu}^{\text{II}}]^+[\text{SbF}_6]^-$ (**5**) with the thermal ellipsoids shown at the 50% probability level. All hydrogen atoms and the solvated molecules (Et_2O) are omitted for clarity. Selected bond lengths (Å) and angles (°): Cu1–N1, 1.988(4); Cu1–N2, 1.958(4); Cu1–N3, 1.988(4); Cu1–N4, 1.960(4); N1–Cu1–N2, 89.90(17); N1–Cu1–N3, 171.52(18); N1–Cu1–N4, 91.25(16); N2–Cu1–N3, 90.60(16); N2–Cu1–N4, 166.78(18); N3–Cu1–N4, 90.20(16).

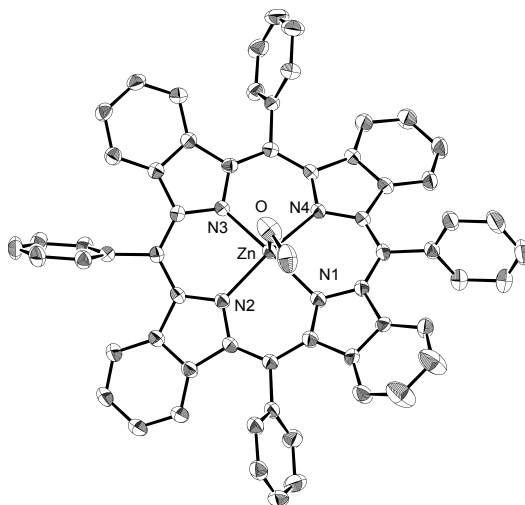


Figure 10. The ORTEP drawing of (TPTBP)Zn^{II}(MeOH) (**6**) with the thermal ellipsoids shown at the 50% probability level. All hydrogen atoms and the solvated molecules (CH₃OH and H₂O) are omitted for clarity. Selected bond lengths (Å) and angles (°): Zn1–N1, 2.096(2); Zn1–N2, 2.087(2); Zn1–N3, 2.062(2); Zn1–N4, 2.083(2); Zn1–O1, 2.074(2); N1–Zn1–N2, 88.45(8); N1–Zn1–N3, 169.08(9); N1–Zn1–N4, 88.41(8); N2–Zn1–N3, 89.70(8); N2–Zn1–N4, 158.58(9); N3–Zn1–N4, 89.39(8).

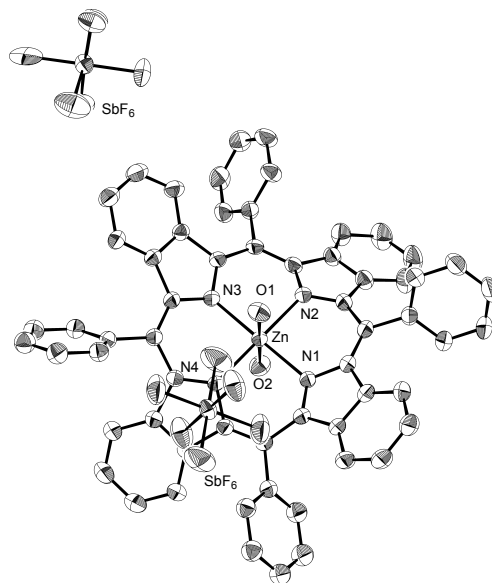
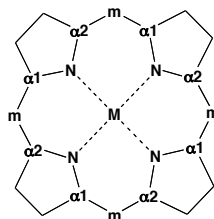


Figure 11. ORTEP diagrams of the 16π [(TPTBP)Zn^{II}(H₂O)₂]²⁺·2[SbF₆][−] complexes (**7**). The thermal ellipsoids are scaled to the 50% probability level. All hydrogen atoms and the molecules are omitted for clarity. Selected lengths (Å) and angles (°): (b) Zn1–N1, 2.071(1); Zn1–N2, 2.069(1); Zn1–N3, 2.067(1); Zn1–N4, 2.064(1); Zn1–O1, 2.216(1); Zn1–O2, 2.232(0); N1–Zn1–N2, 89.96(5); N1–Zn1–N3, 179.48(5); N1–Zn1–N4, 89.95(5); N1–Zn1–O1, 89.75(3); N2–Zn1–N3, 89.59(5); N2–Zn1–N4, 179.63(4); N2–Zn1–O1, 91.31(3); N3–Zn1–N4, 90.50(5); N3–Zn1–O1, 90.00(3); N4–Zn1–O1, 89.04(3).

Table 1. Structural parameters of the porphyrin cores for **3-7**.

Compound	no. of π electron	$M \cdots \Delta 4N^{[b]}$ (Å)	average bond distance (Å)		RMS ^[e]	Ref
			$\Delta N-C_a^{[c]}$	$\Delta C_m-C_a^{[d]}$		
(TPTBP)Cu ^{II} (3) ^[a] (Mol 1)	18	0.010	0.007(8)	0.002(9)	0.612	this work
(Mol 2)		0.003	0.011(8)	0.012(8)	0.642	this work
(TPTBP)Zn ^{II} (MeOH) (6)	18	0.293	0.003(3)	0.001(4)	0.473	this work
[(TPTBP)Cu ^{II}] ⁺ [SbF ₆] ⁻ (5)	17	0.040	0.000(6)	0.006(7)	0.628	this work
[(TPTBP)Cu ^{II} (H ₂ O)] ²⁺ ·2[SbF ₆] ⁻ (4)	16	0.142	0.0095(6)	0.111(6)	0.654	this work
[(TPTBP)Zn ^{II} (H ₂ O) ₂] ²⁺ ·2[SbF ₆] ⁻ (7)	16	0.001	0.098(2)	0.102(2)	0.617	this work
(OiBTTP)Cu ^{II}	18	0.010	0.021(4)	0.002(4)	0.690	[1b]
(OiBTTP)Zn ^{II} (EtOH)	18	0.338	0.004(6)	0.008(7)	0.641	[1b]
[(OiBTTP)Cu ^{II}] ⁺ [SbF ₆] ⁻	17	0.001	0.066(5)	0.055(6)	0.821	[1b]
[(OiBTTP)Zn ^{II} (Cl)] ⁺ [Zn ^{II} Cl ₃] ⁻ (2)	16	0.643	0.101(6)	0.114(7)	0.888	[1b]
[(TPP)Li] ⁺ [BF ₄] ⁻	16	0.440	0.092(3)	0.105(3)	0.381	[9]

[a] Two independent molecules. [b] The distance between M and the mean plane consisting of the four nitrogen atoms. [c] Difference in the average bond distance between N–C_{a1} and N–C_{a2}. [d] Difference in the average bond distance between C_m–C_{a1} and C_m–C_{a2}. [e] The root-mean-square of the sum of the squares of the distance of each atom from the mean plane defined by the 24 core atoms. TPP = tetraphenylporphyrin.

On the other hand, in the 17 π [(TPTBP)Cu^{II}]⁺[SbF₆]⁻ species **5**, the differences between these bond lengths are significantly smaller (**5**: $\Delta(N-C_a) = 0.000$ Å, $\Delta(C_m-C_a) = 0.006$ Å). This is in marked contrast with the π cation radical metalloporphyrins reported by Ghosh *et al.* in which bond alternation was observed in most of their compounds due to pseudo-Jahn-Teller distortion effects.^[8]

The core porphyrin ligand portion of the π -systems of all of the TPTBP metal species, including the parent 18 π complexes, are nonplanar. Figure 12 provides the deviation of each atom from the mean plane defined by the 24 atoms for **3-7**. The 18 π complexes, **3** and **6**, are distorted primarily at the β -positions with slight distortions at the meso-positions resulting in a saddle-type structure. The conformation of the 17 π complex, **5**, is very similar and this may account for the heteroaromatic nature of the radical ring (*vide supra*). In the case of the 16 π complexes **4** and **7**, both the meso-positions and the

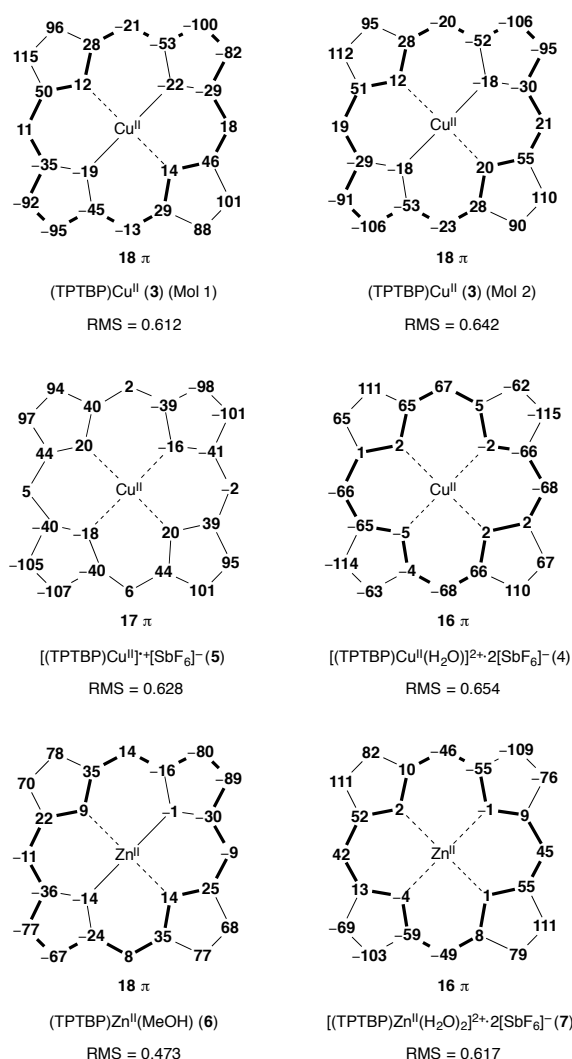


Figure 12. Deviation of each atom from the mean plane (in units of 0.01 Å) along with RMS values for the molecular structures of **3** (two independent molecules) and **4-7**.

β -positions exhibit large deviations from the mean plane. These species have an essentially saddle-type conformation with an additional ruffling-type distortion. The degree of overall distortion of the porphyrin portion of the π -system can be evaluated by the root-mean-square values of the deviation of each atom from the mean plane defined by the 24 core atoms (RMS value). The RMS values are 0.654 and 0.617, respectively, for the 16 π copper(II) and the zinc(II) complexes. These values are considerably smaller than that reported for the 16 π [(OiBTTP)Zn^{II}(Cl)]⁺[Zn^{II}Cl₃]⁻ complex, but unfortunately, they are larger than that of 16 π [(TPP)Li]⁺[BF₄]⁻ prepared by Vaid *et al.*^[9] The introduction of the benzo-ring, therefore, does not help to enhance the planarity of the ligand. However, it should be noted that the difference in RMS values between the corresponding 18 π and 16 π complexes is reduced significantly. Thus, for the copper(II) complexes, the average difference is only +0.027, markedly smaller than that of the corresponding OiBTTP zinc(II) complexes (+0.247).^[1b] Furthermore, although it may not be proper in a

strict sense due to the difference in the number of Li^{I} cations associated with each porphyrin ligand, a comparison with the RMS values of 16π $[\text{Li}^{\text{I}}(\text{TPP})]^+[\text{BF}_4]^-$ (0.381)^[9] and its 18π parent complex, $\text{Li}^{\text{I}}_2(\text{TPP})$ (0.055)^[10] also highlights how small the structural deviation is in the context of the copper(II) complexes. The RMS value of the 17π $[(\text{TPTBP})\text{Cu}^{\text{II}}]^+[\text{SbF}_6]^-$ species (0.628) is practically equal to the average RMS value of the 18π complex (0.627), as would be anticipated, since they adopt similar conformations, in contrast the 17π $[(\text{OiBTTP})\text{Cu}^{\text{II}}]^+[\text{SbF}_6]^-$ species is more distorted than the corresponding 18π complex by +0.131 with only a slight alternation observed in the bond lengths ($\Delta(\text{X}-\text{C}_a) = \text{ca. } 0.06$, where $\text{X} = \text{N}$ or C_m). This indicates that the structural deviation among the three copper(II) complexes is minimal and thus the differences observed in their spectroscopic data are mainly associated with differences in the electronic structure. This makes this series of species ideal for making direct spectroscopic comparisons in this regard.

In contrast, the RMS value of the 16π $[(\text{TPTBP})\text{Zn}^{\text{II}}(\text{H}_2\text{O})_2]^{2+} \cdot 2[\text{SbF}_6]^-$ species (0.617) is substantially larger than that of the 18π zinc(II) complex (0.473), and the difference between the 18π and 16π values (+0.144) is larger than that between the corresponding copper(II) species. Nevertheless, this difference is still smaller than that between the analogous pair of OiBTTP structures. Thus, these findings suggest that the use of a TPTBP ligand is an effective way to minimize structural differences between 18π and 16π metal complexes.

3-4. Evaluation of Antiaromaticity by ^1H NMR Spectroscopy and NICS Calculations

The antiaromaticity of the 16π zinc complex (**7**) was evaluated based on an analysis of ^1H NMR spectra and nucleus-independent chemical shift (NICS) calculations. Generally in the ^1H NMR spectra of aromatic porphyrins, the signals of the outer protons of the porphyrin ring exhibit low-field shifts due to the diatropic ring current, whereas those of anti-aromatic porphyrins are shifted to high-field due to the paratropic ring current.^[11] NICS values derived from a type of theoretical calculation, first proposed by Schleyer *et al.*, in which a dummy atom is placed at the center of a ring, are widely used to determine whether the π -system has aromatic or anti-aromatic character.^[12] Negative values are anticipated for aromatic compounds, while positive values are predicted for anti-aromatic compounds. A value of zero indicates that the compound has non-aromatic character due to the absence of a ring current.

As shown in Figure 13a, the protons of the meso-phenyl groups and peripheral benzo-rings, which are located on the outer part of the porphyrin core, appear in the downfield region at 8.27 (*o*-Ph), 7.95 (*p*-Ph), 7.88 (*m*-Ph), 7.23 and 7.14 (benzo-H) ppm, respectively, in the ^1H NMR spectrum of the 18π $(\text{TPTBP})\text{Zn}^{\text{II}}$ complex (**6**), which is consistent with a diatropic ring current. The assignments of the proton chemical shifts of the meso-phenyl groups and the peripheral benzo-rings were determined unambiguously by H-H COSY (see Experimental Section). In contrast, the protons of the meso-phenyl

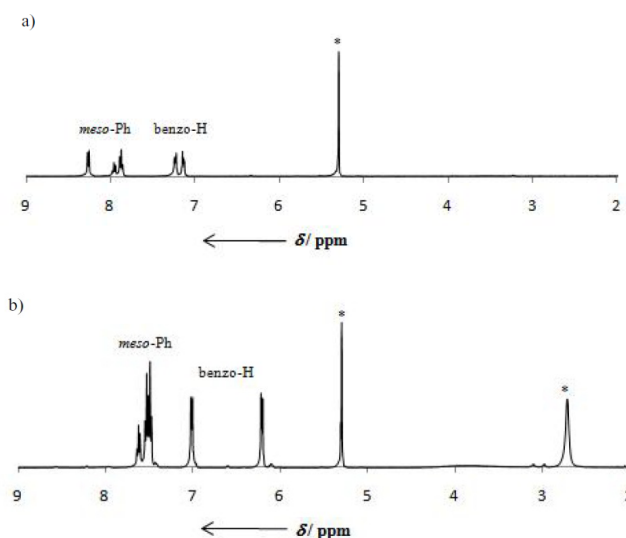
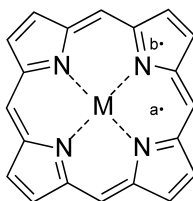


Figure 13. ^1H NMR spectra of a) **6** in CD_2Cl_2 and b) **7** in CD_2Cl_2 at r.t. Signals marked with an asterisk (*) arise from residual solvents and impurities.

Table 2. NICS Values (ppm, B3LYP/6-31G*) for the Porphyrin Metal Complexes



Compound	no. of π electron	point a ^[b]	point b ^[c]	Ref
(TPTBP) Cu^{II} (3) ^[a]	18	-15.04	-3.17	this work
(TPTBP) Zn^{II} (6) ^[a]	18	-14.34	-3.80	this work
[(TPTBP) Cu^{II}] ²⁺ (4) ^[a]	16	+7.55	+3.24	this work
[(TPTBP) Zn^{II}] ²⁺ (7) ^[a]	16	+12.93	+2.38	this work
(OiBTTP) Cu^{II} ^[a]	18	-15.38	-5.12	[1b]
(OiBTTP) Zn^{II} ^[a]	18	-14.02	-5.36	[1b]
[(OiBTTP) Zn^{II} (Cl)] ⁺ ^[a]	16	+4.38	-0.46	[1b]

[a] X-ray geometry. [b] Average of the values for the centers of the square area defined by two C-N bonds connecting a meso carbon. [c] Average of the values for the centers of pyrrole rings.

groups lie at 7.62 (*p*-Ph) and 7.51 (*o*-Ph, *m*-Ph) ppm in the ^1H NMR spectrum of the 16π $[(\text{TPTBP})\text{Zn}^{\text{II}}(\text{H}_2\text{O})_2]^{2+} \cdot 2[\text{SbF}_6]^-$ species (**7**), Figure 13b, and those of the benzo-rings lie at 7.02 and 6.22 ppm. Although these high field shifts are relatively small compared to those of $[\text{Li}^{\text{I}}(\text{TPP})]^+[\text{BF}_4]^-$,^[9] this result provides direct spectroscopic evidence for a paratropic ring current. NICS calculations were performed at the B3LYP/6-31G* level of theory at the centers of the square area defined by the two C–N bonds on either side of a meso carbon (point a) and at the centers of the pyrrole rings (point b) using the X-ray geometries. The results are summarized in Table 2 along with previously reported data.^[1b] The average NICS values at point a for the 18π (TPTBP) Cu^{II} and (TPTBP) Zn^{II} complexes (**3** and **6**) were calculated to be -15.04 and -14.34 , respectively, which are comparable with those reported for representative aromatic porphyrins.^[12b] In marked contrast, positive average NICS values of $+7.55$ and $+12.93$ were calculated for the 16π $[(\text{TPTBP})\text{Cu}^{\text{II}}(\text{H}_2\text{O})]^{2+} \cdot 2[\text{SbF}_6]^-$ and $[(\text{TPTBP})\text{Zn}^{\text{II}}(\text{H}_2\text{O})_2]^{2+} \cdot 2[\text{SbF}_6]^-$ species (**4** and **7**), respectively, which are larger than that reported previously for 16π $[(\text{OiBTPP})\text{Zn}^{\text{II}}(\text{Cl})]^+[\text{Zn}^{\text{II}}\text{Cl}_3]^-$ ($+4.38$). Especially, in the case of the 16π zinc(II) complex (**7**), the NICS value is substantial and this indicates that the TPTBP ligand is more anti-aromatic in character in the 16π state than the corresponding OiBTPP species. Positive values are also predicted at point b for both the copper(II) and the zinc(II) complexes, in contrast with the $[(\text{OiBTPP})\text{Zn}^{\text{II}}(\text{Cl})]^+[\text{Zn}^{\text{II}}\text{Cl}_3]^-$ complex, which has a near zero value. This suggests that the introduction of benzo-rings was found to be useful for inducing antiaromaticity although the degree of antiaromaticity is not so much compared with more planar $[(\text{TPP})\text{Li}]^+[\text{BF}_4]^-$.

3-5. Magnetic Circular Dichroism (MCD) Spectra and MO Analysis

The spectral properties of TPTBP complexes of divalent main group and closed shell d^{10} metal ions such as Mg^{II} and Zn^{II} can be readily accounted for based on Gouterman's 4-orbital model^[13] and Michl's $4N+2$ -perimeter model.^[14] The perimeter model approach is based on the fact that the MOs of cyclic polyenes retain their nodal patterns even after symmetry-lowering perturbations to the structure. Key trends in the optical properties of porphyrinoid π -systems can, therefore, be readily predicted based

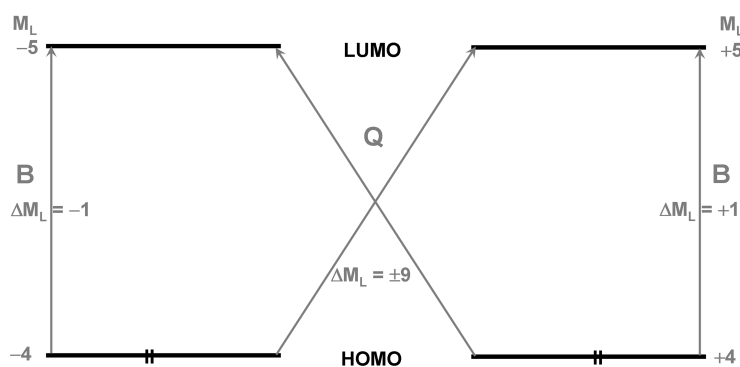


Figure 14. The origin of the Q and B bands in Gouterman's 4-orbital model.^[16]

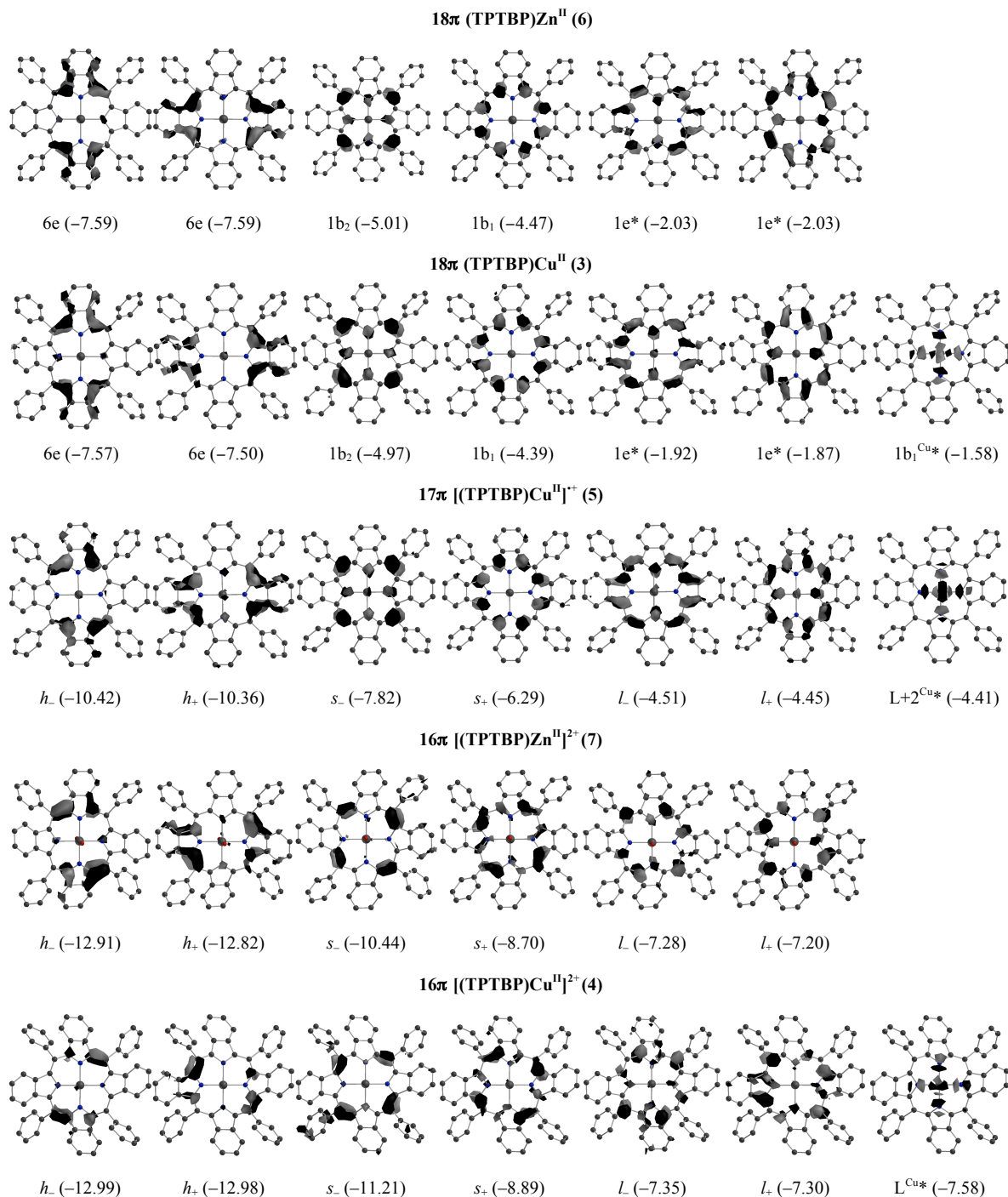


Figure 15. Nodal patterns of the key frontier π -MOs of 18 π (TPTBP)Zn^{II}, 18 π (TPTBP)Cu^{II}, 17 π [(TPTBP)Cu^{II}]⁺, 16 π [(TPTBP)Zn^{II}]²⁺ and 16 π [(TPTBP)Cu^{II}]²⁺ in TD-DFT calculations at an isosurface value of 0.04 a.u. D_{2d} symmetry is assumed for both 18 π (TPTBP)Zn^{II} and (TPTBP)Cu^{II} for ease of comparison, despite the fact that there is a slight deviation from four-fold symmetry in the case of (TPTBP)Cu^{II}. Michl's h_- , h_+ , s_- , s_+ , L and L_+ terminology is adopted for the MOs of 17 π [(TPTBP)Cu^{II}]⁺ and 16 π [(TPTBP)Cu^{II}]²⁺ with $M_L = \pm 3, \pm 4, \pm 5$ nodal properties, respectively, Figure 16. L in the context of the $d_{x^2-y^2}$ MO denotes the LUMO. MO energies predicted for the b-electrons in the TD-DFT calculations, Table 3, are included in parentheses in units of eV.

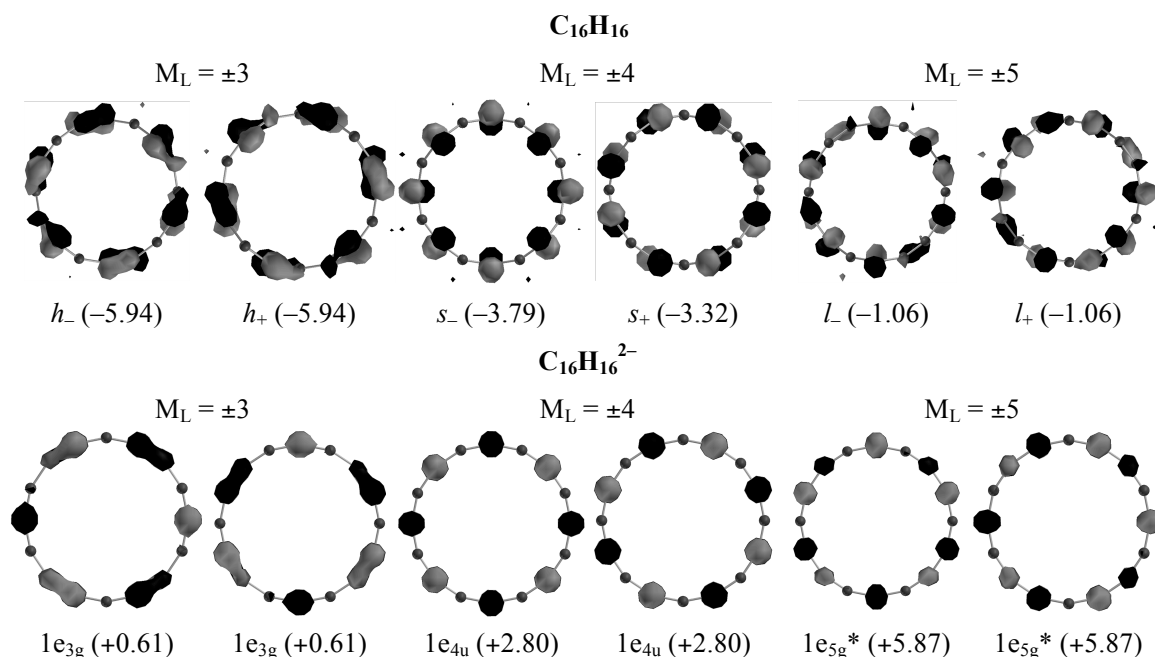


Figure 16. Nodal patterns of the key frontier π -MOs of $C_{16}H_{16}$ and $C_{16}H_{16}^{2-}$ parent perimeters in TD-DFT calculations at an isosurface value of 0.04 a.u. Michl's h_- , h_+ , s_- , s_+ , L_- and L_+ terminology^[16] is adopted for the MOs with $M_L = \pm 3, \pm 4, \pm 5$ nodal properties (Figure 15). MO energies are included in parentheses in units of eV.

on changes in the relative energies of the frontier π -MOs derived from the HOMO and LUMO of a parent hydrocarbon perimeter. The MOs of the 16 atom 18 π -electron $C_{16}H_{16}^{2-}$ parent perimeter of (TPTBP) M^{II} complexes are arranged in an $M_L = 0, \pm 1, \pm 2, \pm 3, \pm 4, \pm 5, \pm 6, \pm 7, 8$ sequence in ascending energy terms.^[15] This results in an allowed $\Delta M_L = \pm 1$ and a forbidden $\Delta M_L = \pm 9$ transition in the context of Gouterman's 4-orbital model (Figure 14), which are associated with the Q and B (or Soret) bands, respectively.^[13] The Q band is referred to as the L band in Michl's 4N+2-perimeter model.^[14] The HOMO and HOMO-1 of 18 π (TPTBP) Zn^{II} and (TPTBP) Cu^{II} retain the $M_L = \pm 4$ nodal properties of the parent perimeter, while the $M_L = \pm 5$ nodal patterns are retained by the LUMO and LUMO+1 (Figures 15 and 16). The key difference in the electronic structure of 18 π (TPTBP) Cu^{II} is the presence of a partially filled $d_{x^2-y^2}$ MO due to the open shell d^9 configuration of the central metal. Many of the key breakthroughs in the understanding of the electronic structure of the porphyrinoids have been derived from MCD spectroscopy based on the orbital angular momentum properties associated with the magnetic quantum number.^[15] Analysis of MCD spectra is based on the three Faraday terms, \mathcal{A}_1 , \mathcal{B}_0 and \mathcal{C}_0 , which arise from the Zeeman splitting of the absorption bands for left and right circularly polarized light into an orbitally degenerate excited state, the field-induced mixing of zero-field states and Zeeman splittings associated with the population adjustment for an orbitally degenerate ground state, respectively. Saddling of tetraphenylporphyrinoids due to steric crowding typically results in π -systems with D_{2d} symmetry, which retain an S_4 axis of symmetry and, orbitally degenerate Q and B excited states.^[16] The \mathcal{A}_1 terms associated

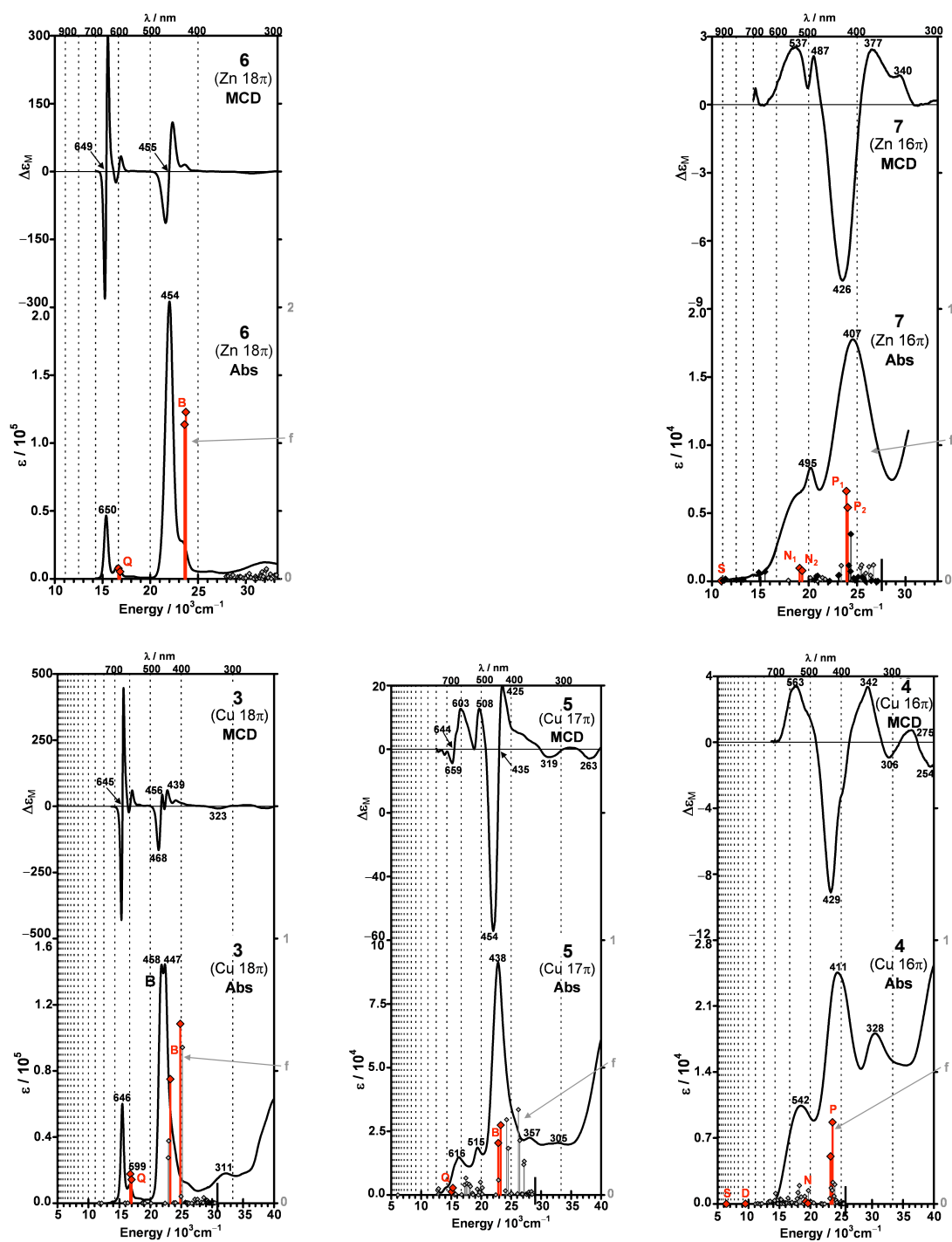


Figure 17. Absorption and MCD data for 18 π (TPTBP)Zn^{II} (**6**), 16 π [(TPTBP)Zn^{II}]²⁺ (**7**), 18 π (TPTBP)Cu^{II} (**3**), 17 π [(TPTBP)Cu^{II}]⁺ (**5**) and 16 π [(TPTBP)Cu^{II}]²⁺ (**4**) plotted against energy and wavelength scales. Calculated TD-DFT spectra are plotted against a right-hand axis. The bands predicted in the TD-DFT calculations to arise primarily from the Q and B transitions of (TPTBP)Zn^{II}, (TPTBP)Cu^{II} and [(TPTBP)Cu^{II}]⁺ and S, D, N and P transitions of [(TPTBP)Zn^{II}]²⁺ and [(TPTBP)Cu^{II}]²⁺ are highlighted in red. Details of the calculations are tabulated in Table 3.

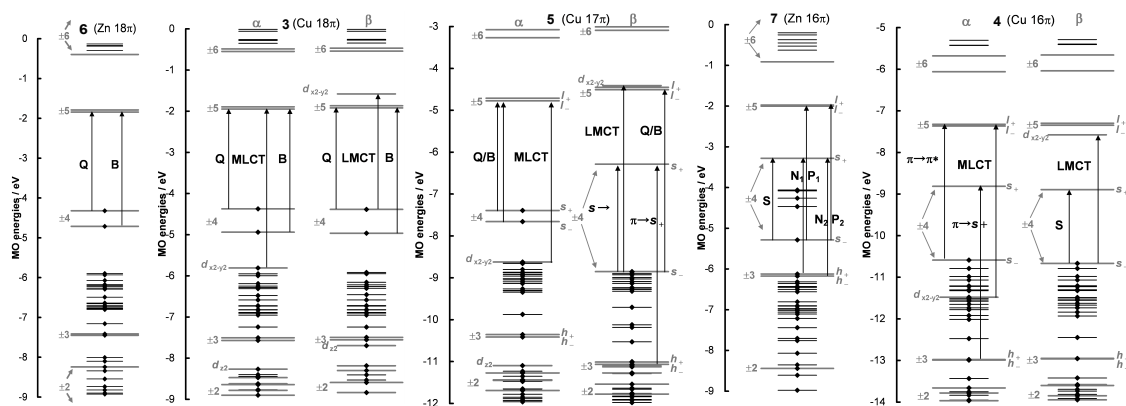


Figure 18. MO energies for the α - and β -electrons of 18 π (TPTBP)Zn^{II} (6), 16 π [(TPTBP)Zn^{II}]²⁺ (7), 18 π (TPTBP)Cu^{II} (3), 17 π [(TPTBP)Cu^{II}]⁺ (5) and 16 π [(TPTBP)Cu^{II}]²⁺ (4) relative to the LUMO in TD-DFT calculations (Figure 17). MOs associated with the d orbitals of the central metal, and the parent cyclic perimeter, are highlighted with narrower and wider dark gray lines, respectively. Michl's h , h +, s , s +, l , and l + terminology^[16] is adopted for the MOs of [(TPTBP)Cu^{II}]⁺ and [(TPTBP)Cu^{II}]²⁺ with $M_L = \pm 3, \pm 4, \pm 5$ nodal properties (Figures 15 and 16). The structures of (TPTBP)Cu^{II} and [(TPTBP)Cu^{II}]⁺ are heteroaromatic, while that of [(TPTBP)Cu^{II}]²⁺ is unaromatic.

with the Q and B bands can be readily identified based on their distinctive first-derivative shape, while Gaussian-shaped \mathcal{B}_0 terms can also be observed for vibrational bands and transitions to non-degenerate excited states. Since the ground states are orbitally non-degenerate, no \mathcal{C}_0 terms are anticipated.

The bands which lie at 650 and 454 nm in the electronic absorption spectrum of 18 π (TPTBP)Zn^{II} can be readily assigned to the Q and B transitions based on Gouterman's 4-orbital model, since a marked intensification is observed in the Faraday \mathcal{A}_1 term at 649 nm relative to that at 455 nm due to the larger ΔM_L value associated with the Q transition. Since there is only limited scope for metal-to-ligand and ligand-to-metal charge transfer (MLCT and LMCT) bands in the spectrum of 18 π (TPTBP)Cu^{II}, the bands at 646 and 458 nm can also be assigned as $Q00$ and $B00$ bands,^[13,16] based on the results of TD-DFT calculations (Figure 17). An intense pseudo- \mathcal{A}_1 term is observed in the MCD spectrum for the $Q00$ band at 646 nm, with a second weaker pseudo- \mathcal{A}_1 term observed in the vibrational band envelope centered slightly to the blue at 599 nm. A more complex set of bands is observed in the B band region with two absorption band maxima of similar intensities at 458 and 447 nm. Since no absorption band or shoulder is observed at 468 nm, corresponding to the trough of negative MCD intensity, it seems safe to assume on the basis of TD-DFT calculations that a pseudo- \mathcal{A}_1 term associated with the B transitions is centered at 458 nm, which overlaps with an intense MLCT band. The -ve / +ve sign sequence observed in ascending energy terms for the Q and B bands in the MCD spectrum is consistent with Michl's perimeter model since this sign sequence is normally observed when the splitting of the MOs derived from the HOMO of the parent perimeter is greater than that of the MOs derived from the LUMO (Figure 16 and Table 3).^[14] An intense absorption band is observed at 438 nm in the spectrum of

Table 3. Calculated TD-DFT electronic excitation spectra of (TPTBP)Zn^{II}, (TPTBP)Cu^{II}, [(TPTBP)Cu^{II}]⁺, [(TPTBP)Zn^{II}]²⁺ and [(TPTBP)Cu^{II}]²⁺ (Figure 17).

18π (TPTBP)Zn ^{II} (<i>D</i> _{2d})									
Band ^a	# ^b	Sym ^c	Calc ^d	Exp ^e		Wave Function ^f =			
Q	1,2	16.8	595	(0.09)	15.4	651	66% 1b ₁ → 1e [*] ; 32% 1b ₂ → 1e [*] ; ...		
B	3,4	24.1	416	(1.24)	21.8	459	51% 1b ₂ → 1e [*] ; 13% 1b ₁ → 1e [*] ; ...		
18π (TPTBP)Cu ^{II} (<i>D</i> _{2d})									
Q	6	16.8	597	(0.11)	15.5	646	34% 1b ₁ ^B → 1e [*] ^B ; 33% 1b ₁ ^A → 1e [*] ^A ; 23% 1b ₂ ^B → 1e [*] ^B ; ...		
Q	7	17.0	589	(0.09)		34% 1b ₁ ^B → 1e [*] ^B ; 31% 1b ₁ ^A → 1e [*] ^A ; 20% 1b ₂ ^B → 1e [*] ^B ; ...			
--	13	22.9	437	(0.17)	---	---	24% 2b ₁ ^{CuA} → 1e [*] ^A ; 12% 1b ₁ ^A → 2a ₂ ^{*A} ; 12% 1b ₁ ^B → 2a ₂ ^{*B} ; ...		
--	14	23.0	435	(0.24)	---	---	27% 2b ₁ ^{CuA} → 1e [*] ^A ; 10% 1b ₁ ^A → 2a ₂ ^{*A} ; 10% 1b ₁ ^B → 2a ₂ ^{*B} ; ...		
B	15	23.2	430	(0.47)	21.8	458	42% 2b ₁ ^{CuA} → 1e [*] ^A ; 17% 1b ₂ ^B → 1e [*] ^B ; 16% 1b ₂ ^A → 1e [*] ^A ; ...		
B	18	24.8	403	(0.68)		43% 2b ₁ ^{CuA} → 1e [*] ^A ; 15% 1b ₂ ^B → 1e [*] ^B ; 11% 1b ₂ ^A → 1e [*] ^A ; ...			
--	20	25.2	397	(0.59)	---	---	52% 2b ₁ ^{CuA} → 1e [*] ^A ; 13% 1b ₂ ^B → 1e [*] ^B ; ...		
17π [(TPTBP)Cu ^{II}] ⁺									
s → s	1	6.12	1635	(0.00)	--	--	103% H(s.) ^B → L(s ₊) ^B ; ...		
Q	4	15.1	664	(0.01)	15.5	644	66% H-1(s.) ^A → L(<i>L</i>) ^A ; 21% H(s ₊) ^A → L+1(<i>L</i>) ^A ; 11% H(s.) ^B → L+1(<i>L</i>) ^B ; ...		
Q	5	15.3	654	(0.03)		55% H-1(s.) ^A → L+1(<i>L</i>) ^A ; 29% H(s ₊) ^A → L(<i>L</i>) ^A ; ...			
p → p	12	17.5	573	(0.07)	--	--	29% H-9 ^{PhB} → L(s ₊) ^B ; 16% H(s.) ^B → L+2(<i>L</i>) ^B ; 14% H(s ₊) ^A → L(<i>L</i>) ^A ; 13% H-1(s.) ^A → L+1(<i>L</i>) ^A ; ...		
p → p	22	19.9	503	(0.05)	--	--	61% H-14 ^{PhB} → L(s ₊) ^B ; 15% H-12 ^B → L(s ₊) ^B ; ...		
B	26	22.8	438	(0.20)	22.8	438	23% H-2 ^{CuA} → L(<i>L</i>) ^A ; 20% H(s.) ^B → L+1(<i>L</i>) ^B ; 19% H-16 ^B → L(s ₊) ^B ; 16% H-3 ^{NA} → L(<i>L</i>) ^A ; ...		
p → p	27	22.9	437	(0.06)		74% H-16 ^B → L(s ₊) ^B ; ...			
B	28	23.3	430	(0.27)	28% H(s.) ^B → L+2(<i>L</i>) ^B ; 22% L-2 ^{CuA} → L+1(<i>L</i>) ^A ; 17% H-3 ^{NA} → L+1(<i>L</i>) ^A ; ...				
MLCT	30	24.3	412	(0.30)	--	--	19% H(s.) ^B → L+1(<i>L</i>) ^B ; 18% L-2 ^{CuA} → L(<i>L</i>) ^A ; 17% H-3 ^{NA} → L(<i>L</i>) ^A ; 15% H-18(<i>h</i>) ^B → L(s ₊) ^B ; ...		
MLCT	31	24.5	408	(0.18)	--	--	25% 2b ₁ ^{CuA} → 1e [*] ^A ; 24% H-17(<i>h</i> ₊) ^B → L(s ₊) ^B ; 19% H-3 ^{NA} → L+1(<i>L</i>) ^A ; 14% H-1(s.) ^A → L+1(<i>L</i>) ^A ; ...		

$h \rightarrow s$	35	26.2	382	(0.34)	--	--	45% $H-17(h_+)^B \rightarrow L(s_+)^B$; ...
$h \rightarrow s$	36	26.4	378	(0.21)	--	--	43% $H-18(h_+)^B \rightarrow L(s_+)^B$; ...
$p \rightarrow p^*$	39	27.1	369	(0.12)	--	--	31% $H-5^A \rightarrow L(L)^A$; 10% $H-3^B \rightarrow L+1(L)^B$; ...
$p \rightarrow p^*$	40	27.2	368	(0.13)	--	--	19% $H-8^A \rightarrow L(L)^A$; 17% $H-18(h_+)^B \rightarrow L(s_+)^B$; ...

 $16\pi [(TPTBP)Zn^{II}]^{2+}$

S	1	9.40	1063	(0.00)	--	--	89% $H(s_-) \rightarrow L(s_+)$; ...
N ₁	2	14.6	684	(0.07)	20.2	495	89% $H-1 \rightarrow L(s_+)$; ...
N ₂	3	15.0	668	(0.08)	20.5	487	88% $H-2 \rightarrow L(s_+)$; ...
P ₁	18	22.9	437	(0.53)	23.5	426	74% $H(s_-) \rightarrow L+1(L)$; 4% $H-18(h_+) \rightarrow L(s_+)$; ...
P ₂	19	23.4	428	(0.50)	26.5	377	77% $H(s_-) \rightarrow L+2(L_+)$; 3% $H-19(h_-) \rightarrow L(s_+)$; ...
$p \rightarrow p^*$	37	29.3	341	(0.10)	--	--	34% $H-9 \rightarrow L+2(L_+)$; 30% $H-18(h_+) \rightarrow L(s_+)$; 17% $H-10 \rightarrow L+1(L)$; ...
$p \rightarrow p^*$	38	29.6	337	(0.06)	--	--	28% $H-10 \rightarrow L+1(L)$; 22% $H-8 \rightarrow L+2(L_+)$; 14% $H-18(h_+) \rightarrow L(s_+)$; ...
$p \rightarrow p^*$	39	29.7	337	(0.07)	--	--	39% $H-8 \rightarrow L+2(L_+)$; 16% $H-10 \rightarrow L+1(L)$; 14% $H-11 \rightarrow L+1(L)$;
$p \rightarrow p^*$	40	29.8	335	(0.12)	--	--	34% $H-9 \rightarrow L+2(L_+)$; 18% $H-18(h_+) \rightarrow L(s_+)$; 14% $H-12 \rightarrow L+1(L)$; ...

 $16\pi [(TPTBP)Cu^{II}]^{2+}$

S	1	6.40	1562	(0.00)	--	--	69% $H(s_-)^A \rightarrow L(s_+)^A$; 52% $H(s_-)^B \rightarrow L(s_+)^B$; ...
D	2	9.48	1054	(0.00)	--	--	52% $H(s_-)^B \rightarrow L(s_+)^B$; 39% $H(s_-)^A \rightarrow L(s_+)^A$; ...
$p \rightarrow s_+$	10	14.4	695	(0.04)	--	--	48% $H-3^A \rightarrow L(s_+)^A$; 15% $H-5^{PhA} \rightarrow L(s_+)^A$; 13% $H-3^B \rightarrow L(s_+)^B$; ...
$p \rightarrow s_+$	28	18.0	556	(0.04)			25% $H-14^B \rightarrow L(s_+)^B$; 10% $H(s_-)^B \rightarrow L+1^{CuB}$; ...
MLCT	29	18.2	549	(0.07)			12% $H-8^{CuA} \rightarrow L(s_+)^A$; 11% $H-14^A \rightarrow L(s_+)^A$; 10% $H(s_-)^B \rightarrow L+1^{CuB}$; ...
N ₁	33	19.3	519	(0.00)	17.8	563	34% $H(s_-)^A \rightarrow L+1(L)^A$; 24% $H(s_-)^B \rightarrow L+2(L)^B$; 11% $H-13^B \rightarrow L(s_+)^B$; ...
N ₂	35	19.6	510	(0.00)			22% $H(s_-)^A \rightarrow L+2(L_+)^A$; 22% $H-20^{CuB} \rightarrow L+1^{CuB}$; 14% $H(s_-)^B \rightarrow L+3(L_+)^B$; ...
$p \rightarrow s_+$	36	19.7	508	(0.05)			45% $H-13^A \rightarrow L(s_+)^A$; 22% $H-13^B \rightarrow L(s_+)^B$;

									10% H-14 ^A → L(s ₊) ^A ; ...
P ₁	44	23.3	430	(0.18)					35% H(s)^B → L+2(L)^B ; 17% H-3 ^B → L+1 ^{CuB} ; 14% H-2 ^{PhB} → L+1 ^{CuB} ; 13% H(s)^A → L+1(L)^A ; ...
p → p*	45	23.4	428	(0.06)					36% H-1 ^{PhA} → L+1(L) ^A ; 12% H-1 ^{PhB} → L+2(L) ^B
p → p*	46	23.6	425	(0.05)	23.3	429			23% H-1 ^{PhA} → L+2(L) ^A ; 12% H-1 ^{PhB} → L+3(L) ^B ; 10% H-3 ^A → L+1(L) ^A ; 10% H-3 ^B → L+2(L) ^B ; ...
P ₂	47	23.6	424	(0.31)					34% H(s)^B → L+3(L)^B ; 26% H(s)^A → L+2(L)^A ; ...
LMCT	48	23.7	423	(0.08)					63% H-3 ^B → L+1 ^{CuB} ; ...
p → p*	50	24.0	417	(0.07)					54% H-1 ^{PhB} → L+2(L) ^B ; 24% H-1 ^{PhA} → L+1(L) ^A ; ...
p → s ₊	58	25.3	395	(0.00)	--	--			38% H-18(h)^B → L(s₊)^B ; 14% H-18(h₊)^A → L(s₊)^A ; 12% H-5 ^B → L+1 ^{CuB} ; 11% H-19(h)^A → L(s₊)^A ; ...
p → s ₊	60	25.4	394	(0.00)	--	--			25% H-17(h₊)^B → L(s₊)^B ; 19% H-4 ^B → L+1 ^{CuB} ; 11% H-18(h₊)^A → L(s₊)^A ; ...

[a] Band assignment is described in the text. [b] The number of the state assigned in terms of ascending energy within the TD-DFT calculation. Only states located below 33, 333 cm⁻¹ resulting from allowed electronic transitions with an oscillator strength of greater than 0.10 are included. [c] The symmetry of the state. [d] Calculated band energies (10³.cm⁻¹), wavelengths (nm) and oscillator strengths (f) in parentheses. [e] Observed energies (10³.cm⁻¹) and wavelengths (nm). [f] The wave functions based on the eigenvectors predicted by TD-DFT. D_{2d} symmetry is assumed for both (TPTBP)Zn^{II} and (TPTBP)Cu^{II} for ease of comparison, despite the fact that there is a slight deviation from four-fold symmetry in the case of (TPTBP)Cu^{II}. H and L denote the HOMO and LUMO respectively, while Michl's h₋, h₊, s₋, s₊, l₋ and l₊ nomenclature is used to denote MOs of [(TPTBP)Cu^{II}]⁺, [(TPTBP)Zn^{II}]²⁺ and [(TPTBP)Cu^{II}]²⁺ with M_L = ±3, ±4 and ±5 nodal properties (Figure 18). Strictly speaking this nomenclature is only applicable to the even-electron π-system of the unaromatic [(TPTBP)Zn^{II}]²⁺ and [(TPTBP)Cu^{II}]²⁺ species but adopting it for [(TPTBP)Cu^{II}]⁺ aids comparison of the contributions made by specific one-electron transitions. Cu^{II}, N and Ph as superscripts denote MOs associated primarily with the central metal, the pyrrole nitrogen lone pairs and phenyl substituents, respectively. A and B denote the α- and β-electrons, respectively. Bold fonts are used to highlight one-electron transitions associated with Gouterman's 4-orbital model in the context of the (TPTBP)Zn^{II} and (TPTBP)Cu^{II} calculations and to one-electron transitions between the h₋, h₊, s₋, s₊, l₋ and l₊ MOs in the [(TPTBP)Zn^{II}]²⁺, [(TPTBP)Cu^{II}]⁺ and [(TPTBP)Cu^{II}]²⁺ calculations.

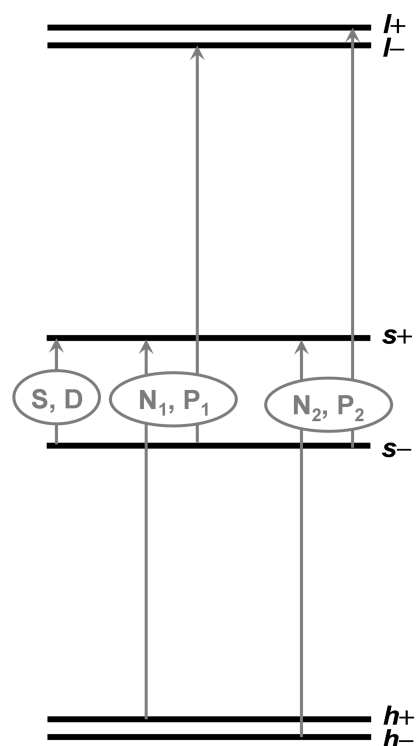


Figure 19. The origin of the S, D, N₁, P₁, N₂ and P₂ bands in Michl's 4N-perimeter model.

17π [(TPTBP)Cu^{II}]⁺, which lies close to the B band of 18π (TPTBP)Cu^{II} and is associated with a pseudo- \mathcal{A}_1 term in the MCD spectrum, but a much more complex set of bands is observed in the visible region with no obvious intense pseudo- \mathcal{A}_1 term corresponding to the Q band. Due to the loss of an electron from the π -system, additional $\pi \rightarrow \pi$ bands are predicted to lie between 500 – 700 nm and a significant loss of intensity can be anticipated in the MCD spectrum due to quenching of the orbital angular momentum properties of the MOs associated with the HOMO of the parent perimeter. Bands centered at 644 and 438 nm are tentatively assigned to the Q and B transitions but the spectrum is clearly comprised of a very complex envelope of bands arising from $\pi \rightarrow \pi$, MLCT and LMCT transitions in addition to the $\pi \rightarrow \pi^*$ transitions associated with Gouterman's 4-orbital model, which dominate the spectra of 18π (TPTBP)Zn^{II}.

On moving to the non-aromatic 16π -electron system in the case of 16π [(TPTBP)Zn^{II}]²⁺ and [(TPTBP)Cu^{II}]²⁺, the Q and B band nomenclature associated with Gouterman's 4-orbital model is no longer applicable. The h_- , h_+ , s_- , s_+ , l_- , l_+ terminology used in Michl's 4N-perimeter model for non-aromatic π -systems^[17] has been adopted to denote MOs with $M_L = \pm 3, \pm 4, \pm 5$ nodal properties derived from the HOMO, SOMO and LUMO levels of the parent C₁₆H₁₆ perimeter, respectively (Figure 19). This is in marked contrast with the (4N+2)-electron perimeter model where the Q and B bands arise from transitions between the four frontier π -MOs derived from the HOMO and LUMO of the parent hydrocarbon perimeter.^[14] Michl *et al.* adopted new terminology to describe even-electron cyclic

4N- π -systems.^[17] The term “anti-aromatic” is reserved for π -systems that have very strong biradical-like character, while 4N-electron perimeter in which the structural perturbations are strong enough to remove the biradical-like character are described as “unaromatic”. The lowest-energy bands of unaromatic compounds arise from the $s_- \rightarrow s_+$ transition (Figure 19). Since the transition is of an intrashell nature in the perimeter model, the transition is magnetic-dipole allowed, but the absorption and hence also the MCD intensity of the S and D bands are predicted to be zero.^[17] The other four electronic transitions are intershell being derived from HOMO \rightarrow SOMO and SOMO \rightarrow LUMO one-electron transitions (Figure 19). Two weakly (N_1 , N_2) and two strongly (P_1 , P_2) electric-dipole allowed transitions are predicted. The N and P transitions are somewhat analogous to the L and B transitions in aromatic systems 4N+2-perimeter model.^[14] Configuration interaction between states arising from the $h_+ \rightarrow s_+$ and $s_- \rightarrow l_-$ transitions causes cancellation and intensification of the transition dipole moments, resulting in weak and intense N_1 and P_1 bands, respectively. Weak N_2 and intense P_2 bands arise from the $h_- \rightarrow s_+$ and $s_- \rightarrow l_+$ transitions in a similar manner (Figure 19).

The presence of a paramagnetic central metal and/or the additional π -MOs associated with fused-ring-expansion of the π -system makes the application of Michl’s 4N-perimeter model for non-aromatic π -systems^[16] problematic in the case of 16π [(TPTBP)Zn^{II}]²⁺ and [(TPTBP)Cu^{II}]²⁺. As was the case previously with the unaromatic 16 π -electron systems of OiBTPPs,^[1b] no predictions of the MCD signs have been attempted. Although Michl’s S, D, N_1 , N_2 , P_1 and P_2 band nomenclature cannot be fully applied in the case of 16π [(TPTBP)Cu^{II}]²⁺ due to the presence of charge transfer bands, one-electron transitions between the h_- , h_+ , s_- , s_+ , L_- and L_+ MOs still play a major role in the spectral bands predicted by TD-DFT, Table 3. Weak forbidden bands, which are predicted to lie beyond 1000 nm, have been assigned as S and D bands, since they arise from $s_- \rightarrow s_+$ transitions. The broad envelope of bands centered at 542 nm in the spectrum of 16π [(TPTBP)Cu^{II}]²⁺ and the shoulder of intensity observed at similar wavelengths in the spectrum of 16π [(TPTBP)Zn^{II}]²⁺ (Figure 17), are tentatively assigned as arising from weak $\pi \rightarrow s_+$ transitions on the basis of the TD-DFT calculation (Table 3), while the more intense bands at 411 and 407 nm, respectively, are assigned as being primarily arising from the P transitions based on the large contributions from the $s_- \rightarrow L_-$ and $s_- \rightarrow L_+$ one-electron transitions (Figures 17, 18, 19 and Table 3), which are predicted for the most intense bands in this region of the spectrum in the TD-DFT calculation.

3-6. Excited-state Relaxation Dynamics

Time correlated single photon counting (TCSPC) and femtosecond transient absorption (TA) experiments were carried out to explore the excited state relaxation dynamics of **3** - **7** and how it is affected by the number of π -electrons on the inner ligand perimeter. Initially, the photophysical properties of the two 18π TPTBP metal complexes (**3** and **6**) were investigated. (TPTBP) Cu^{II} (**3**) exhibits a fast deactivation process with a lifetime of 27.5 ps in CH_2Cl_2 in fs-TA measurements (Figure 20). Previously, Rodgers *et al.*^[18] investigated the deactivation dynamics of **3** in toluene and benzonitrile. According to this research the LMCT state is located between the Q excited state and the ground state and provides an effective deactivation channel. These authors observed fast relaxation dynamics with a lifetime of a few tens of a picosecond. It, therefore, seems reasonable to conclude that the fast relaxation dynamics of **3** originates from the existence of a low-lying LMCT state. In contrast, (TPTBP) Zn^{II} (**6**) exhibits slower excited state dynamics. Rentzepis *et al.*^[19] reported the deactivation dynamics of **6** in benzene based on picosecond transient absorption measurements. It proved difficult to assign the pure S_1 state lifetime in this study, however, due to the complex overlap of transient singlet and triplet excited state signals, which results in excited state absorption (ESA), ground state bleaching recovery (GSB), and stimulated emission (SE) in the TA spectra. We were able to observe the fluorescence spectrum of **6** in CH_2Cl_2 , and the

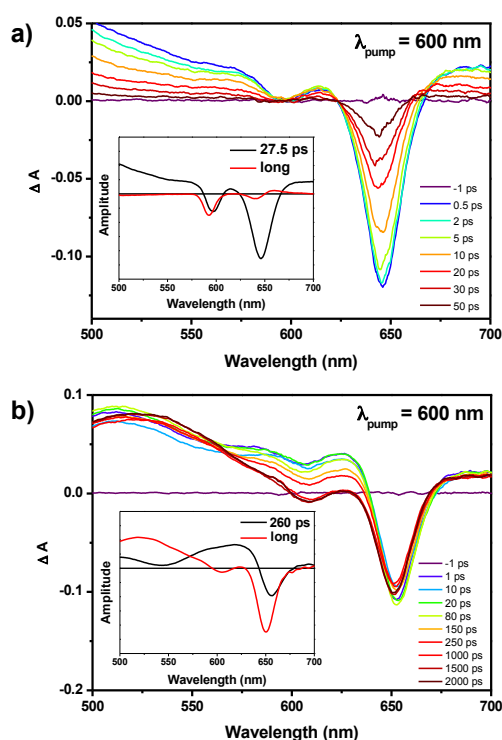


Figure 20. Femtosecond transient absorption spectra of (a) **3** and (b) **6** in CH_2Cl_2 . The insets show the decay-associated spectra obtained from global analysis.

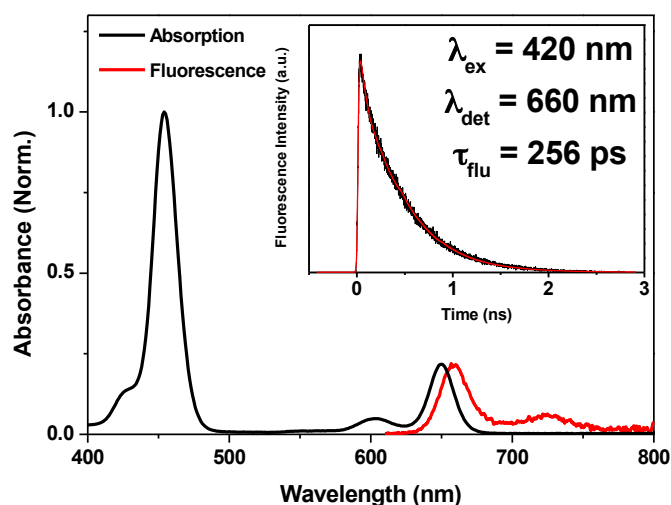


Figure 21. Absorption (black line) and fluorescence spectrum (red line) of **6** in CH_2Cl_2 . The inset shows the fluorescence decay profile of **6**.

fluorescence lifetime was estimated to be 256 ps based on TCSPC measurements (Figure 21). In addition, we have also elucidated a similar time constant of 260 ps by applying the global analysis technique to the TA spectra, which could be assigned as the S_1 state lifetime of **6** (Figure 20). It is worth noting that **6** has an S_1 state lifetime, which is six times shorter than that of the planar meso-free Zn^{II} benzoporphyrin (1.56 ns)^[20]. In general, non-planar porphyrins exhibit shorter excited state lifetimes due to enhanced nonradiative decay processes.^[21] The X-ray crystal structure of **6** reveals a saddle-type distorted structure due to steric interactions between the benzo-fused moieties and the phenyl substituents.

The excited state dynamics of the two anti-aromatic 16π metallobenzoporphyrin species (**4** and **7**) have also been analyzed. It is worth noting that the two 16π metallobenzoporphyrins exhibit dramatically faster decay dynamics in TA spectra (Figure 22) than the heteroaromatic 18π complexes (**3** and **6**). The temporal profiles of **4** and **7** can be fitted with a double exponential decay function with time constants of <1 ps and 10~18 ps, respectively. In previous studies, various anti-aromatic $[4n]\pi$ porphyrinoids, such as 20π SiTPP(py)₂,^[21] 20π orangarin,^[22] 24π rosarin,^[23] and vinylene bridged 28π hexaphyrin^[24] were revealed to have shorter excited state lifetimes than those of corresponding aromatic $[4n+2]\pi$ porphyrinoids. High symmetry heteroaromatic $[4n+2]\pi$ porphyrinoids often have near degenerate frontier orbitals (HOMO-1/HOMO and LUMO/LUMO+1). Thus, when two electrons are added to the LUMO or removed from the HOMO of $[4n+2]\pi$ porphyrinoids, the HOMO-LUMO gap of $[4n]\pi$ porphyrinoids should decrease significantly. The lowest energy excited states are one-photon forbidden (or dark) and provide an effective non-radiative deactivation channel due to the markedly reduced HOMO-LUMO gap. Anti-aromatic $[4n]\pi$ porphyrinoids, therefore, exhibit shorter excited state lifetimes

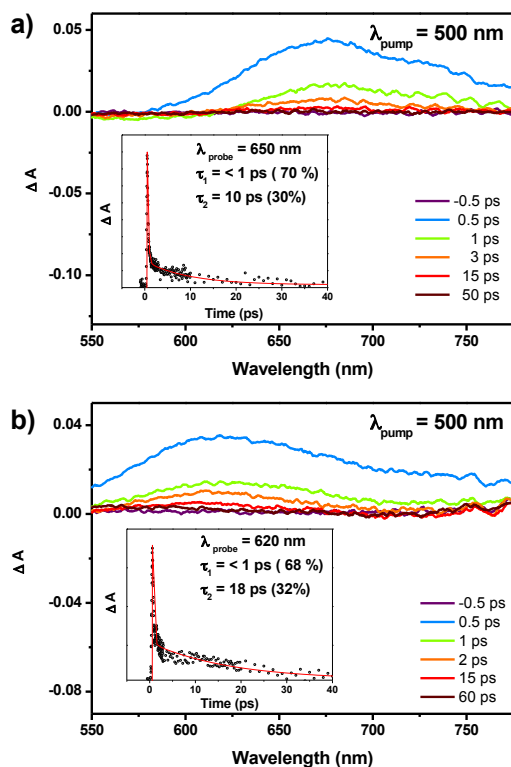


Figure 22. Femtosecond transient absorption spectra of (a) **4** and (b) **7** in CH_2Cl_2 . The insets show representative decay profiles of **4** and **7**, respectively.

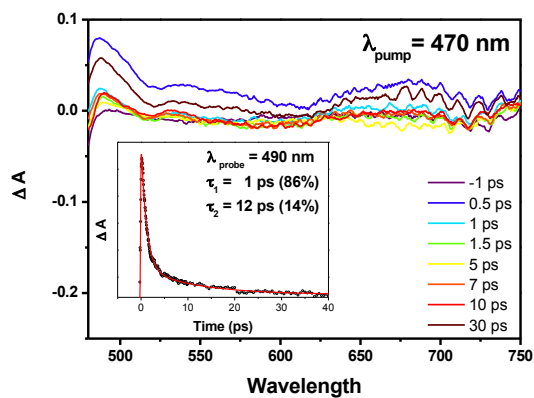


Figure 23. Femtosecond transient absorption spectra of **5** in CH_2Cl_2 . The inset shows the representative decay profile of **5**.

than their $[4n+2]\pi$ aromatic congeners. The TD-DFT results of **4** and **7** clearly demonstrate the existence of forbidden states (S and D) beyond 1000 nm (Table 3). In light of these photophysical characteristics, the fast deactivation dynamics (< 1 ps) are consistent with the internal conversion time from the higher excited state to the lowest dark state and the second deactivation process with 10~18 ps lifetimes corresponds to the decay of the lowest dark state.

The relaxation dynamics of 17π [(TPTBP)Cu^{II}]⁺[SbF₆]⁻ (**5**), which exhibits cation radical characteristics, was also investigated (Figure 23). Biexponential decays were observed in the fs-TA measurements with the time constants of 1 and 12 ps. It is worth noting that the overall excited state dynamics of **5** exhibits significantly faster decay than that of the heteroaromatic 18π complex (**3**). Interestingly, the mono radical cation species of meso-free hexaphyrin also had a shorter lifetime than that of the neutral species due to the greater density of the states, which results from the presence of the singly occupied molecular orbital.^[25] Additionally, the electrochemically oxidized [(TPP)Zn^{II}]⁺ cation radical exhibits faster relaxation dynamics with a lifetime of ca. 17 ps due to the smaller energy gap between the lowest excited and ground states.^[26] The 17π species has a greater density of the states than the 18π complex due to the states associated with the additional $\pi \rightarrow \pi$, MLCT, and $\pi \rightarrow \pi^*$ bands in the absorption spectrum. Furthermore, in TD-DFT calculations, the lowest excited band of **5**, arising from $s_- \rightarrow s_+$ transition (Table 3), lies at 1635 nm. It is safe to conclude, therefore, that the non-radiative deactivation dynamics of **5** seems to arise from the combination of the greater density of the states and the small energy gap between the lowest energy excited state and the ground state of **5**. The transient absorption results of the five metallobenzoporphyrins (16, 17 and 18π) demonstrate the critical roles of the number of π -electrons and the identity of the central metal in the relaxation dynamics.

3-7. Electrochemistry and Electrosynthesis

Redox properties of the 16, 17 and 18π -electron forms of the TPTBP copper(II) complex and the 16 and 18π -electron forms of the TPTBP zinc(II) complex were examined in CH₂Cl₂ and PhCN containing 0.1 M TBAP with the goal of characterizing the electrochemistry and electrosynthesis of these species in nonaqueous media. UV-visible spectra of the products formed in each stepwise one-electron addition or abstraction were also elucidated as a function of applied potential in a thin-layer spectroelectrochemical cell. Examples of cyclic voltammograms (CV) for the three related Cu^{II} derivatives in CH₂Cl₂, 0.1 M TBAP are illustrated in Figure 24 which also shows the spectral changes obtained under the application of a fixed oxidizing or reducing potential to give the desired species.

(TPTBP)Cu^{II} (**3**) in CH₂Cl₂, 0.1 M TBAP undergoes two reversible one-electron oxidations at $E_{1/2} = 0.56$ and 0.86 V and two reversible one-electron reductions at $E_{1/2} = -1.18$ and -1.78 V, leading to a π -cation radical (17π), dication (16π), π -anion radical (19π) and dianion (20π), respectively. The two oxidations at positive potentials generate the 17 and 16π -electron forms of the porphyrin, transitions

which are reversible and rapid under the electrochemical conditions as judged by the well-defined cyclic voltammogram illustrated in the lower part of Figure 24. The doubly oxidized 16 π -electron $[(\text{TPTBP})\text{Cu}^{\text{II}}(\text{H}_2\text{O})]^{2+} \cdot 2[\text{SbF}_6]^-$ (**4**) exhibits three reversible one-electron reductions in CH_2Cl_2 , the first two of which are located at $E_{1/2} = 0.87$ and 0.58 V to give the 17 and 18 π -electron forms of the compound (see CV at top of Figure 24) while the singly oxidized 17 π -electron $[(\text{TPTBP})\text{Cu}^{\text{II}}]^+[\text{SbF}_6]^-$ (**5**) undergoes a reversible one-electron oxidation at $E_{1/2} = 0.86$ V and a reversible one-electron reduction at $E_{1/2} = 0.56$ V. The fact that potentials for the three related Cu^{II} porphyrins are identical within experimental error suggests the absence of coupled chemical reactions in the stepwise electrochemical conversion between $(\text{TPTBP})\text{Cu}^{\text{II}}$ (**3**), $[(\text{TPTBP})\text{Cu}^{\text{II}}]^+[\text{SbF}_6]^-$ (**5**) and $[(\text{TPTBP})\text{Cu}^{\text{II}}(\text{H}_2\text{O})]^{2+} \cdot 2[\text{SbF}_6]^-$ (**4**) under the given solution conditions. This is also suggested by the thin-layer spectroelectrochemical data described below.

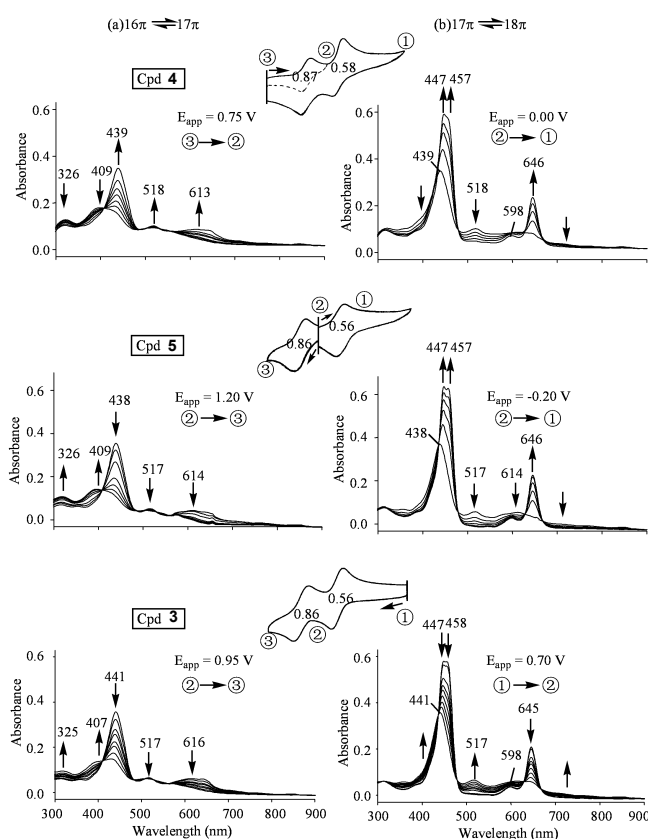


Figure 24. Cyclic voltammograms and corresponding UV-vis spectral changes for **3-5** in CH_2Cl_2 , 0.2 M TBAP during (a) the 16 π /17 π electron conversions and (b) the 17 π /18 π electron conversions at the indicated potentials where ③ gives a 16 π -electron species, ② gives a 17 π -electron species and ① gives an 18 π -electron species.

A CH_2Cl_2 solution of chemically generated $[(\text{TPTBP})\text{Cu}^{\text{II}}]^+[\text{SbF}_6]^-$ (**5**) exhibits absorptions at 438, 517 and 614 nm (see Figure 3a) and virtually the same spectral pattern is observed under conditions of the electrochemical experiments, i.e., in solutions containing 0.1 or 0.2 M TBAP (Figure 24, center). The same UV-visible spectrum is also seen after the one-electron controlled potential reduction of $[(\text{TPTBP})\text{Cu}^{\text{II}}(\text{H}_2\text{O})]^{2+} \cdot 2[\text{SbF}_6]^-$ (**4**) at 0.75 V (③ to ② in Figure 24, top left) or after the one-electron controlled potential oxidation of $(\text{TPTBP})\text{Cu}^{\text{II}}$ (**3**) at 0.70 V in the thin-layer cell (① to ② in Figure 24, bottom right).

Electrochemical generation of the 16 π -electron porphyrin from its 17 or 18 π -electron form, $[(\text{TPTBP})\text{Cu}^{\text{II}}]^+[\text{SbF}_6]^-$ (**5**) and $(\text{TPTBP})\text{Cu}^{\text{II}}$ (**3**), in CH_2Cl_2 , 0.2 M TBAP (② to ③ or ① to ② to ③ in Figure 24) also gives virtually the same UV-visible spectrum as the chemically generated $[(\text{TPTBP})\text{Cu}^{\text{II}}(\text{H}_2\text{O})]^{2+} \cdot 2[\text{SbF}_6]^-$ (**4**) in CH_2Cl_2 without TBAP although the doubly oxidized compound under the electrochemical conditions would contain one or two associated ClO_4^- counterions rather than just SbF_6^- . Thus, the potential driven conversion between the three forms of the Cu^{II} porphyrins is rapid and easily accomplished on the electrochemical timescale in CH_2Cl_2 and there is no obvious effect of supporting electrolyte on UV-visible spectra of the electrogenerated species in a given oxidation state.

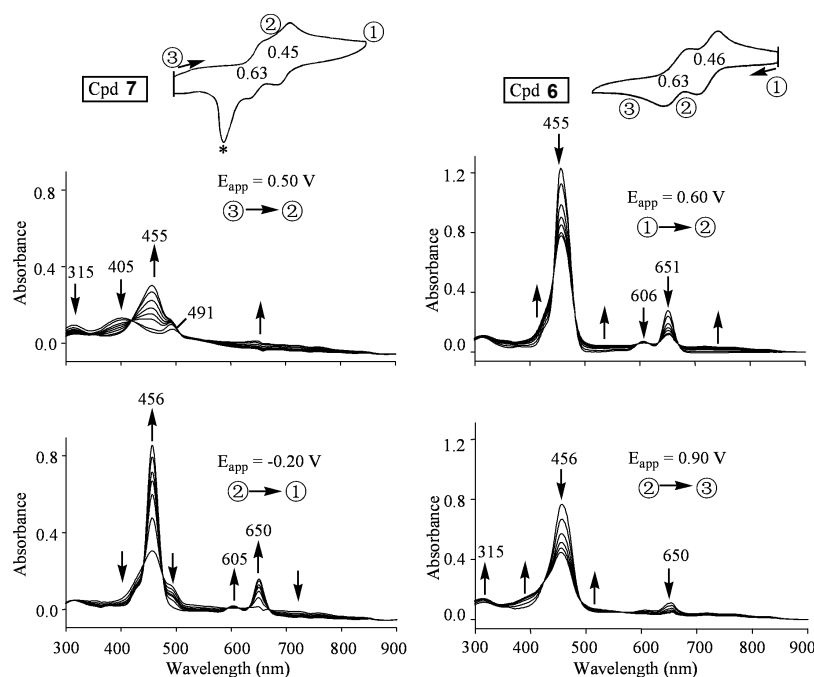


Figure 25. Cyclic voltammograms and corresponding UV-vis spectral changes during controlled potential reduction and oxidation of zinc(II) compounds **6** and **7** in CH_2Cl_2 , 0.1 M TBAP at the indicated potentials where ③ gives a 16 π -electron species, ② gives a 17 π -electron species and ① gives an 18 π -electron species. The peak marked with an asterisk in the CV of **7** is due to a surface reaction involving oxidation of H_2O from the compound.

An electrochemical conversion between 16π and 18π Zn^{II} porphyrins was also examined. Cyclic voltammetric measurements of 18π (TPTBP) Zn^{II} (**6**) and 16π [(TPTBP) $\text{Zn}^{\text{II}}(\text{H}_2\text{O})_2$] $^{2+} \cdot 2[\text{SbF}_6]^-$ (**7**) show no obvious effect of solvent or compound oxidation state on the measured half wave potentials. For example, in CH_2Cl_2 containing 0.1 M TBAP, [(TPTBP) $\text{Zn}^{\text{II}}(\text{H}_2\text{O})_2$] $^{2+} \cdot 2[\text{SbF}_6]^-$ (**7**) is reduced stepwise at $E_{1/2} = 0.63$ and 0.45 V to give (TPTBP) Zn^{II} (**6**) as a final product while **6** is stepwise oxidized at $E_{1/2} = 0.46$ and 0.63 V as shown in Figure 25 to give [(TPTBP) Zn^{II}] $^{2+}$ which contains one or two associated ClO_4^- counterions and no H_2O . Both sets of half wave potentials are shifted positively by about 100 mV upon changing the solvent from CH_2Cl_2 to PhCN, but again there is no difference between the measured $E_{1/2}$ values for reduction of the 16π -electron porphyrin ($E_{1/2} = 0.73$ and 0.52 V) or oxidation of the 18π -electron porphyrin ($E_{1/2} = 0.52$ and 0.73 V) in this solvent (see CV in Figure 26, inset). Although identical redox potentials are obtained in both solvents starting from the oxidized or reduced forms of the Zn^{II} porphyrins, this is not the case for the UV-visible spectra. As described earlier in this chapter, [(TPTBP) $\text{Zn}^{\text{II}}(\text{H}_2\text{O})_2$] $^{2+} \cdot 2[\text{SbF}_6]^-$ (**7**) reacts with the CH_2Cl_2 solvent to give a side product, possibly the singly reduced 17π -electron form of the porphyrin, having an absorption band at 489-491 nm. A spontaneous reduction of **7** also occurs in PhCN, 0.2 M TBAP but in this solvent the electrochemically examined species in solutions to which [(TPTBP) $\text{Zn}^{\text{II}}(\text{H}_2\text{O})_2$] $^{2+} \cdot 2[\text{SbF}_6]^-$ (**7**) has been added is actually

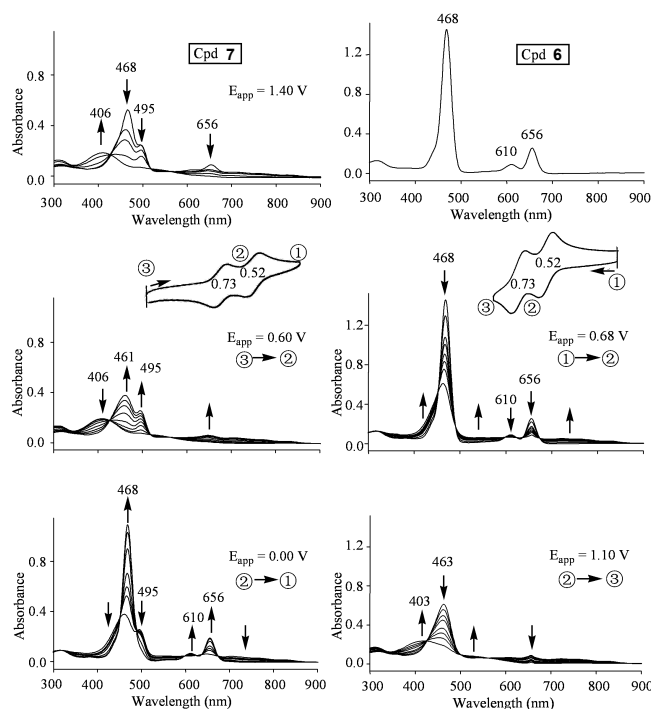


Figure 26. Cyclic voltammograms and corresponding UV-vis spectral changes for **6** and **7** in PhCN, 0.2 M TBAP where ③ gives a 16π -electron species, ② gives a 17π -electron species and ① gives an 18π -electron species.

a mixture of the singly and doubly reduced forms of the compound which would formally be the 17 and 18 π -electron porphyrins. The lack of stability of **7** in PhCN is illustrated in the top of Figure 26 where UV-vis bands for the species added to solution are seen at 468, 495 and 656 nm. The 468 and 656 nm absorptions are characteristic of the unoxidized 18 π -electron Zn^{II} porphyrin while the 495 nm band is associated with the singly oxidized 17 π -electron porphyrin.

Despite the fact that a rapid reduction of the 16 π -electron porphyrin occurs in the PhCN solutions, the desired $[(\text{TPTBP})\text{Zn}^{\text{II}}(\text{H}_2\text{O})_2]^{2+} \cdot 2[\text{SbF}_6]^-$ (**7**) could be quantitatively regenerated *in situ* by applying a fixed oxidizing potential of 1.40 V to the thin-layer cell after which conversion to the porphyrin's 17 and 18 π -electron forms could be studied under the application of a fixed reducing potential. The spectral changes associated with the quantitative *in situ* generation of $[(\text{TPTBP})\text{Zn}^{\text{II}}(\text{H}_2\text{O})_2]^{2+} \cdot 2[\text{SbF}_6]^-$ in solution are shown in the top illustration of Figure 26 where the 468, 495 and 656 nm bands disappear and a new band at 406 nm characteristic of **7** is formed under the application of the fixed oxidizing potential. Having quantitatively generated the 16 π -electron porphyrin, the applied potential was first switched to 0.60 V and then to 0.00 V to stepwise generate the 17 and 18 π -electron compounds respectively. These spectral changes are also shown in Figure 26.

A similar sequence of reactions involving a potential driven interconversion between **6** and **7** is observed in CH_2Cl_2 containing 0.1 or 0.2 M TBAP and examples of the thin-layer spectral changes at specific oxidizing or reducing potentials are shown in Figure 25. The UV-visible spectrum of **7** is characterized by a band at 315 and 405 nm but there is also a band at 491 nm associated with some reductions to the 17 π -electron form of the porphyrin.

3-8. Conclusions and Outlook

In summary, we have succeeded in synthesizing novel 16 π copper(II) and zinc(II) complexes, [(TPTBP)Cu^{II}(H₂O)]²⁺·2[SbF₆]⁻ (**4**) and [(TPTBP)Zn^{II}(H₂O)₂]²⁺·2[SbF₆]⁻ (**7**), and a 17 π -electron cation radical complex [(TPTBP)Cu^{II}]^{•+}[SbF₆]⁻ (**5**) by the controlled oxidation of the parent 18 π complexes (TPTBP)M (**3** (M = Cu^{II}) and **6** (M = Zn^{II})). The copper(II) complexes are the first series of porphyrinoid structures to be reported which have 16 to 18 π -electrons and the same atom composition. X-ray analysis revealed that the TPTBP ligand retains planarity in the 16 π state to a greater extent than the OiBTPP in the context of their metal complexes. This planarity may have led to a paratropic ring current which in turn induces greater anti-aromatic character in **7** as demonstrated by ¹H NMR spectroscopy and predicted by NICS calculations. Femtosecond transient absorption results demonstrate that the number of π -electrons and the nature of the central metal of **3-7** play a key role in determining the overall excited state relaxation dynamics of metallobenzoporphyrins. An analysis based on MCD spectroscopy and TD-DFT calculations demonstrated that the spectra of the anti-aromatic 16 π species and heteroaromatic 18 π complexes consistent with what would be anticipated on the basis of Michl's 4N and 4N+2 perimeter models. The combined electrochemical and spectroelectrochemical data of the five investigated compounds are self-consistent and indicate that reversible potential driven interconversions between the 16, 17 and 18 π -electron forms of the porphyrins may be accomplished in solutions of CH₂Cl₂ or PhCN without any apparent interference from the supporting electrolyte. Thin-layer spectroelectrochemistry can also be used as an electrosynthetic tool to quantitatively generate the porphyrin in a specifically desired oxidation state prior to in situ spectroscopic characterization which might not be otherwise possible in the absence of an applied potential.

Experimental Section

General. The melting points were measured with a Yanagimoto micro melting point apparatus and are uncorrected. Column chromatography was carried out using Merck neutral alumina 1077. The ^1H NMR (400 MHz) spectra and ^{13}C NMR (100 MHz) were recorded using a JEOL EX-400 or AL-400 spectrometer. The chemical shifts are reported (σ scale) relative to internal tetramethylsilane for ^1H spectra. The ESR spectra were acquired on a Bruker ELEXSYS E500 instrument at 85K. UV-visible absorption spectra were recorded using Shimadzu UV-2200 and Jasco V-570 spectrophotometers. The elemental analyses were performed using a Perkin-Elmer 2400 CHN elemental analyzer. Mass spectra were recorded with a Thermo Fisher Scientific model LTQ Orbitrap XL by using the ESI-TOF method in the positive ion mode with acetonitrile solution samples. Magnetic circular dichroism (MCD) spectra were recorded using a Jasco J-725 spectrodichrometer and a Jasco electromagnet that produces a magnetic field of up to 1.09 T. Tetraphenyltetrabenzoporphyrin copper(II) and zinc(II) complexes (**3** and **6**) were prepared using the literature methods.^[3, 6]

Single crystal X-ray analyses of 3-7: Single crystals of **3** and **5-7** suitable for the X-ray structural determination were mounted on a Bruker SMART APEXII CCD diffractometer and irradiated with graphite monochromated Mo-K α radiation ($\lambda = 0.71073 \text{ \AA}$) for data collection. The data were processed using the APEX program suite. Single crystals of **4** were obtained from a $\text{ClCH}_2\text{CH}_2\text{Cl}$ /hexane solution as green blocks. A single crystal of **4** with dimensions of $0.20 \times 0.10 \times 0.10 \text{ mm}$ was coated with oil (Paratone-N, Hampton Research Corp.) and mounted on a MicroMountTM (MiTeGen, LLC). Diffraction data were collected, using a RIGAKU AFC-8 diffractometer equipped with a Saturn70 CCD detector with Mo K α radiation, by an ω -scan method with 0.5° oscillation for each frame at 90 K. The X-ray was monochromated and focused by a confocal mirror. Bragg spots were integrated using the HKL2000 program package,^[27] and empirical absorption corrections (multi-scan) were applied.

The structures were solved by a direct method using the SIR2004 program,^[28] and refined by a full-matrix least squares method using the SHELXL-97 program.^[29] Anisotropic temperature factors were applied to all non-hydrogen atoms. The hydrogen atoms were placed at calculated positions, and refined applying riding models. The crystallographic data are summarized in Table 4.

Theoretical Calculations: TD-DFT calculations were carried out for the X-ray structures of $(\text{TPTBP})\text{Zn}^{\text{II}}$, $(\text{TPTBP})\text{Cu}^{\text{II}}$, $[(\text{TPTBP})\text{Cu}^{\text{II}}]^+$, $[(\text{TPTBP})\text{Zn}^{\text{II}}]^{2+}$ and $[(\text{TPTBP})\text{Cu}^{\text{II}}]^{2+}$ and for $\text{C}_{16}\text{H}_{16}$ and $\text{C}_{16}\text{H}_{16}^{2-}$ parent hydrocarbon perimeters using the B3LYP functional of the G03W^[30] software package with 6-31G(d) basis sets. NICS(0) calculations were carried out using the X-ray coordinates of **3**, **4**, **6**, **7** using the B3LYP functional of the G09W^[31] software package with 6-31G(d) basis sets.

Time Correlated Single Photon Counting Measurements. Time-resolved fluorescence lifetime experiments were performed by the time-correlated single photon counting (TCSPC) and femtosecond fluorescence up-conversion techniques. In the TCSPC system, we used a mode-locked Ti:sapphire laser (Spectra Physics, MaiTai BB) which provides ultrashort pulse (80 fs at full width half maximum, fwhm) with high repetition rate (80 MHz) as an excitation light source. This high repetition rate was slowed to 1M ~ 800 kHz using a homemade pulse-picker. The pulse-picked output was frequency-doubled with a BBO crystal with a thickness of 1 mm (EKSMA). The fluorescence was collected by a microchannel plate photomultiplier (MCP-PMT, Hamamatsu, R3809U-51) with a thermoelectric cooler (Hamamatsu, C4878) connected to a TCSPC board (Becker&Hickel SPC-130). The overall instrumental response function was about 25 ps (fwhm). A vertically polarized pump pulse by a Glan-laser polarizer was used to irradiate the samples, and a sheet polarizer, set at an angle complementary to the magic angle (54.7°), was placed in the fluorescence collection path to obtain polarization-independent fluorescence decays. Deconvolution fitting was performed using the vfit software package (version 2.02)

Femtosecond Transient Absorption Measurements. A femtosecond time-resolved transient absorption (TA) spectrometer pumped by a Ti:sapphire regenerative amplifier system (Quantronix, Integra-C) operating at 1 kHz repetition rate and an optical detection system were used. The frequency doubled 400 nm pulses had a pulse width of ~ 100 fs and an average power of 1 mW which were used as pump pulses. White light continuum (WLC) probe pulses were generated using a sapphire window (2 mm of thickness) by focusing of a small portion of the fundamental 800 nm pulses. The time delay between the pump and probe beams was carefully controlled by making the pump beam travel along a variable optical delay (Newport, ILS250). Intensities of the spectrally dispersed WLC probe pulses were monitored by a miniature spectrograph (OceanOptics, USB2000+). To obtain the time-resolved transient absorption difference signals (ΔA) at a specific time, the pump pulses were chopped at 25 Hz and absorption spectra intensities were saved alternately with or without a pump pulse. Typically, 6000 pulses were used to excite samples to obtain the TA spectra at a particular delay time. The polarization angle between the pump and probe beams was set at the magic angle (54.7°) in order to prevent polarization-dependent signals. The cross-correlation fwhm in the pump-probe experiments was less than 200 fs and the chirp of the WLC probe pulses was determined to be 800 fs in the 400-800 nm region. To minimize the chirp, all reflection optics in the probe beam path were used with a quartz cell having a 2 mm path length. The three-dimensional data sets of ΔA versus time and wavelength were subjected to singular value decomposition and global fitting using the Surface Explorer software to obtain the kinetic time constants and their associated spectra.

Electrochemical and Spectroelectrochemical Measurements. Dichloromethane (CH_2Cl_2) was purchased from EMD Chemicals and used as received for electrochemistry and spectroelectrochemistry experiments. Benzonitrile (PhCN) was obtained from Aldrich Co. and distilled over P_2O_5 under vacuum prior to use. High purity N_2 from Tri-gas was used to deoxygenate the solution before each electrochemical and spectroelectrochemical experiment. Tetra-*n*-butylammonium perchlorate (TBAP, 99%) from Fluka Chemika Co. was used as supporting electrolyte (0.1 M for cyclic voltammetry and 0.2 M for spectroelectrochemistry) and stored under vacuum at 40 °C prior to use.

Cyclic voltammetry was performed with an EG&G Model 173 Potentiostat coupled to an EG&G Model 175 Universal Programmer. Current-voltage curves were recorded on an EG&G Princeton Applied Research model R-0151 X-Y recorder. A three-electrode system was used, consisting of a glassy carbon working electrode, a platinum counter electrode and a saturated calomel reference electrode (SCE). UV-visible spectroelectrochemical experiments were carried out with a home made thin-layer cell^[32] which has a light-transparent platinum gauze working electrode. The applied potential was monitored with an EG&G Model 173 potentiostat and UV-visible spectra were recorded on a Hewlett-Packard Model 8453 diode array spectrophotometer.

Synthesis of $[(\text{TPTBP})\text{Cu}^{\text{II}}(\text{H}_2\text{O})]^{2+} \cdot 2[\text{SbF}_6]^-$ (**4**)

Under Ar, silver hexafluoroantimonate (52 mg, 0.15 mmol) was added to a solution of **3** (40 mg, 0.046 mmol) in dry CH_2Cl_2 (2 mL) at rt in a reaction vessel shielded from ambient light. The resulting solution was stirred for 30 min at rt. The metallic Ag that formed was removed by filtration under N_2 and then the solution was concentrated by applying a flow of N_2 to afford **4** (48 mg, 0.036 mmol, 78%) as a brown solid. Single crystals suitable for X-ray crystallography were obtained by recrystallization from hexane/1,2-dichloroethane at -4 °C. M.p. > 300 °C; UV/Vis (CH_2Cl_2): λ_{max} (log ϵ): 328 (4.27), 410 (4.40), 540 (4.03) nm; elemental analysis calcd (%) for $\text{C}_{60}\text{H}_{36}\text{N}_4\text{CuF}_{12}\text{Sb}_2 + 2\text{C}_2\text{H}_4\text{Cl}_2$: C 49.72, H 2.87, N 3.62; found: C 49.37; H 2.49; N 3.64.

Synthesis of $[(\text{TPTBP})\text{Cu}^{\text{II}}]^{+}[\text{SbF}_6]^-$ (**5**)

Under Ar, silver hexafluoroantimonate (35 mg, 0.10 mmol) was added to a solution of **3** (50 mg, 0.057 mmol) in dry CH_2Cl_2 (5 mL) at rt in a reaction vessel shielded from ambient light. The resulting solution was stirred for 30 min at rt. The metallic Ag that formed was removed by filtration and then the solution was evaporated to give **5** quantitatively as a green solid stable to air. Single crystals suitable for X-ray crystallography were obtained by recrystallization from ether/ CH_2Cl_2 at rt. M.p. > 300 °C; UV/Vis (CH_2Cl_2), λ_{max} (log ϵ): 438 (4.94), 517 (4.30), 614 nm (4.22); elemental analysis calcd (%) for $\text{C}_{60}\text{H}_{36}\text{N}_4\text{CuF}_{12}\text{Sb}_2 + \text{C}_4\text{H}_{10}\text{O}$: C 61.41, H 3.81, N 4.41; found: C 61.42, H 3.89, N 4.15.

Synthesis of $[(\text{TPTBP})\text{Zn}^{\text{II}}(\text{H}_2\text{O})_2]^{2+} \cdot 2[\text{SbF}_6]^-$ (7**)**

Under Ar, silver hexafluoroantimonate (45 mg, 0.13 mmol) was added to a solution of **6** (20 mg, 0.023 mmol) in dry CH_2Cl_2 (3 mL) at rt in a reaction vessel shielded from ambient light. The resulting solution was stirred for 30 min at rt. The metallic Ag that formed was removed by filtration under N_2 and then the solution was concentrated by applying a flow of N_2 to afford **7** (17 mg, 0.012 mmol, 54%) as a brown solid. Single crystals suitable for X-ray crystallography were obtained by recrystallization from hexane/ CH_2Cl_2 at -4°C . M.p. $> 300^\circ\text{C}$; ^1H NMR (CD_2Cl_2): $\delta = 7.62$ (m, 4H; *p*-Ph), 7.51 (m, 16H; *o*-Ph, *m*-Ph), 7.02 (m, 8H; benzo), 6.22 ppm (m, 8H; benzo); UV/Vis (CH_2Cl_2): λ_{max} (log ϵ): 316 (4.25), 407 (4.37), 510 nm (3.94); ^{13}C NMR (CD_2Cl_2): 127.3 (CH), 130.2 (CH), 130.3 (CH), 130.9 (CH), 131.9 (CH), 134.4 (C), 138.4 (C), 139.5 (C), 165.9 (C); HR-MS(ESI): calcd. for $\text{C}_{60}\text{H}_{36}\text{N}_4\text{Zn}^{\text{II}} [\text{M}]^{2+}$ 438.1116, found 438.1120.

2D H-H COSY of TPTBP zinc(II) complexes

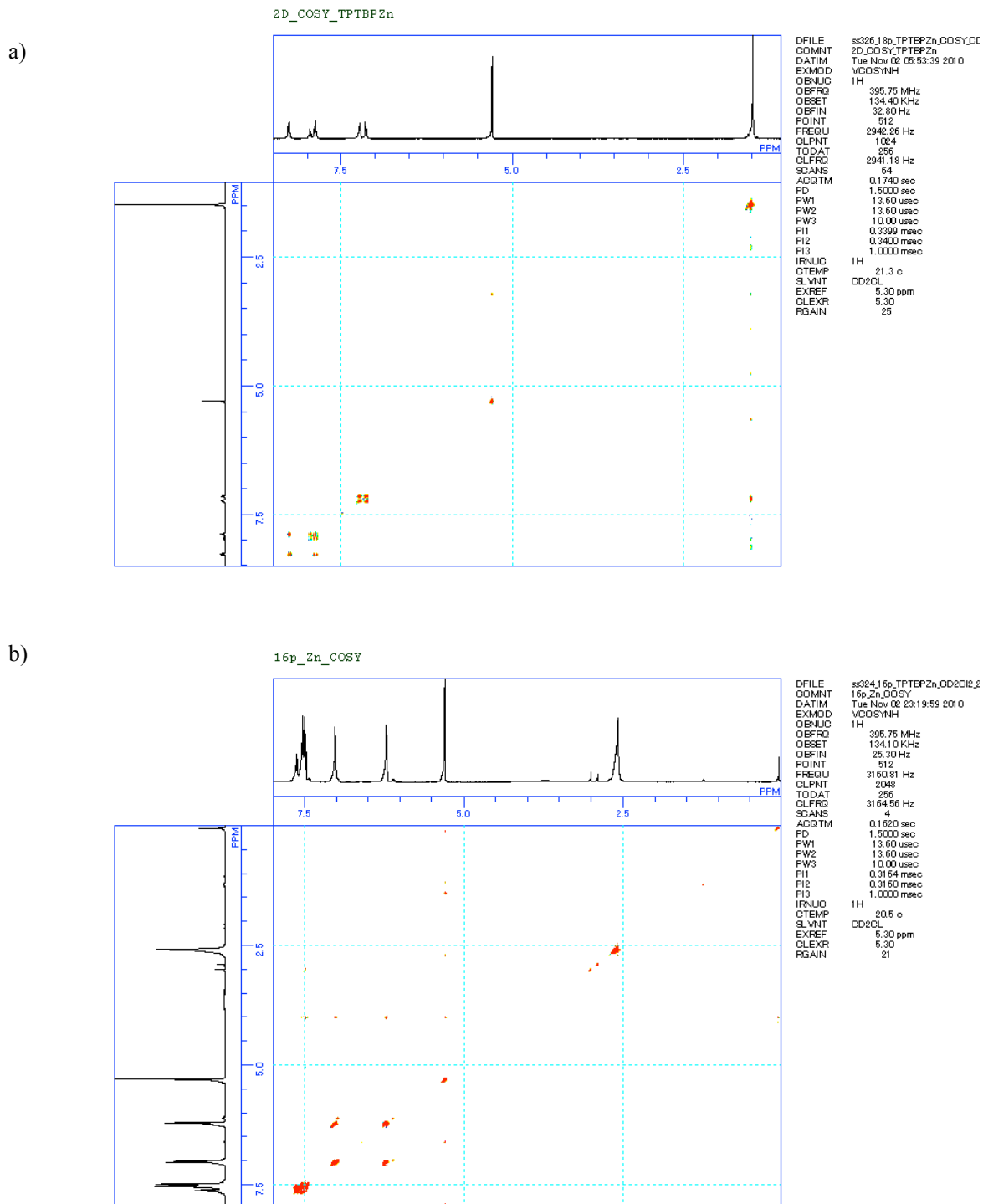


Figure 27. H-H COSY of a) 18π (TPTBP) Zn^{II} (**6**) and b) 16π [(TPTBP) $Zn^{II}(H_2O)_2$] $^{2+} \cdot 2[SbF_6]^-$ (**7**) in CD_2Cl_2 .

Table 4. Crystallographic data for **3-7**.^[a]

	3 ·1.06CH ₂ Cl ₂ ·0.22CH ₃ OH	4 ·ClCH ₂ CH ₂ Cl	5 ·2.28C ₄ H ₁₀ O	6 ·CH ₂ Cl ₂ ·3CH ₃ OH	7 ·2CH ₂ Cl ₂ ·H ₂ O
Formula	C _{61.28} H ₃₉ Cl _{2.13} CuN ₄ O _{0.22}	C ₆₂ H ₄₂ Cl ₂ CuF ₁₂ N ₄ OSb ₂	C _{67.53} H _{55.62} CuF ₆ N ₄ O _{2.28} Sb	C ₆₅ H ₅₄ Cl ₂ ZnN ₄ O ₄	C ₆₂ H ₄₆ Cl ₄ ZnF ₁₂ N ₄ O ₃ Sb ₂
Mol wt	973.88	1464.94	1258.92	1091.39	1573.70
Crystal system	triclinic	monoclinic	monoclinic	monoclinic	monoclinic
Space group	<i>P</i> =1	<i>P</i> c	<i>P</i> 2 ₁ / <i>a</i>	<i>P</i> 2 ₁ / <i>n</i>	<i>P</i> 2 ₁ / <i>c</i>
Color	blue–green	green	black	green	blown
Habit	plate	block	plate	plate	plate
Cryst dims, mm	0.07 x 0.06 x 0.02	0.20 x 0.10 x 0.10	0.18 x 0.10 x 0.04	0.17 x 0.14 x 0.02	0.16 x 0.10 x 0.03
<i>a</i> , Å	12.667(3)	9.93910(10)	14.0532(13)	19.678(2)	15.716(2)
<i>b</i> , Å	14.497(3)	10.0044(2)	35.488(4)	10.8211(13)	25.870(4)
<i>c</i> , Å	28.971(6)	28.0850(5)	11.3015(15)	25.221(3)	17.121(2)
α , deg	80.544(3)	90	90	90	90
β , deg	78.307(3)	90.9288(8)	94.7040(10)	91.0380(10)	114.8430(10)
γ , deg	65.248(3)	90	90	90	90
<i>V</i> , Å ³	4712.1(17)	2792.26	5617.2(11)	5369.6(11)	6316.7(15)
<i>Z</i>	4	2	4	4	4
<i>D</i> _{calc} , g cm ^{−3}	1.373	1.742	1.489	1.350	1.655
Abs coeff, mm ^{−1}	0.631	1.522	0.931	0.611	1.478
<i>F</i> (000)	2007	1446	2564	2272	3112
Temp, K	173(2)	90	173(2)	173(2)	173(2)
Reflections	22532	64233	30980	29647	35364
Independent	16723	16160	12569	12156	14343
<i>R</i> _{int}	0.0664	0.0542	0.0380	0.0351	0.0344
Parameters	1348	806	818	752	964
<i>R</i> ₁ [<i>I</i> > 2σ(<i>I</i>)]	0.0854	0.0484	0.0721	0.0529	0.064
<i>wR</i> ₂ (all data)	0.2372	0.1221	0.1757	0.1568	0.2158
Goodness of fit	1.022	1.080	1.093	1.037	1.08
solv for crystallization	<i>n</i> –hexane/CH ₂ Cl ₂	<i>n</i> –hexane/ClCH ₂ CH ₂ Cl	ether/CH ₂ Cl ₂	CH ₃ OH/CH ₂ Cl ₂	<i>n</i> –hexane/CH ₂ Cl ₂

[a] These crystals contained solvent molecules in the crystal lattice (**3**: CH₂Cl₂, **4**: 1,2-dichloroethane, **5**: diethyl ether, **6**: CH₂Cl₂ and CH₃OH, **7**: CH₂Cl₂ and H₂O).

References

- [1] a) Y. Yamamoto, A. Yamamoto, S. Furuta, M. Horie, M. Kodama, W. Sato, K.-y. Akiba, S. Tsuzuki, T. Uchimar, D. Hashizume, F. Iwasaki, *J. Am. Chem. Soc.* **2005**, *127*, 14540-14541; b) Y. Yamamoto, Y. Hirata, M. Kodama, T. Yamaguchi, S. Matsukawa, K.-y. Akiba, D. Hashizume, F. Iwasaki, A. Muranaka, M. Uchiyama, P. Chen, K. M. Kadish, N. Kobayashi, *J. Am. Chem. Soc.* **2010**, *132*, 12627-12638.
- [2] O. S. Finikova, A. V. Cheprakov, I. P. Beleskaya, P. J. Carroll, S. A. Vinogradov, *J. Org. Chem.* **2004**, *69*, 522-535.
- [3] N. G. Connelly, W. E. Geiger, *Chem. Rev.* **1996**, *96*, 877-910.
- [4] M. W. Renner, K. M. Barkigia, Y. Zhang, C. J. Medforth, K. M. Smith, J. Fajer, *J. Am. Chem. Soc.* **1994**, *116*, 8582-8592.
- [5] a) S. Ito, T. Murashima, H. Uno, N. Ono, *Chem. Commun.* **1998**, 1661; b) S. Ito, N. Ochi, T. Murashima, H. Uno, N. Ono, *Heterocycles* **2000**, *52*, 399-411; c) T. Okujima, N. Komobuchi, H. Uno, N. Ono, *Heterocycles* **2006**, *67*, 255-267.
- [6] M. W. Renner, R.-J. Cheng, C. K. Chang, J. Fajer, *J. Phys. Chem.* **1990**, *94*, 8508-8511.
- [7] In the unit cell, there are two independent molecules having two different conformations of 18π (TPTBP)Cu^{II}.
- [8] T. Vangberg, R. Lie, A. Ghosh, *J. Am. Chem. Soc.* **2002**, *124*, 8122-8130.
- [9] J. A. Cissell, T. P. Vaid, G. P. A. Yap, *Org. Lett.* **2006**, *8*, 2401-2404.
- [10] D. Y. Dawson, J. Arnold, *J. Porphyrins Phthalocyanines* **1997**, *1*, 121-124.
- [11] M. Stępień, B. Szyszko, L. Latos-Grażyński, *J. Am. Chem. Soc.* **2010**, *132*, 3140-3152.
- [12] a) P. v. R. Schleyer, C. Meaerker, A. Dransfeld, H. Jiao, N. J. R. v. E. Hommes, *J. Am. Chem. Soc.* **1996**, *118*, 6317-6318; b) K. M. Cyrański, T. M. Krygowski, M. Wisiorowski, N. J. R. v. E. Hommes, P. v. R. Schleyer, *Angew. Chem.* **1998**, *110*, 187-190; *Angew. Chem. Int. Ed.* **1998**, *37*, 177-180.
- [13] M. Gouterman, in *The Porphyrins* (Eds.; D. Dolphin), Academic Press, New York, **1978**, Vol. III, Part A, pp 1-165.
- [14] a) J. Michl, *J. Am. Chem. Soc.* **1978**, *100*, 6801-6811; b) J. Michl, *J. Am. Chem. Soc.* **1978**, *100*, 6812-6818; c) J. Michl, *Pure Appl. Chem.* **1980**, *52*, 1549-1563.
- [15] J. Mack, M. J. Stillman, N. Kobayashi, *Coord. Chem. Rev.* **2007**, *251*, 429-453.
- [16] J. Mack, Y. Asano, N. Kobayashi, M. J. Stillman, *J. Am. Chem. Soc.* **2005**, *127*, 17697-17711.
- [17] a) U. Höweler, J. W. Downing, J. Fleischhauer, J. Michl, *J. Chem. Soc., Perkin Trans. 2* **1998**, 1101-1117; b) J. Fleischhauer, U. Höweler, J. Michl, *Spectrochim. Acta A* **1999**, *55*, 585-606; c) J. Fleischhauer, U. Höweler, J. Michl, *J. Phys. Chem. A* **2000**, *104*, 7762-7775.
- [18] G. V. N. Rajapakse, A. V. Soldatova, M. A. J. Rodgers, *J. Phys. Chem. B*, **2010**, *114*,

14205-14213.

- [19] P. Chen, I. V. Tomov, A. S. Dvornikov, M. Nakashima, J. F. Roach, D. M. Alabran, P. M. Rentzepis, *J. Phys. Chem.*, **1996**, *100*, 17507-17512.
- [20] P. Kim, J. Sung, H. Uoyama, T. Okujima, H. Uno, D. Kim, *J. Phys. Chem. B*, **2011**, *115*, 3784-3792.
- [21] H. Song, J. A. Cisell, T. P. Vaid, D. J. Holten, *J. Phys. Chem. B* **2007**, *111*, 2138-2142.
- [22] S. Cho, Z. S. Yoon, K. S. Kim, M.-C. Yoon, D.-G. Cho, J. L. Sessler, D. Kim, *J. Phys. Chem. Lett.*, **2010**, *1*, 895-900.
- [23] B. Lament, J. Dobkowski, J. L. Sessler, S. J. Weghorn, J. Waluk, *Chem.-Eur. J.* **1999**, *5*, 3039-3045.
- [24] M. Yoon, S. Cho, M. Suzuki, A. Osuka, D. Kim, *J. Am. Chem. Soc.* **2009**, *131*, 7360-7367.
- [25] T. Koide, G. Kashiwazaki, M. Suzuki, K. Furukawa, M.-C. Yoon, S. Cho, D. Kim, A. Osuka, *Angew. Chem., Int. Ed.* **2008**, *47*, 9661-9665.
- [26] A. N. Okhrimenko, A. V. Gusev, M. A. J. Rodgers, *J. Phys. Chem. A* **2005**, *109*, 7653-7656.
- [27] Z. Otwinoski, W. Minor, Processing of X-ray Diffraction Data Collected in Oscillation Mode, *Methods in Enzymol.* **1997**, *276*, 307-326
- [28] M. C. Burla, R. Caliendo, M. Camalli, B. Carrozzini, G. L. Casciaro, L. De Caro, C. Giacovazzo, G. Polidori, R. Spagna, *J. Appl. Cryst.* **2005**, *38*, 381-388.
- [29] G. M. Sheldrick, *Acta Crystallogr. Sect. A*, **2008**, *64*, 112-122.
- [30] Gaussian 03, Revision D.01, M. J. Frisch, G.W. Trucks, H. B. Schlegel, G. E. Scuseria, M. A. Robb, J. R. Cheeseman, J. A. Montgomery, Jr., T. Vreven, K. N. Kudin, J. C. Burant, J. M. Millam, S. S. Iyengar, J. Tomasi, V. Barone, B. Mennucci, M. Cossi, G. Scalmani, N. Rega, G. A. Petersson, H. Nakatsuji, M. Hada, M. Ehara, K. Toyota, R. Fukuda, J. Hasegawa, M. Ishida, T. Nakajima, Y. Honda, O. Kitao, H. Nakai, M. Klene, X. Li, J. E. Knox, H. P. Hratchian, J. B. Cross, V. Bakken, C. Adamo, J. Jaramillo, R. Gomperts, R. E. Stratmann, O. Yazyev, A. J. Austin, R. Cammi, C. Pomelli, J. W. Ochterski, P. Y. Ayala, K. Morokuma, G. A. Voth, P. Salvador, J. J. Dannenberg, V. G. Zakrzewski, S. Dapprich, A. D. Daniels, M. C. Strain, O. Farkas, D. K. Malick, A. D. Rabuck, K. Raghavachari, J. B. Foresman, J. V. Ortiz, Q. Cui, A. G. Baboul, S. Clifford, J. Cioslowski, B. B. Stefanov, G. Liu, A. Liashenko, P. Piskorz, I. Komaromi, R. L. Martin, D. J. Fox, T. Keith, M. A. Al-Laham, C. Y. Peng, A. Nanayakkara, M. Challacombe, P. M. W. Gill, B. Johnson, W. Chen, M. W. Wong, C. Gonzalez, J. A. Pople, Gaussian, Inc., Wallingford CT, **2004**.
- [31] Gaussian 09, Revision A.02, M. J. Frisch, G. W. Trucks, H. B. Schlegel, G. E. Scuseria, M. A. Robb, J. R. Cheeseman, G. Scalmani, V. Barone, B. Mennucci, G. A. Petersson, H. Nakatsuji, M. Caricato, X. Li, H. P. Hratchian, A. F. Izmaylov, J. Bloino, G. Zheng, J. L. Sonnenberg, M. Hada, M. Ehara, K. Toyota, R. Fukuda, J. Hasegawa, M. Ishida, T. Nakajima, Y. Honda, O. Kitao, H.

Nakai, T. Vreven, J. A. Montgomery, Jr., J. E. Peralta, F. Ogliaro, M. Bearpark, J. J. Heyd, E. Brothers, K. N. Kudin, V. N. Staroverov, R. Kobayashi, J. Normand, K. Raghavachari, A. Rendell, J. C. Burant, S. S. Iyengar, J. Tomasi, M. Cossi, N. Rega, J. M. Millam, M. Klene, J. E. Knox, J. B. Cross, V. Bakken, C. Adamo, J. Jaramillo, R. Gomperts, R. E. Stratmann, O. Yazyev, A. J. Austin, R. Cammi, C. Pomelli, J. W. Ochterski, R. L. Martin, K. Morokuma, V. G. Zakrzewski, G. A. Voth, P. Salvador, J. J. Dannenberg, S. Dapprich, A. D. Daniels, O. Farkas, J. B. Foresman, J. V. Ortiz, J. Cioslowski, and D. J. Fox, Gaussian, Inc., Wallingford CT, **2009**.

[32] X. Q. Lin, K. M. Kadish, *Anal. Chem.* **1985**, 57, 1849.

Chapter 4

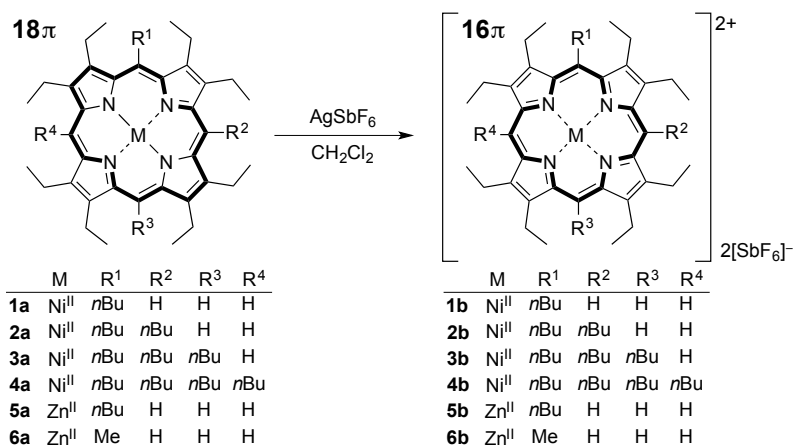
Anti-aromatic 16π Porphyrin Metal Complexes with meso-Alkyl Substituents

4-1. Introduction

As stated in Chapter 1, our 16π octaalkyltetraphenylporphyrins were rationalized to have been stabilized by deformation of the conjugated core induced by steric hindrance. Due to this insufficient conjugation, it was found that these highly distorted 16π porphyrins are essentially nonaromatic as estimated by NICS calculations.^[1] Vaid's 16π tetraphenylporphyrin lithium(I) complex, $[(\text{TPP})\text{Li}]^+[\text{BF}_4]^-$ showed the ^1H NMR signal for the protons at the β -position to be shifted to high-field ($\delta = 5.94$ ppm)^[2] relative to that of an ordinary aromatic 18π porphyrin (*e.g.* $\delta = 8.91$ for non-metal TPP^[3]). However, this chemical shift is typical of an internal alkene proton and it just indicates that this proton is part of an alkene moiety not participating in the circuit of ring current, and there is no direct experimental evidence on the electronic nature of the ring current. In order to evaluate antiaromaticity, it would be desirable to have meso-protons, since these protons are directly connected to the ring circuit and thus would be strongly affected by the property of the ring current. To this end, we decided to examine porphyrins with different numbers of alkyl groups at the meso-positions. Since higher substitution is known to deform the porphyrin plane for 18π porphyrins,^[4] we envisioned that systematic evaluation of the relationship between planarity of the 16π complexes and the degree of antiaromaticity by ^1H NMR spectroscopy would be possible. Furthermore, an increase in the number of the electron-donating alkyl groups was expected to lead to an increase in the stability of the electron-deficient 16π porphyrins and also to reduce the oxidation potentials. In this chapter, we report on the synthesis and comparison of a series of 16π -electron meso-butylated octaethylporphyrin (OEP) nickel(II) complexes, and the characterization of 16π monoalkylated OEP zinc(II) complexes (Bu and Me).

4-2. Synthesis and Characterization

18π 5-butyl, 5,10-dibutyl, 5,10,15-tributyl and 5,10,15,20-tetrabutyl OEP nickel(II) complexes **1a-4a** (Scheme 1, left), previously reported by Senge and co-workers, were prepared according to their protocol.^[4] To determine the first and second oxidation potentials of these porphyrins which were unknown, we examined their electrochemical properties by cyclic voltammetry in CH_2Cl_2 versus SCE (Figure 1). The results summarized in Table 1 reveal that the oxidation potentials clearly become lower as the number of butyl groups is increased, thereby indicating the gradual increase of electron density of the 18π -electron porphyrins. Encouraged by these results, the chemical oxidations of **1a-4a** were attempted with silver(I) hexafluoroantimonate (AgSbF_6) as the oxidant. The use of excess amounts of AgSbF_6 yielded the corresponding porphyrin nickel(II) complexes **1b-4b** with 16π -electron cores (Scheme 1). Although traces of the excess oxidants could not be completely removed, the novel 16π porphyrins could be unambiguously identified by UV-vis spectra, ^1H NMR spectra, high-resolution mass spectra (for **1b** and **2b**) and elemental analysis (for **3b** and **4b**). The UV-vis spectra of all of the 16π porphyrins showed the Soret-like bands to be highly blue-shifted compared with the 18π analogs.



Scheme 1. Oxidation of 18 π Ni^{II}-complexes **1a-4a** and Zn^{II}-complexes **5a** and **6a** with AgSbF₆ to give 16 π Ni^{II} and Zn^{II} complexes.

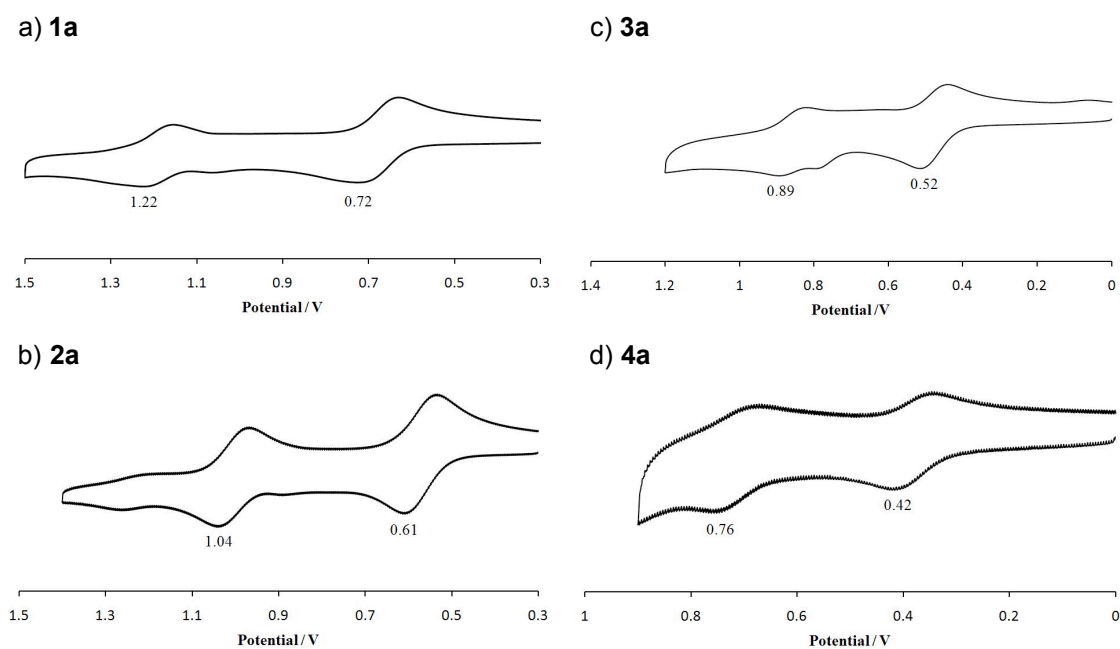


Figure 1. Cyclic voltammograms of 18 π a) monobutyl Ni^{II} complex **1a**, b) dibutyl Ni^{II} complex **2a**, c) tributyl Ni^{II} complex **3a**, d) tetrabutyl Ni^{II} complex **4a** in CH₂Cl₂ containing 0.1 M TBAPF₆.

Table 1. Oxidation potentials based on CV measurements.

compound	$E_{p, \text{ox1}} / \text{V}^{[a]}$	$E_{p, \text{ox2}} / \text{V}^{[a]}$
1a	0.72	1.22
2a	0.61	1.04
3a	0.52	0.89
4a	0.42	0.76
5a	0.64	0.85
6a	0.69	0.90

[a] First and second peak potentials (V vs SCE) in CH_2Cl_2 containing 0.1 M TBAPF₆.

To evaluate the relative stabilities of **1b-4b**, the time courses of the decomposition of the four species were monitored by UV-vis spectroscopy using highly pure CH_2Cl_2 (Figure 2). It was found that decomposition became slower as the number of butyl groups increased. Particularly, the tetra-substituted species **4b** remained essentially intact throughout the whole measurement while the mono-substituted **1b** was almost completely decomposed within 3 h. This result revealed that meso-alkyl substitution is very effective for enhancing the stability of 16π porphyrins in accordance with our expectations.

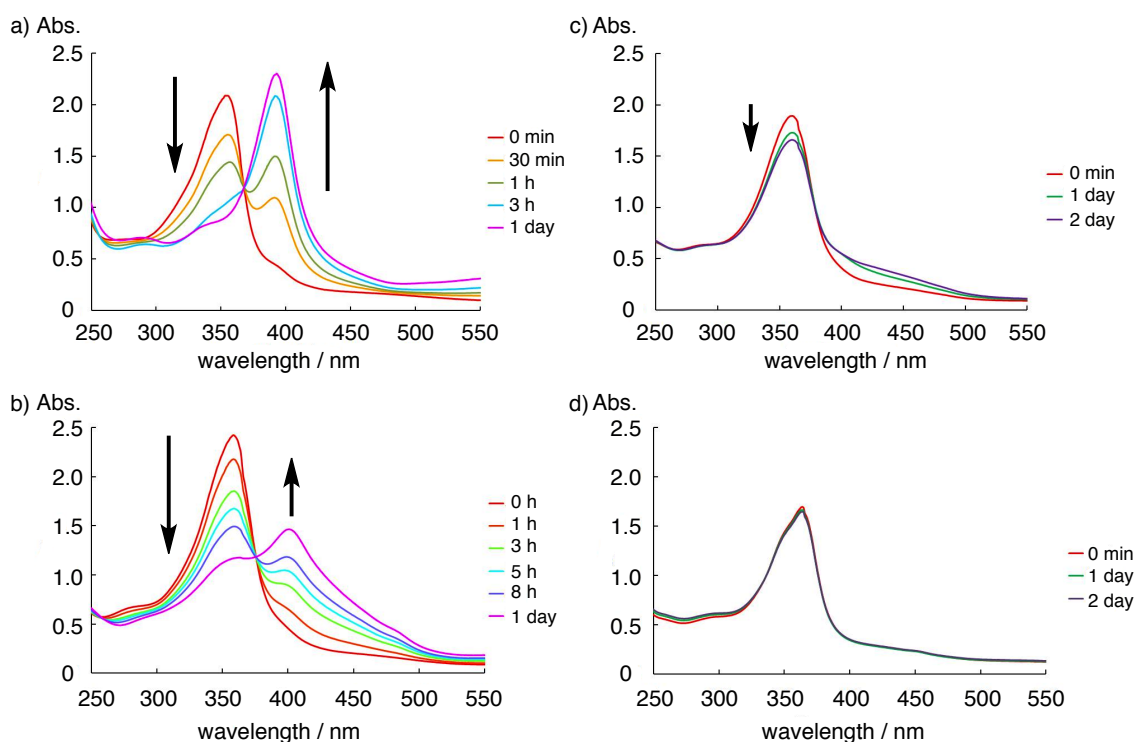


Figure 2. Time course of the decomposition of a) 16π monobutyl Ni^{II} complex **2b**, b) 16π dibutyl Ni^{II} complex **3b**, c) 16π tributyl Ni^{II} complex **3b** and d) 16π tetrabutyl Ni^{II} complex **4b** in CH_2Cl_2 monitored by UV-vis measurements at rt.

Since the structures of the 16π porphyrin nickel(II) complexes could not be determined, we decided to examine mono-alkylated OEP zinc(II) complexes. 5-Butyl and 5-methyl OEP zinc(II) complexes (**5a** and **6a**) were prepared by the reaction of the known free-base analogs^[4, 5] with zinc(II) acetate in 77% and 80% yields, respectively. The oxidation of **5a** and **6a** using AgSbF_6 gave the 16π porphyrin zinc(II) complexes **5b** and **6b** as black crystalline solids (Scheme 1). The structures of **5b** and **6b** were unambiguously determined by single-crystal X-ray diffraction analysis (Figure 3 and 4). In contrast to the 18π species, clear bond alternations of the porphyrin core are observed for both of the 16π zinc(II) complexes. However, the differences in bond lengths are smaller than those for previously reported 16π porphyrins^[1, 2] (Table 2). This suggests that the π -electrons are more delocalized in the conjugated cores of **5b** and **6b**. Table 2 shows the root-mean-square values of the deviation of each atom from the mean plane defined by the 24 core atoms (RMS value), which are indicators of the degree of overall distortion of the porphyrin core. The RMS values of **5b** and **6b** are 0.339 and 0.291, respectively. The latter is the smallest value reported so far, thereby indicating that **6b** is the most planar 16π porphyrin to date.

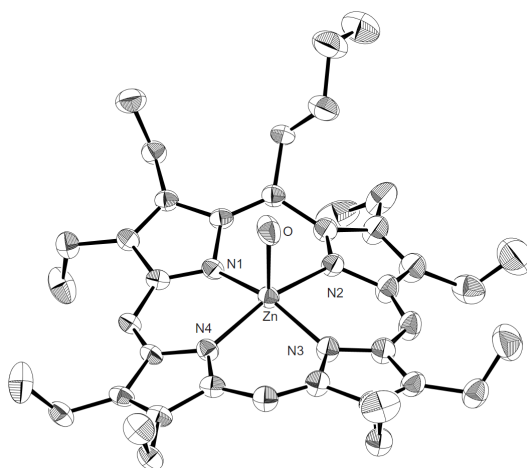


Figure 3. The ORTEP drawing of 16π monobutyl Zn^{II} complex **5b** with the thermal ellipsoids shown at the 50% probability level. All hydrogen atoms, the solvated molecules (CH_2Cl_2) and the counter anions are omitted for clarity. Selected bond lengths (\AA) and angles ($^\circ$): Zn1-N1 , 2.065(3); Zn1-N2 , 2.069(2); Zn1-N3 , 2.065(3); Zn1-N4 , 2.047(2); Zn1-O1 , 2.056(3); N1-Zn1-N2 , 86.90(10); N1-Zn1-N3 , 157.46(11); N1-Zn1-N4 , 90.04(10); N1-Zn1-O1 , 101.36(11); N2-Zn1-N3 , 88.23(10); N2-Zn1-N4 , 161.35(10); N2-Zn1-O1 , 94.40(10); N3-Zn1-N4 , 87.59(10); N3-Zn1-O1 , 100.96(11); N4-Zn1-O1 , 104.24(10).

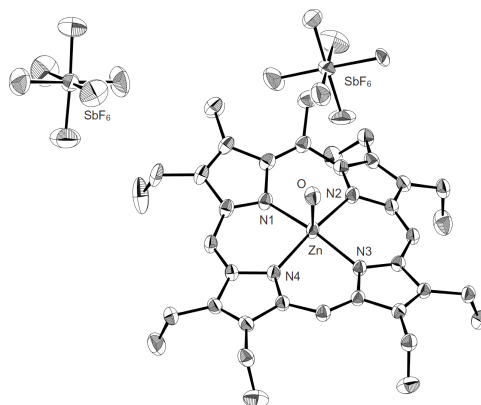
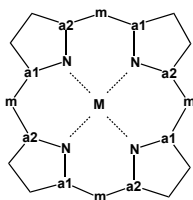


Figure 4. The ORTEP drawing of 16 π monomethyl Zn^{II} complex **6b** with the thermal ellipsoids shown at the 50% probability level. The compound was obtained as a monohydrate with the water molecule coordinated to the zinc metal. All hydrogen atoms are omitted for clarity. Selected bond lengths (Å) and angles (°): Zn1-N1, 2.067(3); Zn1-N2, 2.061(4); Zn1-N3, 2.055(3); Zn1-N4, 2.055(4); Zn1-O1, 2.085(3); N1-Zn1-N2, 89.1(1); N1-Zn1-N3, 164.8(2); N1-Zn1-N4, 90.3(1); N1-Zn1-O1, 97.9(1); N2-Zn1-N3, 88.8(1); N2-Zn1-N4, 168.5(2); N2-Zn1-O1, 97.9(1); N3-Zn1-N4, 88.7(1); N3-Zn1-O1, 97.3(1); N4-Zn1-O1, 93.6(1).

Table 2. Structural parameters of the porphyrin cores.



compound	no. of π electrons	difference of average bond distances (Å)		RMS ^[c]
		$\Delta(\text{N}-\text{C}_a)^{[a]}$	$\Delta(\text{C}_m-\text{C}_a)^{[b]}$	
5a ^[d]	18	0.001(3)	0.001(3)	0.084
6a ^[e]	18	0.007(7)	0.001(8)	0.018
5b ^[d]	16	0.090(4)	0.104(4)	0.339
6b ^[d]	16	0.087(7)	0.097(7)	0.291
[(TPP)Li] ⁺ [BF ₄] ⁻ ^[f]	16	0.092(3)	0.105(3)	0.381
OETPP ^[g]	16	0.114(3)	0.118(4)	0.836
OiBTTP ^[g]	16	0.114(3)	0.122(4)	0.921

[a] Difference in the average bond distance between N-C_{a1} and N-C_{a2}. [b] Difference in the average bond distance between C_m-C_{a1} and C_m-C_{a2}. [c] The root-mean-square of the distances of each atom from the mean plane defined by the 24 core atoms. [d] This work. [e] ref [6]. [f] ref. [2]. [g] ref. [1a].

4-3. Evaluation of Antiaromaticity

The ^1H NMR chemical shifts of the meso protons of the 18π porphyrins **1a-3a** showed progressive high field shifts with the increasing number of alkyl groups. This suggests that aromaticity decreases with increasing distortion of the ring caused by an increase in the number of alkyl-alkyl repulsions.^[4] On the other hand, a comparison of the ^1H NMR chemical shifts for the corresponding signal among 16π porphyrins **1b-3b** shows the opposite trend with lower field shifts with higher alkyl substitution. Since crystallographic analysis of the 16π porphyrin nickel(II) complexes could not be carried out, direct structural comparisons could not be carried out. However, it is reasonable to assume in analogy with the corresponding 18π porphyrins that higher alkyl substitution induces larger distortion of the porphyrin ring. Therefore, the observed trend in the chemical shift of the meso protons can be rationalized as stronger antiaromaticity being induced by higher degree of planarity of the porphyrin ring. Thus, with a highly planar porphyrin, both aromatic and anti-aromatic character appear strongly, thereby giving rise to a large difference in meso chemical shifts ($\Delta\delta$) as in the case of 18π complex **1a** and the 16π complex **1b** with $\Delta\delta = 4.85$ (Figure 5), as compared with the distorted pair of **3a** and **3b** of which the difference is reduced to only $\Delta\delta = 2.92$.

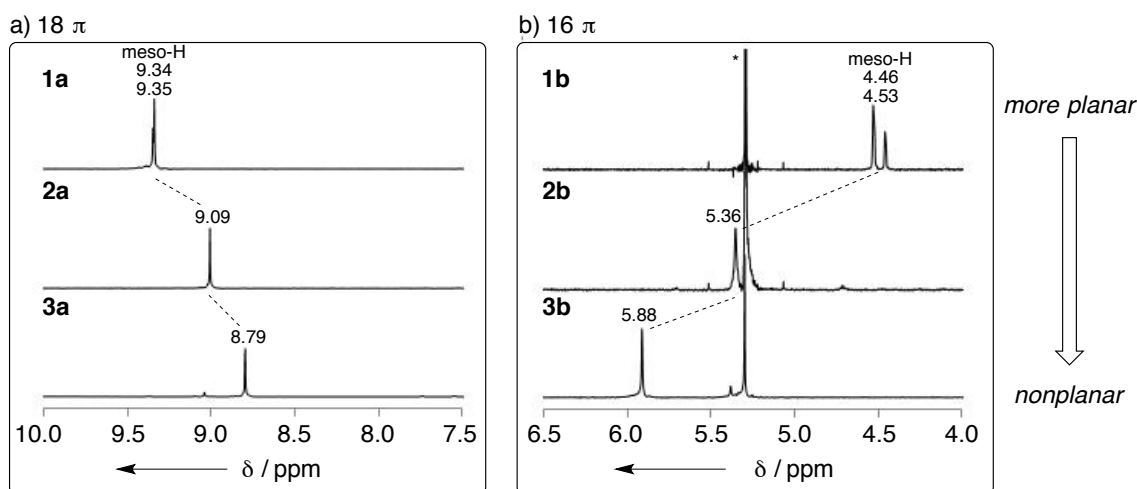
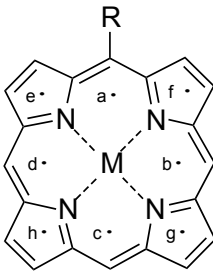


Figure 5. ^1H NMR spectra of a) 18π Ni^{II} -complexes **1a**, **2a** and **3a**, b) 16π Ni^{II} -complexes **1b**, **2b** and **3b** in CDCl_3 at rt. Signals marked with an asterisk (δ 5.26) arise from residual CH_2Cl_2 .

A comparison of the ^1H NMR signals for the meso-protons of 18π porphyrin zinc(II) complexes **5a** and **6a** with those of 16π porphyrins **5b** and **6b** also suggests strong antiaromaticity in **5b** and **6b** showing the differences in the chemical shifts to be $\Delta\delta = 4.89$ for **5a** and **5b** and $\Delta\delta = 5.14$ for **6a** and **6b**, respectively, which are comparable with the difference of $\Delta\delta = 4.85$ for the corresponding nickel(II) complexes. A comparison between **5b** and **6b** unambiguously shows that although the differences are small, here again, the more planar 16π complex is more anti-aromatic. These results are also supported by nucleus-independent chemical shift (NICS) calculations^[7] carried out at the B3LYP/6-31G* level at the centers of the square areas formed by two C–N bonds connected to the same meso carbon (point **a-d**) and at the centers of the pyrrole rings (point **e-f**) using the X-ray geometries (Table 3).^[8] In contrast to the highly distorted 16π porphyrins which have small positive values at point **a** (+2.83 for OETPP and +2.40 for OiBTTP)^[1b], the NICS values of **5b** and **6b** at this point were calculated to be significantly larger (+19.71 and +20.08), suggesting that the more planar structure induces larger positive NICS values or in other words more antiaromaticity in 16π porphyrins.

Table 3. NICS values (ppm, B3LYP/6-31G*) for porphyrins and their metal complexes.



compound	5a ^[a]	6a ^[b]	5b ^[a]	6b ^[a]
no. of π electrons	18	18	16	16
point a ^[c]	-17.22	-17.09	+19.71	+20.08
point b ^[c]	-17.19	-17.14	+19.94	+20.79
point c ^[c]	-17.17	-17.07	+20.92	+21.95
point d ^[c]	-17.00	-17.27	+20.04	+21.35
point e ^[d]	-7.31	-7.35	+3.11	+2.90
point f ^[d]	-7.19	-7.68	+6.82	+6.87
point g ^[d]	-6.43	-6.66	+5.51	+6.36
point h ^[d]	-6.78	-6.87	+6.32	+6.33

[a] Calculated using X-ray geometry. [b] Since the reported X-ray structure had disorder, the structural data was modified to give one specific structure for use in the calculations.^[6] [c] Value at the center of the square area defined by two C–N bonds connected to the same meso carbon. [d] Value at the center of the pyrrole ring.

4-4. Conclusions and Outlook

In conclusion, a series of novel meso-mono- to tetra-alkylated OEP nickel(II) complexes with 16 π -electron cores was prepared. Monitoring of the decomposition using UV-vis spectroscopy revealed that the stability of 16 π porphyrins increased as the number of the butyl groups at meso-positions increased. Especially, the 5,10,15,20-tetrabutyl OEP nickel(II) complex showed extraordinary stability. ^1H NMR spectroscopy suggested that the degree of antiaromaticity diminished with the increase of the butyl groups. The synthesis of 5-alkylated OEP 16 π zinc(II) complexes was also successful, and in these cases, X-ray analysis could be carried out. 5-Methyl OEP zinc(II) complex **6b** was found to have the most planar structure among all reported 16 π porphyrins and analysis of the series of 16 π porphyrins indicates that the degree of antiaromaticity has a strong relationship with the planarity of 16 π porphyrins.

Experimental Section

General. Melting points were measured with a Yanagimoto micro melting point apparatus and are uncorrected. Column chromatography was carried out using Merck neutral alumina 1077. ^1H NMR (400 MHz) spectra were recorded using a JEOL EX-400 or AL-400 spectrometer. The chemical shifts are reported (σ scale) from internal tetramethylsilane. UV-visible spectra were recorded using a Shimadzu UV-2200 spectrophotometer using Nacalai Tesque dichloromethane as the solvent for spectroscopic measurements. The elemental analyses were performed using a Perkin-Elmer 2400 CHN elemental analyzer. Mass spectra were measured with a Thermo Fisher Scientific model LTQ Orbitrap XL by using the ESI-TOF method in the positive ion mode with acetonitrile solution samples. Crystals suitable for the X-ray structural determination were mounted on a Bruker SMART APEXII CCD diffractometer and irradiated with graphite monochromated Mo-K α radiation ($\lambda = 0.71073 \text{ \AA}$) for data collection. The data were processed using the APEX program suite. The structures were solved by a direct method using the SIR-2004 program.^[9] Refinement on F^2 was carried out by full-matrix least-squares using the SHELXL-97 program.^[10] All non-hydrogen atoms were refined using anisotropic thermal parameters except for disordered atoms. The hydrogen atoms were included in the refinement with isotropic thermal parameters. The crystallographic data are summarized in Table 4. Cyclic voltammetric measurements were performed in CH_2Cl_2 solutions containing 0.1 M TBAPF₆ at a scan rate of 100 mV/s with an ALS1200 electrochemical analyzer. A three electrode cell, which was equipped with a glassy carbon working electrode, a saturated calomel electrode (SCE) as reference electrode, and a platinum coil counter electrode, was used.

Octaethylporphyrin(OEPH₂), 5-Butyl-OEPH₂, (5-Butyl-OEP)Ni^{II} (**1a**), (5,10-Dibutyl-OEP)Ni^{II} (**2a**), (5,10,15-Tributyl-OEP)Ni^{II} (**3a**), (5,10,15,20-Tetrabutyl-OEP)Ni^{II} (**4a**) were prepared by literature methods.^[4, 11]

Computational Details. All computations were performed using the Gaussian 09 package of programs.^[8] The B3LYP hybrid functional was used with the 6-31G* basis set. NICS values were calculated at the GIAO-B3LYP/6-31G* level of theory using the X-ray geometries.

Synthesis of 5-methyl-OEPH₂

Free base OEPH₂ (100 mg, 0.19 mmol) was dissolved in dry THF (50 mL) and the solution was cooled to 0 °C under Ar. Tetramethylethylenediamine (0.68 mL, 5.2 mmol) and methyl lithium (1.09 M in diethyl ether, 2.4 mL, 2.6 mmol) were added dropwise. The reaction mixture was stirred for 6 h at rt. The reaction mixture was quenched by the addition of a mixture of water (1.0 mL) and THF (6.0 mL) and then by a 0.06 M solution of DDQ in CH_2Cl_2 (10 mL) were added. The mixture was stirred for 30 min and filtered through neutral alumina (grade I). Chromatographic purification was achieved on alumina (grade

III) eluting with hexane/CH₂Cl₂ 1:1 (v/v). Recrystallization from CH₂Cl₂/MeOH gave 5-methyl-OEPH₂ (40 mg, 0.073 mmol, 39 %) as purple crystals. The data of this compound were identical with those of the same compound prepared by a different procedure.^[5]

General procedure for the synthesis of the zinc(II) complexes.

A suspension of the free base porphyrin and excess Zn^{II}(OAc)₂ (14 eq.) in THF (120 mL/1 mmol) was heated to reflux for 30 min. The solution was extracted with CH₂Cl₂, washed with water and brine, and then dried over Na₂SO₄. The organic layer was evaporated to give the zinc(II) complex. Recrystallization from CH₂Cl₂/MeOH gave the pure product.

(5-Butyl-OEP)Zn^{II} (5a): Single crystals suitable for X-ray crystallography were obtained by recrystallization from CH₂Cl₂/ MeOH at 0 °C. Yield. 77%. M.p. 247-250 °C; ¹H NMR (CDCl₃, 400 MHz): δ = 0.67 (3H, t, *J* = 7.3 Hz), 1.19 (2H, m), 1.54 (2H, m), 1.73-1.88 (24H, m), 3.91-4.06 (16H, m), 5.05 (2H, t, *J* = 7.3 Hz), 9.82 (1H, s), 9.93 ppm (2H, s); UV/Vis (CH₂Cl₂): λ_{max} (log ε) = 330 (4.19), 410 (5.32), 540 (3.99), 573 nm (3.84); elemental analysis calcd (%) for C₄₀H₅₂N₄Zn^{II}: C 73.43, H 8.01, N 8.56; found: C 73.55, H 7.68, N 8.47.

(5-Methyl-OEP)Zn^{II} (6a): Yield. 80%. The data of this compound were identical with those previously reported.^[5]

Synthesis of [(5-butyl-OEP)Ni^{II}]²⁺•2[SbF₆]⁻ (1b) using AgSbF₆.

Silver hexafluoroantimonate (650 mg, 1.89 mmol) was added to a solution of (5-butyl-OEP)Ni^{II} (20 mg, 0.031 mmol) in dry CH₂Cl₂ (5.0 mL) at rt under Ar. After the reaction vessel was shielded from ambient light, the solution was stirred for 5 min at rt. The metallic Ag that formed was removed by filtration under N₂ and then the solution was concentrated in vacuo to give **1b** as a brown solid. Data other than ¹H NMR and UV/Vis spectrum could not be obtained due to residues from the excess reagents that could not be completely removed and to the instability of the product. ¹H NMR (CDCl₃, 400 MHz): δ = 0.72, 0.76, 0.85 (24H, t, *J* = 8.0 Hz), 1.23 (3H, t, *J* = 7.2 Hz), 1.60-1.77 (18H, m), 2.19 (2H, m), 2.30 (2H, m), 4.46 (1H, s), 4.53 ppm (2H, s); UV/Vis (CH₂Cl₂): λ_{max} = 353 nm.

Synthesis of [(5-butyl-OEP)Ni^{II}]²⁺•2[SbCl₆]⁻ (1c) using SbCl₅.

A solution of antimony pentachloride (1.0 M solution in CH₂Cl₂, 0.19 mL, 0.19 mmol) was added to a solution of (5-butyl-OEP)Ni^{II} (30 mg, 0.046 mmol) in dry CH₂Cl₂ (3.0 mL) at rt under Ar. The solution was stirred for 10 min at rt and then concentrated in vacuo to give a crude product. After the solid was washed with dry hexane, the solvent was decanted and pumped out to give **1c** as a brown solid. M.p. 122-126 °C (decomp.); ¹H NMR (CDCl₃, 400 MHz): δ = 0.72-0.92 (24H, m), 1.22 (3H, t, *J* = 7.4 Hz),

1.63-1.82 (18H, m), 2.26 (2H, m), 2.44 (2H, m), 4.58 (1H, s), 4.61 ppm (2H, s); UV/Vis (CH_2Cl_2): λ_{max} (log ϵ) = 272 (4.30), 357 (4.37), 390 nm (4.24); HRMS (ESI): m/z : calcd for $\text{C}_{40}\text{H}_{52}\text{N}_4\text{Ni}^{\text{II}}$ $[\text{M}]^{2+}$ 323.1773; found 323.1774.

Synthesis of [(5,10-dibutyl-OEP) Ni^{II}] $^2 \cdot 2[\text{SbF}_6]^-$ (**2b**).

Silver hexafluoroantimonate (ca. 150 mg, 0.437 mmol) was added to a solution of (5,10-dibutyl-OEP) Ni^{II} (47 mg, 0.031 mmol) in dry CH_2Cl_2 (5.0 mL) at rt. After the reaction vessel was shielded from ambient light, the solution was stirred for 5 min at rt under Ar. The metallic Ag that formed was removed by filtration under N_2 and then the solution was concentrated in vacuo to give **2b** as a brown solid. M.p. $>300^\circ\text{C}$; ^1H NMR (CDCl_3 , 400 MHz): δ = 0.86, 0.90, 0.92, 0.95 (24H, t, J = 7.6 Hz), 1.17 (3H, t, J = 7.6 Hz), 1.71 (4H, sext., J = 7.6 Hz), 1.88-2.11 (16H, m), 2.22 (4H, brs), 2.51 (4H, brs), 5.36 ppm (2H, s); UV/Vis (CH_2Cl_2): λ_{max} (log ϵ) = 359 nm (4.42); HRMS (ESI): m/z : calcd for $\text{C}_{44}\text{H}_{60}\text{N}_4\text{Ni}^{\text{II}}$ $[\text{M}]^{2+}$ 351.2086; found 351.2092.

Synthesis of [(5,10,15-tributyl-OEP) Ni^{II}] $^2 \cdot 2[\text{SbF}_6]^-$ (**3b**).

Silver hexafluoroantimonate (ca. 70 mg, 0.20 mmol) was added to a solution of (5,10,15-tributyl-OEP) Ni^{II} (40 mg, 0.053 mmol) in dry CH_2Cl_2 (5.0 mL) at rt. After the reaction vessel was shielded from ambient light, the solution was stirred for 5 min at rt under Ar. The metallic Ag that formed was removed by filtration under N_2 and then the solution was concentrated in vacuo to give **3b** as a brown solid. M.p. 118-121 $^\circ\text{C}$ (decomp.); ^1H NMR (CDCl_3 , 400 MHz): δ = 0.96, 0.97, 1.00, 1.02 (24H, t, J = 8.0 Hz), 1.11, 1.13 (9H, t, J = 7.2 Hz), 1.65 (6H, sext., J = 7.2 Hz), 1.90-2.29 (22H, m), 2.72 (6H, m), 5.88 ppm (1H, s); UV/Vis (CH_2Cl_2): λ_{max} (log ϵ) = 360 nm (4.51); elemental analysis calcd (%) for $\text{C}_{48}\text{H}_{68}\text{F}_{12}\text{N}_4\text{Ni}^{\text{II}}\text{Sb}_2 + \text{CH}_2\text{Cl}_2$: C 44.71, H 5.36, N 4.26; found: C 44.73, H 5.49, N 3.95.

Synthesis of [(5,10,15,20-tetrabutyl-OEP) Ni^{II}] $^2 \cdot 2[\text{SbF}_6]^-$ (**4b**).

Silver hexafluoroantimonate (30 mg, 0.087 mmol) was added to a solution of (5,10,15,20-tetrabutyl-OEP) Ni^{II} (25 mg, 0.031 mmol) in dry CH_2Cl_2 (5.0 mL) at rt. After the reaction vessel was shielded from ambient light, the solution was stirred for 5 min at rt under Ar. The metallic Ag that formed was removed by filtration under N_2 and then the solution was concentrated in vacuo to give **4b** as a brown solid. M.p. 208-211 $^\circ\text{C}$ (decomp.); ^1H NMR (CDCl_3 , 400 MHz): δ = 0.60, 0.62 (32H, t, J = 7.2 Hz), 1.15 (8H, sext., J = 7.2 Hz), 1.50 (8H, m), 1.95 (16H, m), 2.37 ppm (8H, t, J = 7.2 Hz); UV/Vis (CH_2Cl_2): λ_{max} (log ϵ) = 363 nm (4.56); elemental analysis calcd (%) for $\text{C}_{52}\text{H}_{76}\text{F}_{12}\text{N}_4\text{Ni}^{\text{II}}\text{Sb}_2 + \text{CH}_2\text{Cl}_2$: C 46.39, H 5.73, N 4.08; found: C 46.10, H 5.62, N 3.94.

Synthesis of [(5-butyl-OEP) $\text{Zn}^{\text{II}}(\text{H}_2\text{O})$] $^2 \cdot 2[\text{SbF}_6]^-$ (**5b**).

Silver hexafluoroantimonate (ca. 30 mg, 0.087 mmol) was added to a solution of (5-butyl-OEP) Zn^{II} (23

mg, 0.035 mmol) in dry CH_2Cl_2 (5.0 mL) at rt. After the reaction vessel was shielded from ambient light, the solution was stirred for 5 min at rt under Ar. The metallic Ag that formed was removed by filtration under N_2 and then the solution was concentrated in vacuo to give **5b** as a brown solid, quantitatively. Single crystals suitable for X-ray crystallography were obtained by recrystallization from heptane/ CH_2Cl_2 at 0 °C. M.p. >300 °C; ^1H NMR (CDCl_3 , 400 MHz): δ = 0.83-0.95 (24H, m), 0.98 (3H, t, J = 7.2 Hz), 1.53 (2H, m), 1.69 (2H, m), 1.87-2.09 (16H, m), 2.31 (2H, t, J = 7.2 Hz), 4.96 (1H, s), 5.03 ppm (2H, s); UV/Vis (CH_2Cl_2): λ_{max} (log ϵ) = 342 nm (4.67); elemental analysis calcd (%) for $\text{C}_{40}\text{H}_{54}\text{F}_{12}\text{N}_4\text{Zn}^{\text{II}}\text{OSb}_2 + 2\text{CH}_2\text{Cl}_2$: C 38.40, H 4.45, N 4.26; found: C 38.14, H 4.33, N 4.19.

Synthesis of [(5-methyl-OEP)Zn^{II}(H₂O)]²⁺•2[SbF₆]⁻ (6b**).**

Silver hexafluoroantimonate (40 mg, 0.12 mmol) was added to a solution of (5-methyl-OEP)Zn^{II} (17 mg, 0.028 mmol) in dry CH_2Cl_2 (5.0 mL) at rt. After the reaction vessel was shielded from ambient light, the solution was stirred for 5 min at rt under Ar. The metallic Ag that formed was removed by filtration under N_2 and then the solution was concentrated in vacuo to give **6b** as a brown solid, quantitatively. Single crystals suitable for X-ray crystallography were obtained by recrystallization from heptane/ CH_2Cl_2 at 0 °C. M.p. >300 °C; ^1H NMR (CDCl_3 , 400 MHz): δ = 0.85-0.99 (24H, m), 1.25 (3H, s), 1.83-2.03 (16H, m), 4.84 (1H, s), 4.91 ppm (2H, s); UV/Vis (CH_2Cl_2): λ_{max} (log ϵ) = 342 nm (4.64); elemental analysis calcd. for $\text{C}_{37}\text{H}_{46}\text{F}_{12}\text{N}_4\text{Zn}^{\text{II}}\text{OSb}_2 + \text{CH}_2\text{Cl}_2$: C 39.05, H 4.14, N 4.79; found: C 38.88, H 3.96, N 4.53.

Table 4. Crystallographic data for **5a**, **5b** and **6b**.

	5a	5b ^[a]	6b
Formula	C ₄₀ H ₅₂ N ₄ Zn ^{II}	C ₄₁ H ₅₆ Cl ₂ F ₁₂ N ₄ OSb ₂ Zn ^{II}	C ₃₇ H ₄₈ F ₁₂ N ₄ OSb ₂ Zn ^{II}
Mol wt	654.23	1228.67	1101.66
Crystal system	triclinic	orthorhombic	triclinic
Space group	<i>P</i> -1	<i>P</i> 2 ₁ 2 ₁ 2 ₁	<i>P</i> -1
Color	purple	black	black
Habit	plate	block	plate
Cryst dims, mm	0.13 x 0.07 x 0.03	0.20 x 0.10 x 0.10	0.16 x 0.13 x 0.03
<i>a</i> , Å	8.6909(16)	9.0366(11)	9.625(2)
<i>b</i> , Å	14.504(3)	17.391(2)	13.283(3)
<i>c</i> , Å	15.211(3)	31.035(4)	17.357(4)
α , deg	74.690(2)	90	73.009(2)
β , deg	74.553(2)	90	78.323(3)
γ , deg	75.728(2)	90	85.285(3)
<i>V</i> , Å ³	1750.3(5)	4877.2(10)	2077.6(8)
<i>Z</i>	2	4	2
<i>D</i> _{calc} , g cm ⁻³	1.241	1.673	1.761
Abs coeff, mm ⁻¹	0.735	1.779	1.953
<i>F</i> (000)	700	2448	1092
Temp, K	173(2)	173(2)	173(2)
Reflections	9889	27829	11626
Independent	7558	11018	8924
<i>R</i> _{int}	0.0206	0.0323	0.0195
Parameters	415	613	586
<i>R</i> ₁ [<i>I</i> > 2σ(<i>I</i>)]	0.0355	0.0286	0.0467
<i>wR</i> ₂ (all data)	0.0926	0.0739	0.1286
Goodness of fit	1.063	1.013	1.071
solv for crystallization	MeOH/CH ₂ Cl ₂	<i>n</i> -heptane/CH ₂ Cl ₂	<i>n</i> -heptane/CH ₂ Cl ₂

[a] These crystals contained solvent molecules in the crystal lattice (**5b**: CH₂Cl₂).

References

- [1] a) Y. Yamamoto, A. Yamamoto, S. Furuta, M. Horie, M. Kodama, W. Sato, K. Akiba, S. Tsuzuki, T. Uchimaru, D. Hashizume, F. Iwasaki, *J. Am. Chem. Soc.* **2005**, *127*, 14540-14541; b) Y. Yamamoto, Y. Hirata, M. Kodama, T. Yamaguchi, S. Matsukawa, K. Akiba, D. Hashizume, F. Iwasaki, A. Muranaka, M. Uchiyama, P. Chen, K. M. Kadish, N. Kobayashi, *J. Am. Chem. Soc.* **2010**, *132*, 12627-12638.
- [2] J. A. Cissell, T. P. Vaid, G. P. A. Yap, *Org. Lett.* **2006**, *8*, 2401-2404.
- [3] Z. Dong, P. J. Scammells, *J. Org. Chem.* **2007**, *72*, 9881-9885.
- [4] a) W. W. Kalisch, M.O. Senge, *Angew. Chem. Int. Ed. Engl.* **1998**, *37*, 1107-1109; b) M. O. Senge, W. W. Kalisch, I. Bischoff, *Chem. Eur. J.* **2000**, *6*, 2721-2738; c) M. O. Senge, I. Bischoff, *Eur. J. Org. Chem.* **2001**, 1735-1751.
- [5] G.-Z. Wu, H.-K. Leung, W.-X. Gan, *Tetrahedron* **1990**, *46*, 3233-3244.
- [6] M. O. Senge, T. P. Forsyth, K. Smith, *Z. Kristallogr.* **1996**, *211*, 176.
- [7] a) P. v. R. Schleyer, C. Meaerker, A. Dransfeld, H. Jiao, N. J. R. v. E. Hommes, *J. Am. Chem. Soc.* **1996**, *118*, 6317-6318; b) Z. Chen, C. S. Wannere, C. Corminboueuf, R. Puchta, P. v. R. Schleyer, *Chem Rev.* **2005**, *105*, 3842-3888.
- [8] Gaussian 09, Revision A.02, M. J. Frisch, G. W. Trucks, H. B. Schlegel, G. E. Scuseria, M. A. Robb, J. R. Cheeseman, G. Scalmani, V. Barone, B. Mennucci, G. A. Petersson, H. Nakatsuji, M. Caricato, X. Li, H. P. Hratchian, A. F. Izmaylov, J. Bloino, G. Zheng, J. L. Sonnenberg, M. Hada, M. Ehara, K. Toyota, R. Fukuda, J. Hasegawa, M. Ishida, T. Nakajima, Y. Honda, O. Kitao, H. Nakai, T. Vreven, J. A. Montgomery, Jr., J. E. Peralta, F. Ogliaro, M. Bearpark, J. J. Heyd, E. Brothers, K. N. Kudin, V. N. Staroverov, R. Kobayashi, J. Normand, K. Raghavachari, A. Rendell, J. C. Burant, S. S. Iyengar, J. Tomasi, M. Cossi, N. Rega, J. M. Millam, M. Klene, J. E. Knox, J. B. Cross, V. Bakken, C. Adamo, J. Jaramillo, R. Gomperts, R. E. Stratmann, O. Yazyev, A. J. Austin, R. Cammi, C. Pomelli, J. W. Ochterski, R. L. Martin, K. Morokuma, V. G. Zakrzewski, G. A. Voth, P. Salvador, J. J. Dannenberg, S. Dapprich, A. D. Daniels, O. Farkas, J. B. Foresman, J. V. Ortiz, J. Cioslowski, D. J. Fox, Gaussian, Inc., Wallingford CT, **2009**.
- [9] M. C. Burla, R. Caliendo, M. Camalli, B. Carrozzini, G. L. Cascarano, L. De Caro, C. Giacovazzo, G. Polidori, R. Spagna, *J. Appl. Cryst.* **2005**, *38*, 381-388.
- [10] G. M. Sheldrick, *SHELX-97*; University of Göttingen: Göttingen, Germany, **1997**.
- [11] N. Ono, H. Kawamura, M. Bougauchi, K. Maruyama, *Tetrahedron* **1990**, *46*, 7483-7496.

Chapter 5

Synthesis of the Most Anti-aromatic 16π Porphyrin: An Octaethylporphyrin Zinc(II) Complex with No meso-Substituents

5-1. Introduction

As mentioned above in Chapter 4, we have revealed that the degree of antiaromaticity has a strong relationship with the planarity of the 16π porphyrins, that is, more planar 16π porphyrins have stronger anti-aromatic nature, according to nucleus-independent chemical shift (NICS) calculations on X-ray determined structures.^[1] Among a series of zinc complexes which were structurally determined in our laboratory (Figure 1), the highly distorted 16π octaisobutyltetraphenylporphyrin zinc(II) complex $[(\text{O}i\text{BTTP})\text{Zn}^{\text{II}}\text{Cl}]^+$ (**1**) showed the lowest positive value within the porphyrin ring, indicating weak antiaromaticity (RMS value = 0.888, NICS value = +4.38).^[1] In contrast, the 16π meso-monomethylated octaethylporphyrin zinc(II) complex $[5\text{-Me}(\text{OEP})\text{Zn}^{\text{II}}]^{2+}$ (**3**) was found to have the most planar structure and the strongest antiaromaticity reported thus far in terms of NICS values (RMS value = 0.291, NICS value = +21.04).^[1] Furthermore, experimental evaluation of the degree of antiaromaticity by ^1H NMR spectroscopy could be performed due to the presence of protons at the meso positions in complex **3**, and significant high-field shifts for these protons compared with those of the corresponding 18π porphyrin (average $\Delta\delta = 5.14$ ppm) could be observed.

Based upon these premises, it could be envisioned that reducing steric hindrance around the porphyrin ring would lead to higher planarity of the ring and thus induce higher antiaromaticity. This was anticipated to be achieved by using meso-substituent free octaethylporphyrin (OEP), in which steric repulsion between substituents at the meso- and β - positions has been eliminated, but at the expense of an increase in the oxidation potential of the precursor 18π porphyrin and a decrease in the stability of the target 16π porphyrin. To this end, the oxidation of the meso-substituent free octaethylporphyrin (OEP) system with strong oxidants such as SbF_5 and $\text{AgSbF}_6/\text{I}_2$ was investigated. Herein, we report on the successful synthesis of the 16π OEP zinc(II) complex and on the evaluation by ^1H NMR spectroscopy of the paramagnetic ring current to establish the novel species as the most anti-aromatic known 16π porphyrin.

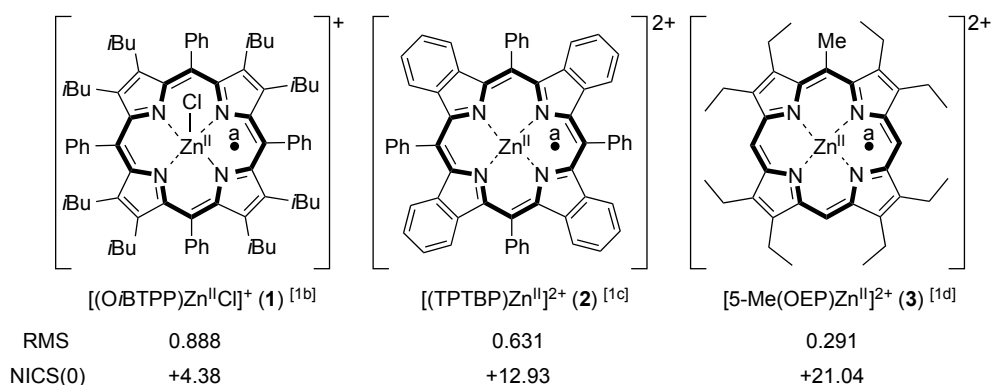
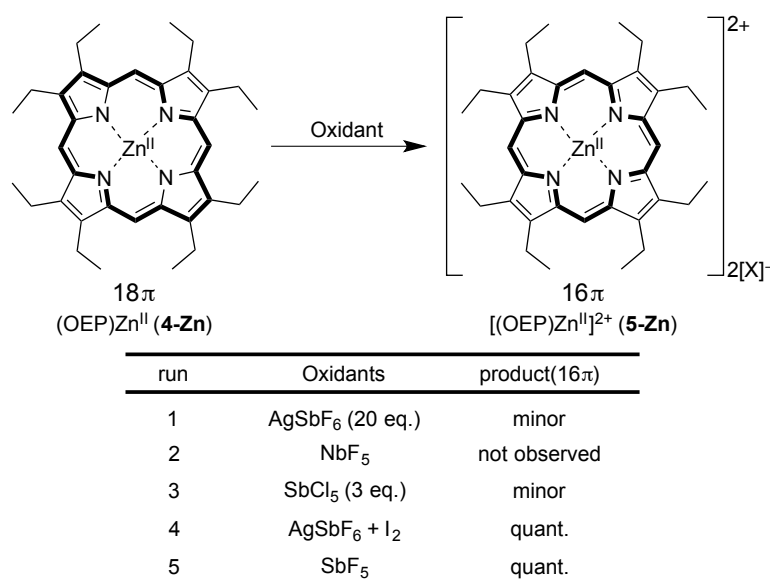


Figure 1. A series of 16π porphyrinato zinc(II) complexes and their RMS and NICS(0) values. The NICS(0) values are the average of values estimated at points a, the centers of the area defined by two C-N bonds connected to a meso carbon.

5-2. Results and Discussion

The parent 18π (OEP) H_2 (**4**) and the zinc(II) complex **4-Zn** were prepared using a literature method.^[1c, 2] To determine the first and second oxidation potentials of **4-Zn**, cyclic voltammetric measurements in CH_2Cl_2 versus SCE (SCE vs. $\text{Fc}/\text{Fc}^+ = +0.46$ V) were carried out. The cyclic voltammogram of **4-Zn** showed two reversible oxidation peaks at +0.69 V and +1.07 V. Although these oxidation potentials are slightly higher than those of 18π 5-Me(OEP) Zn^{II} (**3**) (1st and 2nd oxidation potentials: +0.69 V, +0.90 V versus SCE, respectively),^[1] this result implied that quantitative two electron oxidation of **4-Zn** would be possible with oxidants stronger than silver(I) hexafluoroantimonate (AgSbF_6) by which zinc(II) complex **3** could be oxidized to the 16π state. Encouraged by this result, the chemical oxidation of **4-Zn** was examined using strong oxidants such as $\text{AgSbF}_6/\text{I}_2$, NbF_5 , SbCl_5 and SbF_5 .^[3] Among these oxidants, the reaction with an excess amount of $\text{AgSbF}_6/\text{I}_2$ or SbF_5 gave the desired 16π porphyrin zinc(II) complex (**5-Zn**) cleanly and almost quantitatively, as determined by UV-vis spectroscopy (Scheme 1 and Figure 2). UV-vis spectroscopy has been an important method for identifying 16π porphyrins. All of the 16π porphyrins previously investigated by us and Vaid's group have been found to show a unique blue-shifted Soret-like band at around 340 nm and no Q band,^[1,4] while the parent 18π porphyrins have a Soret band at around 400 nm and a Q band at around 550-600 nm. The electronic absorption spectrum of **5-Zn** contains a band at 339 nm, which is blue-shifted compared to that of the parent 18π complex at 401 nm and is very similar to the corresponding value of ca. 340 nm for



Scheme 1. Synthesis of 16π octaethylporphyrin zinc(II) complex **5-Zn**.

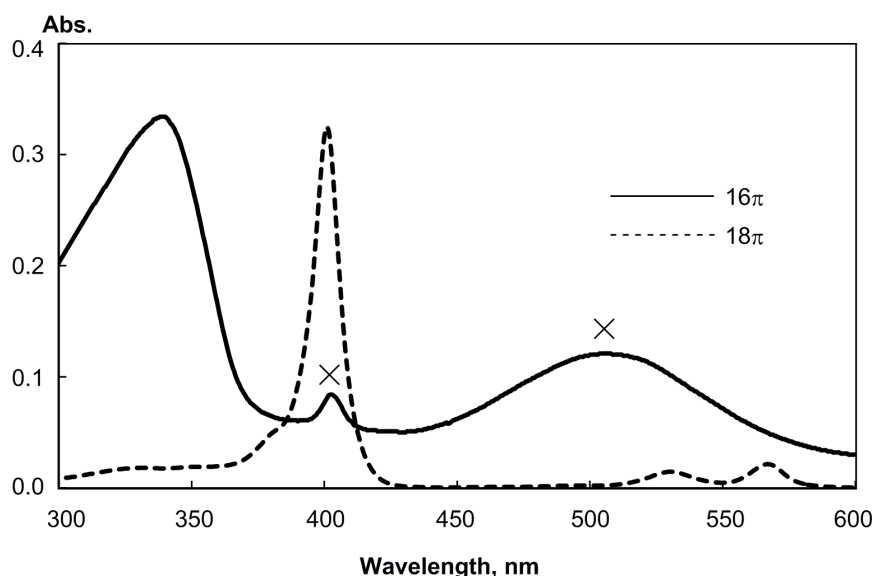


Figure 2. UV/Vis spectra of 18 π **4-Zn** and 16 π **5-Zn** in CH₂Cl₂. The absorbances denoted with an X symbol correspond to impurities (see the text). Relative intensities are arbitrary.

other 16 π porphyrins of the OEP series structurally established.^[1d] This provides proof for the formation of the 16 π porphyrin from its 18 π precursor. However, a species formed by the decomposition of the generated 16 π species with an absorption band at around 400 nm was observed along with the 16 π species in the UV-vis spectrum, indicating that **5-Zn** is very labile in solution. The broad band at 500 nm was found to be from the excess oxidants. Although we could not determine the precise identity of the product of decomposition, it is likely to be some sort of a two-electron reduced species (18 π porphyrin) and not the 17 π cation radical of (OEP)Zn^{II}, since the radical species has been shown to have a Soret-like band at 386 nm which is at shorter wavelength than that of the product of decomposition.^[5]

Unfortunately, all attempts to obtain single crystals of the 16 π species **5-Zn** suitable for X-ray analysis ended in failure due to its unstable nature. However, ¹H NMR measurements of **5-Zn** under an inert atmosphere were possible and they provided us with interesting insight on the 16 π species. In our previous work,^[1d] we investigated the relationship between antiaromaticity and planarity of a series of meso-*n*Bu substituted (OEP)Ni^{II} complexes. The ¹H NMR chemical shifts of the meso protons of the 18 π mono-*n*Bu to tri-*n*Bu porphyrins showed progressive high-field shifts with the increasing number of *n*Bu groups. This suggested that aromaticity decreases with increasing distortion of the ring caused by an increase in the number of *n*Bu-*n*Bu repulsions. On the other hand, a comparison of the ¹H NMR chemical shifts for the corresponding signal among 16 π porphyrins showed the opposite trend, with lower field shifts with higher *n*Bu substitution. The observed trend in the chemical shift of the meso protons could be rationalized as stronger antiaromaticity being induced by a higher degree of planarity of the porphyrin ring. Thus, with a highly planar porphyrin, both high aromatic (18 π) and high anti-aromatic (16 π)

character are expected, and in turn, a large difference in meso chemical shifts ($\Delta\delta$) between the 18π and the 16π states. Specifically, in the case of the highly planar 18π mono-*n*Bu complex and the corresponding 16π complex, the difference was $\Delta\delta = 4.85$, while with the highly distorted pair of tri-*n*Bu complexes, the difference was reduced to only $\Delta\delta = 2.92$. In the previously most planar and anti-aromatic 16π porphyrin **3** (RMS = 0.291, $\delta = 4.84, 4.91$ ppm), the $\Delta\delta$ with 18π 5-Me(OEP)Zn^{II} ($\delta = 9.93, 10.01$ ppm) was the largest (average $\Delta\delta = 5.14$ ppm) reported at that time. For the meso-unsubstituted OEP system here, the difference between those of **4-Zn** ($\delta = 10.11$ ppm) and **5-Zn** ($\delta = 3.55$ ppm) is $\Delta\delta = 6.56$ ppm (Figure 3), which is significantly larger than the previous maximum value of 5.14. This experimentally indicates that the 16π species **5-Zn** is the most anti-aromatic 16π porphyrin among all previously reported. Thus, **5-Zn** is speculated to be the most planar known 16π porphyrin, according to our previous findings on the relationship between planarity and antiaromaticity for 16π porphyrins.

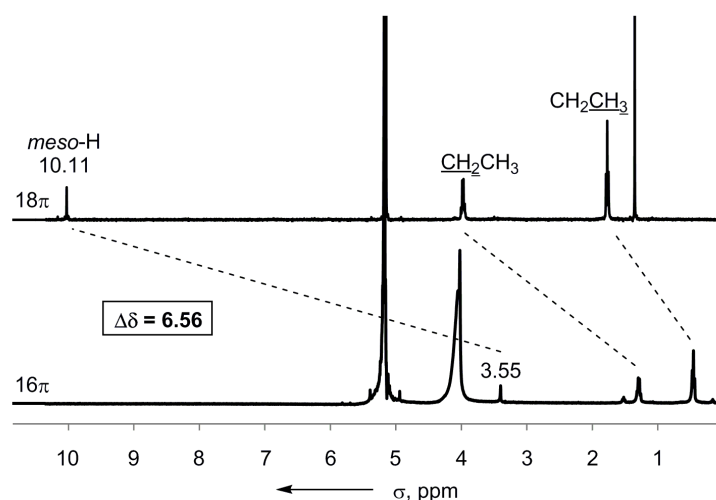
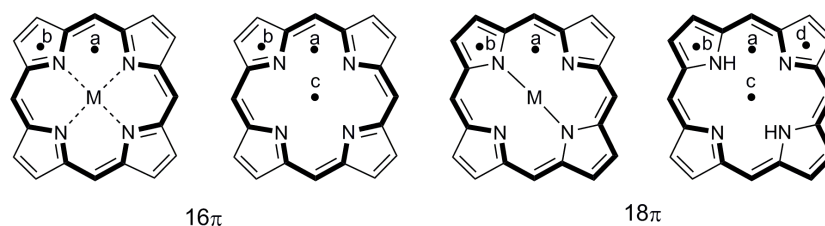


Figure 3. ¹H NMR spectra of 18π **4-Zn** and 16π **5-Zn** in CD₂Cl₂.

In order to estimate the structure of 16π **5-Zn** and to examine the effect of the central metal, DFT calculations at the B3LYP/6-31G* level^[6] were carried out for **5-Zn** and the metal-free 16π OEP, as well as their corresponding 18π species. The calculations showed the meso-unsubstituted [(OEP)Zn^{II}]²⁺ (**5-Zn**) (RMS = 0.001) to be of highly planar structure, thereby providing support for its planar structure assumed from ¹H NMR. Metal-free 16π OEP (RMS = 0.326) was calculated to be distorted compared with **5-Zn**, and thus it can be reasoned that the central Zn^{II} metal plays an important role for the planarization of the core of **5-Zn**. Nucleus-independent chemical shift (NICS(0)) calculations of [(OEP)Zn^{II}]²⁺ (**5-Zn**) and metal-free 16π OEP together with their corresponding 18π species were carried out at the centers of the areas formed by the two C-N bonds connected to the same meso-carbon (point a), at the centers of the pyrrole rings (points b and d), and at the center of the core for the metal-free species (point c; Table 1) using the calculated geometries.^[7] As was expected, the NICS(0) values were significantly larger than those of corresponding points for the previously most anti-aromatic 16π

Table 1. NICS values (ppm, B3LYP/6-31G*)



Compound	Number of π electrons	RMS value	NICS(0) value			
			point a ^[a]	point b ^[b]	point c ^[c]	point d ^[b]
$[(\text{OEP})\text{Zn}^{\text{II}}]^{2+}$ (5-Zn)	16π	0.001	+43.61	+11.32		
$[(\text{OEP})]$ (5)	16π	0.326	+15.80	+10.37	-2.62	
$(\text{OEP})\text{Zn}^{\text{II}}$ (4-Zn)	18π	0.015	-17.72	-6.33		
(OEPH_2) (4)	18π	0.018	-18.88	-11.98	-15.24	-1.51

[a] Average of the values for the centers of the area defined by two C-N bonds connected to a meso carbon. [b] Average of the values for the centers of the pyrrole rings. [c] The value of the center of the four nitrogen atoms.

porphyrin **3**. Especially noteworthy is the average value at point a where that of [(OEP)Zn^{II}]²⁺ (**5-Zn**) is +43.61 while that of **3** is +21.04.^[1d] Thus, we can conclude that **5-Zn** is the most anti-aromatic 16 π porphyrin reported thus far.

Since the metal-free 16π porphyrin would be a fascinating precursor for the introduction of various transition-metals to form novel 16π porphyrin metal complexes, we attempted the oxidation of free-base (OEP) H_2 (**4**).^[1] However, the desired metal-free 16π porphyrin could not be obtained even in the reaction with SbF_5 , with no apparent change in the UV-vis spectra, although the purple solution of **4** changed to green-brown.

5-3. Conclusions and Outlook

Based upon our previous studies, we envisioned that decreasing steric hindrance between peripheral substituents of 16π porphyrins would be effective for enhancing planarity of the porphyrin core and thus the antiaromaticity of the porphyrins. To this end, the meso-substituent free OEP system was selected as a suitable skeleton and examined. The two electron oxidation of the zinc(II) complex (OEP)Zn^{II} (**4-Zn**) was successful using an excess of strong oxidants such as AgSbF₆/I₂ and SbF₅. Although we could not determine the crystal structure of the 16π porphyrin, we were able to establish its formation by the observation of an absorbance significantly blue-shifted in the UV-vis spectra from that of the 18π precursor and agreeing well with those of previously reported 16π species. The meso-protons showed the largest high field-shift relative to its parent 18π species in ¹H NMR reported thus far, thereby suggesting that the novel species is the most anti-aromatic 16π porphyrin to date.

Experimental Section

General. All manipulations as well as ^1H NMR and UV-vis measurements were conducted under an argon atmosphere. Dichloromethane and dichloromethane- d_2 were distilled from CaH_2 . Dry hexane was purified by passing through a Glass Contour solvent dispensing system under a nitrogen atmosphere. Column chromatography was carried out using Merck neutral alumina 1077. ^1H NMR (400 MHz) spectra were recorded using a JEOL EX-400 or an AL-400 spectrometer. The chemical shifts are reported (s scale) from internal tetramethylsilane. UV-visible spectra were recorded with a Shimadzu UV-2200 spectrophotometer using Nacalai Tesque spectroscopic grade dichloromethane as the solvent for spectroscopic measurements.

Computational Details. All computations were performed using the Gaussian 09 package of programs.^[8] The B3LYP hybrid functional was used with the 6-31G* basis set. NICS values were calculated at the GIAO-B3LYP/6-31G* level of theory using the X-ray geometries.

Synthesis of $[(\text{OEP})\text{Zn}^{\text{II}}]^{2+}$ (**5-Zn**) using $\text{AgSbF}_6/\text{I}_2$

Complex **4-Zn** (5.0 mg, 0.0076 mmol), excess AgSbF_6 (54 mg, 0.16 mmol) and iodine (9.6 mg, 0.038 mmol) were placed in a Schlenk flask shielded from light and purged with Ar. Then, dry CH_2Cl_2 was added and the resulting mixture was stirred at room temperature for 30 min. The excess AgSbF_6 and iodine were filtered off under N_2 , and the solvent was evacuated to give the doubly oxidized species **5-Zn** as a brown solid containing a small amount of some unidentified product of decomposition.

Synthesis of $[(\text{OEP})\text{Zn}^{\text{II}}]^{2+}$ (**5-Zn**) using SbF_5

Under Ar, excess SbF_5 was added to a solution of **4-Zn** (19 mg, 0.028 mmol) in dry CH_2Cl_2 (10 mL) at -78°C . The mixture was stirred at this temperature for 30 min and then was allowed to warm to rt. After removal of the solvent in vacuo, the residue was washed with dry hexane under Ar at -78°C and dried to give the doubly oxidized species **5-Zn** as a brown solid. ^1H NMR (CD_2Cl_2 , 400 MHz): $\delta = 0.61$ ppm (t, 24H, $^3J = 8$ Hz), 1.44 (q, 16H, $^3J = 8$ Hz), 3.55 ppm (s, 4H); UV-vis (CH_2Cl_2): $\lambda_{\text{max}} = 339$ nm.

References

- [1] a) Y. Yamamoto, A. Yamamoto, S. Furuta, M. Horie, M. Kodama, W. Sato, K. Akiba, S. Tsuzuki, T. Uchimaru, D. Hashizume, F. Iwasaki, *J. Am. Chem. Soc.* **2005**, *127*, 14540-14541; b)– Y. Yamamoto, Y. Hirata, M. Kodama, T. Yamaguchi, S. Matsukawa, K. Akiba, D. Hashizume, F. Iwasaki, A. Muranaka, M. Uchiyama, P. Chen, K. M. Kadish, N. Kobayashi, *J. Am. Chem. Soc.* **2010**, *132*, 12627-12638; c) S. Sugawara, M. Kodama, Y. Hirata, S. Kojima, Y. Yamamoto, *J. Porphyrins Phthalocyanines* **2011**, *15*, 1326-1334; d) T. Kakui, S. Sugawara, Y. Hirata, K. Kojima, Y. Yamamoto, *Chem. Eur. J.* **2011**, *17*, 7768-7771; e) S. Sugawara, Y. Hirata, S. Kojima, Y. Yamamoto, E. Miyazaki, K. Takimiya, S. Matsukawa, D. Hashizume, J. Mack, N. Kobayashi, Z. Fu, K. M. Kadish, Y. M. Sung, K. S. Kim, D. Kim, *Chem. Eur. J.* **2012**, *18*, 3566-3581.
- [2] N. Ono, H. Kawamura, M. Bougauchi, K. Maruyama, *Tetrahedron* **1990**, *46*, 7483-7496.
- [3] a) N. G. Connelly, W. E. Geiger, *Chem. Rev.* **1996**, *96*, 877-910; b) R. Rathore, A. S. Kumar, S. V. Lindeman, J. K. Kochi, *J. Org. Chem.* **1998**, *63*, 5847-5856; c) T. Nishinaga, A. Wakamiya, D. Yamazaki, K. Komatsu, *J. Am. Chem. Soc.* **2004**, *126*, 3163-3174; d) F. Marchetti, C. Pinzino, S. Zacchini, G. Pampaloni, *Angew. Chem. Int. Ed.* **2010**, *49*, 5268-5272.
- [4] J. A. Cissel, T. P. Vaid, G. P. A. Yap, *Org. Lett.* **2006**, *8*, 2401-2404.
- [5] H. Song, R. D. Orosz, C. A. Reed, W. R. Scheidt, *Inorg. Chem.* **1990**, *29*, 4274-4282.
- [6] 8Gaussian 09, Revision A.02, M. J. Frisch, G. W. Trucks, H. B. Schlegel, G. E. Scuseria, M. A. Robb, J. R. Cheeseman, G. Scalmani, V. Barone, B. Mennucci, G. A. Petersson, H. Nakatsuji, M. Caricato, X. Li, H. P. Hratchian, A. F. Izmaylov, J. Bloino, G. Zheng, J. L. Sonnenberg, M. Hada, M. Ehara, K. Toyota, R. Fukuda, J. Hasegawa, M. Ishida, T. Nakajima, Y. Honda, O. Kitao, H. Nakai, T. Vreven, J. A. Montgomery, Jr., J. E. Peralta, F. Ogliaro, M. Bearpark, J. J. Heyd, E. Brothers, K. N. Kudin, V. N. Staroverov, R. Kobayashi, J. Normand, K. Raghavachari, A. Rendell, J. C. Burant, S. S. Iyengar, J. Tomasi, M. Cossi, N. Rega, J. M. Millam, M. Klene, J. E. Knox, J. B. Cross, V. Bakken, C. Adamo, J. Jaramillo, R. Gomperts, R. E. Stratmann, O. Yazyev, A. J. Austin, R. Cammi, C. Pomelli, J. W. Ochterski, R. L. Martin, K. Morokuma, V. G. Zakrzewski, G. A. Voth, P. Salvador, J. J. Dannenberg, S. Dapprich, A. D. Daniels, O. Farkas, J. B. Foresman, J. V. Ortiz, J. Cioslowski, D. J. Fox, Gaussian, Inc., Wallingford CT, **2009**.
- [7] a) P. R. Schleyer, C. Meaerker, A. Dransfeld, H. Jiao, N. J. R. V. E. Hommes, *J. Am. Chem. Soc.* **1996**, *118*, 6317-6318; b) Z. Chen, C. S. Wannere, C. Corminboueuf, R. Puchta, P. R. Schleyer, *Chem. Rev.* **2005**, *105*, 3842-3888.

Chapter 6

Synthesis of New Cyclic Aromatic Carbene Ligands Bearing Remote Amino Groups and Their Palladium(II) Complexes

6-1. Introduction

Since the first isolations of singlet carbenes reported by Bertrand^[1a] and Arduengo^[1b], there has been much interest in stable singlet carbenes due to their prominent coordinating ability to transition-metals. Among the variety of carbenes, mainly *N*-heterocyclic carbenes (NHCs) and their derivatives have been utilized as ligands for transition-metal catalysts.^[2] The extraordinary stability of NHCs is derived from the π -electron donation from the adjacent electron-rich nitrogen atoms into the vacant p-orbital at the carbene center.^[3] Since it has been revealed that a single adjacent nitrogen atom is enough to extensively stabilize singlet carbenes and that it might not be necessary to place heteroatoms α to the carbene carbon at all, new classes of carbenes such as “abnormal” and “remote” carbenes have been widely developed in recent years.^[4]

In relation with our recent interest in carbenes,^[5] we chose to focus on cyclic aromatic carbenes, which are also potential scaffolds for ligands for transition-metal catalysts. Previous work on cyclic aromatic carbenes, investigated as transient species by Schuster *et al.*, revealed that the ground state multiplicity (the singlet and triplet states) was dependent on the identity of the bridged heteroatom.^[6] As for metal complexes, there are a few reports on the synthesis of carbene complexes,^[7] but little is known about their structure and catalytic properties other than the catalytic ability of a sole acridinylidene palladium(II) complex.^[7c] In order to prepare isolable carbenes, we envisaged that thermodynamic stabilization by the introduction of amino groups into conjugating positions of the carbene skeleton would be appropriate (Figure 1). We also envisioned that further substitution of the aryl rings might allow for fine-tuning. Herein, we report on the synthesis of novel cyclic aromatic carbene ligands and their palladium(II) complexes.

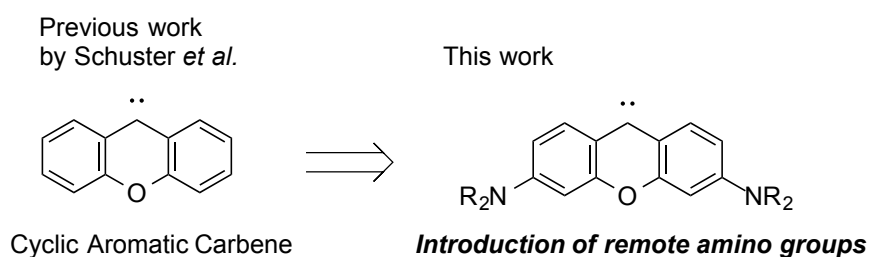
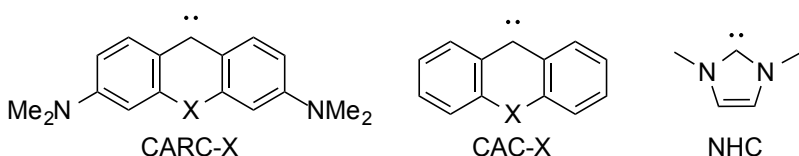


Figure 1. Cyclic aromatic carbenes with remote amino groups designed in this work.

6-2. Theoretical Calculation

To determine the energy gap between singlet and triplet states of the novel carbene species, we performed density functional theory (DFT) calculations^[8] on model compounds that have methyl groups on the nitrogen atoms. As shown in Table 1, the calculation results revealed that singlet states are more favored when electron-donating groups like the nitrogen or oxygen atom are introduced at X. On the other hand, electron-withdrawing groups like the sulfinyl group decreased the energy gap and the multiplicity of the more stable ground state shifted to the triplet state when the boron atom was placed at X. These results are in good agreement with experimental observations in the photophysical study of 9-mesityl-9,10-dihydro-9-boraanthrylidene and 9-xanthylidene.^[6] In addition, Feng and Schaefer III. *et al.* recently reported more comprehensive theoretical studies of cyclic aromatic carbenes with remote amino groups.^[9] While their calculations were performed at the level of M06/cc-pVTZ which was different from ours, the results showed similar tendencies of singlet-triplet energy differences and HOMO-LUMO gaps.

Table 1. DFT calculations of model compounds of novel cyclic aromatic carbenes and reported carbenes.

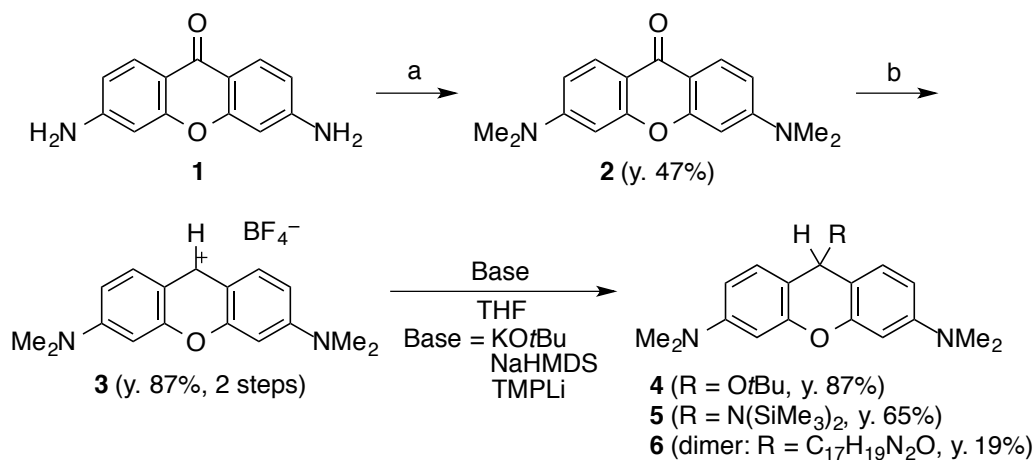


Calculated compound ^[a]	Ground state (ΔE_{S-T}) ^[b] (kcal/mol)	HOMO (eV) ^[c]	LUMO (eV) ^[c]
CARC-NMe	singlet (−14.4)	−3.67	−1.00
CARC-O	singlet (−13.7)	−3.98	−1.28
CARC-S	singlet (−8.0)	−3.86	−1.39
CARC-CH ₂	singlet (−4.6)	−3.74	−1.37
CARC-SO	singlet (−3.0)	−4.21	−1.94
CARC-BMes	triplet (+9.6)	−3.94	−2.32
CAC-O	singlet (−6.5)	−4.76	−2.27
CAC-BMes	triplet (+12.8)	−5.04	−3.14
NHC	singlet (−77.6)	−5.34	+1.18

CARC = Cyclic aromatic and remote carbenes. CAC = Cyclic aromatic carbenes. [a] Geometries optimized at the level of B3LYP/6-31G(d). [b] Energies include zero-point energy (ZPE) correction. [c] Energies of the HOMO and the LUMO in singlet states.

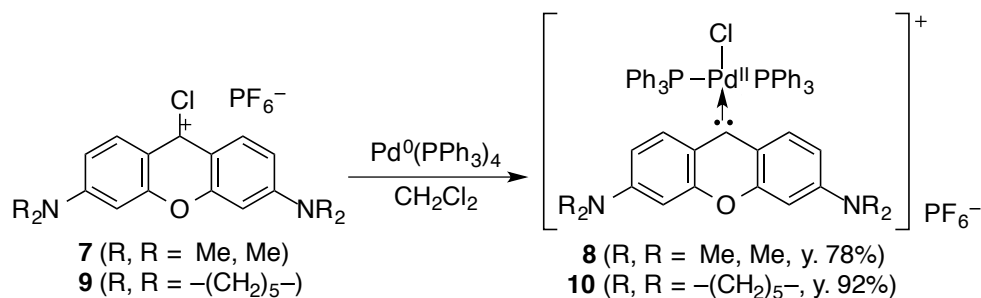
6-3. Synthesis and Characterization

From the perspective of expected easier preparation and handling, we chose to synthesize new cyclic aromatic carbenes with an oxygen atom as the bridging atom. The required carbene precursor **3**^[10] was prepared in 3 steps in 41% overall yield from 3,6-diamino-9*H*-xanthen-9-one (**1**)^[11] as shown in Scheme 1. Although deprotonation of compound **3** was then investigated with sterically hindered bases, the adducts **4** and **5** were obtained in the same manner as reactions using a phenanthridinium salt as reported by Bertrand.^[12] Consequently, the more sterically hindered base, lithium tetramethylpiperidide (TMPLi), was attempted for generating the free carbene, but the resulting product was found to be the dimer **6** bearing a saturated bridging bond. The mechanism of this reaction probably involves single electron transfer from TMPLi to give radical species which underwent dimerization. Although the attempted direct observation of the free carbene was to no avail, it was found that adduct **4** reacted with S₈ in refluxing THF to afford the corresponding thioketone product in 52% yield. In light of the report^[13] that an isoquinolin-1-ylidene is generated from its alcohol adduct analogous to **4** upon heating, it can be assumed that this result indicates the generation of a carbene species. Thus, it is suggested that in order to generate and isolate the free carbene, it is at least necessary to add kinetic stability by introducing bulky substituents at the 1,8-positions of the cyclic aromatic carbenes.



Scheme 1.– Synthesis of carbene precursor **3** and attempted deprotonation of **3** with sterically hindered bases. a) NaH, MeI, THF, reflux. b) (1) LiAlH₄, THF, r.t. (2) [Ph₃C]⁺[BF₄][−], CH₂Cl₂, r.t..

Toward the preparation of metal complexes with the ligand, oxidative addition of low valent metal into the chloride precursor was considered to be an alternative approach to a method via the free carbene for this aim. Indeed, a variety of carbene metal complexes, especially those which were difficult to synthesize through simple ligand exchange, have been obtained with this methodology.^[14] Treatment of 3,6-bis(dimethylamino)-9*H*-xanthen-9-one (**2**) with oxalyl chloride in CCl₄ followed by a counter anion exchange reaction gave the desired chloride precursor **7** as an hexafluorophosphate salt in moderate yield. Subsequently, precursor **7** was reacted with 1.2 equivalents of Pd(PPh₃)₄ in refluxing CH₂Cl₂ to



Scheme 2. Oxidative addition of palladium(0) into the chloride precursors.

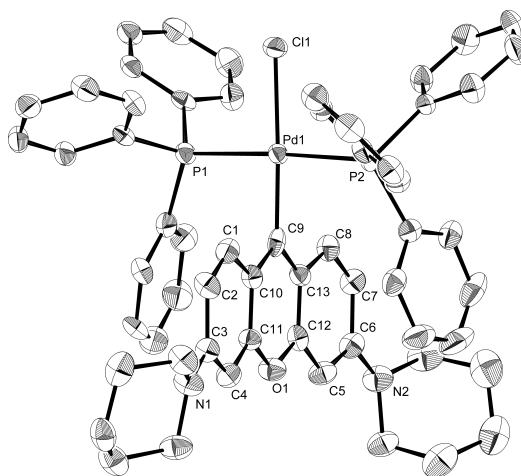


Figure 2. The ORTEP drawing of **10** (three independent molecules) with the thermal ellipsoids shown at the 50% probability level. All hydrogen atoms and the counter anion are omitted for clarity. Selected bond lengths (Å) and angles (°): C9-Pd1, 1.974(6); C9-C10, 1.431(7); C9-C13, 1.410(7); C10-C1, 1.428(7); C1-C2, 1.352(7); C2-C3, 1.439(7); C3-N1, 1.341(6), Pd1-P1, 2.3209(13); Pd1-P2, 2.3346(12); Pd1-C11, 2.3779(14); C10-C9-C13, 116.0(5); C10-C9-Pd1, 121.8(4); C13-C9-Pd1, 122.2(4); C9-Pd1-P1, 88.80(13); P1-Pd1-C11, 89.01(5); P1-Pd1-P2, 176.82(5).

afford the novel palladium(II) complex **8** (Scheme 2). The singlet peak in ^{31}P NMR at 24.02 ppm clearly indicated the complex to be in the *trans*-configuration and ^{13}C NMR showed a characteristic triplet peak ($^2J_{\text{C-P}} = 6$ Hz) at 214.8 ppm for the C9 carbon.^[15] However, a pure ^{13}C NMR spectrum of **8** could not be obtained due to degradation during measurements in CDCl_3 and even CD_2Cl_2 . In addition, despite many attempts at recrystallization of the complex, crystals suitable for X-ray analysis could not be obtained. Since the solubility of the complex was relatively low, corresponding palladium(II) complex **10**, bearing piperidinyl substituents instead of dimethylamino groups, was prepared in the same manner as **8**. Although the difference between **8** and **10** was minute, the ^{13}C NMR spectrum of **10** indicated no decomposition of the sample during measurements in CD_2Cl_2 in contrast with **8**. A symbolic triplet peak appeared at 213.7 ppm for the C9 carbon as in the case of **8**, which was significantly downfield shifted

compared to that of precursor **9** ($\delta_{\text{C}} = 157.8$ ppm). The structure of **10** could be unambiguously determined by X-ray crystallographic analysis (Scheme 2 and Figure 2). The crystals contained three independent molecules and all of them showed *trans*-configuration which was also supported by the presence of only a singlet peak in the ^{31}P NMR spectrum. As is the case for classical NHCs,^{1b} the bond angle surrounding the carbene center (C10–C9–C13: 117.12° (average value)) is somewhat narrow compared to that of the precursor **9** (121.87°). In addition, the lengths of the carbon-carbon bonds connected at the carbene center in **10** (the range is 1.390–1.432 Å) were slightly elongated in comparison with those of **9** (1.389, 1.397 Å). It was also found that the ligand is perpendicular to the plane composed of the phosphorus and chloride atoms.

For the purpose of investigating the donor ability of the ligand, comparison with other reported palladium(II) complexes was performed in terms of the degree of *trans*-influence on the Pd–Cl bonds. As shown in Figure 3, the average Pd–Cl bond of complex **10** is undoubtedly longer than that of complex **A** and **B** which bears a classical NHC^[14a] and is comparable to that of complex **C**^[14c] which has recently been reported as member of a new class of singlet carbene ligands stabilized by lateral enamine moieties. This suggests that the donor ability of the carbene ligand in **10** and **C** is much stronger than that of classical NHC ligands like in **A** and **B**. This character could be due to the relatively lower σ -electron withdrawing ability of the carbon atoms adjacent to the carbene center in **10** and **C** compared with the corresponding nitrogen atoms in classical NHCs. As for the ^{13}C NMR shift of the carbene center, although multiple factors must be operative, we see a trend in the chemical shift that parallels bond elongation except for **B**, with **10** showing an intermediate value (213.6 ppm) among the four complexes.

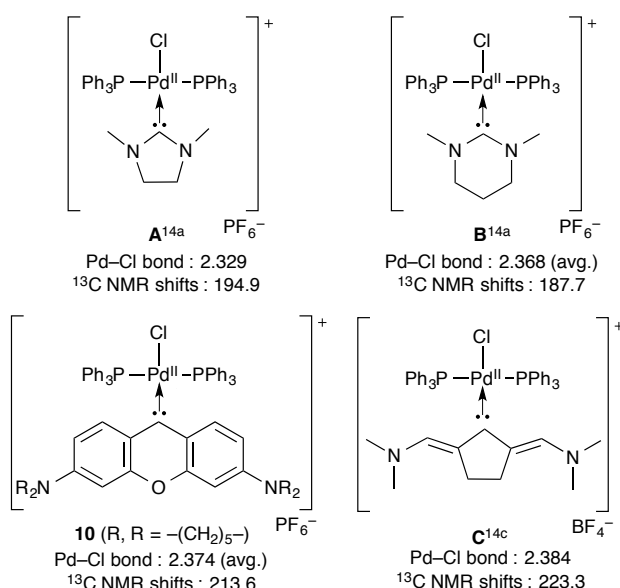
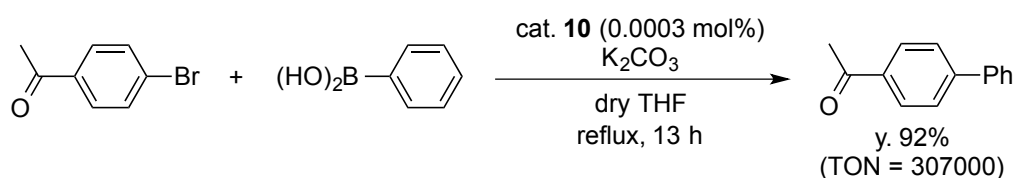


Figure 3. Comparison of Pd–Cl bonds (Å) and ^{13}C NMR shifts (ppm) of the carbene center of carbene Pd^{II} complexes.

6-4. Catalytic Activity

With the Pd^{II} complex **10** in hand, preliminary catalytic performance in the Suzuki-Miyaura cross-coupling reaction was investigated. According to a previous report, the cross-coupling reaction of 4-bromoacetophenone with PhB(OH)₂ in the presence of 1 mol% of the NHC complex **A** afforded the expected biphenyl product in 79% isolated yield.^[14a] In comparison, with 0.001 mol% of complex **10** in the same cross-coupling reaction, the biphenyl product was yielded quantitatively. Surprisingly, even in the presence of only 0.0003 mol% of **10**, the catalytic reaction proceeded, giving the product in 92% isolated yield (Scheme 3). This corresponds to a turnover number (TON) of 3.07×10^5 . This result suggested that the strong donor ability of this diaryl carbene ligand enhanced the catalytic activity of the transition-metal catalyst.



Scheme 3. Suzuki-Miyaura cross coupling reaction of bromoacetophenone with phenylboronic acid catalyzed by the palladium(II) complex **10**.

6-5. Conclusions and Outlook

In conclusion, novel cyclic aromatic carbene ligands bearing a bridged oxygen atom was developed. Although the attempted deprotonation of carbocation **3** which is a precursor to the free carbene failed, the reaction of the alcohol adduct **4** with S₈ gave the corresponding thioketone species, which suggested that the adduct can be regarded as a precursor of the free carbene. Oxidative insertion of palladium(0) to chlorine derivatives afforded the palladium(II) complexes **8** and **10**. The X-ray structure of **10** implied that the donor ability of the ligand is stronger than that of the classical NHC ligand, and high catalytic activity of **10** in the Suzuki-Miyaura cross-coupling reaction attributable to this electronic feature was disclosed. These results indicated that the novel cyclic aromatic carbene ligand is promising as a useful ligand for transition-metal catalysts. Based upon our findings here, further investigations for isolating the free carbene by introduction of bulky substituents at the 1,8-positions will be discussed in the following chapters.

Experimental Section

General. Melting points were measured with a Yanagimoto micro melting point apparatus and are uncorrected. Column chromatography was carried out using Merck silica gel 60. ^1H NMR (400 MHz), ^{13}C NMR (100 MHz), ^{19}F NMR (376 MHz) and ^{31}P NMR (160 MHz) spectra were recorded using a JEOL EX-400 or AL-400 spectrometer. The ^1H NMR chemical shifts are reported (δ scale) from internal tetramethylsilane. The ^{13}C NMR chemical shifts are reported (δ scale) from internal tetramethylsilane. The ^{19}F NMR chemical shifts are reported (δ scale) from external CFCl_3 . The ^{31}P NMR chemical shifts are reported (δ scale) from external 85% H_3PO_4 . Tetrahydrofuran (THF) and diethyl ether (Et_2O) were freshly distilled from Na-Benzophenone. The elemental analyses were performed using a Perkin-Elmer 2400 CHN elemental analyzer. Mass spectra were measured with a Thermo Fisher Scientific model LTQ Orbitrap XL by using the ESI-TOF method in the positive ion mode with acetonitrile solution samples. Crystals suitable for X-ray structural determination were mounted on a Bruker SMART APEXII CCD diffractometer or a Rigaku SCXmini diffractometer and irradiated with graphite monochromated Mo-K α radiation ($\lambda = 0.71073 \text{ \AA}$) at 173 K for data collection. The data were processed using the APEX program suite or the Rigaku SCXmini program. The structures were solved by a direct method using the SIR-2004 program.^[16] Refinement on F^2 was carried out by full-matrix least-squares using the SHELXL-97 program.^[17] All non-hydrogen atoms were refined using anisotropic thermal parameters except for disordered atoms. The hydrogen atoms were included in the refinement with isotropic thermal parameters. The crystallographic data are summarized in Table 2.

3,6-Diamino-9*H*-xanthen-9-one (**1**) was prepared by a literature method.^[11]

Computational Details

All computations were performed using the Gaussian 09 package of programs.^[8] The B3LYP hybrid functional was used with the 6-31G* basis set. All structures were optimized without any symmetry assumptions. Harmonic vibration frequency calculations at the same level were performed to verify that all the stationary points were local minima (with no imaginary frequency).

Synthesis of 3,6-bis(dimethylamino)-9*H*-xanthen-9-one (**2**)

3,6-Diamino-9*H*-xanthen-9-one (**1**) (645 mg, 2.85 mmol) and sodium hydride (60%, 729 mg, 18.2 mmol) were dissolved in dry THF (40 mL) under Ar and methyl iodide (1.42 mL, 22.8 mmol) was added dropwise. The reaction mixture was heated at reflux for 18 h. The reaction mixture was quenched by the addition of water and the solvent was concentrated. The remaining solution was extracted with CH_2Cl_2 (x3) and the combined organic layer was dried over Na_2SO_4 . After the solvent was evaporated, chromatographic purification was achieved on neutral alumina (grade I) with AcOEt containing 1% NEt_3 as the eluent. The solution was evaporated in vacuo and the resulting solid was recrystallized from CH_2Cl_2 /hexane to give **2** (376 mg, 1.33 mmol, 47%) as dark red crystals. M.p. 235-240 °C; ^1H NMR

(CDCl₃, 400 MHz): δ = 3.09 (12H, s), 6.47 (2H, d, 5J = 2 Hz), 6.69 (2H, dd, 3J = 9 Hz, 5J = 2 Hz), 8.13 ppm (2H, d, 3J = 9 Hz); ¹³C NMR (CDCl₃, 100 MHz) δ = 40.14 (CH₃), 96.94 (CH), 108.89 (CH), 111.94 (C), 127.57 (CH), 154.23 (C), 158.10 (C), 175.14 ppm (C); HRMS (ESI): m/z : calcd for C₁₇H₁₈N₂O₂ [M+H]⁺ 283.1441; found 283.1443; elemental analysis calcd (%) for C₁₇H₁₈N₂O₂: C 72.32, H 6.43, N 9.92; found: C 72.06, H 6.65, N 9.90.

Synthesis of 3

A solution of **2** (800 mg, 2.83 mmol) in dry THF (80 mL) was added to a solution of lithium aluminum hydride (215 mg, 5.66 mmol) in dry THF (27 mL) under Ar. After the reaction mixture was stirred for 3 h at ambient temperature, the mixture was quenched by the addition of AcOEt at 0 °C and then water. The solvent was concentrated and the remaining solution was extracted with CH₂Cl₂ (x3). The combined organic layer was washed with water and then dried over Na₂SO₄. Evaporation of the solvent gave a cationic product as a purple solid labile to air. ¹H NMR (CDCl₃, 400 MHz): δ = 2.93 (12H, s), 3.86 (2H, s), 6.42 (2H, d, 5J = 3 Hz), 6.45 (2H, dd, 3J = 8 Hz, 5J = 3 Hz), 7.01 ppm (2H, d, 3J = 8 Hz).

The resulting product and triphenylmethylium tetrafluoroborate (1.04 g, 3.15 mmol) were dissolved in dry CH₂Cl₂ (40 mL) and the reaction mixture was stirred for 5 h at ambient temperature. After the solvent was removed in vacuo, the crude product was washed with diethyl ether (x3). Recrystallization from CH₃CN / ether gave **3** (876 mg, 2.47 mmol, 87% for 2 steps) as a red-purple solid. M.p. > 300 °C; ¹H NMR (CD₃CN, 400 MHz): δ = 3.21 (12H, s), 6.63 (2H, d, 5J = 2 Hz), 7.00 (2H, dd, 3J = 9 Hz, 5J = 2 Hz), 7.64 (2H, d, 3J = 9 Hz), 8.34 ppm (1H, s); ¹³C NMR (CD₃CN, 100 MHz) δ = 41.36 (CH₃), 97.03 (CH), 115.13 (C), 115.32 (CH), 133.94 (CH), 147.13 (CH), 158.81 (C), 158.88 ppm (C); ¹⁹F NMR (CD₃CN, 376 MHz) δ = -150.21 (s, 1F), -150.26 ppm (s, 3F); HRMS (ESI, positive): m/z : calcd for C₁₇H₁₉N₂O [M]⁺ 267.1492; found 267.1491; elemental analysis calcd (%) for C₁₇H₁₉BF₄N₂O: C 57.65, H 5.41, N 7.91; found: C 57.22, H 5.30, N 7.84.

Synthesis of 4

To a solution of **3** (20 mg, 0.056 mmol) in dry THF (5 mL) was added 1.0 M KO^tBu in THF (0.060 mL, 0.060 mmol). The reaction mixture was stirred for 2 h at ambient temperature and then the solvent was removed in vacuo. After the resulting solid was dissolved with diethyl ether, the solution was filtered and the filtrate was evaporated to give **4** (17 mg, 0.048 mmol, 87%) as a gray solid. M.p. 138-142 °C; ¹H NMR (C₆D₆, 400 MHz): δ = 1.26 (9H, s), 2.50 (12H, s), 5.58 (1H, s), 6.47 (2H, dd, 3J = 9 Hz, 5J = 2 Hz), 6.68 (2H, d, 5J = 2 Hz), 7.41 ppm (2H, d, 3J = 9 Hz); ¹³C NMR (C₆D₆, 100 MHz) δ = 29.84 ((CH₃), 40.11 (CH₃), 65.13 (CH), 73.73 (C), 100.63 (CH), 108.18 (CH), 114.51 (C), 129.82 (CH), 151.25 (C), 155.04 ppm (C); HRMS (ESI, positive): m/z : calcd for C₂₁H₂₉N₂O₂ [M+H]⁺ 341.2224; found 341.2221.

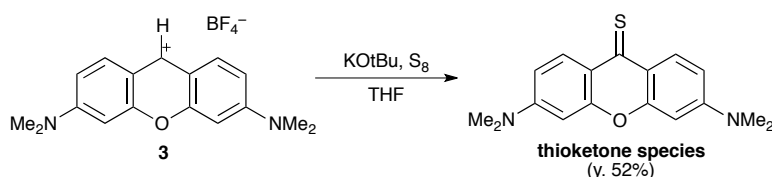
Synthesis of 5

To a solution of **3** (30 mg, 0.085 mmol) in dry THF (3 mL) was added 1.1 M NaHMDS in THF (0.086 mL, 0.094 mmol). The reaction mixture was stirred for 2 h at ambient temperature and then the solvent was removed in vacuo. After the resulting solid was dissolved with diethyl ether, the solution was filtered and the filtrate was evaporated to give **4** (24 mg, 0.055 mmol, 65%) as a yellow solid. M.p. 154-161 °C; ^1H NMR (C_6D_6 , 400 MHz): δ = 0.08 (9H, br s), 0.39 (9H, br s), 2.52 (12H, s), 5.53 (1H, s), 6.46 (2H, d, 5J = 2 Hz), 6.62 (2H, dd, 3J = 9 Hz, 5J = 2 Hz), 7.56 ppm (2H, d, 3J = 9 Hz); ^{13}C NMR (CDCl_3 , 100 MHz) δ = 2.91 (CH_3), 4.04 (CH_3), 40.07 (CH_3), 49.80 (CH), 99.86 (CH), 108.04 (CH), 115.42 (C), 129.67 (CH), 151.04 (C), 152.14 ppm (C); HRMS (ESI, positive): m/z : calcd for $\text{C}_{23}\text{H}_{38}\text{N}_3\text{OSi}_2$ $[\text{M}+\text{H}]^+$ 428.2548; found 428.2544.

Synthesis of 6

1.63 M *n*-Butyl lithium in hexane (0.19 mL, 0.31 mmol) was added to a solution of tetramethylpiperidine (0.052 mL, 0.31 mmol) in THF (5 mL) at -78 °C. The reaction mixture was stirred for 30 min at -78 °C and then added to a solution of **3** (100 mg, 0.282 mmol) in THF (10 mL) at -78 °C. The reaction mixture was stirred for 4 h at ambient temperature and then the solvent was removed in vacuo. After the resulting solid was dissolved with diethyl ether, the solution was filtered and the filtrate was evaporated. The crude product was recrystallized from ether/hexane to give **6** (14 mg, 0.027 mmol, 19%) as a purple solid. M.p. 142-144 °C (decomp.); ^1H NMR (CDCl_3 , 400 MHz): δ = 2.90 (24H, s), 4.00 (2H, s), 6.21 (4H, d, 5J = 2 Hz), 6.34 (4H, dd, 3J = 9 Hz, 5J = 2 Hz), 6.53 ppm (4H, d, 3J = 9 Hz); HRMS (ESI, positive): m/z : calcd for $\text{C}_{34}\text{H}_{39}\text{N}_2\text{O}_2$ $[\text{M}+\text{H}]^+$ 535.3068; found 535.3060.

Synthesis of 3,6-bis(dimethylamino)-9H-xanthene-9-thione



To a solution of **3** (101 mg, 0.285 mmol) and sulfur (91 mg, 2.8 mmol) in dry THF (20 mL) was added 1.0 M KOtBu in THF (0.35 mL, 0.35 mmol). The reaction mixture was refluxed for 1.5 h and the solvent was evaporated. The residual solid was purified by silica gel column chromatography with CH_2Cl_2 as the eluent and the resulting product was recrystallized from CH_2Cl_2 /hexane to give 3,6-bis(dimethylamino)-9H-xanthene-9-thione (44 mg, 0.15 mmol, 52%) as a dark green solid. M.p. 280-285 °C; ^1H NMR (CDCl_3 , 400 MHz): δ = 3.12 (12H, s), 6.41 (2H, d, 5J = 2 Hz), 6.74 (2H, dd, 3J = 9 Hz, 5J = 2 Hz), 8.68 ppm (2H, d, 3J = 9 Hz); ^{13}C NMR (CDCl_3 , 100 MHz) δ = 40.20 (CH_3), 95.93 (CH), 110.46 (CH), 119.97 (C), 131.77 (CH), 153.01 (C), 154.56 (C), 196.19 ppm (C); HRMS (ESI, positive): m/z : calcd for $\text{C}_{17}\text{H}_{19}\text{N}_2\text{OS}$ $[\text{M}+\text{H}]^+$ 299.1213; found 299.1213.

Synthesis of 3,6-di(piperidin-1-yl)-9H-xanthen-9-one

Compound **1** (750 mg, 3.31 mmol) and sodium hydride (60%, 840 mg, 20.8 mmol) were dissolved in dry THF (50 mL) under Ar and 1,5-diiodopentane (1.23 mL, 8.30 mmol) was added dropwise. The reaction mixture was heated at reflux for 18 h. The reaction mixture was quenched by the addition of water and the solvent was concentrated. The remaining solution was extracted with CH₂Cl₂ (x3) and the combined organic layer was dried over Na₂SO₄. After the solvent was evaporated, the chromatographic purification was achieved on silica gel with AcOEt/hexane = 1:1 as the eluent. The solution was evaporated in vacuo and the resulting solid was recrystallized from CH₂Cl₂/hexane to give 3,6-di(piperidine-1-yl)-9H-xanthen-9-one (397 mg, 1.09 mmol, 33%) as a red solid. M.p. 148-152 °C; ¹H NMR (CDCl₃, 400 MHz): δ = 1.68 (12H, m), 3.39 (8H, m), 6.66 (2H, d, ⁵J = 2 Hz), 6.86 (2H, dd, ³J = 9 Hz, ⁵J = 2 Hz), 8.10 ppm (2H, d, ³J = 9 Hz); ¹³C NMR (CDCl₃, 100 MHz) δ = 24.34 (CH₂), 25.30 (CH₂), 48.68 (CH₂), 99.55 (CH), 111.38 (CH), 113.00 (C), 127.51 (CH), 155.26 (C), 158.25 (C), 175.00 ppm (C); HRMS (ESI): *m/z*: calcd for C₂₃H₂₇N₂O₂ [M+H]⁺ 363.2067; found 363.2062.

General procedure for the conversion of the xanthenes into the chlorides (7 and 9)

Oxalyl chloride (1.2 eq.) was added to a solution of the xanthone in dry CCl₄ (7 mL/1 mmol). The reaction mixture was stirred for 16 h at 60 °C. After the reaction was completed, the solution was diluted with CH₃CN and evaporated. The crude product was recrystallized from CH₃CN/ether to give the chloride species. The chloride species and potassium hexafluorophosphate (5.0 eq.) were dissolved in CH₃CN and stirred at room temperature for 16 h. After the solvent was evaporated and replaced with CH₂Cl₂, the solution was filtered and the filtrate was evaporated. The crude product was recrystallized from CH₃CN/ether to give the corresponding hexafluorophosphate salts.

Data for **7**: Yield, 75% (2 steps, a brown solid); M.p. 250-254 °C (decomp.); ¹H NMR (CD₃CN, 400 MHz): δ = 3.27 (12H, s), 6.75 (2H, d, ⁵J = 2 Hz), 7.16 (2H, dd, ³J = 9 Hz, ⁵J = 2 Hz), 8.03 ppm (2H, d, ³J = 9 Hz); ¹³C NMR (CD₃CN, 100 MHz): δ = 42.13 (CH₃), 97.42 (CH), 113.80 (C), 116.81 (CH), 130.70 (CH), 153.17 (C), 158.89 (C), 159.37 ppm (C); ¹⁹F NMR (CD₃CN, 376 MHz): δ = -71.72 ppm (d, *J*_{P-F} = 706 Hz); ³¹P NMR (CD₃CN, 160 MHz): δ = -143.37 ppm (sept, *J*_{P-F} = 706 Hz); HRMS (ESI, positive): *m/z*: calcd for C₁₇H₁₈N₂OCl [M]⁺ 301.1102; found 301.1108; elemental analysis calcd (%) for C₁₇H₁₈ClF₆N₂OP: C 45.70, H 4.06, N 6.27; found: C 45.85, H 3.74, N 6.21.

Data for **9**: Yield, 61% (2 steps, a green solid); M.p. 202-207 °C (decomp.); ¹H NMR (CD₃CN, 400 MHz): δ = 1.72 (12H, m), 3.71 (8H, m), 6.83 (2H, d, ⁵J = 2 Hz), 7.23 (2H, dd, ³J = 9 Hz, ⁵J = 2 Hz), 7.95 ppm (2H, d, ³J = 9 Hz); ¹³C NMR (CD₃CN, 100 MHz) δ = 24.72 (CH₂), 26.73 (CH₂), 49.86 (CH₂), 97.37 (CH), 113.43 (C), 116.46 (CH), 130.44 (CH), 151.40 (C), 157.79 (C), 159.01 ppm (C); ¹⁹F NMR (CD₃CN, 376 MHz): δ = -71.71 ppm (d, *J*_{P-F} = 708 Hz); ³¹P NMR (CD₃CN, 160 MHz): δ = -143.36 ppm (sept, *J*_{P-F} =

708 Hz); HRMS (ESI, positive): m/z : calcd for $C_{23}H_{26}N_2O_2Cl [M]^+$ 381.1728; found 381.1722; elemental analysis calcd (%) for $C_{23}H_{26}ClF_6N_2OP$: C 52.43, H 4.97, N 5.32; found: C 52.15, H 5.04, N 5.23.

General procedure for the oxidative addition into the chloride species (7 and 9)

The chloride species and $Pd(PPh_3)_4$ (1.2 eq.) were dissolved in dry CH_2Cl_2 and the reaction mixture was refluxed under argon for 3 h. After the solvent was removed in vacuo, the resulting solid was washed with hexane (x3) to remove triphenylphosphines and then the crude product was recrystallized from CH_2Cl_2 /hexane to give the palladium(II) complexes.

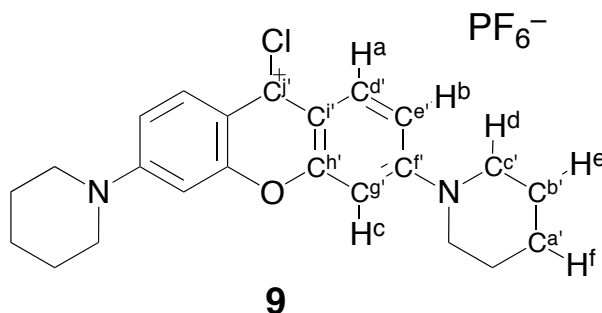
Data for **8**: Yield, 78% (a pale purple solid); M.p. 160-165 °C; 1H NMR ($CDCl_3$, 400 MHz): δ = 3.15 (12H, s), 6.10 (2H, d, 5J = 2 Hz), 6.62 (2H, dd, 3J = 9 Hz, 5J = 2 Hz), 7.20-7.42 (18H, m), 7.46-7.62 (12H, m), 8.25 ppm (2H, d, 3J = 9 Hz); ^{19}F NMR ($CDCl_3$, 376 MHz): δ = -73.98 ppm (d, J_{P-F} = 717 Hz); ^{31}P NMR ($CDCl_3$, 160 MHz): δ = 24.02 (s), -143.61 ppm (sept, J_{P-F} = 717 Hz); HRMS (ESI, positive): m/z : calcd for $C_{53}H_{49}ClN_2OP_2Pd [M]^+$ 931.1965; found 931.1971; elemental analysis calcd (%) for $C_{53}H_{48}ClF_6N_2OP_3Pd$: C 59.06, H 4.49, N 2.60; found: C 59.26, H 4.64, N 2.19.

Data for **10**: Yield, 92% (a red-green solid); M.p. 198-200 °C; 1H NMR ($CDCl_3$, 400 MHz): δ = 1.69 (12H, m), 3.54 (8H, m), 6.22 (2H, d, 5J = 2 Hz), 6.80 (2H, dd, 3J = 9 Hz, 5J = 2 Hz), 7.21-7.26 (12H, m), 7.30-7.36 (6H, m), 7.46-7.53 (12H, m), 8.18 ppm (2H, d, 3J = 9 Hz); ^{13}C NMR (CD_2Cl_2 , 100 MHz): δ = 24.50 (CH_2), 25.93 (CH_2), 48.90 (CH_2), 95.90 (CH), 113.38 (CH), 121.98 (C, t, J = 3 Hz), 128.50 (CH, t, J = 3 Hz), 129.36 (C, t, J = 24 Hz), 131.40 (CH), 134.52 (CH, t, J = 5 Hz), 137.39 (CH), 152.61 (C), 156.39 (C), 213.72 ppm (C, t, J = 6 Hz); ^{19}F NMR ($CDCl_3$, 376 MHz): δ = -73.97 ppm (d, J_{P-F} = 712 Hz); ^{31}P NMR ($CDCl_3$, 160 MHz): δ = 24.08 (s), -143.61 ppm (sept, J_{P-F} = 712 Hz); HRMS (ESI, positive): m/z : calcd for $C_{59}H_{56}ClN_2OP_2Pd [M]^+$ 1011.2586; found 1011.2584; elemental analysis calcd (%) for $C_{59}H_{56}ClF_6N_2OP_3Pd+0.5CH_2Cl_2$: C 59.54, H 4.79, N 2.33; found: C 59.76, H 4.65, N 2.06.

General procedure for the Suzuki-Miyaura cross-coupling reaction

A solution of phenylboronic acid (2.4 mmol, 1.2 equiv.), 4-bromoacetophenone (2.0 mmol, 1 equiv.), the Pd complex **10** (0.001 or 0.0003 mol%), and K_2CO_3 (3.0 mmol, 1.5 equiv.) in THF (2 mL) was refluxed for 13 h under argon. After cooling, the reaction mixture was diluted with water, and the aqueous phase was extracted with ethyl acetate (x3). The combined organic layer was washed with brine and dried over Na_2SO_4 . After the solvent was evaporated, the residue was purified by silica gel column chromatography with CH_2Cl_2 /hexane = 1:1 as the eluent to give 4-phenyl-acetophenone, the analytical and spectroscopic data of which were identical to those of an authentic sample.^[18]

2D NMR spectra of compound 9



In order to assign the quaternary carbon atom at C9 position (C^j in above figure), we performed ^1H - ^1H COSY, ^1H - ^{13}C COSY, and ^1H - ^{13}C COLOC measurements as follows. Each of the protons was identified using ^1H - ^1H COSY as shown in Figure 4. Then, the secondary and the tertiary carbon atoms were assigned with correlation spectroscopy between directly attached protons and carbons as shown in Figure 5. Finally, each of the quaternary carbons could be determined with correlation spectroscopy for long-range coupling (COLOC), through 2- and 3-bond correlations between proton and carbon nuclei. Judging from the correlation in Figure 6, the targeted peak of C^j could be determined to be the signal at 157.79 ppm since peak j' only had a correlation with proton H^a .

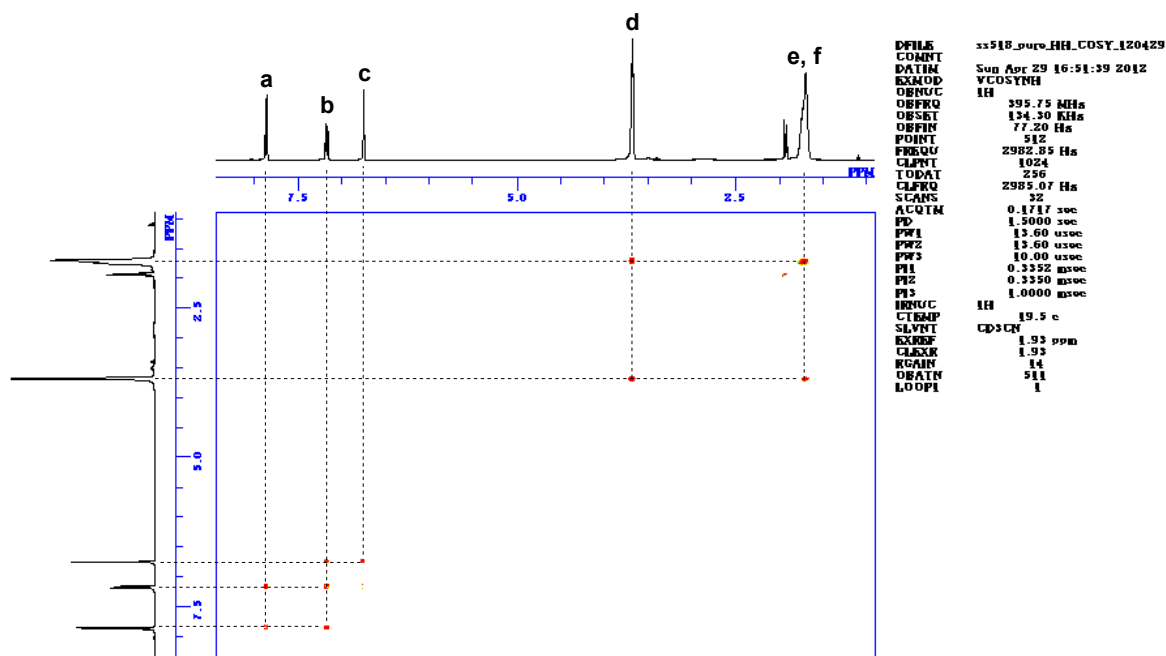


Figure 4. ^1H - ^1H COSY spectrum of compound 9 in CD_3CN .

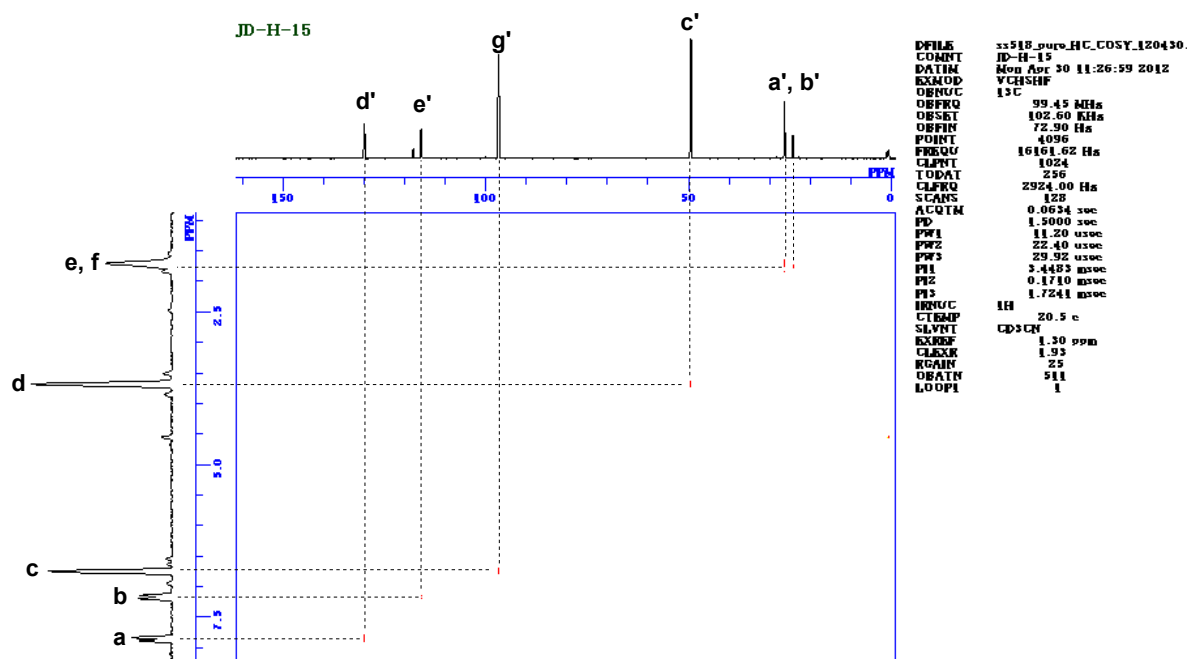


Figure 5. ^1H - ^{13}C COSY spectrum of compound **9** in CD_3CN .

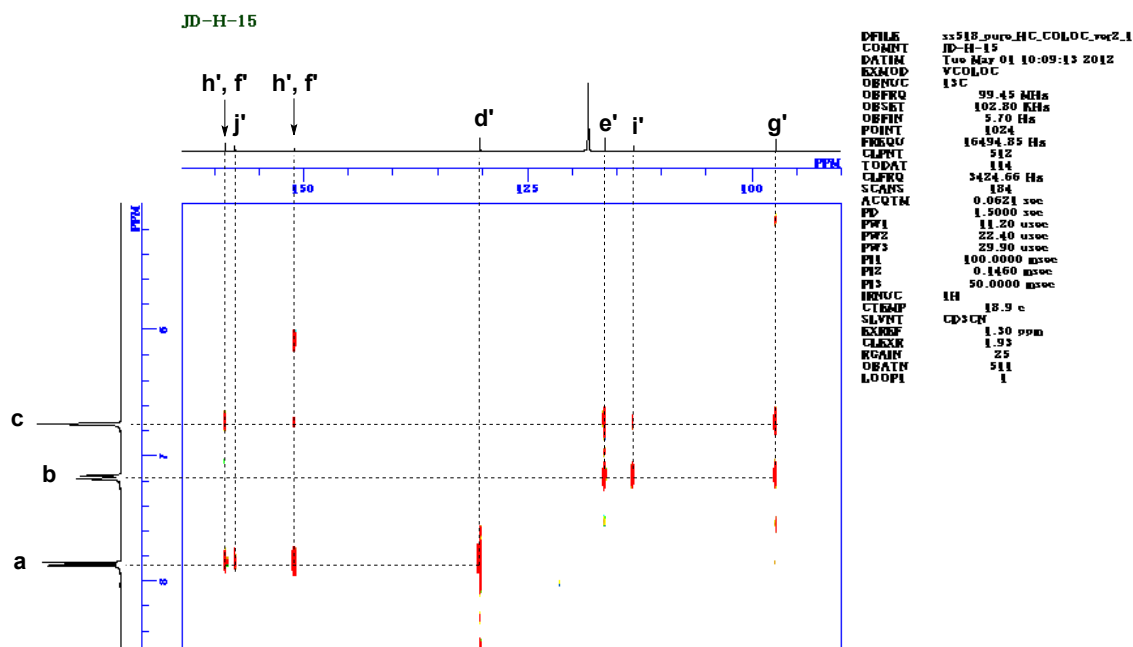


Figure 6. ^1H - ^{13}C COLOC spectrum of compound **9** in CD_3CN .

X-ray Crystallographic Details

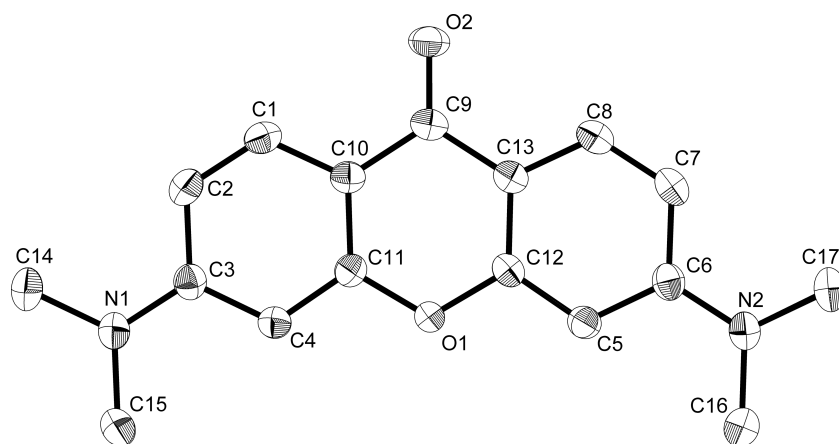


Figure 7. The ORTEP drawing of 3,6-bis(dimethylamino)-9*H*-xanthen-9-one (**2**) with the thermal ellipsoids shown at the 50% probability level. All hydrogen atoms are omitted for clarity. Selected bond lengths (Å) and angles (°): C9-O2, 1.2362(14); C9-C10, 1.4533(16); C9-C13, 1.4508(17); C10-C1, 1.4033(17); C1-C2, 1.3646(18); C2-C3, 1.4176(17); C3-N1, 1.3615(15); C10-C9-C13, 114.36(10); C10-C9-O2, 122.74(11); C13-C9-O2, 122.90(11).

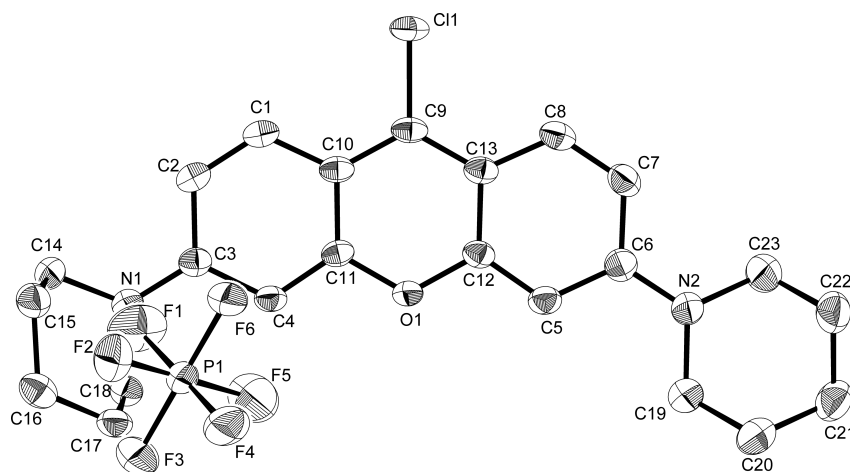


Figure 8. The ORTEP drawing of **9** with the thermal ellipsoids shown at the 50% probability level. All hydrogen atoms are omitted for clarity. Selected bond lengths (Å) and angles (°): C9-Cl1, 1.7138(18); C9-C10, 1.397(3); C9-C13, 1.389(3); C10-C1, 1.413(3); C1-C2, 1.356(3); C2-C3, 1.434(3); C3-N1, 1.344(2); C10-C9-C13, 121.87(17); C10-C9-Cl1, 118.45(15); C13-C9-Cl1, 119.68(15).

Table 2. Crystallographic data for **2**, **9** and **10**.

	2	9 ^[a]	10 ^[b]
Formula	C ₁₇ H ₁₈ N ₂ O ₂	C ₂₅ H ₂₉ ClF ₆ N ₃ OP	C ₅₉ H ₅₆ F ₆ N ₂ OOP ₃ Pd
Mol wt	282.33	567.93	1157.82
Crystal system	monoclinic	triclinic	triclinic
Space group	<i>P</i> 2 ₁ /n	<i>P</i> -1	<i>P</i> -1
Color	red	purple	red
Habit	block	block	plate
Cryst dimens, mm	0.88 x 0.60 x 0.44	0.81 x 0.43 x 0.34	0.12 x 0.07 x 0.05
<i>a</i> , Å	12.1248(10)	9.0244(10)	13.4314(18)
<i>b</i> , Å	8.8762(8)	11.0496(12)	23.977(3)
<i>c</i> , Å	13.9060(12)	14.0165(15)	28.786(4)
<i>a</i> , deg	90	103.630(3)	99.891(2)
<i>b</i> , deg	107.207(2)	91.184(3)	96.290(2)
<i>g</i> , deg	90	109.380(3)	105.059(2)
<i>V</i> , Å ³	1429.6(2)	1273.9(2)	8702(2)
<i>Z</i>	4	2	6
<i>D</i> _{calc} , g cm ⁻³	1.321	1.481	1.326
Abs coeff, mm ⁻¹	0.087	0.282	0.508
<i>F</i> (000)	600	588	3564
Temp, K	173(2)	173(2)	173(2)
Reflections	14303	13249	30765
Independent	3265	5818	30765
<i>R</i> _{int}	0.0302	0.0282	0.0000
Parameters	194	335	1902
<i>R</i> ₁ [<i>I</i> > 2s(<i>I</i>)]	0.0411	0.0511	0.0595
<i>wR</i> ₂ (all data)	0.1169	0.1503	0.1679
Goodness of fit	1.041	1.068	1.011
solv for crystallization	hexane/CH ₂ Cl ₂	ether/CH ₃ CN	hexane/CH ₂ Cl ₂

[a] These crystals contained solvent molecules in the crystal lattice (**9**: CH₃CN). [b] In these crystal structures, there are disordered solvent molecules, and their contribution to the scattering values have been removed by using the PLATON SQUEEZE program.^[19]

References

- [1]. a) A. Igau, H. Grutzmacher, A. Baceiredo, G. Bertrand, *J. Am. Chem. Soc.* **1988**, *110*, 6463-6466; b) A. J. Arduengo, III., R. L. Harlow, M. Kline, *J. Am. Chem. Soc.* **1991**, *113*, 361-363. The term 'classical NHCs' refers to cyclic carbenes with two nitrogen atoms adjacent to the carbene center such as in Arduengo-type carbenes. Abnormal and remote carbenes are precluded from this category.
- [2]. *N-Heterocyclic carbenes in Transition Metal Catalysis and Organocatalysis*, ed. C. S. J. Cazin, Springer, Netherlands, **2011**.
- [3]. a) C. Heinemann, T. Müller, Y. Apeloig, H. Schwarz, *J. Am. Chem. Soc.* **1996**, *118*, 2023-2038; b) C. Boehme, G. Frenking, *J. Am. Chem. Soc.* **1996**, *118*, 2039-2046.
- [4]. a) O. Schuster, L. Yang, H. G. Raubenheimer, M. Albrecht, *Chem. Rev.* **2009**, *109*, 3445; b) M. Melaimi, M. Soleilhavoup, G. Bertrand, *Angew. Chem. Int. Ed.* **2010**, *49*, 8810-8849.
- [5]. a) T. Yamaguchi, S.-i. Fuku-en, S. Sugawara, S. Kojima, Y. Yamamoto, *Aust. J. Chem.* **2010**, *63*, 1638-1644; b) S.-i. Fuku-en, T. Yamaguchi, S. Kojima, Y. Yamamoto, *J. Phys. Org. Chem.* **2011**, *24*, 1009-1017.
- [6]. a) S. C. Lapin, B. E. Brauer, G. B. Schuster, *J. Am. Chem. Soc.* **1984**, *106*, 2092-2100; b) S. C. Lapin, G. B. Schuster, *J. Am. Chem. Soc.* **1985**, *107*, 4243-4248.
- [7]. a) K. H. Dötz, J. Pfeiffer, *Chem. Commun.* **1996**, 895; b) J. Pfeiffer, K. H. Dötz, *Organometallics* **1998**, *17*, 4353-4361; c) S. K. Schneider, P. Roembke, G. R. Julius, H. G. Raubenheimer, W. A. Herrmann, *Adv. Synth. Catal.* **2006**, *348*, 1862-1873.
- [8]. Gaussian 09, Revision A.02, M. J. Frisch, G. W. Trucks, H. B. Schlegel, G. E. Scuseria, M. A. Robb, J. R. Cheeseman, G. Scalmani, V. Barone, B. Mennucci, G. A. Petersson, H. Nakatsuji, M. Caricato, X. Li, H. P. Hratchian, A. F. Izmaylov, J. Bloino, G. Zheng, J. L. Sonnenberg, M. Hada, M. Ehara, K. Toyota, R. Fukuda, J. Hasegawa, M. Ishida, T. Nakajima, Y. Honda, O. Kitao, H. Nakai, T. Vreven, J. A. Montgomery, Jr., J. E. Peralta, F. Ogliaro, M. Bearpark, J. J. Heyd, E. Brothers, K. N. Kudin, V. N. Staroverov, R. Kobayashi, J. Normand, K. Raghavachari, A. Rendell, J. C. Burant, S. S. Iyengar, J. Tomasi, M. Cossi, N. Rega, J. M. Millam, M. Klene, J. E. Knox, J. B. Cross, V. Bakken, C. Adamo, J. Jaramillo, R. Gomperts, R. E. Stratmann, O. Yazyev, A. J. Austin, R. Cammi, C. Pomelli, J. W. Ochterski, R. L. Martin, K. Morokuma, V. G. Zakrzewski, G. A. Voth, P. Salvador, J. J. Dannenberg, S. Dapprich, A. D. Daniels, O. Farkas, J. B. Foresman, J. V. Ortiz, J. Cioslowski, D. J. Fox, Gaussian, Inc., Wallingford CT, **2009**.
- [9]. Y. Zeng, H. Fang, Y. Xie, H. F. Schaefer III., *J. Org. Chem.* **2014**, *79*, 2926-2933.
- [10]. Compound **2** has also been prepared by other methods: a) S. Kenmoku, Y. Urano, H. Kojima, T. Nagano, *J. Am. Chem. Soc.* **2007**, *129*, 7313-7318; b) B. D. Calitree, M. R. Detty, *Synlett* **2010**, 89-92. The chloride salt of **3** is well known as Pyronin G or Pyronin Y. This compound and their

derivatives are very useful on broad areas of research as organic dyes, fluorescent probes and other materials. However, there is no report on their use as carbene precursors.

- [11]. Y. H. Ahn, J. S. Lee, Y. T. Chang, *J. Am. Chem. Soc.* **2007**, *129*, 4510-4511.
- [12]. X. Cattoën, D. Bourissou, G. Bertrand, *Tetrahedron Lett.* **2006**, *47*, 531-534.
- [13]. S. Gómex-Bujedo, M. Alcarazo, C. Pichon, E. Álvarez, R. Fernández, J. M. Lassaletta, *Chem. Commun.* **2007**, 1180-1182.
- [14]. a) D. Kremzow, G. Seidel, C. W. Lehmann, A. Fürstner, *Chem. Eur. J.*, **2005**, *11*, 1833-1853; b) T. Ksterke, T. Pape, F. E. Hahn, *J. Am. Chem. Soc.*, **2011**, *133*, 2112; c) M. Alcarazo, K. Radkowski, R. Goddard and A. Fürstner, *Chem. Commun.* **2011**, *47*, 776-778.
- [15]. D. Tpu, D. A. Dixon, C. Roe, *Chem. Rev.* **2009**, *109*, 3385-3478.
- [16]. M. C. Burla, R. Caliendo, M. Camalli, B. Carrozzini, G. L. Cascarano, L. De Caro, C. Giacovazzo, G. Polidori, R. Spagna, *J. Appl. Cryst.* **2005**, *38*, 381-388.
- [17]. G. M. Sheldrick, *SHELX-97*; University of Göttingen: Göttingen, Germany, **1997**.
- [18]. A. M. Echavarren, J. K. Stille, *J. Am. Chem. Soc.* **1987**, *109*, 5478-5486.
- [19]. PLATON SQUEEZE program: a) A. L. Spek, *PLATON, A Multipurpose Crystallographic Tool*, Utrecht University, Utrecht, The Netherlands, **2005**; b) P. van der Sluis, A. L. Spek, *Acta Crystallogr. Sect. A*, **1990**, *46*, 194-201.

Chapter 7

1,8-Disubstituted Xanthyliene-based Remote Carbenes: Photolytic Generation and Isolation of Low-coordinate Palladium(II) Complex

7-1. Introduction

Prior to the identification of persistent carbenes, several transient species of carbenes, generated via photolysis of diazo precursors, have been studied using spectroscopic methods. As mentioned in above chapters, Schuster *et al.* have generated transient cyclic aromatic carbenes, 9-xanthylidene and 9-mesityl-9,10-dihydro-9-boraanthrydene, via photolysis, and have investigated their photophysical properties, reactivity, and ground states.^[1] In their study, irradiation of 9-xanthylidene with nitrogen laser led to the formation of decomposition products, predominantly the dimer. Therefore, we envisioned that introduction of sterically bulky substituents at the C1 and C8 positions can be effective in preventing dimerization. Furthermore, the different steric environment produced by the ligand can also generate a metal complex with unusual coordination number in contrast to our previous work on isolating the carbene palladium(II) complex (**Pd_{1,8-H}**) with 16 electrons (Figure 1). In this chapter, we report the direct observation of novel xanthylidene carbene derivatives bearing remote amino groups via photolysis of the tosylhydrazone lithium salts and the isolation of a low-coordinate cationic palladium(II) complex bound to the carbene ligand with phenyl groups at the C1 and C8 positions.

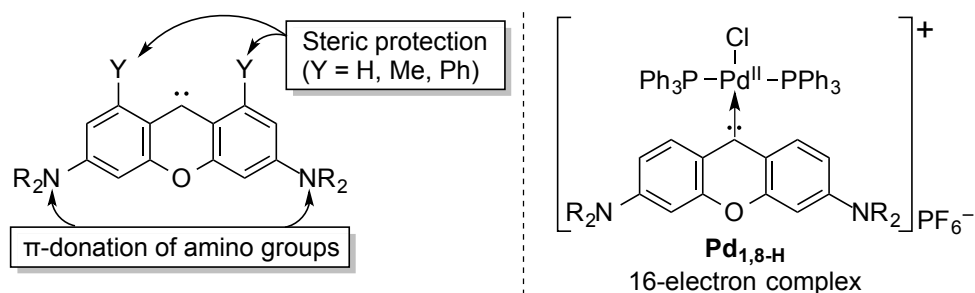
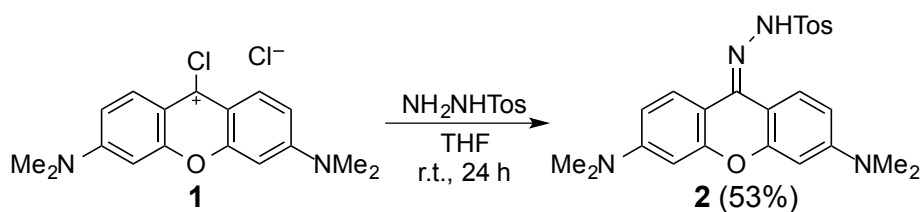


Figure 1. General structure of novel xanthylidene carbene derivatives (left) and previously isolated 16-electron palladium(II) complex **Pd_{1,8-H}** (right).

7-2. Synthesis

Diazo compounds are typical precursors used in the photochemical generation of free carbenes.^[2] Most well-behaved diazo compounds have electron-withdrawing substituents, such as carbonyl, phosphoryl, and sulfonyl substituents, adjacent to the diazo carbon, while simple diazoalkanes and aryl-substituted diazomethane derivatives have been proven to be thermally less stable. Indeed, attempts to generate the diazo species based on cyclic aromatic carbene structures with 3,6-diamino substituents were unsuccessful in our hands. Therefore, we decided to synthesize tosylhydrazone alkali metal salts. Thermolysis or photolysis of the salt could then generate the corresponding diazo species, followed by the spontaneous denitrogenation to afford the free carbene *in situ*.^[3] Towards this, chloride **1**^[4] was treated with three equivalent of tosylhydrazide to afford the desired tosylhydrazone **2** (53% yield) as an orange solid (Scheme 1). The structure of the product was confirmed by ¹H NMR, ¹³C NMR, high resolution ESI-MS, and elemental analysis. The NMR spectra displayed peaks attributed to the asymmetric structure. In addition, suitable crystals for single crystal X-ray diffraction were obtained by recrystallization from CH₂Cl₂/hexane (Figure 2). To the best of our knowledge, the X-ray crystal structure



Scheme 1. Synthesis of tosylhydrazone **2**.

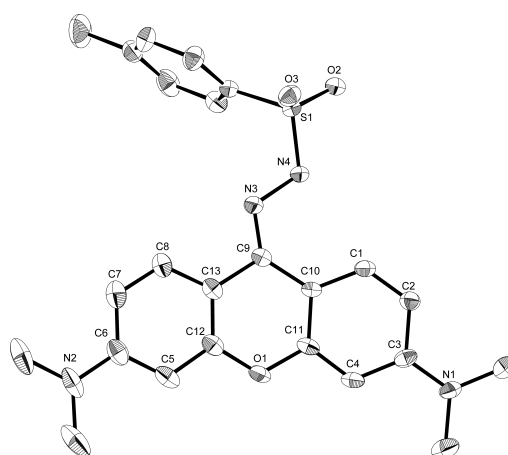
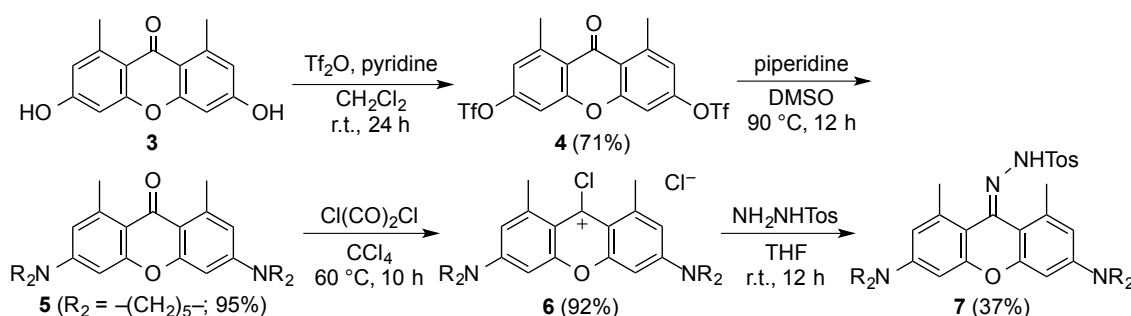


Figure 2. ORTEP drawing of **2** (two independent molecule) with thermal ellipsoids shown at 50% probability level. Hydrogen atoms, solvent, and the other molecule are omitted for clarity. Selected bond lengths (Å) and angles (°): C9–C13, 1.466(6); C9–C10, 1.466(6); C9–N3, 1.304(6); N3–N4, 1.423(5); N4–S1, 1.630(4); C10–C9–C13, 115.0(4); C13–C9–N3, 114.3(4); C10–C9–N3, 130.7(4); C9–N3–N4, 115.4(4); N3–N4–S1, 113.6(3).

of **2** shown in Figure 2 represents the first structural elucidation of a biaryl tosylhydrazone, although a number of examples for such derivatives have been synthesized previously.^[5] In the structure, bond angles around C9 are slightly distorted from that of a regular sp^2 hybridization. However, thermolysis of the alkali metal salt of hydrazone **2** did not yield the carbene, rather it yielded the corresponding ketone or other decomposition products, suggesting that the reactivity of the diazo species was high even at ambient temperature (more than that of 9-diazoxanthene)^[1b] Consequently, we chose to perform photolysis of the tosylhydrazone lithium salt to facilitate matrix isolation and measure steady-state and transient UV-vis absorption data (see below).

With a view to prevent dimerization of free carbenes, we designed precursors bearing bulky groups at the 1 and 8 positions. Since methyl groups hamper the dimerization of free carbenes, enhancing steric repulsion in the resulting bis(xanthene)-based olefin species, synthesis of 1,8-dimethyl substituted compound **5** was performed (Scheme 2). The starting material **3**, which was synthesized using a reported protocol,^[6] was treated with trifluoromethanesulfonic anhydride in CH_2Cl_2 in the presence of pyridine. Subsequently, the resulting triflates of compound **4** were substituted with piperidine in an aromatic nucleophilic substitution reaction to provide 3,6-diamino substituted ketone **5** (67% yield for 2 steps). In a protocol similar to that used for the preparation of tosylhydrazone **2**, the 1,8-dimethyl analogue **7** was also prepared (34% yield for 2 steps). The structures of both **5** and **7** were confirmed using single crystal X-ray diffraction analysis (Figure 3, 4). In the structure of **7**, similar distortion of bond angles around C9 could be found to accommodate for the steric demands of the hydrazone moiety on C9 and the methyl groups at the C1 and C8. This steric congestion is also evident by marginal inclination of the substituent methyl groups (C10–C1–C14, 121.8(2); C13–C8–C15, 121.6(2)).



Scheme 2. Synthesis of the 1,8-dimethyl tosylhydrazone **7**.

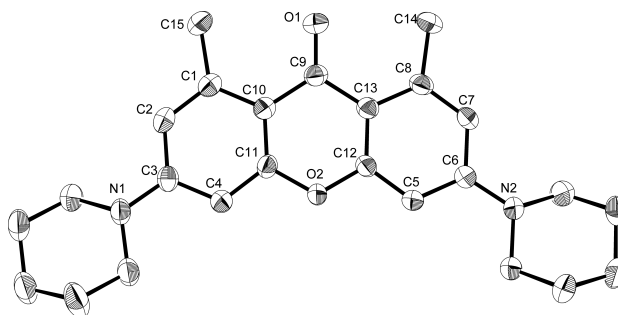


Figure 3. ORTEP drawing of **5** with thermal ellipsoids shown at the 50% probability level. Hydrogen atoms and the solvent are omitted for clarity. Selected bond lengths (Å) and angles (°): C9–C13, 1.468(2); C9–C10, 1.465(2); C9–O1, 1.233(2); C10–C9–C13, 115.41(14); C10–C9–O1, 122.22(16); C13–C9–O1, 122.36(15).

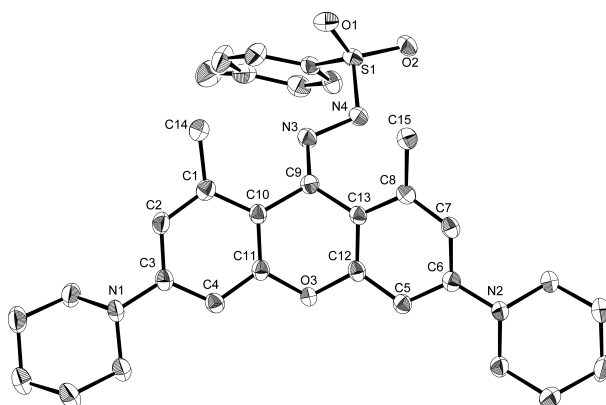
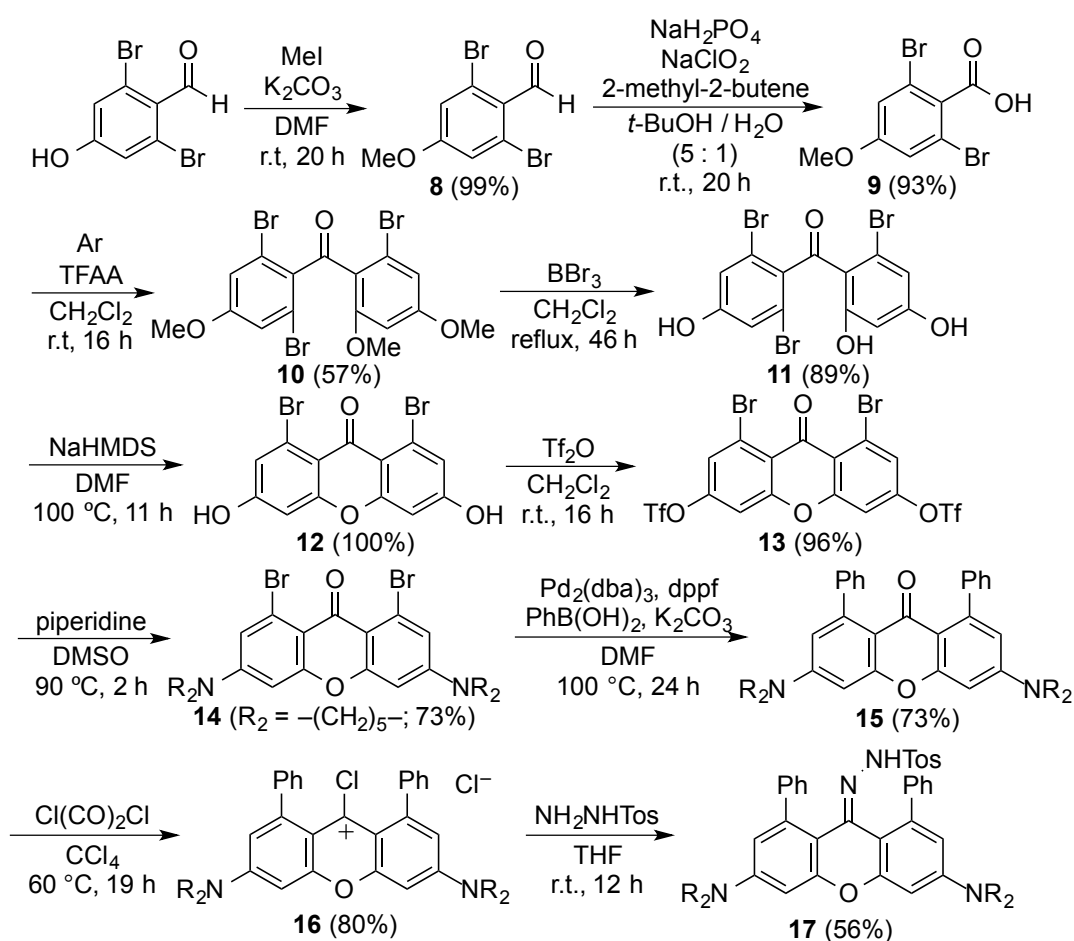


Figure 4. ORTEP drawing of **7** with thermal ellipsoids shown at the 50% probability level. Hydrogen atoms are omitted for clarity. Selected bond lengths (Å) and angles (°): C9–C13, 1.463(3); C9–C10, 1.479(3); C9–N3, 1.297(3); N3–N4, 1.414(3); N4–S1, 1.642(2); C10–C9–C13, 114.10(19); C13–C9–N3, 128.2(2); C10–C9–N3, 117.0(2); C9–N3–N4, 114.73(19); N3–N4–S1, 112.48(16).

With a view to generate a structure providing more effective steric protection of the carbene than that provided by the 1,8-dimethyl analogue, we pursued the synthesis of 1,8-diphenyl substituted tosylhydrazone **17** (Scheme 3). Since aryl groups can be readily introduced at the C1 and C8 positions via cross coupling reactions, we designed the synthesis of **17** with 1,8-dibromo-substituted xanthone derivative **14** as the starting material. As described in experimental section in more detail, condensation of 2,6-dibromo-4-methoxybenzoic acid **9** with 1-bromo-3,5-dimethoxybenzene in the presence of trifluoroacetic anhydride in CH_2Cl_2 gave the tribromo-substituted biaryl ketone **10** in moderate yields. Successive demethylation and intermolecular aromatic nucleophilic substitution produced 1,8-dibromo-substituted species **12**, the dibromo analog of **3**. Nucleophilic substitutions of the triflate **13** with piperidine yielded the desired compound C3 and C6 bispiperidine compound **14**. Then, phenyl substitutions at positions C1 and C8 were accomplished by Suzuki–Miyaura cross coupling, to generate

the 1,8-diphenyl substituted ketone **15** (73% yield). The desired tosylhydrazone **17** (48% yield in 2 steps) was prepared from **15** following protocols used for the synthesis of **7**. The X-ray structural analysis of **10**, **14**, **15**, and **17** were successfully carried out as show in Figure 5, 6, 7, and 8, respectively. Although **17** could be identified by ^1H NMR, ^{13}C NMR, high resolution MS, elemental analysis, and X-ray analysis (Figure 8), **17** was found to be relatively more sensitive to light in the solution when compared with that of **2** or **7**. This suggested that increased steric repulsion between hydrazone moiety and bulkier phenyl groups led to the relative instability of **17**, an indication of the ease of decomposition to the corresponding diazo species.



Scheme 3. Synthesis of 1,8-diphenyl tosylhydrazone **17**. Ar = 1-bromo-3,5-dimethoxybenzene; TFAA = trifluoroacetic anhydride; NaHMDS = sodium hexamethyldisilazane; dppf = Bis(diphenylphosphino)ferrocene.

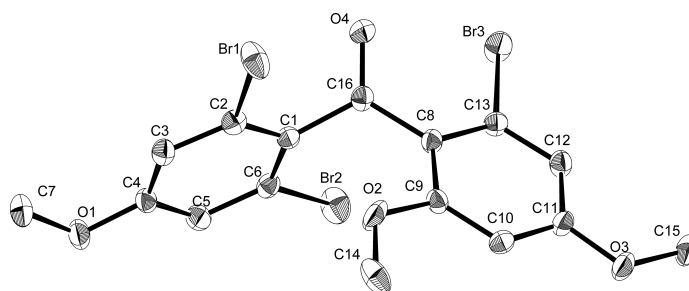


Figure 5. ORTEP drawing of **10** with the thermal ellipsoids shown at the 50% probability level. Hydrogen atoms are omitted for clarity. Selected bond lengths (Å) and angles (°): C1-C16, 1.514(4); C8-C16, 1.486(4); C16-O4, 1.211(4); C1-C16-C8, 120.5(3); C1-C16-O4, 117.8(3); C8-C16-O4, 121.7(3).

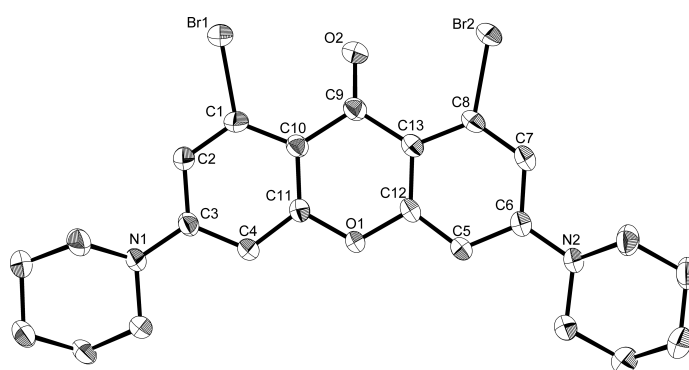


Figure 6. ORTEP drawing of **14** with the thermal ellipsoids shown at the 50% probability level. Hydrogen atoms and the solvent are omitted for clarity. Selected bond lengths (Å) and angles (°): C9-C10, 1.478(6); C9-C13, 1.472(6); C9-O2, 1.226(5); C10-C9-C13, 114.6(4); C10-C9-O2, 122.6(4); C13-C9-O2, 122.8(4).

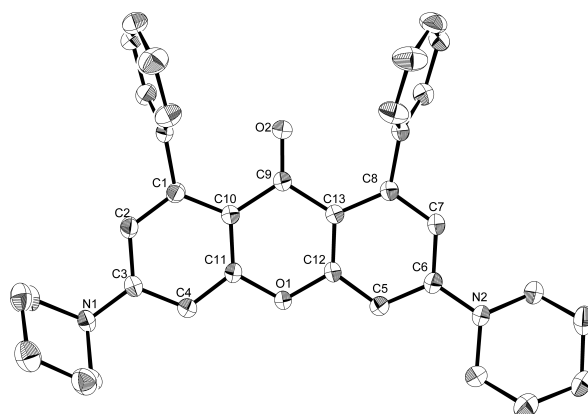


Figure 7. ORTEP drawing of **15** (two independent molecules) with the thermal ellipsoids shown at the 50% probability level. Hydrogen atoms, the solvent and another molecule are omitted for clarity. Selected bond lengths (Å) and angles (°): C9-C10, 1.474(3); C9-C13, 1.474(3); C9-O2, 1.226(2); C10-C9-C13, 114.96(16); C10-C9-O2, 122.63(17); C13-C9-O2, 122.39(17).

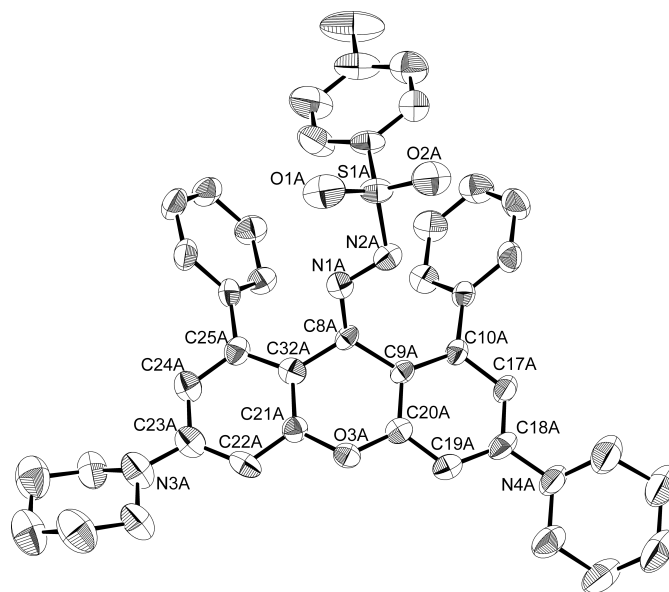
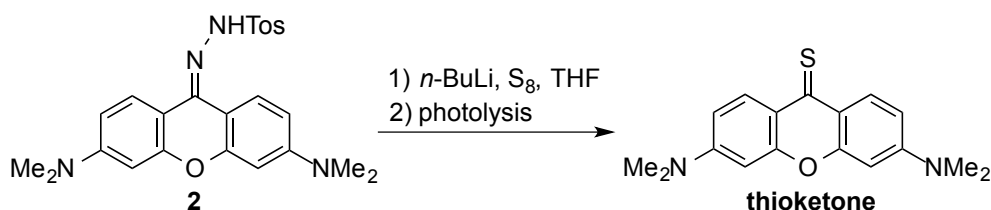


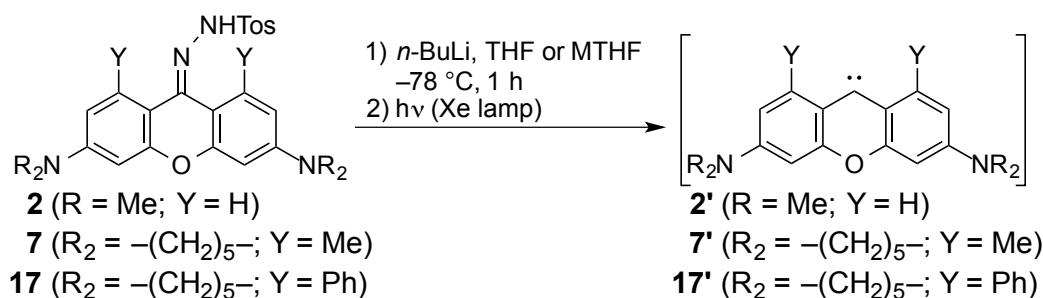
Figure 8. ORTEP drawing of **17** (two independent molecule) with the thermal ellipsoids shown at the 50% probability level. Hydrogen atoms, the solvent, and another molecule are omitted for clarity. Selected bond lengths (Å) and angles (°): C8A–C9A, 1.493(6); C8A–C32A, 1.471(7); C8A–N1A, 1.300(6), N1A–N2A, 1.337(5); C9A–C8A–C32A, 115.5(4); C32A–C8A–N1A, 114.8(4); C9A–C8A–N1A, 128.6(4); C8A–N1A–N2A, 117.9(4). N1A–N2A–S1A, 115.8(3).

7-3. Photolysis of Tosylhydrazones

Tosylhydrazone lithium salts, prepared by the lithiation of tosylhydrazones with *n*-butyllithium in THF, were photo-irradiated and the properties of the generated free carbenes were investigated. As previously stated, carbenes were not detected when the lithium salts were subjected to thermal decomposition conditions (r.t., 21 h). Lithium salts were photolysed because *in situ* generation of the carbene was considered to effectively prevent the decomposition of the intermediate diazo species. Photochemical decomposition products generated on the irradiation of the lithium salt of **2** with a Hg lamp through a Pyrex filter for 1 h at room temperature were analyzed to prove the generation of a free carbene. While complex mixtures were observed in the photolysate in the absence of trapping reagents, addition of excess elemental sulfur allowed for the isolation of the corresponding thioketone species as the major product (scheme 4). This trapping of the decomposition products of **2** by sulfur indicates the *in situ* formation of free carbenes. The isolation of only low quantities of the thioketone (29%) on purification over silica gel by preparative thin layer chromatography was attributed to the unstable nature of the thioketone. However, the recorded spectroscopic data of the thioketone were consistent with that reported by us previously.^[4] This result clearly indicated that, on photolysis of lithium salt **2**, the free carbene **2'** (prime indicates the corresponding carbene) was generated.



Scheme 4. Photolysis of the lithium salts of **2** in the presence of element sulfur.



Scheme 5. Photolysis of tosylhydrazone lithium salts. MTHF = 2-methyltetrahydrofuran.

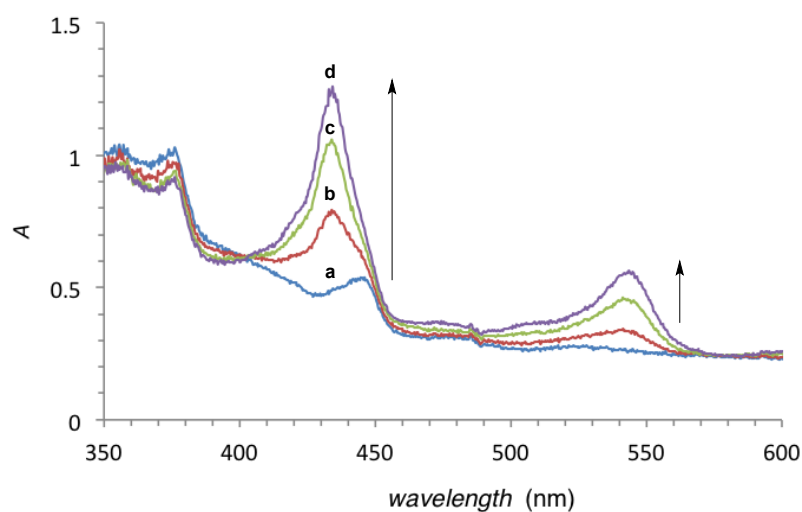


Figure 9. Low-temperature UV-vis absorption spectra of the lithium salt of **2** in dry, degassed MTHF glassy matrix at 78 K after irradiation at 370 nm for (a) 0 min, (b) 1 min, (c) 5 min, and (d) 15 min.

To further confirm the generation of free carbene **2'**, we measured the low temperature UV-vis spectra of the photochemical decomposition of **2** at 78 K in a 2-methyltetrahydrofuran (MTHF) glassy matrix using a Xe lamp. As shown in Figure 9, on irradiation of the lithium salt of **2** at 370 nm, a strong absorption signal at 432 nm and a minor absorption signal at 543 nm increased with increase of the duration of irradiation. These species were stable at 78 K for hours. However, both absorption signals completely disappeared at 103 K during raising the temperature, indicating the transient nature of the

species. Time-dependent (TD) DFT calculations of the carbene, radical, diazo, and cation species at the B3LYP/6-31G(d)//PBEPBE/6-31++G(d,p) level of theory were performed to assign the transient species in the UV-vis spectra. Consistent with the wavelength associated with the observed peak, *i.e.* 432 nm, excitation of the closed-shell singlet carbene was predicted at 421 nm with oscillator strength (f) of 0.635. Theoretical predictions for the other possible species are as follows; radical, $\lambda_{\text{max}} = 452$ nm ($f = 0.5965$); diazo, $\lambda_{\text{max}} = 339.73$ nm ($f = 0.3257$); and cation, $\lambda_{\text{max}} = 491.47$ nm ($f = 0.7028$). These theoretical predictions provided further support that the species with an absorption at 432 nm is the free carbene **2'**. Absence of coincident predicted peaks made the identification of the species with absorption at 543 nm difficult. However, the presence of radical species can influence the spectrum, since the EPR study under similar conditions showed a doublet peak, suggesting the existence of the paramagnetic species (see Experimental Section).

Transient absorption spectra and decay traces during photolysis of tosylhydrazone lithium salts were measured in degassed THF at ambient temperature by laser-flash photolysis ($\lambda_{\text{exc}} = 355$ nm, 5 ns pulse). The time-resolved spectrum apparently showed large decrease in the intensity of absorption at 430 nm, while no change in the intensity is observed at ~ 540 nm, suggesting that the species at 432 nm was observed only in the transient absorption spectrum (Figure 10). According to the decay trace at 430 nm, the lifetime of the transient species in degassed THF at room temperature was determined to be 1.2 μs . When compared to the reported half-life of singlet xanthylidene in pentane (~ 50 μs ; lifetime = 166 μs),^[1b] the lifetime of **2'** is significantly shorter. It is likely that introduction of electron-donating amino groups at the conjugated positions (C3 and C6) makes **2'** kinetically more reactive than the parent xanthylidene.

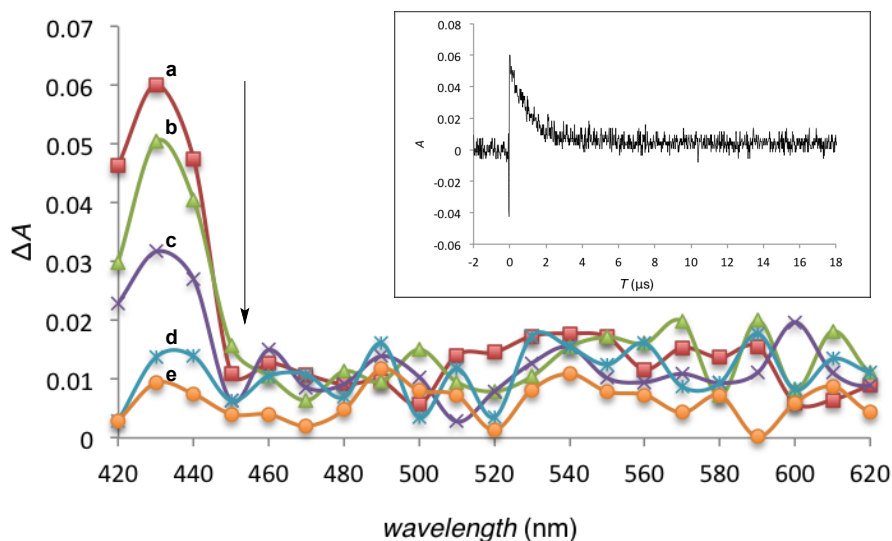


Figure 10. Transient absorption spectrum of the lithium salt of **2** in THF at 293 K at (a) 0, (b) 0.1, (c) 0.6, (d) 1.5, and (e) 10 μs after nanosecond laser excitation at 355 nm. Inset: A time profile at 430 nm corresponding to the decay of free carbene species.

Similar matrix isolation UV-vis and transient absorption measurements for the 1,8-disubstituted species **7'** and **17'** were carried out under identical conditions. In case of **7'**, the absorption intensity at 444 nm increased during the irradiation of the tosylhydrazone lithium salt in MTHF (Figure 11); λ_{max} of the observed absorption peak in the UV-vis spectrum was consistent with the theoretically predicted value of 443.00 nm ($f = 0.628$). A clear decay process at 440 nm was observed in the transient absorption spectroscopic analysis for **7'** (Figure 12). The lifetime of **7'** was determined to be 0.35 μs , which was shorter than that of **2'**. This result suggests that the carbene **7'** is likely to be kinetically less stable than **2'**. Chemical transformations, such as intramolecular C–H insertion or proton migration, are also likely to be occurred.^[7] Thus, we anticipated that the bulkier phenyl groups could hamper the possible C–H activation as well as dimerization. However, irradiation of the tosylhydrazone lithium salt of **17** did not generate measurable quantities of **17'** (only insignificant changes were observed in the UV-vis spectra even after irradiating for a long time as shown in Figure 13). While the observed weak band at ~ 455 nm corresponded with the predicted wavelength of absorption for **17'** (446.67 nm, $f = 0.451$), the weak change in the intensity of absorption did not allow for a definitive assignment. Furthermore, the corresponding transient species could not be observed in the transient absorption spectrum of the lithium salt of **17** (Figure 14), probably due to low absorption efficiency of the intermediate diazo species with low f value (395.29 nm, $f = 0.0721$, see Experimental Section). This result indicates that phenyl groups at C1 and C8 positions, rather than providing a sterically protected environment for the resulting carbene, inhibit efficient light absorption by the compound.

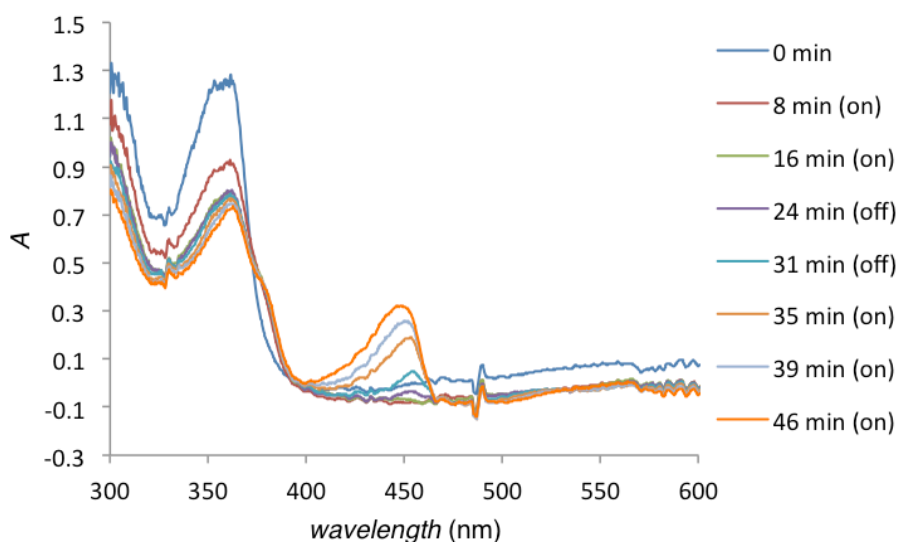


Figure 11. Low temperature UV-vis absorption spectra of the lithium salt of **7** in dry and degassed MTHF glass at 78 K, irradiated at 352 nm for 0–16 min and 31–46 min. The irradiation was suspended from 16 min to 31 min.

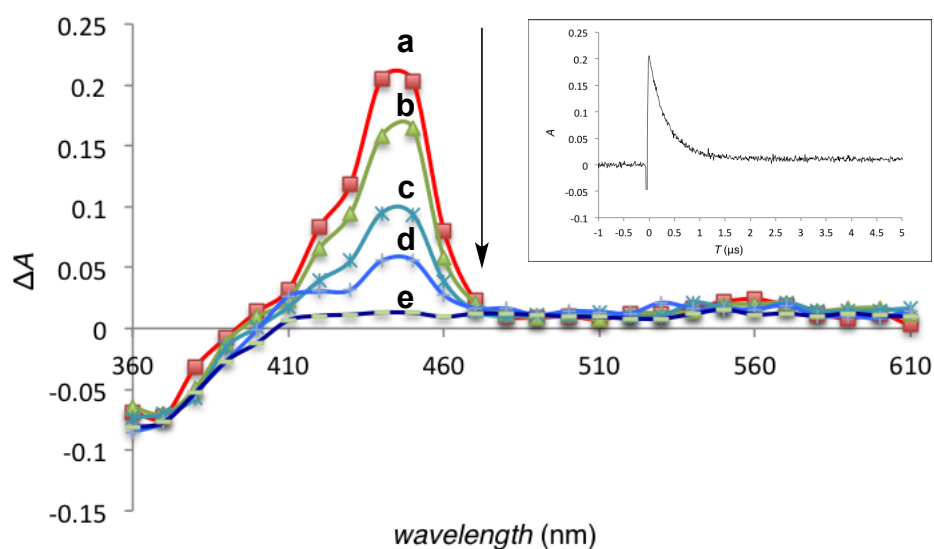


Figure 12. Transient absorption spectrum of the lithium salt of **7** in dry and degassed THF at 293 K at (a) 0, (b) 0.1, (c) 0.3, (d) 0.5, and (e) 5.0 μ s after nanosecond laser excitation at 355 nm. Inset: A time profile at 440 nm corresponding to the decay of free carbene species.

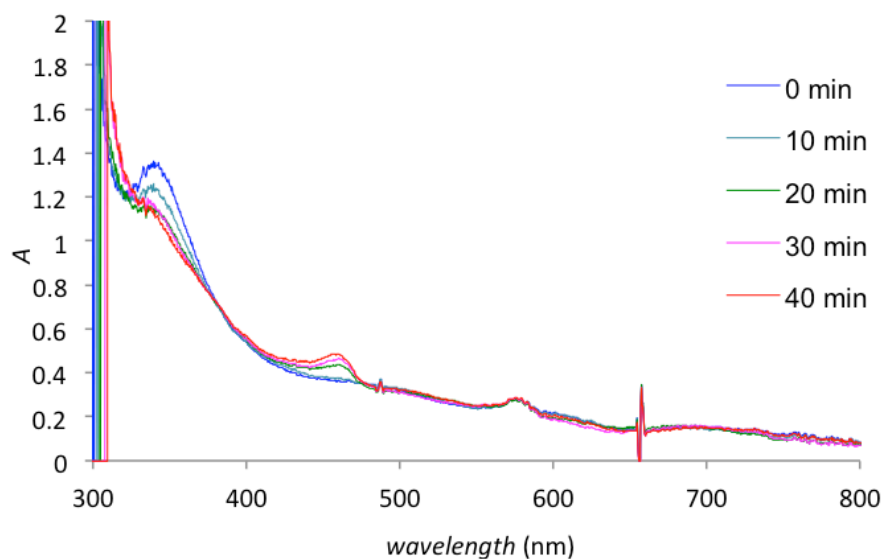


Figure 13. Low temperature UV-vis absorption spectra of the lithium salt of **17** in dry and degassed MTHF glass at 78 K, irradiated at 343 nm for 0-40 min.

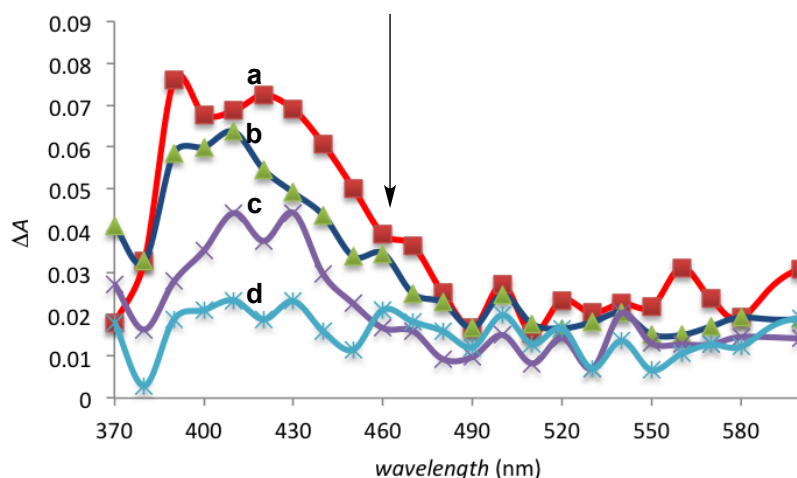
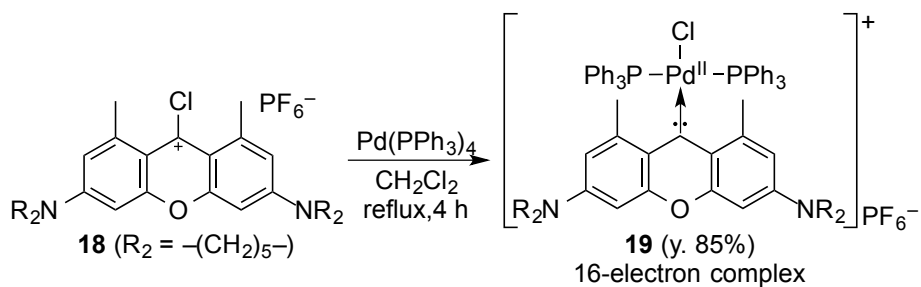


Figure 14. Transient absorption spectrum of the lithium salt of **17** in dry and degassed THF at 293 K at (a) 0, (b) 1.0, (c) 2.0, and (d) 4.0 μ s after nanosecond laser excitation at 355 nm.

7-4. Metal Complexes

To investigate the steric effects of substituents at C1 and C8 positions, we studied the formation of corresponding metal complexes by oxidative addition to the low valent metal. In our previous report, the palladium(II) complex (**Pd_{1,8-H}**; xanthene ligand with protons at C1 and C8, Figure 1) showed a stronger donating ability (supported by elongated palladium-chloride bond length) and a higher catalytic ability than a Pd^{II} NHC complex.^[4] Therefore, we directed our efforts towards the syntheses and evaluation of the Pd-1,8-disubstituted xanthene complexes. Following a protocol similar to that reported previously, 1,8-dimethyl-9-chloro precursor **18** was treated with Pd(PPh₃)₄ in CH₂Cl₂ to give the cationic 16-electron palladium(II) complex **19** (85% yield) as a red solid (Scheme 6). The ¹³C NMR spectrum of **19** showed a characteristic triplet peak at 211.2 ppm (²J_{PC} = 3 Hz), which could be attributed to the carbene carbon atom. In addition, the triplet peak (J_{PC} = 4 Hz) at 26.9 ppm indicated a through space spin coupling between ³¹P nuclei of PPh₃ moiety and ¹³C nuclei of the methyl group.^[8] Furthermore, the ³¹P NMR peak of PPh₃ moiety (12.2 ppm) in **19** was shifted significantly to high field when compared with that of **Pd_{1,8-H}** (24.1 ppm). Finally, the structure of **19** could be clarified by single crystal X-ray diffraction analysis (Figure 16). Both the palladium-chloride and palladium-carbenic carbon bond lengths in crystal structure of **19** were marginally longer than those observed in **Pd_{1,8-H}** (Pd–Cl: 2.3987(18) Å for **19** vs 2.374 Å (avg.) for **Pd_{1,8-H}**; Pd–C: 2.002(8) Å for **19** vs 1.986 Å (avg.) for **Pd_{1,8-H}**), suggesting that the methyl groups at C1 and C8 positions induced higher steric congestion around the metal center. With regards to the above-mentioned through space spin coupling, distance between carbon atoms of the methyl groups and phosphorus atoms were found to be in the 3.642–4.063 Å range, a range that can reasonably account for any non-bonded interactions.^[8]



Scheme 6. Synthesis of the 16-electron palladium(II) complex **19** with 1,8-dimethyl xanthylidene.

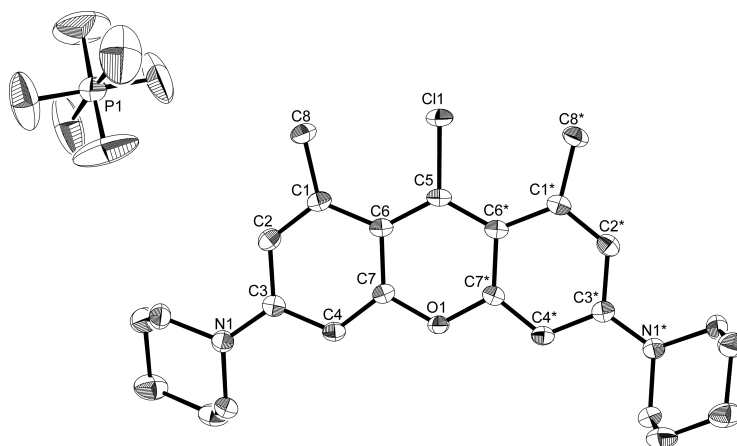


Figure 15. ORTEP drawing of **18** with the thermal ellipsoids shown at the 50% probability level. Hydrogen atoms, solvent molecule, and the disordered parts are omitted for clarity. The shown structure was symmetrically expanded. Selected bond lengths (Å) and angles (°): C5-C6, 1.4126(15); C5-Cl1, 1.7213(18); C6-C5-Cl1, 118.27(8); C6-C5-C6*, 123.45(16).

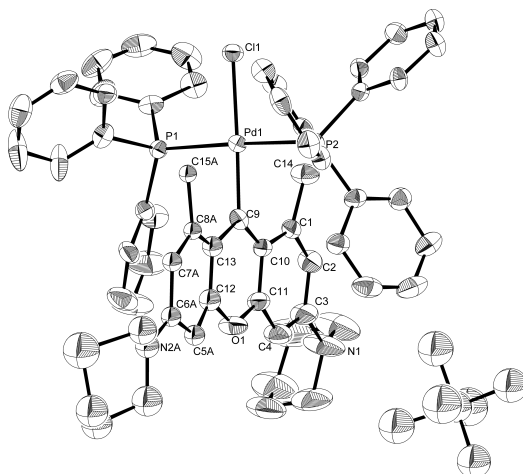
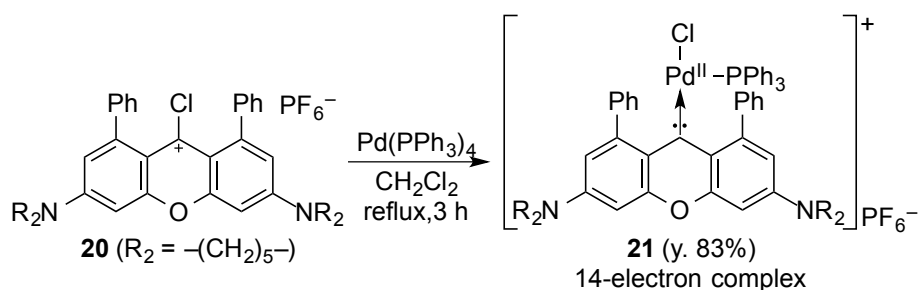


Figure 16. ORTEP drawing of **19** with the thermal ellipsoids shown at the 50% probability level. Hydrogen atoms, the solvent and the disordered parts are omitted for clarity. Selected bond lengths (Å) and angles (°): C9-C10, 1.409(11); C9-C13, 1.455(11); C9-Pd1, 2.002(8), Pd1-P1, 2.364(2); Pd1-P2, 2.368(2); Pd1-Cl1, 2.3987(18); C10-C9-C13, 118.3(7); C10-C9-Pd1, 121.7(6); C13-C9-Pd1, 119.9(6).

Subsequently, oxidative addition of $\text{Pd}(\text{PPh}_3)_4$ to 1,8-diphenyl-9-chloro precursor **20** was also performed (Scheme 6); a purple solid (83% yield), with ^{31}P NMR spectroscopic data (23.9 ppm(s)) identical to that of **Pd_{1,8-H}**, was obtained. However, the multiplet at aromatic region in the ^1H NMR spectrum accounted for protons on only one PPh_3 moiety. In addition, high-resolution ESI-MS also supported that the product was a 14-electron complex with only one PPh_3 moiety. Finally, recrystallization of **21** from CH_2Cl_2 /hexane enabled us to obtain purple crystals suitable for X-ray analysis and the structure could be unambiguously assigned to be the cationic 14-electron Pd^{II} complex, consistent with that of the solution structure predicted by NMR experiments (Figure 18). Compared to the structures of **19** and **Pd_{1,8-H}**, bond lengths of the $\text{Pd}-\text{Cl}$ (2.3621(14) Å) and $\text{Pd}-\text{C}(\text{carbenic carbon})$ (1.981(5) Å) bonds in **21** were significantly contracted, suggesting that lower coordination around the metal center induced enhancement of the bond strengths between the metal and ligands. In addition, the $\text{Pd}-\text{P}$ bond length (2.2763(13) Å) in **21** was also shorter than that in **19** (2.366 Å (avg.)) or **Pd_{1,8-H}** (2.337 Å (avg.)) although the shift in ^{31}P NMR frequency of **21** was quite similar to that of **Pd_{1,8-H}**.

The isolation of intriguing low-coordinate metal complexes, intermediates in the metal catalyzed reactions, remain largely elusive due to their unstable nature.^[9] In particular, there is only one reported example of a stable, formal 14-electron Pd^{II} cation complex involving a carbene ligand.^[10] The bulky and sterically rigid cyclic (alkyl)(amino)carbene played an important role for isolating the low-coordinate Pd^{II} complex. By contrast, structural elucidation of similar NHC complexes have not been realized, even though spectroscopic evidences have been reported.^[11] Thus, **21** can be regarded as the second example of a cationic 14-electron Pd^{II} complex involving a carbene ligand.

In its solid form, **21** was stable under aerobic conditions at room temperature, however, in solution, **21** slowly decomposed to an unidentified compound. The crystal structure of **21** revealed an agostic interaction between Pd and C29 of the phenyl substituent ($\text{Pd}-\text{C}29$: 2.521(5) Å) and the observed stability of **21** was attributed to this interaction. In contrast, the stability of several unsaturated 14-electron metal complexes involve agostic interactions with C–H bond of sp^3 carbon atom.^[12] Additionally, the steric environment around the metal center in **21** is remarkably congested, indicating that the complex could also be kinetically stabilized by the adjacent bulky phenyl groups.



Scheme 7. Synthesis of 14-electron palladium(II) complex **21** involving a 1,8-diphenyl xanthylidene ligand.

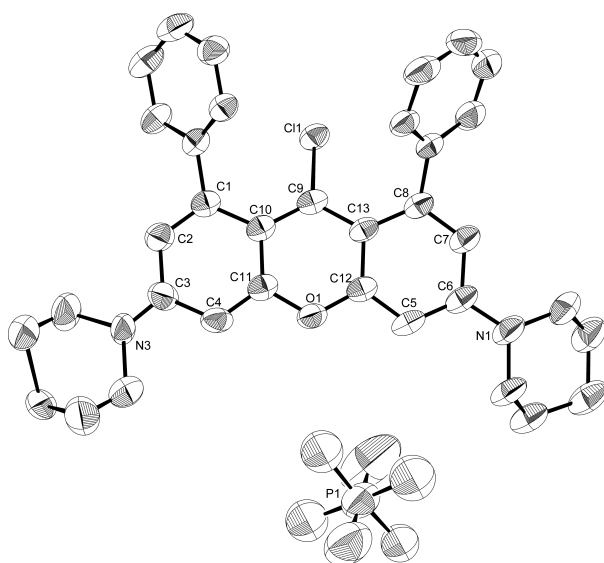


Figure 17. ORTEP drawing of **20** with the thermal ellipsoids shown at the 50% probability level. Hydrogen atoms and the disordered parts are omitted for clarity. Selected bond lengths (Å) and angles (°): C9–C10, 1.405(6); C9–C13, 1.410(5); C9–Cl1, 1.725(4); C10–C9–C13, 122.1(4); C10–C9–Cl1, 120.6(3); C13–C9–Cl1, 117.0(3).

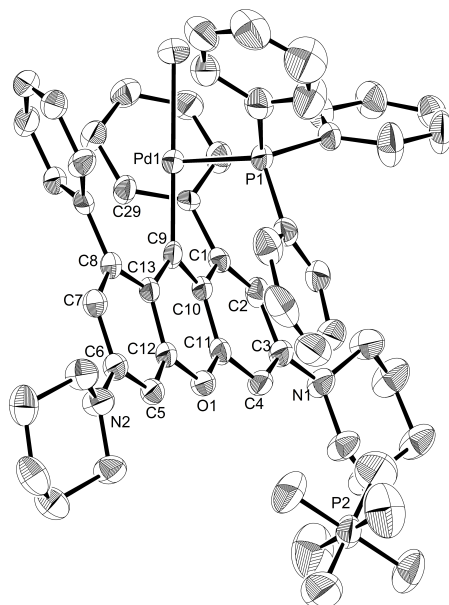


Figure 18. ORTEP drawing of **21** with thermal ellipsoids shown at 50% probability level. Hydrogen atoms are omitted for clarity. Selected bond lengths (Å) and angles (°): C9–C10, 1.423(6); C9–C13, 1.402(6); C9–Pd1, 1.981(5); Pd1–P1, 2.2763(13); Pd1–Cl1, 2.3621(14); C10–C9–C13, 117.2(4); C10–C9–Pd1, 116.1(3); C13–C9–Pd1, 126.6(3); C9–Pd1–Cl1, 177.90(15); P1–Pd1–Cl1, 91.29(5); P1–Pd1–C9, 89.75(14).

7-5. Conclusions and Outlook

In conclusion, 1,8-disubstituted xanthylidene-based remote carbenes were generated by photolysis. Palladium(II) complexes involving these ligand were also prepared. Free carbene resulting from the parent xanthylidene could be identified in the matrix-isolation UV-vis spectroscopic analysis after irradiation of the tosylhydrazone lithium salt. The transient absorption spectrum revealed that the generated carbene was kinetically more reactive than the parent xanthylidene. Although the 1,8-substituents were ineffective at elongating the lifetimes of the corresponding free carbenes, oxidative addition of $\text{Pd}(\text{PPh}_3)_4$ to 1,8-diphenyl substituted carbene afforded the rather elusive low-coordinate 14-electron palladium(II) complex. The structure of the complex displays agostic interaction between the metal center and a phenyl group. Also, this complex is the second example of a low-coordinate cationic palladium(II) complex involving a carbene ligand, thereby, providing new insights for stabilizing the unusual complex.

Experimental Section

General. Melting points were measured with a Yanagimoto micro melting point apparatus and are uncorrected. Column chromatography was carried out using Kanto silica gel 60N. ^1H NMR (400 MHz), ^{13}C NMR (100 MHz), ^{19}F NMR (376 MHz) and ^{31}P NMR (160 MHz) spectra were recorded using a JEOL EX-400 or AL-400 spectrometer. The ^1H and ^{13}C NMR chemical shifts (δ scale) are given in downfield from tetramethylsilane, determined by residual protons of the solvent (^1H) or the solvent itself (^{13}C). The ^{19}F NMR chemical shifts (δ scale) are reported from external CFCl_3 . The ^{31}P NMR chemical shifts (δ scale) were reported from 85% H_3PO_4 (external). Tetrahydrofuran (THF) and diethyl ether (Et_2O) were freshly distilled from Na-Benzophenone. The EPR spectra were acquired on a Bruker ELEXSYS E500 instrument at 78 K. The elemental analyses were performed using a Perkin-Elmer 2400 CHNS elemental analyzer. Mass spectra were measured with a Thermo Fisher Scientific model LTQ Orbitrap XL by using the ESI-TOF or APCI-TOF method in the positive ion mode with acetonitrile or methanol solution samples. Crystals suitable for X-ray structural determination were mounted on a Bruker SMART APEXII CCD diffractometer or a Rigaku SCXmini diffractometer and irradiated with graphite monochromated Mo-K α radiation ($\lambda = 0.71073 \text{ \AA}$) at 173 K for data collection. The data were processed using the APEX program suite or the Rigaku SCXmini program. The structures were solved by a direct method using the SIR-2004 program.^[13] Refinement on F^2 was carried out by full-matrix least-squares using the SHELXL-97 program.^[14] All non-hydrogen atoms were refined using anisotropic thermal parameters except for disordered atoms. The hydrogen atoms were included in the refinement with isotropic thermal parameters. The crystallographic data are summarized in Table 2.

9-Chloro-3,6-bis(dimethylamino)-9H-xanthen-9-ylum chloride (**1**)^[4], 3,6-dihydroxy-1,8-dimethyl-9H-xanthene-9-one (**3**)^[6], and 2,6-dibromo-4-hydroxybenzaldehyde^[15] were prepared by literature methods, respectively.

Synthesis of tosylhydrazone 2

To a solution of **1** (300 mg, 0.893 mmol) in dry THF (10 mL) was added *p*-toluenesulfonyl hydrazide (500 mg, 2.68 mmol). The reaction mixture was stirred at room temperature for 24 h. After the reaction was completed, water was added and the solution was extracted with CH₂Cl₂ (x3). The combined organic layer was washed with brine and dried over Na₂SO₄. The solvent was removed in vacuo and the crude product was purified by silica gel column chromatography eluted with AcOEt/hexane = 2:1. After the solvent was removed in vacuo, the resulting solid was recrystallized from CH₂Cl₂/hexane to afford **2** (221 mg, 0.470 mmol, 53%) as an orange solid. M.p. 180-181 °C (decomp.); ¹H NMR (CD₂Cl₂, 400 MHz): δ = 2.37 (3H, s), 2.98 (6H, s), 3.00 (6H, s), 6.30 (1H, d, ⁴J = 3 Hz), 6.39 (1H, d, ⁴J = 3 Hz), 6.52 (1H, dd, ³J = 9 Hz, ⁴J = 3 Hz), 6.55 (1H, dd, ³J = 9 Hz, ⁴J = 3 Hz), 7.29 (2H, d, ³J = 9 Hz), 7.82 (1H, d, ³J = 9 Hz), 7.86 (2H, d, ³J = 9 Hz), 8.40 ppm (1H, d, ³J = 9 Hz); ¹³C NMR (CD₂Cl₂, 100 MHz): δ = 44.83 (CH₃), 63.24 (CH₃), 63.51 (CH₃), 120.82 (CH), 121.96 (CH), 128.32 (C), 131.02 (CH), 132.28 (C), 132.62 (CH), 148.58 (CH), 151.83 (CH), 152.52 (CH), 152.80 (CH), 159.03 (C), 165.62 (C), 167.39 (C), 176.04 (C), 176.22 (C), 176.96 (C), 179.12 ppm (C); HR-MS(ESI positive): Calcd for C₂₄H₂₇N₄O₃S 451.1798, found 451.1797 for [M+H]⁺; Elemental Analysis: calcd (%) for C₂₄H₂₆N₄O₃S: C 63.98, H 5.82, N 12.44, S 7.12; found: C 63.75, H 5.79, N 12.31, S 7.34.

Synthesis of 4

Dry pyridine (4.10 mL, 50.7 mmol) and dry trifluoromethanesulfonic anhydride (2.88 mL, 17.1 mmol) was added at 0 °C to a solution of **3** (1.40 g, 5.45 mmol) in dry CH₂Cl₂ (40 mL). After the reaction mixture was stirred at room temperature for 16 h, water was added to the mixture and the solution was extracted with CH₂Cl₂ (x3). The combined organic layer was washed with water, 10% HCl aq, and brine and dried over Na₂SO₄. The solvent was evaporated in vacuo and chromatographic purification was achieved on silica gel with CH₂Cl₂ as the eluent. After the solvent was removed in vacuo, the resulting solid was recrystallized with CH₂Cl₂/hexane to give **4** (2.02 g, 3.88 mmol, 71%) as a white solid. M.p. 182-185 °C; ¹H NMR (C₆D₆, 400 MHz): δ = 2.59 (6H, s), 6.48 (2H, d, ⁴J = 2 Hz), 6.75 ppm (2H, d, ⁴J = 2 Hz); ¹⁹F NMR (CDCl₃, 376 MHz): δ = -73.10 ppm (s); ¹³C NMR (C₆D₆, 100 MHz): δ = 23.13 (CH₃), 108.38 (CH), 117.62 (C), 119.73 (CH), 120.90 (C), 145.54 (C), 151.28 (C), 156.75 (C), 177.75 ppm (C); HR-MS(APCI positive): Calcd for C₁₇H₁₁O₈F₆S₂ 520.9794, found 520.9786 for [M+H]⁺; Elemental Analysis: calcd (%) for C₁₇H₁₀O₈F₆S₂: C 39.24, H 1.94, S 12.32; found: C 39.12, H 1.90, S 12.38.

Synthesis of 5

To a solution of **4** (1.90 g, 3.65 mmol) in dry DMSO (20 mL) was added piperidine (3.61 mL, 36.5 mmol). The mixture was stirred at 90 °C for 12 h and the solution was cooled to room temperature. After water was added to the solution, the resulting white solid was collected by filtration and washed with saturated aqueous Na₂CO₃ and water. The solid was dried in vacuo and recrystallized from CH₂Cl₂/hexane to give **5** (1.35 g, 3.46 mmol, 95%) as a yellow solid. M.p. 194-195 °C (decomp.); ¹H NMR (CDCl₃, 400 MHz): δ = 1.66 (12H, m), 2.83 (6H, s), 3.35 (8H, t, ³J = 5 Hz), 6.50 (2H, d, ⁴J = 2 Hz), 6.55 ppm (2H, d, ⁴J = 2 Hz); ¹³C NMR (CD₂Cl₂, 100 MHz): δ = 24.08 (CH₃), 24.36 (CH₂), 25.13 (CH₂), 48.53 (CH₂), 98.07 (CH), 112.81 (C), 113.80 (CH), 142.32 (C), 153.44 (C), 158.61 (C), 178.75 ppm (C); HR-MS(ESI positive): Calcd for C₂₅H₃₁O₂N₂ 391.2380, found 391.2383 for [M+H]⁺; Elemental Analysis: calcd (%) for C₂₅H₃₀N₂O₂: C 76.89, H 7.74, N 7.17; found: C 76.51, H 7.45, N 7.24.

Synthesis of 6

Oxalyl chloride (0.166 mL, 1.92 mmol) was added to a solution of **5** (503 mg, 1.29 mmol) in dry CCl₄ (5 mL). The reaction mixture was stirred for 10 h at 60 °C. After the reaction was completed, the solution was diluted with CH₃CN and evaporated. The crude product was washed with ether (x3) and recrystallized from CH₃CN/ether to give **6** (530 mg, 1.19 mmol, 92%) as a purple solid. M.p. 170-171 °C (decomp.); ¹H NMR (CD₃CN, 400 MHz): δ = 1.67-1.75 (12H, m), 2.86 (6H, s), 3.68 (8H, t, ³J = 5 Hz), 6.70 (2H, d, ⁴J = 2 Hz), 7.06 ppm (2H, d, ⁴J = 2 Hz); HR-MS(ESI positive): Calcd for C₂₅H₃₀ClON₂ 409.2041, found 409.2037 for [M]⁺;

*The low solubility of **6** in CD₃CN and other solvents hampered the ¹³C NMR measurement.

Synthesis of 7

To a solution of **6** (200 mg, 0.449 mmol) in dry THF (10 mL) was added *p*-toluenesulfonyl hydrazide (252 mg, 1.35 mmol). The reaction mixture was stirred at room temperature for 12 h. After the reaction was completed, water was added and the solution was extracted with CH₂Cl₂ (x3). The combined organic layer was washed with brine and dried over Na₂SO₄. The solvent was removed in vacuo and the crude product was purified by silica gel column chromatography eluted with AcOEt/hexane = 1:5. After the solvent was removed in vacuo, the resulting solid was recrystallized from CH₂Cl₂/hexane to afford **7** (94 mg, 0.17 mmol, 37%) as an orange solid. M.p. 160-162 °C (decomp.); ¹H NMR (CDCl₃, 400 MHz): δ = 1.63 (12H, m), 2.37 (6H, s), 2.58 (3H, s), 3.19 (4H, t, ³J = 6 Hz), 3.26 (4H, t, ³J = 6 Hz), 6.45 (1H, d, ⁴J = 2 Hz), 6.50 (1H, d, ⁴J = 2 Hz), 6.55 (1H, d, ⁴J = 2 Hz), 7.21 (2H, d, ³J = 8 Hz), 7.31 (1H, s), 7.76 ppm (2H, d, ³J = 8 Hz); ¹³C NMR (CDCl₃, 100 MHz): δ = 21.31 (CH₃), 21.54 (CH₃), 22.69 (CH₃), 24.31 (CH₂), 25.36 (CH₂), 25.46 (CH₂), 49.00 (CH₂), 49.70 (CH₂), 53.42 (CH₂), 99.56 (CH), 99.83 (CH), 107.76 (C), 112.61 (CH), 114.00 (C), 114.22 (CH), 127.99 (CH), 129.35 (CH), 135.49 (C), 136.56 (C), 136.61 (C), 143.64 (C), 143.85 (C), 151.91 (C), 153.00 (C), 154.96 (C), 156.44 ppm (C); HR-MS(ESI positive):

Calcd for $C_{32}H_{39}O_3N_4S$ 559.2737, found 559.2736 for $[M+H]^+$; Elemental Analysis: calcd (%) for $C_{32}H_{38}N_4O_3S$: C 68.79, H 6.86, N 10.03, S 5.74; found: C 68.58, H 6.98, N 9.99, S 5.91.

Synthesis of 8

2,6-Dibromo-4-hydroxybenzaldehyde (7.43g, 26.6 mmol) and potassium carbonate (7.35 g, 53.2 mmol) were dissolved in dry DMF (40 mL) under Ar and methyl iodide (2.80 mL, 32.1 mmol) was added dropwise. The reaction mixture was stirred at room temperature for 20 h. The reaction mixture was quenched by the addition of water and the organic compound was extracted with AcOEt (x3) and the combined organic layer was washed with water and brine and dried over Na_2SO_4 . The solvent was evaporated to give **8** (7.77 g, 26.4 mmol, 99%) as a white solid. M.p. 139-140 °C; 1H NMR ($CDCl_3$, 400 MHz): δ = 3.87 (3H, s), 7.19 (2H,s), 10.22 ppm (1H, s); ^{13}C NMR ($CDCl_3$, 100 MHz): δ = 56.10 (CH_3), 119.64 (CH), 124.47 (C), 126.94 (C), 162.60 (C), 190.07 ppm (CH); HR-MS(APCI positive): Calcd for $C_8H_7O_2Br_2$ 292.8807 (^{79}Br - ^{79}Br), 294.8786 (^{79}Br - ^{81}Br), 296.8766 (^{81}Br - ^{81}Br), found 292.8809 (^{79}Br - ^{79}Br), 294.8784 (^{79}Br - ^{81}Br), 296.8760 (^{81}Br - ^{81}Br) for $[M+H]^+$; Elemental Analysis: calcd (%) for $C_8H_6O_2Br_2$: C 32.69, H 2.06; found: C 32.68, H 1.91.

Synthesis of 9

To a solution of **8** (7.77 g, 26.3 mmol) in *t*-BuOH/ H_2O (5:1, 450 mL) were added NaH_2PO_4 (4.73 g, 39.5 mmol), $NaClO_2$ (9.51 g, 105 mmol), and 2-methyl-2-butene (16.7 mL, 158 mmol). After the mixture was stirred for 20 h, the solvents were evaporated and the resulting aqueous solution was washed with CH_2Cl_2 (x3). Then, conc. HCl aq. was added to the aqueous layer until a yellow solid was completely formed. The aqueous layer was extracted with AcOEt (x3) and the combined organic layer was washed with brine and dried over Na_2SO_4 . The solvent was evaporated to give **9** (7.60 g, 24.5 mmol, 93%) as a white solid. M.p. 161-162 °C; 1H NMR ($CDCl_3$, 400 MHz): δ = 3.02 (3H, s), 7.10 ppm (2H, s); ^{13}C NMR ($CDCl_3$, 100 MHz): δ = 55.93 (CH_3), 117.59 (CH), 120.03 (C), 128.98 (C), 160.81 (C), 171.44 ppm (C); HR-MS(APCI positive): Calcd for $C_8H_7O_3Br_2$ 308.8756 (^{79}Br - ^{79}Br), 310.8736 (^{79}Br - ^{81}Br), 312.8715 (^{81}Br - ^{81}Br), found 308.8758 (^{79}Br - ^{79}Br), 310.8733 (^{79}Br - ^{81}Br), 312.8707 (^{81}Br - ^{81}Br) for $[M+H]^+$; Elemental Analysis: calcd (%) for $C_8H_6O_3Br_2$: C 31.00, H 1.95; found: C 31.01, H 1.77.

Synthesis of 10

To a solution of **9** (16.3 g, 52.5 mmol) and 1-bromo-3,5-dimethoxybenzene (12.0 g, 55.3 mmol) in CH_2Cl_2 (200 mL) was slowly added trifluoroacetic anhydride (37.2 mL, 263 mmol). After the mixture was stirred at room temperature for 16 h, the reaction was quenched with water. The solution was extracted with CH_2Cl_2 (x3) and the combined organic layer was washed with brine and dried over Na_2SO_4 . After the solvent was evaporated, chromatographic purification was achieved on silica gel with CH_2Cl_2 /hexane (1:1) as the eluent. The solution was evaporated in vacuo and the resulting solid was

recrystallized from CH_2Cl_2 /hexane to give **10** (15.2 g, 29.8 mmol, 57%) as a white solid. M.p. 178 °C; ^1H NMR (CDCl_3 , 400 MHz): δ = 3.58 (3H, s), 3.81 (3H, s), 3.84 (3H, s), 6.35 (1H, d, 4J = 2 Hz), 6.83 (1H, d, 4J = 2 Hz), 7.06 ppm (2H, s); ^{13}C NMR (CDCl_3 , 100 MHz): δ = 55.69 (CH_3), 55.76 (CH_3), 56.10 (CH_3), 98.15 (CH), 111.68 (CH), 117.00 (CH), 121.21 (C), 121.56 (C), 125.31 (C), 135.59 (C), 159.79 (C), 160.97 (C), 162.74 (C), 191.20 ppm (C); HR-MS(APCI positive): Calcd for $\text{C}_{16}\text{H}_{14}\text{O}_4\text{Br}_3$ 506.8436 (^{79}Br - ^{79}Br - ^{79}Br), 508.8416 (^{79}Br - ^{79}Br - ^{81}Br), 510.8395 (^{79}Br - ^{81}Br - ^{81}Br), 512.8375 (^{81}Br - ^{81}Br - ^{81}Br), found 506.8436 (^{79}Br - ^{79}Br - ^{79}Br), 508.8410 (^{79}Br - ^{79}Br - ^{81}Br), 510.8385 (^{79}Br - ^{81}Br - ^{81}Br), 512.8359 (^{81}Br - ^{81}Br - ^{81}Br) for $[\text{M}+\text{H}]^+$; Elemental Analysis: calcd (%) for $\text{C}_{16}\text{H}_{13}\text{O}_4\text{Br}_3$: C 37.76, H 2.57; found: C 38.03, H 2.46.

Synthesis of 11

To a solution of **10** (3.89 g, 7.64 mmol) in CH_2Cl_2 (100 mL) was added boron tribromide (1.0 M CH_2Cl_2 solution, 70.0 mL, 70.0 mmol) under Ar atmosphere. After the mixture was refluxed for 23 h, the additional boron tribromide (7.5 mL, 7.5 mmol) was added and stirred for 23 h. The reaction mixture was cooled to 0 °C with ice bath and 10% HCl aq. was carefully added to the solution. After the bubble releasing was completed, the solvent was evaporated in vacuo and the resulting solution was extracted with ether (x3). The combined organic layer was washed with brine and dried over Na_2SO_4 . The solvent was evaporated to give **11** (3.17 g, 6.79 mmol, 89%) as a white solid. M.p. 261-264 °C; ^1H NMR ($\text{DMSO}-d_6$, 400 MHz): δ = 6.28 (1H, d, 4J = 2 Hz), 6.65 (1H, d, 4J = 2 Hz), 7.03 (2H, s), 10.67 (2H, br s), 11.68 ppm (1H, br s); ^{13}C NMR ($\text{DMSO}-d_6$, 100 MHz): δ = 102.47 (CH), 114.73 (C), 114.90 (CH), 118.78 (CH), 120.29 (C), 124.99 (C), 133.36 (C), 158.97 (C), 163.27 (C), 163.92 (C), 193.72 ppm (C); HR-MS(APCI positive): Calcd for $\text{C}_{13}\text{H}_8\text{O}_4\text{Br}_3$ 464.7967 (^{79}Br - ^{79}Br - ^{79}Br), 466.7946 (^{79}Br - ^{79}Br - ^{81}Br), 468.7926 (^{79}Br - ^{81}Br - ^{81}Br), 470.7905 (^{81}Br - ^{81}Br - ^{81}Br), found 464.7972 (^{79}Br - ^{79}Br - ^{79}Br), 466.7945 (^{79}Br - ^{79}Br - ^{81}Br), 468.7918 (^{79}Br - ^{81}Br - ^{81}Br), 470.7893 (^{81}Br - ^{81}Br - ^{81}Br) for $[\text{M}+\text{H}]^+$; Elemental Analysis: calcd (%) for $\text{C}_{13}\text{H}_7\text{O}_4\text{Br}_3$: C 33.44, H 1.51; found: C 33.66, H 1.41.

Synthesis of 12

To a solution of **11** (3.05 g, 6.53 mmol) in dry DMF (90 mL) was added 1.09 M sodium hexamethyldisilazane (60.0 mL, 65.3 mmol). After the mixture was stirred at 100 °C for 11 h, 10% HCl aq. was added at 0 °C to afford a yellow solid. The resulting solid was collected by filtration and the solid was dried in vacuo (**12**, yellow solid, 2.56 g, 6.62 mmol, 100%). M.p. >300 °C; ^1H NMR ($\text{DMSO}-d_6$, 400 MHz): δ = 6.78 (2H, d, 4J = 3 Hz), 7.08 (2H, d, 4J = 3 Hz), 11.12 ppm (2H, br s); ^{13}C NMR ($\text{DMSO}-d_6$, 100 MHz): δ = 102.42 (CH), 111.85 (C), 119.97 (CH), 121.23 (C), 157.39 (C), 162.00 (C), 171.82 ppm (C); HR-MS(ESI positive): Calcd for $\text{C}_{13}\text{H}_6\text{O}_4\text{Br}_2\text{Na}$ 406.8525 (^{79}Br - ^{79}Br), 408.8505 (^{79}Br - ^{81}Br), 410.8484 (^{81}Br - ^{81}Br), found 406.8530 (^{79}Br - ^{79}Br), 408.8508 (^{79}Br - ^{81}Br), 410.8486 (^{81}Br - ^{81}Br) for $[\text{M}+\text{Na}]^+$.

Synthesis of 13

Dry pyridine (4.74 mL, 58.8 mmol) and dry trifluoromethanesulfonic anhydride (3.47 mL, 20.6 mmol) was added at 0 °C to a solution of **12** (2.28 g, 5.91 mmol) in dry CH₂Cl₂ (35 mL). After the reaction mixture was stirred at room temperature for 16 h, water was added to the mixture and the solution was extracted with CH₂Cl₂ (x3). The combined organic layer was washed with water, 10% HCl aq, and brine and dried over Na₂SO₄. The solvent was evaporated in vacuo and chromatographic purification was achieved on silica gel with CH₂Cl₂/hexane (1:1) as the eluent. After the solvent was removed in vacuo, the resulting solid was recrystallized with CH₂Cl₂/hexane to give **13** (3.68 g, 5.66 mmol, 96%) as a yellow solid. M.p. 157-159 °C; ¹H NMR (CDCl₃, 400 MHz): δ = 7.42 (2H, d, ⁴J = 3 Hz), 7.60 ppm (2H, d, ⁴J = 3 Hz); ¹⁹F NMR (CDCl₃, 376 MHz): δ = -72.01 ppm (s); ¹³C NMR (CDCl₃, 100 MHz): δ = 110.22 (CH), 116.69 (C), 119.45 (C), 119.88 (C), 123.67 (C), 124.50 (CH), 151.14 (C), 156.19 (C), 172.13 ppm (C). (*An unknown peak was included); HR-MS(APCI positive): Calcd for C₁₅H₅O₈Br₂F₆S₂ 648.7691 (⁷⁹Br-⁷⁹Br), 650.7671 (⁷⁹Br-⁸¹Br), 652.7650 (⁸¹Br-⁸¹Br), found 648.7703 (⁷⁹Br-⁷⁹Br), 650.7678 (⁷⁹Br-⁸¹Br), 652.7654 (⁸¹Br-⁸¹Br) for [M+H]⁺; Elemental Analysis: calcd (%) for C₁₅H₄O₈Br₂F₆S₂: C 27.71, H 0.62, S 9.86; found: C 27.92, H 0.34, S 9.54.

Synthesis of 14

To a solution of **13** (3.43 g, 5.27 mmol) in dry DMSO (40 mL) was added piperidine (2.19 mL, 22.1 mmol). The mixture was stirred at 90 °C for 2 h and the solution was cooled to room temperature. After water was added to the solution, the resulting yellow solid was collected by filtration and washed with saturated aqueous Na₂CO₃ and water. The solid was dried in vacuo and recrystallized from CH₂Cl₂/hexane to give **14** (2.01 g, 3.87 mmol, 73%) as a yellow solid. M.p. 281-283 °C (decomp.); ¹H NMR (CDCl₃, 400 MHz): δ = 1.67 (12H, m), 3.38 (8H, m), 6.53 (2H, d, ⁴J = 3 Hz), 7.06 ppm (2H, d, ⁴J = 3 Hz); ¹³C NMR (CDCl₃, 100 MHz): δ = 24.21 (CH₂), 25.20 (CH₂), 48.18 (CH₂), 99.06 (CH), 110.17(C), 117.73 (CH), 122.57 (C), 153.33 (C), 157.90 (C), 172.54 ppm (C); HR-MS(ESI positive): Calcd for C₂₃H₂₅O₂N₂Br₂ 519.0277 (⁷⁹Br-⁷⁹Br), 521.0257 (⁷⁹Br-⁸¹Br), 523.0236 (⁸¹Br-⁸¹Br), found 519.0280 (⁷⁹Br-⁷⁹Br), 521.0258 (⁷⁹Br-⁸¹Br), 523.0233 (⁸¹Br-⁸¹Br) for [M+H]⁺; Elemental Analysis: calcd (%) for C₂₃H₂₄O₂N₂Br₂+0.5CH₂Cl₂: C 50.16, H 4.48, N 4.98; found: C 50.29, H 4.33, N 4.95.

Synthesis of 15

A solution of **14** (1.00 g, 1.92 mmol), phenylboronic acid (1.37 g, 11.3 mmol), Pd₂(dba)₃•CHCl₃ (348 mg, 0.379 mmol), 1,1'-bis(diphenylphosphino)ferrocene (210 mg, 0.379 mmol) and K₂CO₃ (1.05 g, 7.59 mmol) in dry DMF (50 mL) was stirred at 100 °C for 24 h. The reaction mixture was poured into sat. NH₄Cl aq. and the solution was extracted with AcOEt (x3). The combined organic layer was washed with H₂O and brine and dried over MgSO₄. After the solvent was evaporated in vacuo, the crude product was purified by silica gel column chromatography eluted with AcOEt/hexane = 1:4. After the solvent was

removed in vacuo, the resulting solid was recrystallized from CH₂Cl₂/hexane to afford **15** (718 mg, 1.40 mmol, 73%) as a yellow solid. M.p. 236-240 °C (decomp.); ¹H NMR (CDCl₃, 400 MHz): δ = 1.67 (12H, m), 3.38 (8H, m), 6.63 (2H, d, ⁴J = 2 Hz), 6.68 (2H, d, ⁴J = 2 Hz), 7.22-7.33 ppm (10H, m); ¹³C NMR (CDCl₃, 100 MHz): δ = 24.35 (CH₂), 25.31 (CH₂), 48.60 (CH₂), 98.99 (CH), 112.44 (C), 114.80 (CH), 126.58 (CH), 127.38 (CH), 128.59 (CH), 142.26 (C), 144.19 (C), 153.18 (C), 158.50 (C), 175.04 ppm (C); HR-MS(ESI positive): Calcd for C₃₅H₃₅O₂N₂ 515.2693, found 515.2689 for [M+H]⁺.

Synthesis of 16

Oxalyl chloride (0.050 mL, 0.58 mmol) was added to a solution of **15** (200 mg, 0.389 mmol) in dry CCl₄ (2 mL). The reaction mixture was stirred for 19 h at 60 °C. After the reaction was completed, the solution was diluted with CH₃CN and evaporated. The crude product was recrystallized from CH₃CN/ether to give **16** (177 mg, 0.31 mmol, 80%) as a purple solid. M.p. >300 °C; ¹H NMR (CD₃CN, 400 MHz): δ = 1.68 (12H, m), 3.71 (8H, m), 6.89 (2H, d, ⁴J = 2 Hz), 6.99 (2H, d, ⁴J = 2 Hz), 7.25-7.42 ppm (10H, m); ¹³C NMR (CD₃CN, 100 MHz): δ = 24.52 (CH₂), 26.59 (CH₂), 49.49 (CH₂), 96.34 (CH), 114.57 (C), 119.55 (CH), 128.93 (CH), 129.03 (CH), 129.46 (CH), 141.22 (C), 146.27 (C), 154.31 (C), 155.59 (C), 159.37 ppm (C); HR-MS(ESI positive): Calcd for C₃₅H₃₄ClON₂ 533.2356, found 533.2354 for [M]⁺.

Synthesis of 17

To a solution of **16** (100 mg, 0.176 mmol) in dry THF (5 mL) was added *p*-toluenesulfonyl hydrazide (98 mg, 0.53 mmol). The reaction mixture was stirred at room temperature for 24 h. After the reaction was completed, water was added and the solution was extracted with CH₂Cl₂ (x3). The combined organic layer was washed with brine and dried over Na₂SO₄. The solvent was removed in vacuo and the resulting crude product was charged on preparative TLC eluted with AcOEt/hexane (1:1). The fraction was filtered with AcOEt and the solvent was evaporated to give **17** (67 mg, 0.098 mmol, 56%) as a pale purple solid. M.p. 218-220 °C (decomp.); ¹H NMR (CDCl₃, 400 MHz): δ = 1.58-1.75 (12H, m), 2.40 (3H, s), 3.26 (4H, t, ³J = 6 Hz), 3.34 (4H, t, ³J = 6 Hz), 6.63 (1H, d, ⁴J = 2 Hz), 6.68 (1H, d, ⁴J = 2 Hz), 6.73 (2H, s), 6.78 (2H, d, ³J = 8 Hz), 6.99 (2H, d, ³J = 8 Hz), 7.10-7.31 (6H, m), 7.38 (2H, d, ³J = 8 Hz), 7.45 ppm (2H, d, ³J = 8 Hz); ¹³C NMR (CD₂Cl₂, 100 MHz): δ = 21.61 (CH₂), 24.68 (CH₃), 25.72 (CH₂), 49.29 (CH₂), 49.82 (CH₂), 100.95 (CH), 101.06 (CH), 106.25 (C), 112.72 (CH), 115.28 (CH), 126.83 (CH), 127.71 (CH), 127.81 (CH), 127.92 (CH), 128.84 (CH), 129.04 (CH), 129.22 (CH), 129.45 (CH), 135.94 (C), 140.82 (C), 141.05 (C), 141.12 (C), 141.38 (C), 142.06 (C), 148.02 (C), 152.37 (C), 153.43 (C), 155.70 (C), 156.87 ppm (C). (*two peaks corresponded to CH₂ and one peak corresponded to C may be overlapped.); HR-MS(ESI positive): Calcd for C₄₂H₄₃O₃N₄S 683.3053, found 683.3050 for [M+H]⁺; Elemental Analysis: calcd (%) for C₄₂H₄₂N₄O₃S+CH₂Cl₂: C 67.27, H 5.78, N 7.30, S 4.18; found: C 67.54, H 5.96, N 7.35, S 4.40.

Thioketone formation in photolysis of the lithium salt of 2

To a solution of **2** (30 mg, 0.067 mmol) and elemental sulfur (21 mg, 0.67 mmol) in dry and degassed THF (5 mL) was added 1.68 M *n*-butyllithium in hexane (0.060 mL, 0.098 mmol) at $-78\text{ }^{\circ}\text{C}$. The reaction mixture was stirred for 0.5 h at $-78\text{ }^{\circ}\text{C}$. After being warmed up to room temperature, the solution was exposed to Hg light for 1 h. The quantitative formation of thioketone was observed by the ^1H NMR spectroscopic measurement in CDCl_3 . The solvent was removed in vacuo, and then the crude product was purified on silica gel preparative thin layer chromatography eluted with CH_2Cl_2 to give a pure thioketone (5.7 mg, 0.019 mmol, 29%) as a brown solid. The analytical and spectroscopic data of which were identical to those of an authentic sample.^[4]

Synthesis of 18

The chloride **6** (300 mg, 0.674 mmol) and potassium hexafluorophosphate (623 mg, 3.37 mmol) were dissolved in CH_3CN (15 mL) and stirred at room temperature for 17 h. After the solvent was evaporated and replaced with CH_2Cl_2 , the solution was filtered and the filtrate was evaporated. The crude product was recrystallized from CH_3CN /ether to give **18** (119 mg, 0.215 mmol, 32%) as a green solid. M.p. $197\text{--}200\text{ }^{\circ}\text{C}$ (decomp.); ^1H NMR (CD_3CN , 400 MHz): $\delta = 1.67\text{--}1.76$ (12H, m), 2.86 (6H, s), 3.68 (8H, t, $^3J = 5\text{ Hz}$), 6.70 (2H, d, $^5J = 2\text{ Hz}$), 7.06 ppm (2H, d, $^5J = 2\text{ Hz}$); ^{19}F NMR (CD_3CN , 376 MHz): $\delta = -71.71\text{ ppm}$ (d, $J_{\text{P-F}} = 706\text{ Hz}$); ^{31}P NMR (CD_3CN , 160 MHz): $\delta = -143.36\text{ ppm}$ (sept, $J_{\text{P-F}} = 706\text{ Hz}$); ^{13}C NMR (CD_3CN , 100 MHz): $\delta = 24.78$ (CH_2), 26.73 (CH_2), 27.02 (CH_3), 49.32 (CH_2), 96.07 (CH), 114.55 (C), 119.34 (CH), 143.67 (C), 154.60 (C), 155.87 (C), 159.36 ppm (C); HR-MS(ESI positive): Calcd for $\text{C}_{25}\text{H}_{30}\text{N}_2\text{OCl}$ 409.2041, found 409.2044 for $[\text{M}]^+$; Elemental Analysis: calcd (%) for $\text{C}_{25}\text{H}_{30}\text{ClF}_6\text{N}_2\text{OP}$: C 54.11, H 5.45, N 5.05; found: C 54.51, H 5.47, N 5.01.

Synthesis of 19

The chloride **18** (30 mg, 0.054 mmol) and $\text{Pd}(\text{PPh}_3)_4$ (75 mg, 0.065 mmol) were dissolved in CH_2Cl_2 (3 mL) and the reaction mixture was refluxed under Ar for 4 h. After the solvent was removed in vacuo, the resulting solid was washed with hexane (x3) to remove triphenylphosphine and then the crude product was recrystallized from CH_2Cl_2 /hexane to give **19** (54 mg, 0.046 mmol, 85%) as a red solid. M.p. $230\text{--}232\text{ }^{\circ}\text{C}$ (decomp.); ^1H NMR (CDCl_3 , 400 MHz): $\delta = 1.48\text{--}1.83$ (12H, m), 3.48 (8H, t, $^3J = 5\text{ Hz}$), 3.61 (6H, s), 6.18 (2H, d, $^4J = 2\text{ Hz}$), 6.47 (2H, d, $^4J = 2\text{ Hz}$), 7.14–7.24 (12H, m), 7.29–7.36 (6H, m), 7.52–7.62 ppm (12H, m); ^{19}F NMR (CDCl_3 , 376 MHz): $\delta = -74.23\text{ ppm}$ (d, $J_{\text{P-F}} = 715\text{ Hz}$); ^{31}P NMR (CDCl_3 , 160 MHz): $\delta = 12.21$ (s), -143.66 ppm (sept, $J_{\text{P-F}} = 706\text{ Hz}$); ^{13}C NMR (CDCl_3 , 100 MHz): $\delta = 24.22$ (CH_2), 25.67 (CH_2), 26.88 (CH_3 , t, $J = 4\text{ Hz}$), 48.01 (CH_2), 95.14 (CH), 115.21 (CH), 122.07 (C), 128.18 (CH, t, $J = 5\text{ Hz}$), 129.46 (C, t, $J = 22\text{ Hz}$), 130.87 (CH), 134.06 (CH, t, $J = 5\text{ Hz}$), 142.95 (C), 152.03 (C), 154.21 (C), 211.17 ppm (C, t, $^2J = 3\text{ Hz}$); HR-MS(ESI positive): Calcd for $\text{C}_{61}\text{H}_{60}\text{N}_2\text{OCIP}_2\text{Pd}^+$ 1039.2899, found 1039.2907 for $[\text{M}]^+$; Elemental Analysis: calcd (%) for $\text{C}_{61}\text{H}_{60}\text{ClN}_2\text{OP}_2\text{Pd} + 0.5\text{CH}_2\text{Cl}_2$: C 60.13, H 5.01, N

2.28; found: C 60.14, H 5.27, N 2.21.

Synthesis of 20

The chloride **18** (300 mg, 0.674 mmol) and potassium hexafluorophosphate (623 mg, 3.37 mmol) were dissolved in CH₃CN (15 mL) and stirred at room temperature for 17 h. After the solvent was evaporated and replaced with CH₂Cl₂, the solution was filtered and the filtrate was evaporated. The crude product was recrystallized from CH₃CN/ether to give **20** (119 mg, 0.215 mmol, 32%) as a green solid. M.p. 197-200 °C (decomp.); ¹H NMR (CD₃CN, 400 MHz): δ = 1.67-1.76 (12H, m), 2.86 (6H, s), 3.68 (8H, t, ³J = 5 Hz), 6.70 (2H, d, ⁵J = 2 Hz), 7.06 ppm (2H, d, ⁵J = 2 Hz); ¹⁹F NMR (CD₃CN, 376 MHz): δ = -71.71 ppm (d, *J*_{P-F} = 706 Hz); ³¹P NMR (CD₃CN, 160 MHz): δ = -143.36 ppm (sept, *J*_{P-F} = 706 Hz); ¹³C NMR (CD₃CN, 100 MHz): δ = 24.51 (CH₂), 26.58 (CH₂), 49.46 (CH₂), 96.23 (CH), 114.53 (C), 119.50 (CH), 128.94 (CH), 129.02 (CH), 129.44 (CH), 141.15 (C), 146.24 (C), 154.25 (C), 155.51 (C), 159.31 ppm (C); HR-MS(ESI positive): Calcd for C₂₅H₃₀N₂OCl 409.2041, found 409.2044 for [M]⁺; Elemental Analysis: calcd (%) for C₃₅H₃₄ClF₆N₂OP: C 61.90, H 5.05, N 4.13; found: C 61.98, H 5.34, N 4.08.

Synthesis of 21

The chloride **20** (30 mg, 0.054 mmol) and Pd(PPh₃)₄ (75 mg, 0.065 mmol) were dissolved in CH₂Cl₂ (3 mL) and the reaction mixture was refluxed under Ar for 4 h. After the solvent was removed in vacuo, the resulting solid was washed with hexane (x3) to remove triphenylphosphine and then the crude product was recrystallized from CH₂Cl₂/hexane to give **21** (54 mg, 0.046 mmol, 85%) as a red solid. M.p. 225-229 °C (decomp.); ¹H NMR (CD₂Cl₂, 400 MHz): δ = 1.66-1.85 (12H, m), 3.55-3.70 (8H, m), 6.36 (2H, d, ⁴J = 3 Hz), 6.91 (2H, d, ⁴J = 3 Hz), 6.94-7.06 (6H, m), 7.12-7.20 (4H, m), 7.17 (6H, td, ³J = 8 Hz, ⁴J = 3 Hz), 7.35-7.46 (3H, m), 7.46-7.58 (2H, m), 7.68-7.75 (2H, m), 7.76-7.83 (2H, m), 7.83-7.96 ppm (4H, m); ¹⁹F NMR (CDCl₃, 376 MHz): δ = -71.72 ppm (d, ¹J_{PF} = 714 Hz); ³¹P NMR (CDCl₃, 160 MHz): δ = 23.90 (s), -143.64 ppm (sept, *J*_{P-F} = 714 Hz); ¹³C NMR (CD₂Cl₂, 100 MHz): δ = 24.44 (CH₂), 26.08 (CH₂), 49.03 (CH₂), 96.10 (CH, d, *J* = 2 Hz), 114.35 (CH, d, *J* = 5 Hz), 117.67 (CH), 124.97 (C, d, *J* = 2 Hz), 128.18 (CH, d, *J* = 12 Hz), 129.29 (C, d, *J* = 52 Hz), 131.22 (C), 131.50 (CH), 133.34 (C), 134.22 (CH, d, *J* = 12 Hz), 136.17 (CH), 144.13 (C, d, *J* = 2 Hz), 147.52 (C, d, *J* = 2 Hz), 152.63 (C, d, *J* = 2 Hz), 155.89 (C), 205.61 ppm (C, d, *J* = 15 Hz). (*An unknown peak corresponded to a quaternary carbon was included); HR-MS(ESI positive): Calcd for C₅₃H₄₉ON₂ClPPd⁺ 901.2300, found 901.2302 for [M]⁺; Elemental Analysis: calcd (%) for C₅₃H₄₉ClP₂F₆ON₂Pd: C 60.75, H 4.71, N 2.67; found: C 60.59, H 4.35, N 2.62.

General procedure for recording photophysical data of tosylhydrazone lithium salts.

In a schlenk flask, a solution of tosylhydrazone in MTHF or THF was cooled to $-78\text{ }^{\circ}\text{C}$ and excess *n*-butyllithium in hexane was added dropwise. The mixture was stirred for 0.5 h at $-78\text{ }^{\circ}\text{C}$ and the mixture was warmed to room temperature. After transfer to cells for the measurements, the solution was degassed by three freeze-pump-thaw cycles before the measurements.

EPR measurement

The EPR measurement was performed to confirm the presence of paramagnetic species upon irradiation of the lithium salt of **2**. In a EPR tube, tosylhydrazone **2** (1.0 mg, 2.2 μmol) was dissolved in 2-methyltetrahydrofuran (MTHF, 0.2 mL). After cooling the solution at $-78\text{ }^{\circ}\text{C}$, the hexane solution of *n*-butyllithium (1.64 M, 40 μL , 65 μmol) was added dropwise and the solution was stirred for 0.5 h at $-78\text{ }^{\circ}\text{C}$. After the solution was warmed up by room temperature, the solution was degassed by three freeze-pump-thaw cycles and then the tube was completely sealed.

The EPR spectrum of the prepared sample was measured at 78 K after irradiated for 1 min using Xe lump (Figure 19). The doublet peak appeared in the spectrum, suggesting a radical species was generated by photolysis of the lithium salt of **2**.

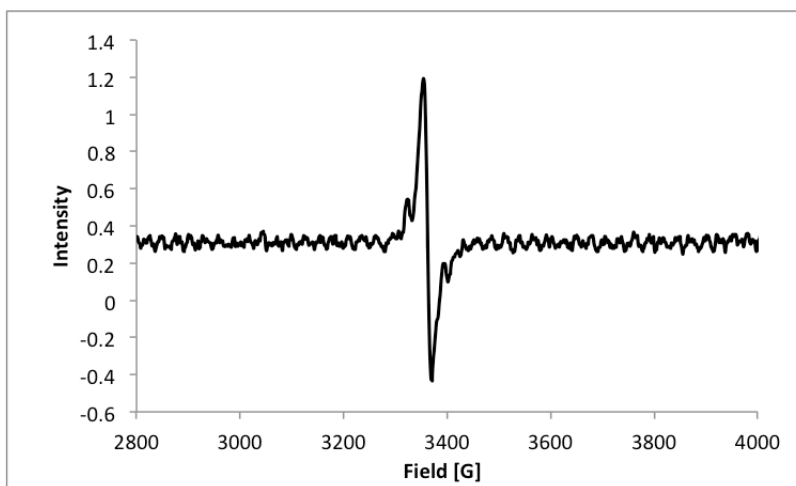
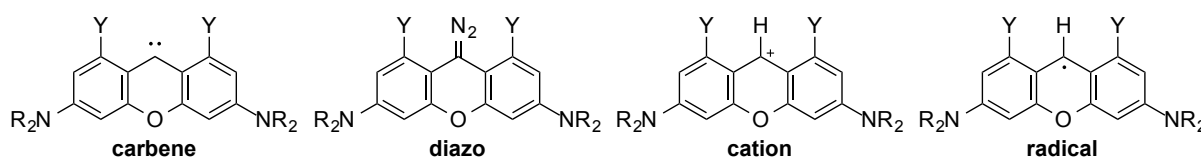


Figure 19. Experimental EPR spectrum of the photo-irradiated product of the lithium salt of **2** in MTHF at 78 K.

Computational Details

All computations were performed using the Gaussian 09 package of programs.^[16] The B3LYP hybrid functional was used with the 6-31G(d) basis set for optimizations and the PBEPBE hybrid functional was used with 6-31G++(d,p) basis set for TD-DFT calculations. All structures were optimized without any symmetry assumptions. Harmonic vibration frequency calculations at the same level were performed to verify that all the stationary points were local minima (with no imaginary frequency).

Table 1. Results of TD-DFT calculations for compounds which could be generated in photolysis of the tosylhydrazone lithium salts. (1,8-H system: R = Me; 1,8-Me and 1,8-Ph systems: R₂ = -(CH₂)₅-)



Compounds ^[a]	carbene	diazo	cation	radical
	λ_{\max} / nm (f)	λ_{\max} / nm (f)	λ_{\max} / nm (f)	λ_{\max} / nm (f)
1,8-H	421.82 (0.6342)	339.73 (0.3257)	491.47 (0.7028)	452.12 (0.5965)
1,8-Me	443.00 (0.6281)	338.44 (0.2761)	515.28 (0.8308)	422.45 (0.4084)
1,8-Ph	446.67 (0.4508)	395.29 (0.0721)	515.06 (0.8036)	545.96 (0.2322)

[a] Geometries optimized at the level of B3LYP/6-31G(d) and TD-DFT calculation was performed at the level of PBEPBE/6-31G++(d,p).

Table 2. Crystallographic data for **2**, **5**, **7**, **10**, **14**, **15**, **17**, **18**, **19**, **20**, and **21**.

	2	5 ^[a]	7 ^[b]	10
Formula	C ₂₅ H ₂₆ N ₄ O ₃ S •CH ₂ Cl ₂	C ₂₅ H ₃₀ N ₂ O ₂ •0.5CH ₂ Cl ₂	C ₃₂ H ₃₈ N ₄ O ₃ S	C ₁₆ H ₁₃ Br ₃ O ₄
Mol wt	535.47	432.97	558.72	508.99
Crystal system	triclinic	monoclinic	triclinic	monoclinic
Space group	<i>P</i> -1	<i>C</i> 2/ <i>c</i>	<i>P</i> -1	<i>P</i> 21/ <i>n</i>
Color	colorless	colorless	colorless	colorless
Habit	plate	block	plate	block
Cryst dims, mm	0.13 x 0.03 x 0.02	0.48 x 0.42 x 0.29	0.26 x 0.22 x 0.09	0.45 x 0.39 x 0.23
<i>a</i> , Å	12.403(3)	13.0511(13)	8.4736(10)	9.9414(12)
<i>b</i> , Å	14.593(4)	13.5902(14)	10.1071(11)	14.7990(18)
<i>c</i> , Å	15.296(4)	25.559(3)	18.108(2)	12.0002(14)
<i>a</i> , deg	76.914(4)	90	81.398(3)	90
<i>b</i> , deg	77.386(4)	101.536(3)	82.099(3)	110.965(3)
<i>g</i> , deg	76.670(4)	90	86.484(3)	90
<i>V</i> , Å ³	2583.4(11)	4441.7(8)	1517.5(3)	1648.6(3)
<i>Z</i>	4	8	2	4
<i>D</i> _{calc} , g cm ⁻³	1.377	1.295	1.223	2.051
Abs coeff, mm ⁻¹	0.367	0.197	0.145	7.357
<i>F</i> (000)	1120	1848	596	984
Temp, K	173(2)	173(2)	173(2)	173(2)
Reflections	14795	22045	6925	17039
Independent	11327	5076	6925	3776
<i>R</i> _{int}	0.0274	0.0475	0.0000	0.0460
Parameters	641	278	368	211
<i>R</i> ₁ [<i>I</i> > 2 <i>s</i> (<i>I</i>)]	0.0922	0.0534	0.0637	0.0358
<i>wR</i> ₂ (all data)	0.2398	0.1442	0.1743	0.0836
Goodness of fit	1.076	1.028	1.067	1.095
solv for crystallization	hexane/CH ₂ Cl ₂	hexane/CH ₂ Cl ₂	hexane/CH ₂ Cl ₂	hexane/CH ₂ Cl ₂

[a] These crystals contained solvent molecules in the crystal lattice (**2**, **5**: CH₂Cl₂). [b] In these crystal structures, there are disordered solvent molecules, and their contribution to the scattering values have been removed by using the PLATON SQUEEZE program.^[17]

	14 ^[a]	15 ^[a]	17	18 ^[a]
Formula	C ₂₃ H ₂₅ Br ₂ N ₂ O ₂ •CHCl ₃	C ₃₆ H ₃₆ N ₂ O ₂ •CH ₂ Cl ₂	C ₄₂ H ₄₂ N ₄ O ₃ S	C ₂₅ H ₃₀ ClF ₆ N ₂ OP •2CH ₃ CN
Mol wt	639.63	599.57	682.85	637.04
Crystal system	monoclinic	triclinic	orthorhombic	orthorhombic
Space group	<i>P</i> 2 ₁ / <i>c</i>	<i>P</i> -1	<i>Pbca</i>	<i>Pbcn</i>
Color	yellow	colorless	colorless	purple
Habit	plate	block	block	plate
Cryst dims, mm	0.13 x 0.08 x 0.05	0.21 x 0.19 x 0.11	0.22 x 0.09 x 0.03	0.11 x 0.04 x 0.02
<i>a</i> , Å	9.8667(7)	11.4934(11)	16.709(2)	20.602(4)
<i>b</i> , Å	9.3429(7)	14.2574(14)	18.217(2)	17.523(3)
<i>c</i> , Å	27.740(2)	20.462(2)	22.760(3)	8.2973(15)
<i>a</i> , deg	90	71.0600(10)	90	90
<i>b</i> , deg	93.5780(10)	76.3360(10)	90	90
<i>g</i> , deg	90	81.0730(10)	90	90
<i>V</i> , Å ³	2552.2(3)	3070.5(5)	6928.2(15)	2995.4(9)
<i>Z</i>	4	4	8	4
<i>D</i> _{calc} , g cm ⁻³	1.665	1.297	1.309	1.413
Abs coeff, mm ⁻¹	3.515	0.247	0.141	0.249
<i>F</i> (000)	1280	1264	2896	1328
Temp, K	173(2)	173(2)	173(2)	173(2)
Reflections	14058	17369	31764	15958
Independent	5853	13401	6118	3444
<i>R</i> _{int}	0.0215	0.0183	0.0586	0.0322
Parameters	298	757	830	221
<i>R</i> ₁ [<i>I</i> > 2s(<i>I</i>)]	0.0634	0.0655	0.0886	0.0373
<i>wR</i> ₂ (all data)	0.1635	0.1899	0.2531	0.1055
Goodness of fit	1.065	1.000	1.088	0.995
solv for crystallization	hexane/CHCl ₃	hexane/CH ₂ Cl ₂	hexane/CH ₂ Cl ₂	Ether/CH ₃ CN

[a] These crystals contained solvent molecules in the crystal lattice (**14**: CHCl₃, **15**: CH₂Cl₂, **18**: CH₃CN).

[b] In these crystal structures, there are disordered solvent molecules, and their contribution to the scattering values have been removed by using the PLATON SQUEEZE program.^[17]

	19 ^[a,b]	20	21 ^[b]
Formula	C ₆₁ H ₆₀ F ₆ N ₂ ClOP ₃ Pd •CHCl ₃	C ₃₅ H ₃₄ ClF ₆ N ₂ OP	C ₅₃ H ₄₉ ClF ₆ N ₂ OP ₂ Pd
Mol wt	1305.24	679.06	1047.73
Crystal system	triclinic	monoclinic	monoclinic
Space group	<i>P</i> -1	<i>P</i> 21/n	<i>P</i> 21/n
Color	purple	green	purple
Habit	Block	block	block
Cryst dims, mm	0.23 x 0.10 x 0.04	0.34 x 0.11 x 0.07	0.17 x 0.15 x 0.07
<i>a</i> , Å	12.0626(15)	9.990(4)	15.142(2)
<i>b</i> , Å	13.4637(17)	16.384(7)	19.407(3)
<i>c</i> , Å	23.567(3)	19.224(8)	16.486(2)
<i>a</i> , deg	91.343(2)	90	90
<i>b</i> , deg	90.755(2)	98.044(6)	91.587(2)
<i>g</i> , deg	113.115(2)	90	90
<i>V</i> , Å ³	3518.2(8)	3116(2)	4842.9(11)
<i>Z</i>	2	4	4
<i>D</i> _{calc} , g cm ⁻³	1.232	1.448	1.437
Abs coeff, mm ⁻¹	0.536	0.243	0.568
<i>F</i> (000)	1336	1408	2144
Temp, K	173(2)	173(2)	173(2)
Reflections	11180	17080	23188
Independent	11180	6811	10491
<i>R</i> _{int}	0.0000	0.0303	0.0279
Parameters	675	465	595
<i>R</i> ₁ [<i>I</i> > 2s(<i>I</i>)]	0.0896	0.0989	0.0646
<i>wR</i> ₂ (all data)	0.2812	0.3220	0.2025
Goodness of fit	1.088	1.027	1.039
solv for crystallization	hexane/CHCl ₃	ether/CH ₂ Cl ₂	hexane/CH ₂ Cl ₂

[a] These crystals contained solvent molecules in the crystal lattice (**19**: CHCl₃). [b] In these crystal structures, there are disordered solvent molecules, and their contribution to the scattering values have been removed by using the PLATON SQUEEZE program.^[17]

References

- [1] a) S. C. Lapin, B. E. Brauer, G. B. Schuster, *J. Am. Chem. Soc.* **1984**, *106*, 2092-2100; b) S. C. Lapin, G. B. Schuster, *J. Am. Chem. Soc.* **1985**, *107*, 4243-4248.
- [2] G. Maas, *Angew. Chem.* **2009**, *121*, 8332-8341; *Angew. Chem. Int. Ed.* **2009**, *48*, 8186-8195.
- [3] a) R. H. Shapiro, *Organic Reactions* **1976**, *23*, New York, Wiley, pp. 405-507; b) G. W. Jones, K. T. Chang, H. Shechter, *J. Am. Chem. Soc.* **1979**, *101*, 3906-3916; c) P. K. Freeman, J. C. Dañino, B. K. Stevenson, G. E. Clapp, *J. Org. Chem.* **1990**, *55*, 3867-3875; d) X. Creary, M. A. Butshko, *J. Am. Chem. Soc.* **2001**, *123*, 1569-1578; e) P. S. Thomas, N. P. Bowling, N. J. Burrmann, R. J. McMahon, *J. Org. Chem.* **2010**, *75*, 6372-6381.
- [4] S. Sugawara, S. Kojima, Y. Yamamoto, *Chem. Commun.* **2012**, *48*, 9735-9737.
- [5] Some of recent examples for biaryl tosylhydrazones: a) H. E. Bronstein, N. Choi, L. T. Scott, *J. Am. Chem. Soc.* **2002**, *124*, 8870-8875; b) P. J. Davis, L. Harris, A. Karim, A. L. Thompson, M. Gilpin, M. G. Moloney, M. J. Pound, C. Thompson, *Tetrahedron Letters* **2011**, *52*, 1663-1556; c) T. Zhang, W. Bao, *J. Org. Chem.* **2013**, *78*, 1317-1322.
- [6] a) A. Ojida, H. Nonaka, Y. Miyahara, S. Tamaru, K. Sada, I. Hamachi, *Angew. Chem.* **2006**, *121*, 8332-8341; *Angew. Chem. Int. Ed.* **2006**, *118*, 5644-5647; b) Y. Kurishita, T. Kohira, A. Ojida, I. Hamachi, *J. Am. Chem. Soc.* **2012**, *134*, 18779-18789.
- [7] Some of the more stable carbenes with an adjacent electron-donating group also caused such reactions: a) S. Solé, H. Gornitzka, W. W. Schoeller, D. Bourissou, G. Bertrand, *Science* **2001**, *292*, 1901-1903; E. Despagne, H. Gornitzka, A. B. Rozhenko, W. W. Schoeller, D. Bourissou, G. Bertrand, *Angew. Chem.* **2002**, *114*, 2959-2961.; *Angew. Chem. Int. Ed.* **2002**, *41*, 2835-2837.
- [8] J.-C. Hierso, *Chem. Rev.* **2014**, *114*, 4838-4867.
- [9] J. P. Collman, L. S. Hegedus, J. R. Norton, R. G. Finke, *Principles and Applications of Organotransition Metal Chemistry*, University Science Books, Milla Valley, **1987**.
- [10] V. Lavallo, Y. Canac, A. DeHope, B. Donnadieu, G. Bertrand, *Angew. Chem.* **2005**, *117*, 7402-7405; *Angew. Chem. Int. Ed.* **2005**, *44*, 7236-7239.
- [11] a) M. S. Viciu, F. K. Zinn, E. D. Stevens, S. P. Nolan, *Organometallics* **2003**, *22*, 3175-3177; b) Y. Ding, R. Goddard, K. R. Pörschke, *Organometallics* **2005**, *24*, 439-445; c) C. Burstein, C. W. Lehmann, F. Glorius, *Tetrahedron* **2005**, *61*, 6207-6217.
- [12] a) A. P. Stambuli, C. D. Incarvito, M. Bühl, J. F. Hartwig, *J. Am. Chem. Soc.* **2004**, *126*, 1184-1194; b) M. Yamashita, J. F. Hartwig, *J. Am. Chem. Soc.* **2004**, *126*, 5344-5345; c) M. Yamashita, I. Takamiya, K. Jin, K. Nozaki, *Organometallics* **2006**, *25*, 4588-4595; d) O. Rivada-Wheelaghan, B. Donnadieu, C. Maya, S. Conejero, *Chem. Eur. J.* **2010**, *16*, 10323-10326; e) M. D. Walter, P. S. White, M. Brookhart, *New. J. Chem.* **2013**, *37*, 1128-1133.
- [13] M. C. Burla, R. Caliendo, M. Camalli, B. Carrozzini, G. L. Cascarano, L. De Caro, C. Giacovazzo, G. Polidori, R. Spagna, *J. Appl. Cryst.* **2005**, *38*, 381-388.

- [14] G. M. Sheldrick, *SHELX-97*; University of Göttingen: Göttingen, Germany, **1997**.
- [15] M. Dąbowski, J. Kubicka, S. Luliński, J. Serwatowski, *Tetrahedron Letters* **2005**, *46*, 4175-4178.
- [16] Gaussian 09, Revision A.02, M. J. Frisch, G. W. Trucks, H. B. Schlegel, G. E. Scuseria, M. A. Robb, J. R. Cheeseman, G. Scalmani, V. Barone, B. Mennucci, G. A. Petersson, H. Nakatsuji, M. Caricato, X. Li, H. P. Hratchian, A. F. Izmaylov, J. Bloino, G. Zheng, J. L. Sonnenberg, M. Hada, M. Ehara, K. Toyota, R. Fukuda, J. Hasegawa, M. Ishida, T. Nakajima, Y. Honda, O. Kitao, H. Nakai, T. Vreven, J. A. Montgomery, Jr., J. E. Peralta, F. Ogliaro, M. Bearpark, J. J. Heyd, E. Brothers, K. N. Kudin, V. N. Staroverov, R. Kobayashi, J. Normand, K. Raghavachari, A. Rendell, J. C. Burant, S. S. Iyengar, J. Tomasi, M. Cossi, N. Rega, J. M. Millam, M. Klene, J. E. Knox, J. B. Cross, V. Bakken, C. Adamo, J. Jaramillo, R. Gomperts, R. E. Stratmann, O. Yazyev, A. J. Austin, R. Cammi, C. Pomelli, J. W. Ochterski, R. L. Martin, K. Morokuma, V. G. Zakrzewski, G. A. Voth, P. Salvador, J. J. Dannenberg, S. Dapprich, A. D. Daniels, O. Farkas, J. B. Foresman, J. V. Ortiz, J. Cioslowski, D. J. Fox, Gaussian, Inc., Wallingford CT, **2009**.
- [17] PLATON SQUEEZE program: (a) A. L. Spek, *PLATON, A Multipurpose Crystallographic Tool*, Utrecht University, Utrecht, The Netherlands, 2005; (b) P. van der Sluis, A. L. Spek, *Acta Crystallogr. Sect. A*, **1990**, *46*, 194.

Chapter 8

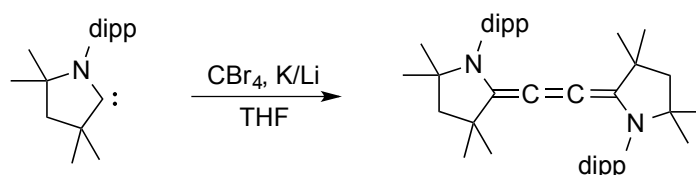
Synthesis of C4 Cumulene featuring Xanthyldene Derivative Units

8-1. Introduction

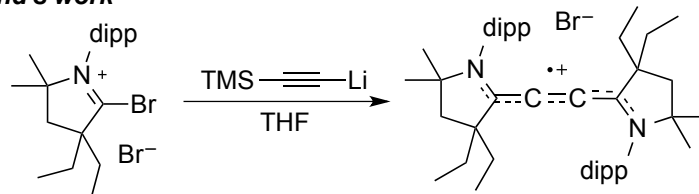
Recent advances in the chemistry of unusual molecules with low-valent elements have been achieved by development of stable singlet carbenes. Notably, *N*-heterocyclic carbenes (NHCs) and cyclic (alkyl)(amino)carbenes (CAACs) were found to be highly useful ligands to stabilize the main group compounds with zero oxidation state.^[1] For example, Roesky *et al.* succeeded in the synthesis of novel acyclic silylone (CAAC)₂Si^[2] and germylone (CAAC)₂Ge^[3], which showed biradicaloid character. In addition, Bertrand *et al.* accomplished isolation of the carbene stabilized carbon(0) species (NHC)₂C, which is recognized as carbodicarbenes.^[4] Furthermore, synthesis of base-stabilized heavier Group 14 diatomic compounds, (NHC)₂Si₂^[5] and (NHC)₂Ge₂^[6], were accomplished by reduction of the NHC adducts with strong reducing reagents. Since these unusual molecules possess peculiar electronic states, there are much interest in their properties and reactivity.^[7]

Very recently, Roesky *et al.*, Bertrand *et al.*, and Kinjo *et al.* separately reported synthesis and structural characterization of C4 cumulenes and their derivatives including carbene moieties (Figure 1).^[8] According to their reports, these compounds could be regarded as L₂C₂ species (L = carbenes) supported by CAACs or 4-pyridylidenes.^[9] In Roesky's work, reduction of CBr₄ with K or Li in the presence of a gem-dimethyl CAAC gave the desired neutral C4 cumulene species although the different ratio of the reagents provided the air-stable cumulene radical cation.^[8a] Additionally, the dication species generated by oxidation of the radical cation or the neutral species was isolated as air-stable crystals. At the same time Bertrand's group also investigated the very similar compounds with gem-ethyl CAACs, but the

Roesky's work



Bertrand's work



Kinjo's work

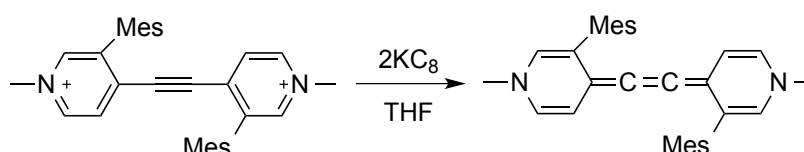


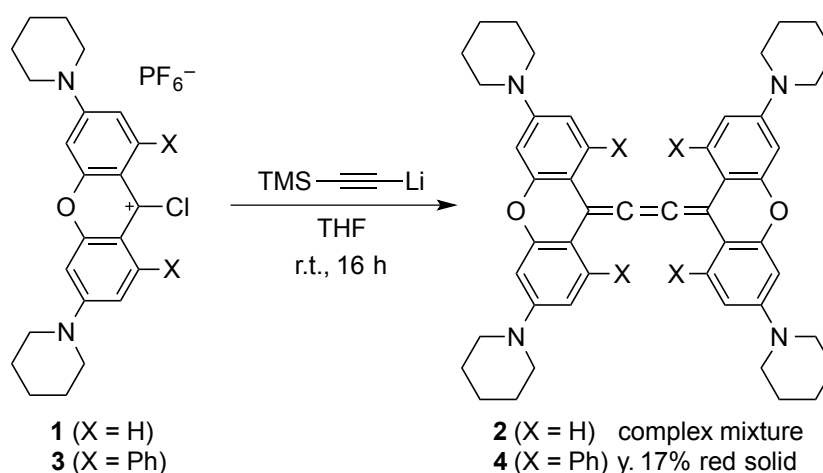
Figure 1. Recent reports on synthesis and characterization of C4 cumulenes featuring carbene units.

preparation method was different from that of Roesky's group. In their study, the air-stable C4 cumulene radical cation was obtained by the reaction of cyclic C-bromo-iminium bromide with a THF solution of lithium trimethylsilyl acetylide in THF. Taking advantage of the reversible redox behavior, the neutral and dicationic species were also isolated in their work. Note that Bertrand suggested that the radical cation could be recognized as a thermally and air-stable organic mixed-valence derivative which has been paid much attention due to potential applications in electronic conductors and non-linear optical materials.^[10] Following these two preceding studies, Kinjo *et al.* achieved synthesis and characterization of a C4 cumulene derivative featuring 4-pyridylidene units, and remarkably, the species easily reacted with ammonia-borane at the central C=C double bond.

As described in the above chapters, we already succeeded in the synthesis of newly cyclic aromatic carbene precursors bearing the remote amino groups.^[11] Thus, we envisioned that application of our carbenes to C4 cumulene chemistry would be possible and the electronic states of the resulting cumulene should be different from the others because of their higher σ -donating and π -accepting abilities than those of CAACs. In this chapter, we discuss the synthesis of C4 cumulene with cyclic aromatic carbene units and experimental and theoretical studies of their electronic properties.

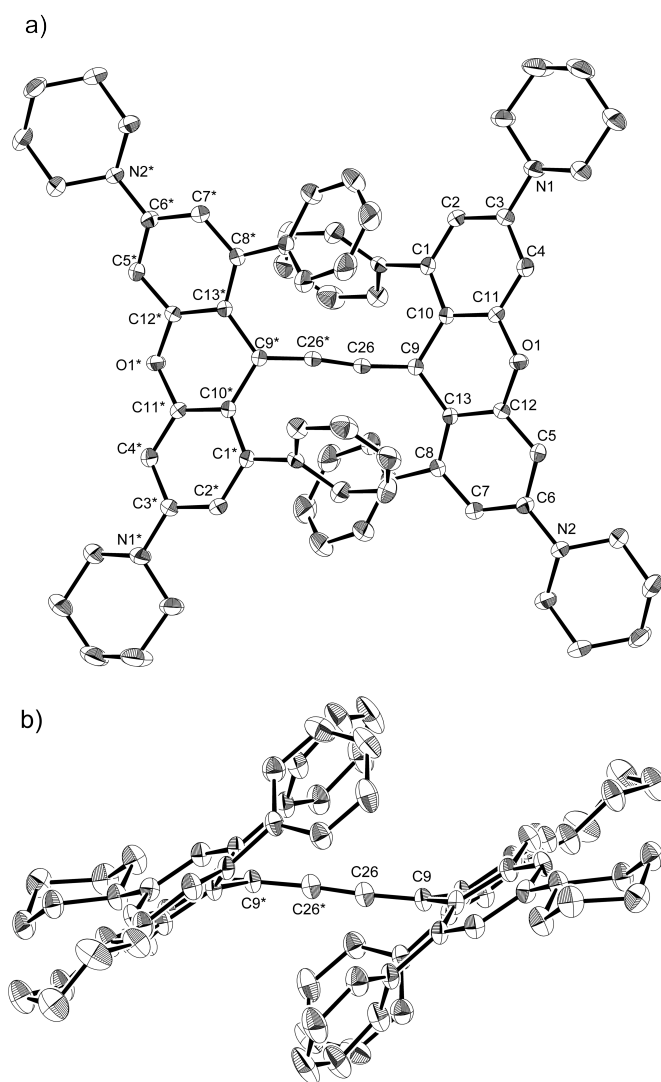
8-2. Synthesis and Characterization

Since the xanthyliene derivatives bearing remote amino groups have not been isolated as the free form, we envisaged that reaction of the chloride precursor with lithium trimethylsilyl acetylide (TMSCLi) should be the most plausible way to obtain the desired C4 cumulene in the similar manner with the Bertrand's procedure.^[8b] First, the chloride precursor **1** with hydrogen atoms at the 1,8-positions was reacted with 3 eq. of the freshly prepared TMSCLi, but the unidentified products were only obtained instead of the expected cumulene radical cation **2**⁺ (Scheme 1). Considering that single electron transfer from TMSCLi followed by possible side reactions of the radical species would compete with



Scheme 1. Synthesis of C4 cumulene bearing xanthyliene-based remote carbenes.

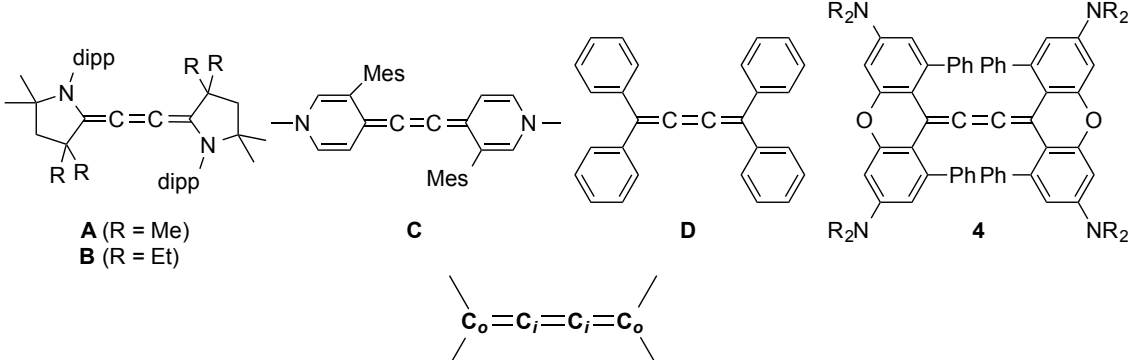
nucleophilic addition of TMSCLi, introduction of bulky phenyl groups at the 1,8-positions of the chloride precursor would hamper the undesired reactions and promote the nucleophilic addition of TMSCLi to the cation center. Indeed, the same reaction was performed with the chloride precursor **3** to give red solids in 17% yield, which could not be identified with ^1H NMR spectroscopy due to the irreproducible data (Scheme 1). However, the generation of C4 cumulene species was supported by high-resolution ESI mass spectrum since a parent ion was found at m/z 1021.5421 as a base peak ($[\text{M}+\text{H}]$; calcd for $\text{C}_{72}\text{H}_{69}\text{O}_2\text{N}_4$: 1021.5415). Based on this positive data, the product was at least found to be the radical cation 4^{++} or the neutral species **4**. Finally, the red crystals suitable for X-ray analysis were obtained by recrystallization from the CH_3CN /ether solution at room temperature (Figure 2). Surprisingly,



the obtained X-ray structure included no counter anion, indicating that the product was a neutral C4 cumulene **4** with the xanthylidene derivative units. The geometry of C4 backbone displays C_2 -symmetry with a slightly bent bond angle from the linear structure (C9-C26-C26', 172.4(3)°). Also, the bond lengths of the xanthylidene moiety shows small bond alternation which is similar to the previously isolated ketone species.^[11b] Although the sum of bond angles around C9 is almost 360°, the xanthylidene moiety is largely deviated from C4 backbone as shown in Figure 2b. This deviation suggests that no effective conjugation between the C4 backbone and the xanthylidene moiety would be conceivable. Focusing on the C4 backbone, the bond lengths of C9-C26 and C26-C26' are 1.338(2) and 1.248(4) Å, respectively. Compared to the analogues **A**, **B**, **C**, and **D**^[12] with other carbene units or tetra phenyl substituents, the C4 backbone structure of **4** is closer to that of **A** and **B**. Among all, the bond lengths of **C** showed the shortest bond length for the inner C_i-C_i bond (1.207(8) Å) and the longest bond length for outer C_i-C_o bond (1.371(5) Å).^[8c] As for **D**, which is an analogue bearing 1,1,4,4,-tetraphenyl moieties, both inner and outer bonds of **D** are slightly lengthened (1.2591(4), 1.3480(4) Å) in comparison with **4**. Thus, all of the inner bond lengths are within typical triple (1.20 Å) and double bond lengths (1.34 Å) whereas the outer bond lengths are closer to typical double bond length.

The reaction mechanism to generate the neutral species **4** instead of the radical cation **4**⁺⁺ is not understandable yet, but it could be considered that the excess amount of TMSCLi would transfer the electrons via sequential single electron transfer process. Unfortunately, the chemical oxidation of **4** could not be performed due to the shortage of the product caused by the irreproducible reaction. In addition, the ¹H NMR spectrum of **4** in CDCl₃ and C₆D₆ also gave useless data since the chemical shift and integration of the product were differently shown in every measurement. Thus, further investigations for reliable generation of **4** are required to overcome those problems.

Table 1. Comparison of bond length of C4 backbone with other C4 cumulene compounds.



Compounds	A ^[b]	B ^[c]	C ^[d]	D ^[e]	4
C_i-C_i / Å	1.249(2)	1.266(2)	1.207(8)	1.2591(4)	1.248(4)
C_i-C_o / Å	1.3236(16)	1.3332(17)	1.371(5)	1.3480(4) ^[a]	1.338(2)

[a] average value of two C_i-C_o bonds. [b] ref [8a]. [c] ref [8b]. [d] ref[8c]. [e] ref[12].

8-3. Electronic Properties

In order to gain further insights into the redox properties of **4**, we examined the electrochemical property by cyclic voltammetry (CV) in CH_2Cl_2 versus SCE (Figure 3). In the CV measurements, two oxidation peaks were found at $E_{1/2} = +0.144$ and $+1.383$ V versus SCE, but the peaks were irreversible, indicating that the resulting dication species $\mathbf{4}^{2+}$ would be unstable and decomposed under the measurement in marked contrast to redox behavior of C4 cumulenes with CAACs.^[8] However, the first oxidation became reversible when the measurement was carried out from -0.5 V to $+0.5$ V. This result suggested that the radical cation $\mathbf{4}^{+\bullet}$ could be stable and generated in terms of the controlled one electron oxidation.

Although isolation of the radical cation generated by air oxidation of **4** in CH_2Cl_2 was unsuccessful, the existence of the radical species was identified by EPR spectroscopy (Figure 4). The EPR signal of the THF solution was detected as a singlet (centered at $g_{\text{iso}} = 2.003$), indicating that the spin would be localized on the C4 backbone without hyperfine couplings with nitrogen atoms. This result is in accordance with negligible conjugation between C4 backbone and the xanthyliene moiety caused by the large steric deformation.

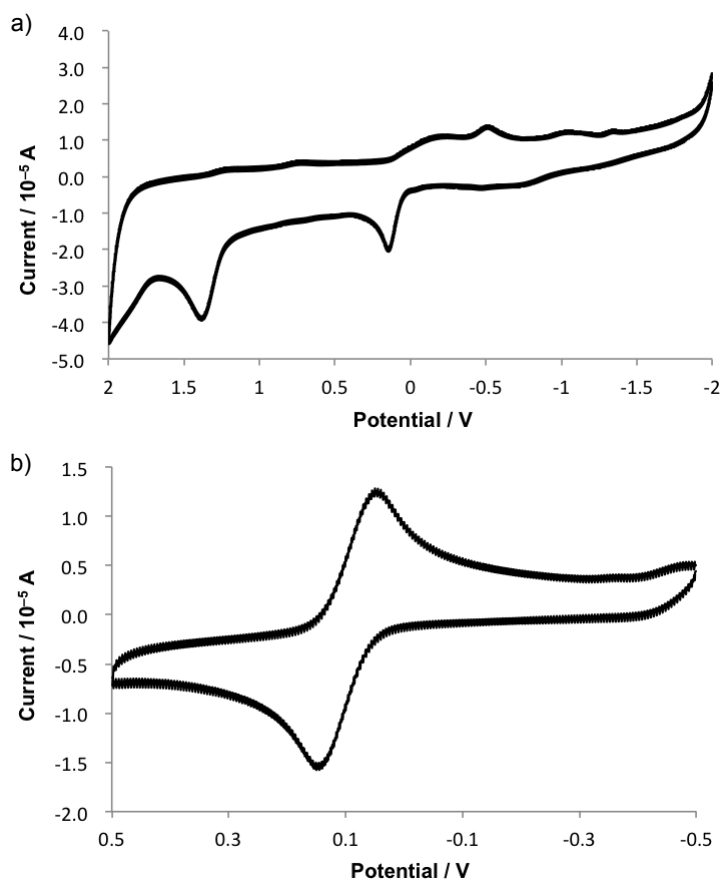


Figure 3. Cyclic voltammograms of **4**. The data was scanned a) from -2.0 V to $+2.0$ V and b) from -0.5 V to $+0.5$ V in CH_2Cl_2 containing 0.1 M TBAPF_6 (SCE vs Fc = 0.46 V).

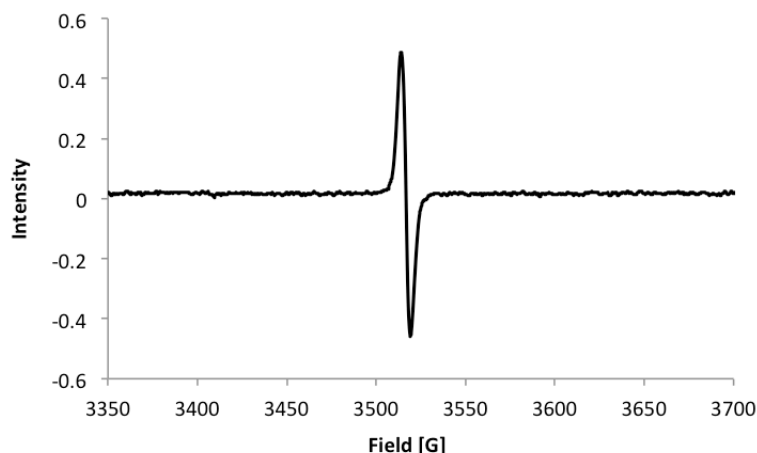


Figure 4. Experimental EPR spectrum of air-oxidized species of **4** in THF at room temperature.

To support the explanation for the electronic state of **4**, theoretical calculations were performed at the level of M06-2X/6-311G(d,p). The optimized structure of **4** showed similar structural parameters to those of the X-ray structure (selected bonds (Å) and angles (°): C26–C26', 1.248(4) (X-ray) vs 1.255 (calcd.); C9–C26, 1.338(2) (X-ray) vs 1.331, 1.332 (calcd.); C9–C26–C26', 172.4(3) (X-ray) vs 170.0 and 177.3 (calcd.)). As for molecular orbitals (MO) of **4**, HOMO–6 and HOMO–3 indicated the perpendicular π -bonding orbitals at the central C=C bond, suggesting the strong interaction on the central C=C bond (Figure 5). Also, HOMO represents the π^* -orbital of the central C=C bond associated with the bonding interaction between the central carbons and p(π) orbital of the carbene carbon in the xanthylidene units. In contrast, the antibonding interactions between the central carbon moiety and the xanthylidene units are found on LUMO. Natural bond order (NBO) analysis showed the Wiberg bond index (WBI) value for the central C26–26' bond (2.10) and the adjacent C9–C26 bond (1.60). The similar calculation results were reported in Roesky's^[8a] and Kinjo's work^[8c], respectively. While the X-ray structure suggested negligible conjugation between C4 backbone and the xanthylidene unit, it is noteworthy that the C9–C26 bond still possesses the partial double bond character, indicating that there is a weak π interaction between the central C2 moiety and the p orbital at the carbenic carbon.

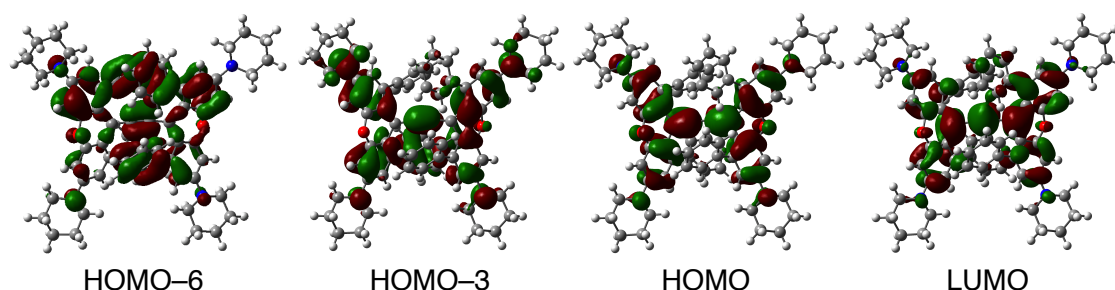


Figure 5. Molecular orbitals of **4** calculated at the level of M06-2X/6-311G(d,p).

8-4. Conclusions and Outlook

In this chapter, we discussed synthesis and characterization of C4 cumulenes featuring xanthyldiene units. Taking advantage of the Bertrand's synthetic method, the desired C4 cumulene was successfully prepared despite the lower yield and irreproducible synthesis. Surprisingly, the product was a neutral species **4** instead of the expected radical cation, which was in contrast to Bertrand's result. Single crystal X-ray structural analysis of **4** revealed that C4 backbone was largely distorted from the xanthyldiene moieties, suggesting that there is little influence from the conjugation of the xanthyldiene units. Cyclic voltammetry and EPR spectroscopy showed that the single electron oxidation would be possible and generate the air-stable radical cation **4**^{•+}. For the further investigations, a new synthetic strategy of **4** is required.

Experimental Section

General. ^1H NMR (400 MHz) and ^{13}C NMR (100 MHz) spectra were recorded using a JEOL EX-400 or AL-400 spectrometer. The ^1H and ^{13}C NMR chemical shifts (δ scale) are given in downfield from tetramethylsilane, determined by residual protons of the solvent (^1H) or the solvent itself (^{13}C). All of the procedures were performed in Ar atmosphere. Tetrahydrofuran (THF), and diethyl ether (Et_2O) were freshly distilled from Na-Benzophenone. The EPR spectra were acquired on a Bruker ELEXSYS E500 instrument at r.t. The elemental analyses were performed using a Perkin-Elmer 2400 CHNS elemental analyzer. Mass spectra were measured with a Thermo Fisher Scientific model LTQ Orbitrap XL by using the ESI-TOF or APCI-TOF method in the positive ion mode with acetonitrile or methanol solution samples. Crystals suitable for X-ray structural determination were mounted on a Bruker SMART APEXII CCD diffractometer or a Rigaku SCXmini diffractometer and irradiated with graphite monochromated Mo-K α radiation ($\lambda = 0.71073 \text{ \AA}$) at 173 K for data collection. The data were processed using the APEX program suite or the Rigaku SCXmini program. The structures were solved by a direct method using the SIR-2004 program.^[13] Refinement on F^2 was carried out by full-matrix least-squares using the SHELXL-97 program.^[14] All non-hydrogen atoms were refined using anisotropic thermal parameters except for disordered atoms. The hydrogen atoms were included in the refinement with isotropic thermal parameters. The crystallographic data are summarized in Table 2.

The chloride precursors **1**^[11a] and **3**^[11b] were prepared by literature methods, respectively.

Computational Details. All computations were performed using the Gaussian 09 package of programs.^[15] The M06-2X hybrid functional was used with the 6-311G(d,p) basis set for optimizations. All structures were optimized without any symmetry assumptions. Harmonic vibration frequency calculations at the same level were performed to verify that all the stationary points were local minima (with no imaginary frequency). Natural bond order (NBO) analysis of **4** was also performed at the same level.

Synthesis of **4**

To the solution of chloride **3** (150 mg, 0.221 mmol) in THF (1 mL) was added the freshly prepared lithium trimethylsilyl acetylide, which was prepared by the lithiation of trimethylsilylacetylene (0.10 mL, 0.72 mmol) with 1.58 M of *n*-butyllithium in hexane (0.44 mL, 0.69 mmol) in THF (1 mL), at -78°C . After stirring at the same temperature for 1 h, the reaction mixture was stirred at r.t. for 16 h. The solvent was then evaporated, and the resulting solid was washed with ether to give **4** (19 mg, 0.019 mmol, 17%) as a red solid. Recrystallization from CH_3CN /ether provided the red crystals suitable for X-ray analysis. HRMS (ESI): m/z : calcd for $\text{C}_{72}\text{H}_{69}\text{O}_2\text{N}_4$ $[\text{M}+\text{H}]^+$ 1021.5415; found 1021.5421.

Table 2. Crystallographic data for **4**.

4	
Formula	$\text{C}_{72}\text{H}_{68}\text{N}_4\text{O}_2$
Mol wt	1021.30
Crystal system	triclinic
Space group	$P\bar{1}$
Color	red
Habit	block
Cryst dims, mm	0.05 x 0.03 x 0.03
a , Å	10.096(4)
b , Å	10.513(4)
c , Å	13.199(5)
α , deg	105.582(5)
β , deg	96.439(5)
γ , deg	94.331(5)
V , Å ³	1332.6(9)
Z	1
D_{calc} , g cm ⁻³	1.273
Abs coeff, mm ⁻¹	0.076
$F(000)$	544
Temp, K	173(2)
Reflections	7530
Independent	5727
R_{int}	0.0206
Parameters	352
R_1 [$I > 2s(I)$]	0.0567
wR_2 (all data)	0.1561
Goodness of fit	1.032
solv for crystallization	hexane/CH ₃ CN

References

- [1]. Selected recent reviews: a) M. Melaimi, M. Soleihavoup, G. Bertrand, *Angew. Chem. Int. Ed.* **2010**, *49*, 8810-8849; b) D. Martin, M. Melaimi, M. Soleihavoup, G. Bertrand, *Organometallics* **2011**, *30*, 5304-5313; c) H. Braunschweig, R. D. Dewhurst, *Organometallics* **2014**, *33*, 6271-6277.
- [2]. a) K. C. Mondal, H. W. Roesky, M. C. Schwarzer, G. Frenking, B. Niepötter, H. Wolf, R. Herbst-Irmer, D. Stalke, *Angew. Chem. Int. Ed.* **2013**, *52*, 2963-2967; b) K. C. Mondal, P. P. Samuel, M. Tretiakov, A. P. Singh, H. W. Roesky, A. C. Stückl, B. Niepötter, E. Carl, H. Wolf, R. Herbst-Irmer, D. Stalke, *Inorg. Chem.* **2013**, *52*, 4736-4743.
- [3]. Y. Li, K. C. Mondal, H. W. Roesky, H. Zhu, P. Stollberg, R. Herbst-Irmer, D. Stalke, D. M. Andrada, *J. Am. Chem. Soc.* **2013**, *135*, 12422-12428.
- [4]. a) R. Tonner, G. Frenking, *Angew. Chem. Int. Ed.* **2007**, *46*, 8695-8698; b) C. A. Dyker, V. Lavallo, B. Donnadieu, G. Bertrand, *Angew. Chem. Int. Ed.* **2008**, *47*, 3206-3209; c) A. Fürstner, M. Alcarazo, R. Goddard, C. W. Lehmann, *Angew. Chem. Int. Ed.* **2008**, *47*, 3210-3214; d) M. Alcarazo, C. W. Lehmann, A. Anoop, W. Thiel, A. Fürstner, *Nat. Chem.* **2009**, *1*, 295-301; e) D. A. Ruiz, M. Melaimi, G. Bertrand, *Chem. Asian. J.* **2013**, *8*, 2940-2942.
- [5]. Y. Wang, Y. Xie, P. Wei, R. B. King, H. F. Schäfer III, P. v. R. Schleyer, G. H. Robinson, *Science* **2008**, *321*, 1069-1071.
- [6]. A. Sidiropoulos, C. Jones, A. Stasch, S. Klein, G. Frenking, *Angew. Chem. Int. Ed.* **2009**, *48*, 9701-9704.
- [7]. Y. Wang, G. H. Robinson, *Inorg. Chem.* **2014**, *53*, 11815-11831. and the references therein.
- [8]. a) Y. Li, C. Mondal, P. P. Samuel, H. Zhu, C. M. Orben, S. Panneerselvam, B. Dittrich, B. Schwederski, W. Kaim, T. Mondal, D. Koley, H. W. Roesky, *Angew. Chem. Int. Ed.* **2013**, *53*, 4168-4172; b) L. Jin, M. Melaimi, L. Liu, G. Bertrand, *Org. Chem. Front.* **2014**, *1*, 351-354; c) D. Wu, Y. Li, R. Ganguly, R. Kinjo, *Chem. Commun.* **2014**, *50*, 12378-12381.
- [9]. a) D. Himmel, I. Krossing, A. Schnepf, *Angew. Chem. Int. Ed.* **2014**, *53*, 370-374; b) G. Frenking, *Angew. Chem. Int. Ed.* **2014**, *53*, 6040-6046; c) D. Himmel, I. Krossing, A. Schnepf, *Angew. Chem. Int. Ed.* **2014**, *53*, 6047-6048.
- [10]. a) D. O. Cowan, C. LeVanda, J. Park, F. Kaufman, *Acc. Chem. Res.* **1973**, *6*, 1-7; b) J. Hankache, O. S. Wenger, *Chem. Rev.* **2011**, *111*, 5138-5178; c) A. Heckmann, C. Lambert, *Angew. Chem. Int. Ed.* **2012**, *51*, 326-392; d) M. Abe, *Chem. Rev.* **2013**, *113*, 7011-7088; e) Y. Su, X. Wang, X. Zheng, Z. Zhang, Y. Song, Y. Sui, Y. Li, X. Wang, *Angew. Chem. Int. Ed.* **2014**, *53*, 2857-2861.
- [11]. a) S. Sugawara, S. Kojima, Y. Yamamoto, *Chem. Commun.* **2012**, *48*, 9735-9737; b) S. Sugawara, M. Abe, Y. Fujiwara, M. Wakioka, F. Ozawa, Y. Yamamoto, *Eur. J. Inorg. Chem.* **2015**, 534-541.
- [12]. Z. Berkovitch-Yellin, L. Leiserowitz, *Acta Cryst.* **1977**, *33*, 3657-3669.
- [13]. M. C. Burla, R. Caliendo, M. Camalli, B. Carrozzini, G. L. Cascarano, L. De Caro, C. Giacovazzo, G. Polidori, R. Spagna, *J. Appl. Cryst.* **2005**, *38*, 381-388.

- [14]. G. M. Sheldrick, *SHELX-97*; University of Göttingen: Göttingen, Germany, **1997**.
- [15]. Gaussian 09, Revision A.02, M. J. Frisch, G. W. Trucks, H. B. Schlegel, G. E. Scuseria, M. A. Robb, J. R. Cheeseman, G. Scalmani, V. Barone, B. Mennucci, G. A. Petersson, H. Nakatsuji, M. Caricato, X. Li, H. P. Hratchian, A. F. Izmaylov, J. Bloino, G. Zheng, J. L. Sonnenberg, M. Hada, M. Ehara, K. Toyota, R. Fukuda, J. Hasegawa, M. Ishida, T. Nakajima, Y. Honda, O. Kitao, H. Nakai, T. Vreven, J. A. Montgomery, Jr., J. E. Peralta, F. Ogliaro, M. Bearpark, J. J. Heyd, E. Brothers, K. N. Kudin, V. N. Staroverov, R. Kobayashi, J. Normand, K. Raghavachari, A. Rendell, J. C. Burant, S. S. Iyengar, J. Tomasi, M. Cossi, N. Rega, J. M. Millam, M. Klene, J. E. Knox, J. B. Cross, V. Bakken, C. Adamo, J. Jaramillo, R. Gomperts, R. E. Stratmann, O. Yazyev, A. J. Austin, R. Cammi, C. Pomelli, J. W. Ochterski, R. L. Martin, K. Morokuma, V. G. Zakrzewski, G. A. Voth, P. Salvador, J. J. Dannenberg, S. Dapprich, A. D. Daniels, O. Farkas, J. B. Foresman, J. V. Ortiz, J. Cioslowski, D. J. Fox, Gaussian, Inc., Wallingford CT, **2009**.

Chapter 9

Attempted Synthesis of Tridentate Pincer-type Cyclic Aromatic Remote Carbene Ligands

9-1. Introduction

Pincer-type ligands, which have two additional neighboring electron donor groups such as amine, sulfide, and phosphine in their skeletons as well as the central anionic or neutral carbon or nitrogen donor site, have been recognized as useful ligands for enhancing the reactivity of the metal complexes. In addition, it is well known that facile fine-tunings of the ligand system allows chemists to design tailor-made ligands.^[1] Indeed, a number of the metal complexes with pincer-type ligands have been developed so far and most of the complexes exhibit their versatile applications to catalytic bond formation and cleavage processes of E–H bonds (E = C, N, O) in small molecules.^[2] On the other hand, *N*-heterocyclic carbenes (NHCs) are widely utilized as strong σ donating ligands for the metal complexes.^[3] However, the carbene-centered pincer ligands have been much less investigated so far.^[4, 5] In particular, the PCP pincer ligands are still rare although the PCP pincer ligands plays a pivotal role due to their strong electron donating abilities to the metal center. While transition metal complexes with the conventional Show's PCP ligand system **I**^[6] and **II**^[7] have exhibited the bond activation of small molecules via oxidative addition,^[2] there are only a few reports on synthesis of the metal complexes with a diarylcarbene-based PCP pincer ligand **III** (Figure 1).^[8,9,10] As for the first report on the PCP ligand with a diarylcarbene unit by Ozerov *et al.*, the ruthenium complex with the ligand based on a dipyrromethane unit was developed via a double C–H activation process.^[8] The study revealed that the strong donating ability and rigidity of the ligand provided very robust metal complexes without carbene/olefin isomerization as seen in the case of the ligand **II**.^[11] In recent years, Piers *et al.* developed the PCP ligand featuring a diphenylcarbene unit and the iridium(I) and nickel(II) complexes were successfully prepared via double C–H activation.^[9] In regard to activation of small molecules, the iridium(I) complex solely reacted with hydrogen,^[9a] but the nickel(II) complex showed higher reactivity with various small molecules including C–H, O–H, and N–H bonds.^[9b] It is notable that the reversible reaction of the nickel(II) complex with ammonia would lead to potential applications in catalysis. The deference of the reactivity was attributed to the electronic state at the carbene center. The former can be regarded as electrophilic “Fischer carbene”, while the latter reacted as nucleophilic “Schrock carbene”. Taking advantage of the developed ligand, Iluc *et al.* investigated the analogous palladium(II) complex with the PCP ligand based on the diphenylcarbene unit, which showed similar reactivity to that of the nickel(II) complex.^[10]

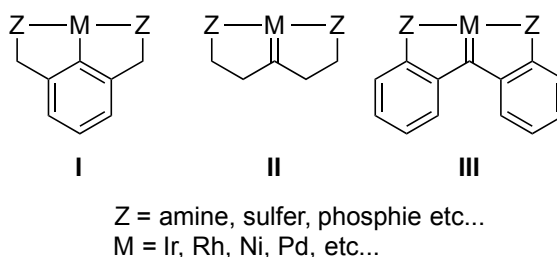


Figure 1. Pincer-type ligands.

Recently, we developed new xanthylidene-based carbene ligands bearing remote amino groups.^[12] Judging from the Pd–Cl bond length of the palladium(II) complex prepared by oxidative addition into the chloride precursor, the carbene ligand exhibited that the donating ability of the ligand is much higher than conventional stable carbenes. In addition, we succeeded in preparing a versatile ketone compound bearing dibromo groups at the 1,8-position, which enables us to introduce various substituents. Therefore, we envisioned that the introduction of the additional donor substituents at the 1,8-positions would give promising tridentate ligands to activate the metal center (Figure 2). Due to the stronger donating ability than the Piers' ligand, the resulting metal complex could be utilized as catalysts in the reaction with small molecules such as water and ammonia. In this chapter, attempted synthesis of the pincer ligand is discussed.

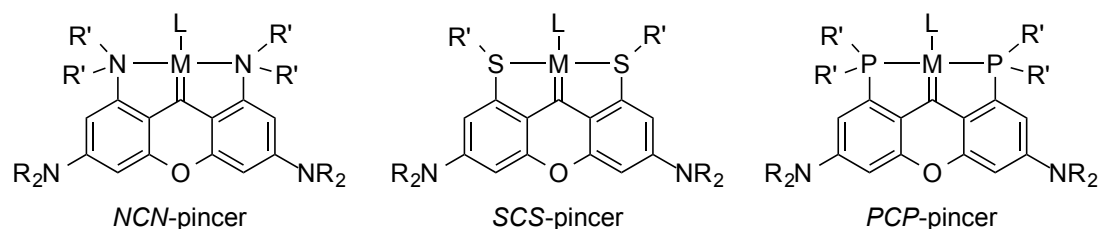
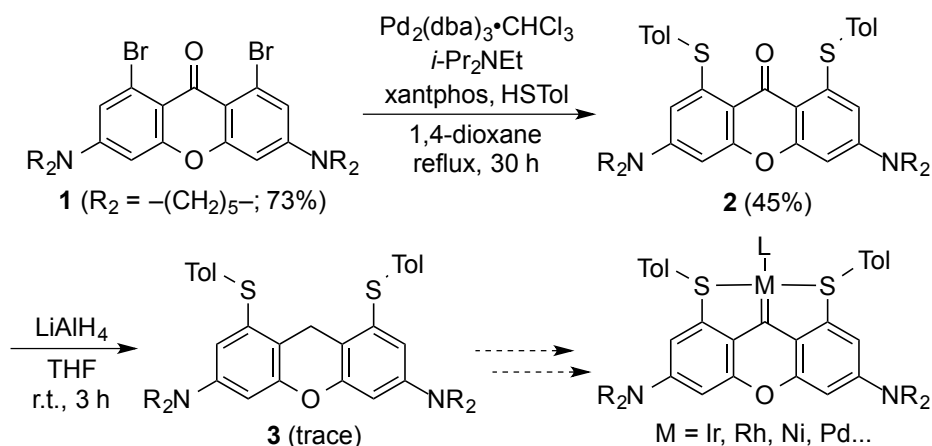


Figure 2. Pincer-type ligands integrated into cyclic aromatic remote carbene scaffolds.

9-2. Results and Discussion

In order to introduce the donor substituents at the 1,8-positions, the previously prepared 1,8-dibromo ketone compound **1** was selected as a suitable starting material.^[12b] Due to predicted easier synthesis and handling, introduction of thioether groups via a cross-coupling reaction was firstly attempted (Scheme 1). The palladium-catalyzed reaction of **1** with *p*-toluenethiol in 1,4-dioxane^[12] furnished the 1,8-STol ketone compound **2** in 45% yield and the formation of compound **2** was ambiguously determined by the X-ray structural analysis (Figure 3). Then, reduction of **2** was successively performed with LiAlH₄ to give the desired product **3**, which can be a precursor for the metal complex via double C–H activation at the central methylene moiety. However, the yield was quite low presumably because of the instability of **3** in air and moisture. Thus, we performed the same reaction followed by the workup under inert gas atmosphere, but the purified product could not be obtained. Thus, alternative reductive methods would be needed to achieve the synthesis. The similar problem would be predicted in more cumbersome synthesis of the ligand bearing 1,8-phosphorus groups. One of the promising solutions is a metal-free reduction with B(C₆F₅)₃ developed by Piers, Stephan, and others, which is recognized as frustrated lewis pair (FLP).^[14] Currently, the FLP-catalyzed reduction of compound **1** and **2** is under investigation.



Scheme 1. Synthesis of the SCS-pincer ligand **3**.

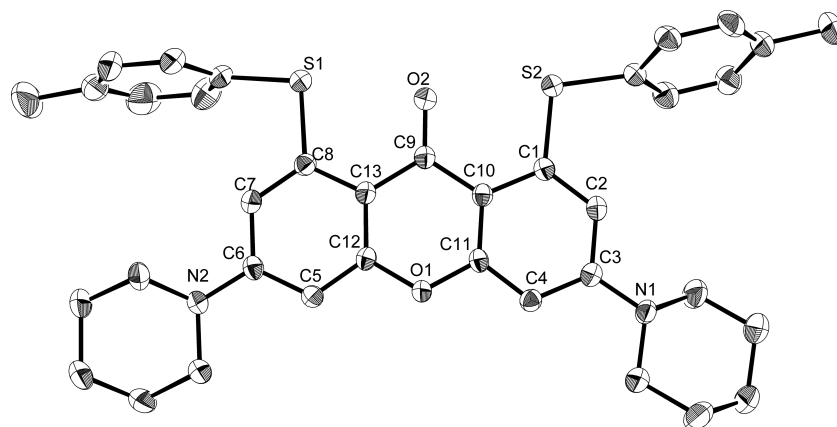


Figure 2. ORTEP drawing of **2** with the thermal ellipsoids shown at the 50% probability level. Hydrogen atoms and the solvent are omitted for clarity. Selected bond lengths (Å) and angles (°): C9-C10, 1.460(2); C9-C13, 1.459(2); C9-O2, 1.2359(18); C8-S1, 1.7932(15); C1-S2, 1.7787(15); C10-C9-C13, 115.82(13); C10-C9-O2, 122.40(13); C13-C9-O2, 121.77(13); C13-C8-S1, 119.06(11); C10-C1-S2, 118.54(11).

9-3. Conclusions and Outlook

In this chapter, we discussed attempted synthesis of tridentate pincer-type ligands based on cyclic aromatic remote carbenes. The metal complexes with the pincer ligands featuring high σ -electron donating ability have been paid much attention to create the new catalytic system utilizing small molecules such as H_2O and NH_3 .^[15] Therefore, we envisioned that our xanthylidene-based carbene ligand would be promising for enhancement of the electronic effects at the metal center because of the presence of electron-rich remote amino groups and bridged oxygen atom. Thus far, we succeeded in introduction of tolylthioether groups into the ligand at the 1,8-positions, but preparation of the suitable precursor are currently investigated yet. Since there are much possibilities for preparing the tridentate pincer carbene complexes, further studies are ongoing in our laboratory.

Experimental Section

General. Melting points were measured with a Yanagimoto micro melting point apparatus and are uncorrected. Column chromatography was carried out using Kanto silica gel 60N. ^1H NMR (400 MHz) and ^{13}C NMR (100 MHz) spectra were recorded using a JEOL EX-400 or AL-400 spectrometer. The ^1H and ^{13}C NMR chemical shifts (δ scale) are given in downfield from tetramethylsilane, determined by residual protons of the solvent (^1H) or the solvent itself (^{13}C). Tetrahydrofuran (THF) and diethyl ether (Et_2O) were freshly distilled from Na-Benzophenone. The elemental analyses were performed using a Perkin-Elmer 2400 CHNS elemental analyzer. Mass spectra were measured with a Thermo Fisher Scientific model LTQ Orbitrap XL by using the ESI-TOF or APCI-TOF method in the positive ion mode with acetonitrile or methanol solution samples. Crystals suitable for X-ray structural determination were mounted on a Bruker SMART APEXII CCD diffractometer and irradiated with graphite monochromated Mo-K α radiation ($\lambda = 0.71073 \text{ \AA}$) at 173 K for data collection. The data were processed using the APEX program suite program. The structures were solved by a direct method using the SIR-2004 program.^[16] Refinement on F^2 was carried out by full-matrix least-squares using the SHELXL-97 program.^[17] All non-hydrogen atoms were refined using anisotropic thermal parameters except for disordered atoms. The hydrogen atoms were included in the refinement with isotropic thermal parameters. The crystallographic data are summarized in Table 2. 1,8-Dibromo-3,6-di(piperidinyl)-9H-xanthen-9-one (**1**) was prepared by literature methods.

Synthesis of 2

To a solution of **1** (100 mg, 0.192 mmol) in dry 1,4-dioxane (3 mL) was added *p*-toluenethiol (60 mg, 0.48 mmol), 4,5-Bis(diphenylphosphino)-9,9-dimethylxanthene (11 mg, 0.019 mmol), and $\text{Pd}_2(\text{dba})_3 \cdot \text{CHCl}_3$ (18 mg, 0.020 mmol), followed by diisopropylethylamine (0.13 mL, 0.77 mmol) in one portion. After the mixture was refluxed for 30 h, the solution was filtered through Celite with CH_2Cl_2 and evaporated to give the crude solid. The solid was washed with hexane and purified on the silica gel column chromatography with CH_2Cl_2 . After the solvent was removed in vacuo, recrystallization from CH_2Cl_2 /hexane furnished the product **2** (52 mg, 0.086 mmol, 45%) as a yellow solid. M.p. 286-287 °C; ^1H NMR (CDCl_3 , 400 MHz): $\delta = 1.46\text{--}1.60$ (12H, m), 2.40 (6H, s), 3.00-3.14 (8H, m), 6.00 (2H, br s), 6.37 (2H, br s), 7.25 (4H, d, $^3J = 7 \text{ Hz}$), 7.53 (4H, d, $^3J = 7 \text{ Hz}$); HR-MS(ESI positive): Calcd for $\text{C}_{37}\text{H}_{39}\text{O}_2\text{N}_2\text{S}_2$ 607.2448, found 607.2448 for $[\text{M}+\text{H}]^+$.

Synthesis of 3

To a solution of **2** (30 mg, 0.049 mmol) in dry THF (2 mL) was added LiAlH_4 (9.6 mg, 0.25 mmol). After the mixture was stirred for 3 h at room temperature, AcOEt followed by H_2O were added to the solution at 0 °C. After the solvent was evaporated, the remaining solid was extracted with CH_2Cl_2 and the solution was washed with H_2O , and dried over Na_2SO_4 . After the solvent was removed in vacuo, silica gel

chromatography was performed with CH_2Cl_2 to give **5** (trace amount) as colorless solid. ^1H NMR (CDCl_3 , 400 MHz): δ = 1.43-1.73 (12H, m), 2.30 (6H, s), 3.06 (8H, t, 3J = 5 Hz), 3.81 (2H, s), 6.49 (2H, br s), 6.63 (2H, d, 4J = 2 Hz), 7.05 (4H, d, 3J = 8 Hz), 7.16 (4H, d, 3J = 8 Hz).

Table 2. Crystallographic data for **2**.

2	
Formula	$\text{C}_{37}\text{H}_{38}\text{N}_2\text{O}_2\text{S}_2$
Mol wt	606.81
Crystal system	triclinic
Space group	$P-1$
Color	colorless
Habit	plate
Cryst dims, mm	0.15 x 0.13 x 0.06
a , Å	10.5129(15)
b , Å	11.4568(16)
c , Å	15.060(2)
α , deg	71.1739(18)
β , deg	83.4103(19)
γ , deg	64.5308(17)
V , Å ³	1549.4(4)
Z	2
D_{calc} , g cm ⁻³	1.301
Abs coeff, mm ⁻¹	0.209
$F(000)$	644
Temp, K	173(2)
Reflections	9463
Independent	7141
R_{int}	0.0197
Parameters	390
R_1 [$I > 2s(I)$]	0.0433
wR_2 (all data)	0.1207
Goodness of fit	1.027
solv for crystallization	hexane/ CH_2Cl_2

References

- [1]. For leading comprehensive reviews of pincer-type compounds: a) J. T. Singleton, *Tetrahedron* **2003**, 59, 1837-1857; b) D. Morales-Morales, C. G. M. Jensen, *The Chemistry of Pincer Compounds*, Elsevier, Amsterdam, **2007**; c) G. van Koten, D. Milstein, *Organometallic Pincer Chemistry; Topics in Organometallic Chemistry* 40, Springer-Verlag, Berlin, **2012**.
- [2]. M. Albrecht, M. M. Lindner, *Dalton Trans.*, **2011**, 40, 8733-8744.
- [3]. Reviews: a) W. A. Herrmann, C. Köcher, *Angew. Chem. Int. Ed. Engl.* **1997**, 36, 2162-2187; b) D. Bourissou, O. Guerret, F. P. Gabbaï, G. Bertrand, *Chem. Rev.* **2000**, 100, 39-91; c) F. E. Hahn, M. C. Jahnke, *Angew. Chem. Int. Ed.* **2008**, 47, 3122-3172; d) T. Dröge, F. Glorius, *Angew. Chem. Int. Ed.* **2010**, 49, 6940-6952; e) M. Melaimi, M. Soleihavoup, G. Bertrand, *Angew. Chem. Int. Ed.* **2010**, 49, 8810-8849.
- [4]. Review: D. Pugh, A. A. Danopoulos, *Coord. Chem. Rev.* **2007**, 251, 610-641.
- [5]. For some selected recent examples on carbene-centered pincer complexes: a) F. E. Hahn, M. C. Janke, T. Pape, *Organometallics* **2006**, 25, 5927-5936; b) C. Romain, B. Heinrich, B. Laponnaz, S. Dagorne, *Chem. Commun.* **2012**, 48, 2213-2215; c) B. K. Shaw, B. O. Patrick, M. D. Fryzuk, *Organometallics* **2012**, 31, 783-786; d) J. A. Thagfi, G. G. Lavoie, *Organometallics* **2012**, 31, 7351-7358; e) A. F. Hill, C. M. A. McQueen, *Organometallics* **2012**, 31, 8051-8054; f) A. J. Arduengo III, J. S. Dolphin, G. Gurău, W. J. Marshall, J. C. Nelson, V. A. Pertov, J. W. Runyon, *Angew. Chem. Int. Ed.* **2013**, 52, 5110-5114; g) S.-i. Fuku-en, J. Yamamoto, M. Minoura, S. Kojima, Y. Yamamoto, *Inorg. Chem.* **2013**, 52, 11700-11702; h) S.-i. Fuku-en, J. Yamamoto, S. Kojima, Y. Yamamoto, *Chem. Lett.* **2014**, 43, 468-470.
- [6]. C. J. Moulton, B. L. Shaw, *J. Chem. Soc., Dalton Trans.* **1976**, 1020-1024.
- [7]. H. D. Empsall, E. M. Hyde, R. Markham, W. S. McDonald, M. C. Norton, B. L. Shaw, B. Weeks, *J. Chem. Soc., Chem. Commun.* **1977**, 589-590.
- [8]. W. Wang, S. Parkin, O. V. Ozerov, *Organometallics* **2006**, 25, 5345-5354.
- [9]. a) R. J. Burford, W. E. Piers, M. Parvez, *Organometallics* **2012**, 31, 2949-2952; b) D. V. Gutsulyak, W. E. Piers, J. Borau-Garcia, M. Parvez, *J. Am. Chem. Soc.* **2013**, 135, 11776-11779; c) R. J. Burford, W. E. Piers, M. Parvez, *Eur. J. Inorg. Chem.* **2013**, 3826-3830; d) R. J. Burford, W. E. Piers, D. H. Ess, M. Parvez, *J. Am. Chem. Soc.* **2014**, 136, 3256-3263.
- [10]. C. C. Comanescu, V. M. Iluc, *Organometallics* **2014**, 33, 6059-6064.
- [11]. a) D. G. Gusev, A. J. Lough, *Organometallics* **2002**, 21, 2601-2603; b) D. G. Gusev, A. J. Lough, *Organometallics* **2002**, 21, 5091-5099.
- [12]. a) S. Sugawara, S. Kojima, Y. Yamamoto, *Chem. Commun.* **2012**, 48, 9735-9737; b) S. Sugawara, M. Abe, Y. Fujiwara, M. Wakioka, F. Ozawa, Y. Yamamoto, *Eur. J. Inorg. Chem.* **2015**, 534-541.
- [13]. T. Itoh, T. Mase, *Org. Lett.* **2004**, 6, 4587-4590.
- [14]. For the selected papers of FLP-catalyzed hydrogenation and hydrosilation with B(C₆F₅)₃. a) D. J.

- Parks, W. E. Piers, *J. Am. Chem. Soc.* **1996**, *118*, 9440-9441; b) D. J. Parks, J. M. Blackwell, W. E. Piers, *J. Org. Chem.* **2000**, *65*, 3090-3098; c) S. Chandrasekhar, C. R. Reddy, B. N. Babu, *J. Org. Chem.* **2002**, *67*, 9080-9082; d) A. Berkefeld, W. E. Piers, M. Parvez, *J. Am. Chem. Soc.* **2010**, *132*, 10660-10661; e) T. Mahdi, D. W. Stephan, *J. Am. Chem. Soc.* **2014**, *136*, 15809-15812; f) D. J. Scott, M. J. Fuchter, A. E. Ashley, *J. Am. Chem. Soc.* **2014**, *136*, 15813-15816.
- [15]. a) J. I. van der Vlugt, *Chem. Soc. Rev.* **2010**, *39*, 2302-2322; b) W. E. Piers, *Organometallics* **2011**, *30*, 13-16; c) J. L. Kinkenberg, J. F. Hartwig, *Angew. Chem. Int. Ed.* **2011**, *50*, 86-95.
- [16]. M. C. Burla, R. Caliandro, M. Camalli, B. Carrozzini, G. L. Cascarano, L. De Caro, C. Giacovazzo, G. Polidori, R. Spagna, *J. Appl. Cryst.* **2005**, *38*, 381-388.
- [17]. G. M. Sheldrick, *SHELX-97*; University of Göttingen: Göttingen, Germany, **1997**.

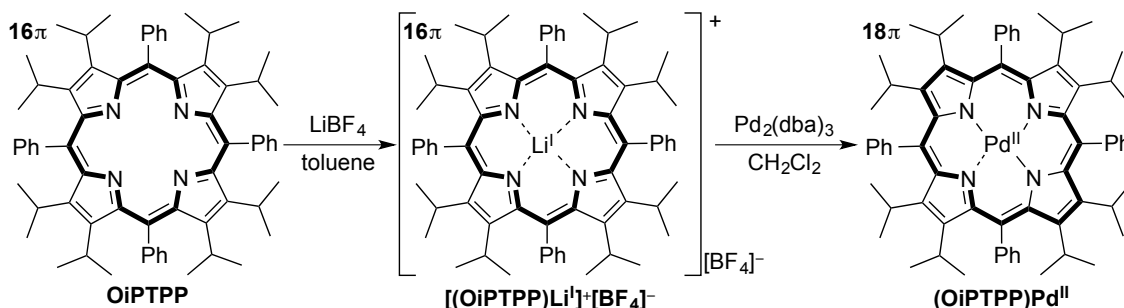
Chapter 10

Conclusions and Outlook

10-1. Summary of Anti-aromatic 16 π Porphyrins

Anti-aromatic molecules, which possess the $4n\pi$ electrons, have been recognized as unstable molecules defined by Hückel's rule, but isolation of anti-aromatic porphyrinoids including expanded porphyrins have been successively accomplished in recent years. In our previous work, we achieved the first isolation of metal-free octaalkyltetraphenylporphyrins with 16 π electron core, whereas Vaid *et al.* reported the isolation of the tetraphenylporphyrin lithium(I) complex in the 16 π state a year later of our report. However, the relationship between antiaromaticity and planarity has been still elusive because there are few examples of 16 π porphyrins. Thus, we envisioned that comprehensive studies of a series of isolable 16 π porphyrins are highly worthwhile for further understanding of the chemistry. Herein, we investigated the 16 π porphyrins with various skeletons from the most hindered porphyrin to the fundamental and planar octaethylporphyrin.

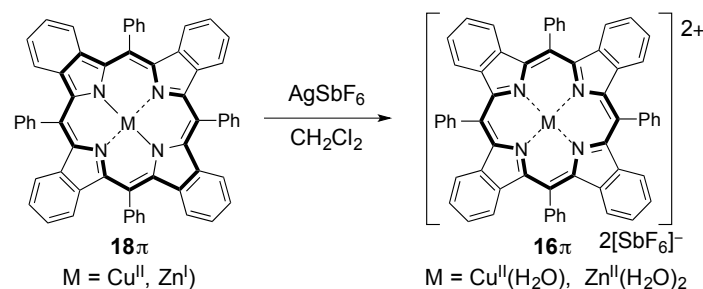
Based on our previous results, we assumed that more stable 16 π porphyrins could be obtained in terms of increasing the distortion of the porphyrin core. Thus, we investigated synthesis of the most hindered porphyrins, octaisopropyltetraphenylporphyrins (OiTPPH₂), which was uncharacterized (Scheme 1). Although the free-base porphyrin could not be crystalized, the reaction of 18 π OiTPPH₂ with SbCl₃ afforded our desired metal-free 16 π octaisopropyltetraphenylporphyrin (OiTPP) as the crystal forms. In agreement of our working hypothesis, X-ray analysis of 16 π OiTPP indicated the most distorted structure among the known 16 π porphyrins. In addition, the reaction of 16 π OiTPP with LiBF₄, followed by Pd₂(dba)₃ furnished the corresponding 18 π OiTPP palladium(II) complex, which was also found to be highly distorted.



Scheme 1. Synthesis of the most distorted 16 π porphyrin and the reaction with metal reagent.

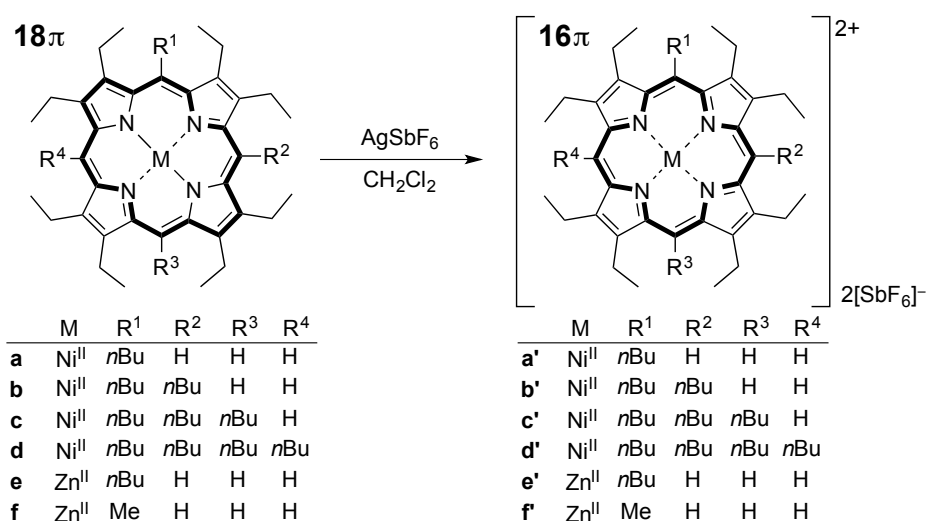
In order to diminish the steric repulsions between β substituents, tetraphenyl-tetrabenzoporphyrins (TPTBPH₂) were chosen as the suitable ligand (Scheme 2). The controlled oxidation of the parent 18 π complexes (TPTBP)M (M = Cu^{II} and Zn^{II}) enabled us to isolate the novel 16 π copper(II) and zinc(II) complexes, [(TPTBP)Cu^{II}(H₂O)]²⁺·2[SbF₆]⁻ and [(TPTBP)Zn^{II}(H₂O)₂]²⁺·2[SbF₆]⁻, as well as singly oxidized 17 π copper(II) complex, [(TPTBP)Cu^{II}]⁺[SbF₆]⁻. The structural studies revealed that the TPTBP skeleton provided more planarity in their 16 π states than the previously isolated octaalkyltetraphenylporphyrins. Attributed to the planarity, TPTBP zinc(II) complexes showed the stronger anti-aromatic character derived from the paratoropic ring current as determined by ¹H NMR

spectroscopy and predicted by NICS calculations. The combined study of MCD spectroscopy and TD-DFT calculations revealed that the electronic transitions of the UV-vis spectra and their assignment were in accord with Michl's $4N$ and $4N+2$ perimeter models. Overall excited state relaxation dynamics of the porphyrins were also investigated using femtosecond transient absorption measurements. In addition, electrochemical and spectroelectrochemical data of the porphyrins clarified the consistency between chemical oxidation and electronic oxidation.



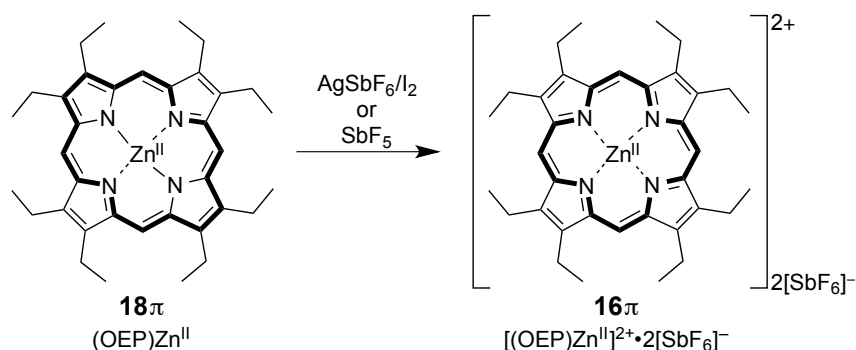
Scheme 2. Oxidation of the benzo-fused 18π porphyrin metal complexes.

A series of novel meso-mono to tetra-alkylated octaethylporphyrin (OEP) nickel(II) complexes with 16π electron core was prepared (Scheme 3). Although they were not isolated in their crystalline forms, the decomposition of the 16π species monitored by UV-vis spectra was found to be slower even in the solution as the number of meso-substituents increased. Also, the ^1H NMR spectra of the 16π porphyrins showed high-field shifts compared to those of the corresponding 18π porphyrins. In particular, the meso-tetrabutyl-substituted (OEP)Ni^{II} in the 16π state showed extraordinary stability in the solution. By replacing the central metal from nickel to zinc, the X-ray structural measurements of two 16π porphyrin zinc(II) complexes with a meso-monobutyl or monomethyl group were accomplished. The results revealed that 16π [5-methyl-(OEP)Zn^{II}]²⁺ was found to have the most planar structure among all isolated 16π porphyrins as well as the distinct anti-aromatic character determined by the ^1H NMR spectra.



Scheme 3. Oxidation of the meso-mono- to tetra-alkyl substituted 18π porphyrin metal complexes.

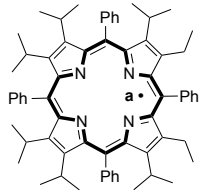
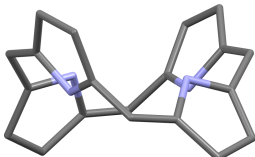
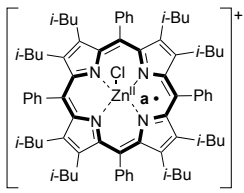
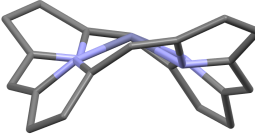
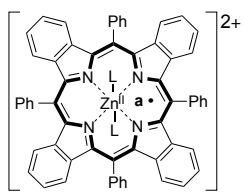
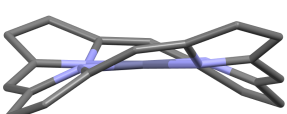
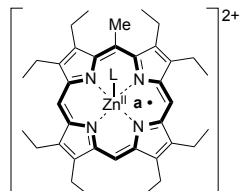
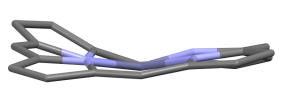
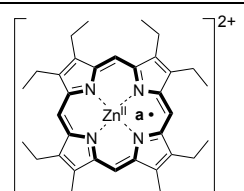
In order to investigate the antiaromaticity of the meso-free 16π porphyrin, the oxidation of the meso-unsubstituted octaethylporphyrin (OEP) zinc(II) complex with strong oxidant was performed (Scheme 4). Although we could not obtain the crystals suitable for X-ray analysis, generation of 16π $(\text{OEP})\text{Zn}^{\text{II}}$ using $\text{AgSbF}_6/\text{I}_2$ or SbF_5 was confirmed by the ^1H NMR spectrum and UV-vis spectrum. In contrast to the most planar 16π porphyrin with a meso-methyl group, the meso-protons of the 16π $[(\text{OEP})\text{Zn}^{\text{II}}]^{2+}$ complex showed a larger high-field shift relative to its parent 18π species in the ^1H NMR spectra. This result indicated that the novel species possess the most anti-aromatic nature among all of the reported 16π porphyrins.



Scheme 4. Oxidation of the most planar 18π octaethylporphyrin zinc(II) complex.

To summarize all of the results for 16π porphyrins, the relationship between the planarity and the antiaromaticity was rationalized through overall findings of our research (Table 1). Our results revealed that the degree of planarity is highly related to the degree of antiaromaticity, that is, the highly planar structure induces distinct antiaromaticity due to the effective conjugation in the porphyrin core. At the same time, the planar 16π porphyrins are unstable when exposed to air and moisture unless an electron-donating substituent is introduced at the meso-position. In addition, all of the 16π porphyrin cores we chose in this study were largely distorted in comparison with the corresponding 18π species upon double oxidation. Thus, in order to evaluate the antiaromaticity of completely planar 16π porphyrins, further studies should be investigated using an anthracene-fused porphyrin skeleton, which could prevent the distortion upon the oxidation due to the β -meso- β -fixed skeleton. The research is ongoing in our laboratory.

Table 1. Overall comparison of relationship between structure and antiaromaticity in our 16 π porphyrins.

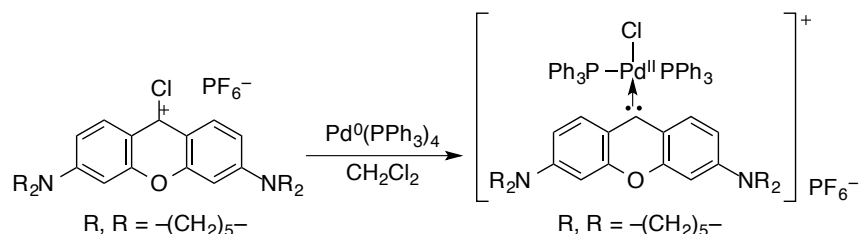
Compounds	X-ray structure	RMS	NICS (point a)	$\Delta\delta_{\text{H}}$ (<i>meso</i> -H)
 16π OiPTPP		1.078	+0.56	n. d.
 16π [(OiBTPP)Zn^{II}Cl]⁺		0.888	+4.38	n. d.
 16π [(TPTBP)Zn^{II}]²⁺ L = H ₂ O		0.631	+12.93	n. d.
 16π [(5-MeOEP)Zn^{II}]²⁺ L = H ₂ O		0.291	+20.08	5.14^[b]
 16π [(OEP)Zn^{II}]²⁺	n. d.	n. d.	+43.61^[a]	6.56

In the X-ray structures, substituents of the porphyrins, counter anions, solvated molecules, and metal-ligated waters are omitted for clarity. All calculations were performed in the level of B3LYP/6-31G(d) using X-ray geometry except for [(OEP)Zn^{II}]²⁺. [a] Calculated using the optimized structure (RMS value of the calculated structure was 0.001). [b] Average value of the *meso*-protons.

10-2. Summary of Cyclic Aromatic Remote Carbenes

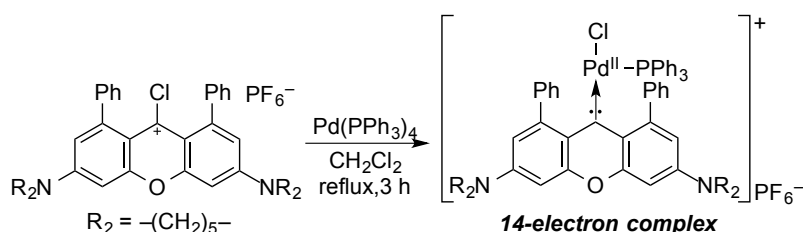
Carbenes are neutral divalent carbon compounds with only six valence electrons and the species have been recognized as reactive intermediates for decades. There are two different electronic states due to two non-bonding electrons: singlet or triplet. As for singlet carbenes in which two electrons occupy one σ -orbital with a parallel spin orientation, stable singlet carbenes have been isolated as the free forms. A leading example of such carbenes is *N*-heterocyclic carbene (NHC), which is highly stable even in air and moisture due to strong π -electron donating ability of the adjacent nitrogen atoms at the carbene carbon atom. In addition to development of the novel carbene species with lower LUMO energy level such as CAACs and DACs than NHCs, “abnormal” and “remote” NHCs have steadily emerged in recent years although there are still few isolated examples as free forms. It is notable that these new generation of carbenes are predicted to have higher nucleophilicity and electrophilicity. Therefore, we envisioned that cyclic aromatic carbenes would be one of the suitable candidates as our target molecules. Cyclic aromatic carbenes have only been studied as transient species, so we envisaged that introduction of remote amino groups at the conjugated position of the carbene carbon atom would be effective to stabilize the carbenes as the free form and enables us to utilize the carbene ligands for the complexes including transition-metals or main group elements. Based on these premises, we investigated the chemistry of cyclic aromatic remote carbenes.

Novel cyclic aromatic carbene ligands bearing a bridged oxygen atom, which were regarded as xanthylidene derivatives, were developed (Scheme 5). Although attempts to generate the free carbenes via deprotonating reaction with strong bases were unsuccessful, the reaction of the alcohol adduct with S8 furnished the corresponding thioketone compound, suggesting that the carbene species would be generated *in situ*. Taking advantage of oxidative addition of low-valent palladium(0) metal into the chloride precursor, isolation of the carbene-palladium(II) complex was accomplished. The X-ray structural analysis revealed that the donating ability of the carbene ligand is stronger than the conventional NHC ligands, resulting higher catalytic activity of the palladium(II) complex in Suzuki-Miyaura cross-coupling reaction.



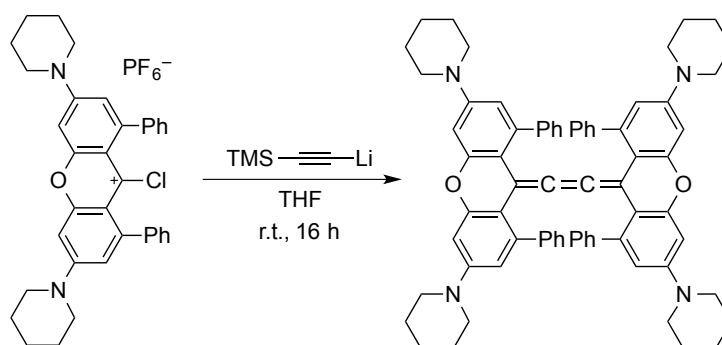
Scheme 5. Oxidative addition of palladium(0) into the xanthylidene-based carbene precursor.

Photophysical studies of 1,8-disubstituted xanthyliene-based remote carbenes were performed. With matrix-isolation UV-vis spectroscopic analysis, the free carbenes could be detected at low temperature, although transient absorption spectra suggested that the xanthyliene-based remote carbenes were to be kinetically more reactive than the parent xanthyliene and the species bearing 1,8-diphenyl groups were less effective to elongate the lifetime. However, oxidative addition of $\text{Pd}(\text{PPh}_3)_4$ furnished a low-coordinate 14-electron palladium(II) complex with the ligand bearing 1,8-diphenyl groups (Scheme 6). In the X-ray structure, agnostic interaction from a surrounding phenyl group was effective to stabilize the unusual complex.



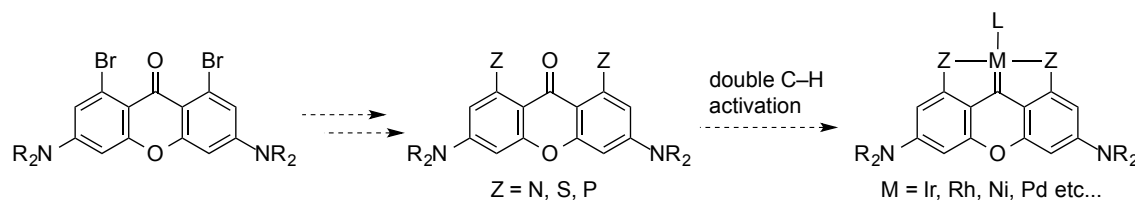
Scheme 6. Oxidative addition of palladium(0) into the xanthyliene-based carbene precursor.

Also, synthesis and characterization of the neutral C4 cumulene featuring xanthyliene units were investigated (Scheme 7). In the similar manner of Bertrand's method, the reaction of the chloride precursor with 1,8-diphenyl groups with TMSCLi gave the unprecedented neutral C4 cumulene instead of the cation radical. Although the reliable synthesis is not established yet, the X-ray analysis revealed that the large deviation between C4 backbone and xanthyliene parts inhibited their effective conjugation. Judging from the crystal structure, it was reasonable that the radical cation species generated by air-oxidation showed a singlet peak in the EPR spectrum without any hyper-fine couplings.



Scheme 7. Oxidative addition of palladium(0) into the xanthyliene-based carbene precursor.

Attempts to prepare the tridentate ligand based on the xanthylidene remote carbenes were also investigated. Introduction of tolylthioether groups was accomplished in terms of the palladium-mediated cross coupling reaction. However, the following reductions to afford the suitable precursor for metal complexes are still underway. It is considered that the tridentate ligand with tolylthioether or dialkylphosphorus groups at the 1,8-positions would be effective to prepare the active metal complexes toward small molecules. Thus, further studies are highly required and ongoing in our laboratory.



Scheme 8. Attempted synthesis of tridentate carbene pincer ligands and the complexes.

As described above, cyclic aromatic remote carbenes are intriguing ligands for organometallic and main-group chemistry, although generation of the carbenes as the free form is still a big challenge. For further ubiquitous application of the carbenes, establishment of the synthetic method for the free carbenes is highly demanded with further fine-tuning of the substituents in the ligands. We hope the dibromo-substituted precursor prepared in this study plays an important role to accomplish the goal.

公表論文

公表論文

- 1) Anti-aromatic 16π Porphyrin Metal Complexes with meso-Alkyl Substituents
T. Kakui, S. Sugawara, Y. Hirata, S. Kojima, Y. Yamamoto,
Chem. Eur. J. **2011**, *17*(29), 8005-8008.
- 2) Synthesis and characterization of the most distorted 16π porphyrin: 16π Octaisopropyltetraphenylporphyrin (OiPTPP)
S. Sugawara, M. Kodama, Y. Hirata, S. Kojima, Y. Yamamoto,
J. Porphyrins. Phthalocyanines. **2011**, *15*(11-12), 1326-1334.
- 3) Synthesis, Characterization and Spectroscopic Analysis of Antiaromatic Benzofused Metalloporphyrin Species
S. Sugawara, Y. Hirata, S. Kojima, Y. Yamamoto, E. Miyazaki, K. Takimiya, S. Matsukawa, D. Hashizume, J. Mack, N. Kobayashi, Z. Fu, K. M. Kadish, Y. M. Sung, K. S. Kim, D. Kim,
Chem. Eur. J. **2012**, *18*(12), 3565-3581.
- 4) Synthesis of new cyclic aromatic carbene ligands bearing remote amino groups and their palladium complexes
S. Sugawara, S. Kojima, Y. Yamamoto,
Chem. Commun. **2012**, *48*, 9735–9737.
- 5) Synthesis of the most anti-aromatic 16π porphyrin: an octaethylporphyrin zinc(II) complex with no meso substituents
S. Hiramatsu, S. Sugawara, S. Kojima, Y. Yamamoto,
J. Porphyrins. Phthalocyanines. **2013**, *17*(12), 1183-1187.
- 6) 1,8-Disubstituted Xanthyliene-based Remote Carbenes: Photolytic Generation and Isolation of Low-coordinate Palladium(II) Complex
S. Sugawara, M. Abe, Y. Fujiwara, M. Wakioka, F. Ozawa, Y. Yamamoto,
Eur. J. Inorg. Chem. **2015**, 534-541.

参考論文

参考論文

- 1) Demethylation of an Allene Bearing Two Dimethoxythioxanthene Groups by Oxidation via a Vinyl Cation Intermediate
T. Yamaguchi, S.-i. Fuku-en, S. Sugawara, S. Kojima, Y. Yamamoto,
Aust. J. Chem. **2010**, 63, 1638-1644.
- 2) Isolation of a Neutral Boron-Containing Radical Stabilized by a Cyclic (Alkyl)(Amino)Carbene
P. Bissinger, H. Braunschweig, A. Damme, I. Krummenacher, A. K. Phukan, K. Radacki, S. Sugawara,
Angew. Chem. Int. Ed. **2014**, 53(28), 7360-7363.
- 3) Alternative synthetic route toward octaisopropylporphyrins and structural deformation caused by a meso-butyl group
S. Sugawara, T. Kakui, Y. Yamamoto,
J. Porphyrins. Phthalocyanines. **2014**, 17(12), 1183-1187.

Acknowledgement

The studies described in this dissertation have been carried out under the direction of Prof. Yohsuke Yamamoto at the Department of Chemistry, Graduate School of Science, Hiroshima University. These works were supported by Research Fellowships of Japan Society for the Promotion of Science for Young Scientists.

The author sincerely wishes to express his appreciation to Prof. Yohsuke Yamamoto for his continuing guidance, valuable discussions and encouragement throughout the course of studies. Grateful acknowledgment is made to Assoc. Prof. Satoshi Kojima (Hiroshima University) and Prof. Atsushi Kawachi (Hosei University) for their helpful discussions and suggestions.

The author is grateful to Prof. Holger Braunschweig, Julius-Maximillians-Universität Würzburg for his valuable discussions, thoughtful advice and encouragement during his stay in his laboratory.

The author wishes to thank Prof. Manabu Abe (Hiroshima University), Assoc. Prof. Yoshihisa Fujiwara (Hiroshima University), Prof. Fumiyuki Ozawa (Kyoto University), Dr. Masayuki Wakioka (Kyoto University), Prof. Kazuo Takimiya (RIKEN), Dr. Eigo Miyazaki (Hiroshima University), Assoc. Prof. Shiro Matsukawa (Toho University), Dr. Daisuke Hashizume (RIKEN), Dr. John Mack (Tohoku University), Prof. Nagao Kobayashi (Tohoku University), Ms. Zhen Fu (University of Houston), Prof. Karl M. Kadish (University of Houston), Mr. Young Mo Sung (Yonsei University), Dr. Kil Suk Kim (Yonsei University), Prof. Dongho Kim (Yonsei University), Prof. Tsutomu Mizuta (Hiroshima University), Prof. Takeharu Haino (Hiroshima University) for their helpful discussions, kind assistance and collaborations.

The author would express his appreciation to Dr. Torahiko Yamaguchi, Dr. Hideaki Yamamichi, Ms. Megumi Kodama, Dr. Jun-ya Nakatsuji, Dr. Yuichi Hirano, Mr. Yusuke Hirata, Mr. Takanari Kakui, Dr. Yusuke Inagaki, Dr. Shin-ichi Fuku-ene, Mr. Hirotaka Yasuda, Dr. Yuan Shi, Mr. Norimasa Nishioka, Mr. Yuki Norimatsu, Mr. Yasuyuki Imada, Mr. Tatsuya Inoue, Mr. Yuya Toya, Mr. Shogo Hiramatsu, Mr.

Tatsuya Hirofuji, Mr. Junki Yamamoto, Mr. Ryosuke Kuramasu, Mr. Naoto Maeta and all of the other members of Prof. Yamamoto's group for their helpful discussions and kind assistance. Also, the author is sincerely grateful to Dr. Philipp Bissinger, Dr. Alexander Damme, Dr. Christian Hörl, Dr. Ivo Krummenacher, Dr. Ashwini K. Phukan, Dr. Krzysztof Radacki, Dr. Rong Shang, Dr. Qing Ye and all of the other members of Prof. Braunschweig's group for their helpful discussions and kind assistance during his stay in Prof. Braunschweig's group.

The author wishes to thank Dr. Hideaki Miyake, Dr. Koh Sugamata, Dr. Katsuhiko Takeuchi, Dr. Tomokatsu Kushida, Dr. Takayuki Tanaka, Dr. Tomoki Yoneda, Dr. Ayumu Karimata, Dr. Takuya Kamimura, Dr. Hiroki Takesawa, Dr. Keita Hagiwara, Dr. Katsuya Mutoh, Dr. Fumiya Hirakawa, Dr. Hiroki Makida, Dr. Tatsuya Wasano, Dr. Tatsurou Annaka, Mr. Hirotaka Mori, Mr. Koichi Nagata, Mr. Yuzuru Kobayashi, and Mr. Kazuyuki Uchida for their fruitful discussion, kind encouragement, and continuous friendship.

The author sincerely wishes to express great thanks to Dr. Wataru Sato, Mr. Susumu Yoshioka, Mr. Takahide Oshita, Mr. Tetsuya Ishimoto, Mr. Akira Takeda, Ms. Karin Schmidt-Singh, Mr. Gurinder Schmidt-Singh, and Ms. Airi Tamaki for encouragement and continuous friendship.

Finally, the author is grateful to his parents Mr. Kouki Sugawara and Ms. Tazuko Sugawara, his brothers Mr. Gaku Sugawara and Mr. Shou Sugawara, his sister-in-law Ms. Ayano Sugawara, and his niece Ms. Sana Sugawara for their constant assistance, affectionate encouragement, and providing the very comfortable environment to concentrate on research.

February, 2015

Shun Sugawara

Department of Chemistry, Graduate School of Science
Hiroshima University